

1-1-1987

## The diffusion of polymers in porous materials as studied by dynamic light scattering/

Matthew T. Bishop  
*University of Massachusetts Amherst*

Follow this and additional works at: [https://scholarworks.umass.edu/dissertations\\_1](https://scholarworks.umass.edu/dissertations_1)

---

### Recommended Citation

Bishop, Matthew T., "The diffusion of polymers in porous materials as studied by dynamic light scattering/" (1987). *Doctoral Dissertations 1896 - February 2014*. 719.  
<https://doi.org/10.7275/70kg-q149> [https://scholarworks.umass.edu/dissertations\\_1/719](https://scholarworks.umass.edu/dissertations_1/719)

This Open Access Dissertation is brought to you for free and open access by ScholarWorks@UMass Amherst. It has been accepted for inclusion in Doctoral Dissertations 1896 - February 2014 by an authorized administrator of ScholarWorks@UMass Amherst. For more information, please contact [scholarworks@library.umass.edu](mailto:scholarworks@library.umass.edu).



THE DIFFUSION OF POLYMERS IN POROUS MATERIALS  
AS STUDIED BY DYNAMIC LIGHT SCATTERING

A Dissertation Presented

by

MATTHEW T. BISHOP

Submitted to the Graduate School of the  
University of Massachusetts in partial fulfillment  
of the requirements for the degree of

DOCTOR OF PHILOSOPHY

February, 1987

Department of Polymer Science and Engineering

© Copyright by Matthew T. Bishop 1987

All Rights Reserved

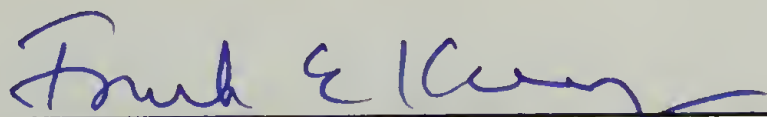
THE DIFFUSION OF POLYMERS IN POROUS MATERIALS  
AS STUDIED BY DYNAMIC LIGHT SCATTERING

A Dissertation Presented

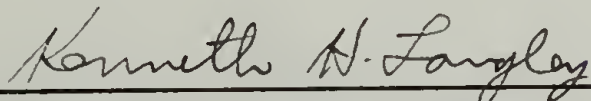
by

MATTHEW T. BISHOP

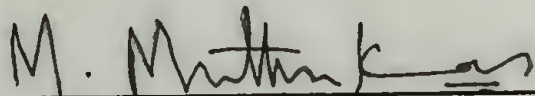
Approved as to style and content by:



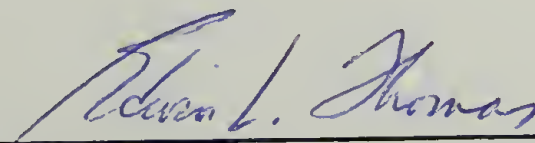
Dr. Frank E. Karasz, Chairperson of Committee



Dr. Kenneth H. Langley, Member



Dr. Murugappan Muthukumar, Member



Dr. Edwin L. Thomas, Department Head  
Polymer Science and Engineering Department

RATIONAL, *adj.* Devoid of all delusions save those of observation, experience, and reflection.

REASON, *v. i.* To weigh probabilities in the scales of desire.

REASON, *n.* Propensitate of prejudice.

Ambrose Bierce, The Devil's Dictionary

## ACKNOWLEDGMENTS

A debt of gratitude is owed my advisors, Professors Frank E. Karasz and Kenneth H. Langley: Dr. Karasz, for allowing me the freedom and providing the support to pursue this project; and Dr. Langley, for his invaluable and generous help, instruction, and encouragement over the years, and for his initiation of this chemist (with synthetic leanings) into the world of physics. It was also a great pleasure to have known and started working with Dr. Paul Russo. He taught me much and is thanked for having provided a substantial foundation for this work--many of the data-taking and data analysis programs, as well as much equipment in the lab, can be traced to his efforts. Machinists Bob Verner and Frank Nalepa are to be thanked for their work; it was they who transformed rough designs into an actual light scattering apparatus, with remarkable skill and precision. The help of Dr. Nalini Easwar, who collected raw data on several samples while this dissertation was being written, is much appreciated. Dr. Wolfgang Haller, of the National Bureau of Standards, kindly provided several porous glass samples, and other useful information. Over the course of this work, Professors Robert Guyer, Murugappan Muthukumar, and Jonathan Machta have provided me with many valuable insights into the problem at hand. The advice of Dr. Steve Bott on implementation of Provencher's CONTIN analysis program was invaluable. Mr. Lou Raboin is thanked for obtaining electron micrographs of the porous glasses. Last but not least, the Air Force Office of Scientific Research (contract 84-0033) has generously funded this work.

My sentence in the tower has been made bearable by my friends in the "6th floor crew", from whence I came, in particular Jack Hirsch, Charlie Dickinson, and Joe Schlenoff, and others long since departed.

My deepest debt is owed my wife, whose love and sacrifice during our tenure in graduate school has been more than most could hope for or deserve, particularly in the waning days.

## ABSTRACT

### THE DIFFUSION OF POLYMERS IN POROUS MATERIALS AS STUDIED BY DYNAMIC LIGHT SCATTERING

February, 1987

Matthew T. Bishop, B. S., University of Chicago, 1977

Ph. D., University of Massachusetts, 1987

Directed by: Professor Frank E. Karasz

Professor Kenneth H. Langley

The diffusion of a flexible polymer in a rigid porous material-- polystyrene in porous silica--is investigated using the technique of dynamic light scattering. Measurements are made entirely within single fragments of porous glass, saturated at equilibrium with dilute solutions of various molecular weights of polystyrene in a thermodynamically good solvent, which is also chosen to match the refractive index of the glass. Adsorption of polymer is absent. Diffusion behavior is investigated as a function of the dimensionless variables  $R_H/R_p$  (the relative size of polymer to pore) and  $qR_p$  (essentially the ratio of pore size to the characteristic diffusion length), where  $R_H$  is the polymer hydrodynamic radius,  $R_p$  the pore radius, and  $q$  the scattering wavevector.

Macroscopic diffusion coefficients,  $D_\infty$ , phenomenological coefficients for diffusion over large distances in the porous glass, are obtained from data at low  $qR_p$ . These macroscopic diffusion results are interpreted

using a combination of phenomenological theories for diffusion of point particles in random porous materials together with theories for the reduced diffusivity of hard spheres and of flexible polymers in cylindrical pores.

The reduced diffusion coefficient in the glass,  $D_{\infty}/D_0$ , with  $D_0$  the diffusivity in unbounded solution, is found to monotonically decrease with an increase in  $R_H/R_p$ , contrary to previous results for polystyrene diffusion in porous glasses, but consistent with results of previous membrane transport experiments. The inverse of the value of  $D_{\infty}/D_0$ , in the limit  $R_H/R_p = 0$ , yields the tortuosity  $T$  of the porous glasses. For these data,  $D_{\infty}$  equals  $D_p$  divided by  $T$ , where the reduced diffusivity  $D_p$  is solely a function of the relative size parameter  $R_H/R_p$ , and where the tortuosity  $T$  depends only on the porous glass structure. The change in diffusivity relative to bulk solution,  $D_p/D_0$ , is due to polymer-wall hydrodynamic interactions, and to changes in intramolecular hydrodynamic interactions for confined polymer. Measured values of  $D_p/D_0$  are in good agreement with existing theories.

## TABLE OF CONTENTS

ACKNOWLEDGMENTS.....	v
ABSTRACT.....	vii
LIST OF TABLES.....	xi
LIST OF FIGURES.....	xiii
 Chapter	
I. INTRODUCTION.....	1
II. PARTITIONING AND DIFFUSION IN POROUS MATERIALS: THEORY AND BACKGROUND.....	14
Equilibrium Partitioning of Polymers.....	15
Diffusion in Single Pores of Simple Geometry.....	26
General Phenomenology of Diffusion in Porous Materials.....	43
Miscellaneous Diffusion Theories.....	69
Experimental Background.....	73
III. DYNAMIC LIGHT SCATTERING: THEORY.....	92
Basics.....	92
Applications to Diffusion in Porous Materials.....	108
IV. MATERIALS.....	117
Polymers and Solvents.....	117
Porous Glass Characterization.....	126
Glass Pretreatment and Adsorption Testing.....	148
Sample Preparation.....	155
V. DYNAMIC LIGHT SCATTERING EXPERIMENTS IN POROUS MATERIALS.....	160
Light Scattering Apparatus and General Procedure.....	160
Technical Details.....	182
Data Analysis.....	201

VI.	RESULTS.....	213
	Experimental Overview.....	213
	Diffusion Regimes: Wavevector Dependence.....	217
	Practical Data Analysis.....	235
	Initial Data Fitting.....	235
	Extraction of Diffusion Coefficients.....	242
	Internal Modes of Strongly Confined Chains.....	245
	Concentration Dependence of Diffusion Coefficients.....	252
VII.	DISCUSSION AND CONCLUSIONS.....	261
	Macroscopic Diffusion.....	261
	Suggestions for Future Work.....	298
	REFERENCES.....	304
Appendix		
A.	MISCELLANEOUS SOLVENT PROPERTIES.....	319
B.	TRACK-ETCHED POROUS PLASTICS.....	321

## LIST OF TABLES

1.	Characteristics of Linear Polystyrene Samples.....	118
2.	Porous Glass Characteristics: Specific Pore Volume $v_p$ , Porosity $\Phi$ , and Nominal Pore Radius $R_p$ .....	133
3.	Silanization Treatments.....	150
4.	Tests of Silanized Glasses for Polystyrene Adsorption.....	153
5.	Comparison of Cumulants and Laplace Inversion Data Analysis Methods for Data in the Macroscopic Diffusion Regime (Polymer P4, Glass B7).....	236
6.	Effect of Baseline Choice and Analysis Method on the Average Decay Rate $\langle \Gamma \rangle$ and Normalized Variance $\mu_2/\langle \Gamma \rangle^2$ for Polymer P3 in Glass B7, at $q^2 = 1.5 \times 10^9 \text{ cm}^{-2}$ .....	240
7.	Internal Modes of Confined Chains: Analysis of Data for Polymer P17 ( $M = 2.1 \times 10^6$ ) in Glass B7 ( $R_p = 893 \text{ \AA}$ ); Relative Size $\lambda_H = 0.47$ .....	248
8.	Master Data Table, Part I: Initial Concentration ( $c_0$ ), Concentration Relative to the Overlap Concentration ( $c_0/c^*$ ), Experimental Temperature ( $T$ ), Hydrodynamic Radius ( $R_H$ ), and Relative Size Parameter ( $\lambda_H$ ) Glass B7 ( $R_p = 893 \text{ \AA}$ ), Glass B5 ( $R_p = 1866 \text{ \AA}$ ), Glass B13 ( $R_p = 703 \text{ \AA}$ ).....	264
9.	Master Data Table, Part 2: Diffusion Coefficient in Bulk Solution ( $D_0$ ), Macroscopic Diffusion Coefficient ( $D_\infty$ ), and Reduced Diffusion Coefficient ( $D_\infty/D_0$ ) for Glasses B7, B5, and B13.....	265
10.	Range (in Microns) of Nuclear Particles in CR-39 Polymer.....	325

11.	dE/dx (in MeV cm <sup>2</sup> /g) for Nuclear Particles in CR-39 Polymer.....	325
12.	Track-Etching Geometry (2L = 150 μm).....	327

## LIST OF FIGURES

1.	Equilibrium partitioning coefficient $K_D$ versus relative size parameter $\lambda_H$ .....	27
2.	Flexible polymers in pores.....	37
3.	Schematic of tortuous and constricted pores.....	53
4.	Schematics of well-connected and non-well- connected pore spaces.....	66
5.	Dynamic light scattering.....	93
6.	Bulk solution diffusion coefficient $D_0$ versus molecular weight for linear polystyrenes in 2-fluorotoluene.....	121
7.	Scanning electron micrographs of porous glasses.....	129
8.	Mercury porosimetry results for controlled pore glasses B7 ( $R_p = 893 \text{ \AA}$ ) and B5 ( $R_p = 1866 \text{ \AA}$ ).....	135
9.	Mercury porosimetry: geometry and ink bottle pores.....	139
10.	Dynamic light scattering apparatus.....	162
11.	Light scattering apparatus: cutaway view of vat parallel to table.....	168
12.	Light scattering apparatus: cutaway view perpendicular to table.....	169
13.	Situation of scattering volume in porous glass fragments.....	176
14.	Angular variation of intensity of light scattered by porous glass fragments.....	179

15.	Correlation function misnormalization due to baseline uncertainty.....	195
16.	Experimental examples of correlation function misnormalization.....	198
17.	Diffusion regimes: differences in the scattered electric field correlation function as $qR_p$ is varied.....	218
18.	Wavevector dependence of the reduced average effective diffusion coefficient $D_{EFF}/D_0$ , and of the normalized variance $V = \mu_2/\langle\Gamma\rangle^2$ of the decay rate distribution, for glasses B7 ( $R_p = 893 \text{ \AA}$ ) and B13 ( $703 \text{ \AA}$ ).....	226
19.	Wavevector dependence of the reduced average effective diffusion coefficient $D_{EFF}/D_0$ , and of the normalized variance $V = \mu_2/\langle\Gamma\rangle^2$ of the decay rate distribution, for glass B5 ( $R_p = 1866 \text{ \AA}$ ).....	228
20.	Relaxation rate spectra as a function of $qR_p$ .....	233
21.	Average relaxation rate $\langle\Gamma\rangle$ versus the square of the scattering wavevector $q^2$ for diffusion in bulk solution and for macroscopic diffusion in a porous glass.....	243
22.	Average relaxation rates for slow and fast modes versus $q^2$ , for $M = 2.1 \times 10^6$ polystyrene in glass B7 ( $R_p = 893 \text{ \AA}$ , $\lambda_H = 0.47$ ).....	251
23.	Concentration dependence of mutual diffusion coefficients, in unbounded solution, and in solution inside a porous glass.....	254
24.	Macroscopic diffusion of linear polystyrenes in porous glasses as a function of relative size of polymer to pore.....	262

25.	Residuals of fits of low Reynolds number hydrodynamics theories to data at small relative size parameter.....	271
26.	Comparison of low $\lambda_H$ data to theories for diffusion of hard spheres in cylindrical pores.....	274
27.	Scaling theory fit to high $\lambda_H$ data.....	280
28.	Transition from non-free draining free draining behavior.....	283
29.	Effective fractal diffusion behavior.....	292
30.	Track-etching geometry.....	327

## CHAPTER I

### INTRODUCTION

This dissertation describes the use of dynamic light scattering to study the diffusion of polymers in porous materials. The purposes of this Introduction are several: first, to place this work in relation to general studies of transport in porous materials, and, more specifically, to studies of polymer transport; second, to briefly describe the experiments, including the system studied, the motivation for using the technique of dynamic light scattering, the research objectives, and the basic accomplishments; and lastly, to outline the content of the dissertation.

The transport of dissolved macromolecules in porous materials, a small subfield of more general studies of transport in porous materials, is central to many phenomena of technological and scientific interest: chromatographic separation of macromolecules using size exclusion or hydrodynamic chromatography; flow of polymer solutions through packed beds or in consolidated porous media, as used, for example, in enhanced oil recovery; separations using membranes, where one wants to selectively control transport by macromolecular size, shape, or charge; flow of blood through small capillaries; polymerization using heterogeneous catalysts; and controlled release from porous substrates.

In the most general case, transport in porous media<sup>1-3</sup> involves convection, diffusion, and chemical reaction; these are coupled processes. ("Chemical reaction" includes physical adsorption and desorption.) These

processes are governed by interactions between the fluid continuum (which may contain suspended particles), the porous medium, and external forces. A few examples of such interactions are the viscous forces involved in low Reynolds number flows;<sup>1-4</sup> interactions of charged species with an external electric field; repulsive or attractive physicochemical interactions between suspended particles and pore walls; and hydrodynamic interactions of large particles with pore walls.<sup>4</sup> Given that the strength of most interactions varies with the distance from the pore surfaces, transport will depend strongly on the detailed geometry of the porous material. Aside from external forces, the structure establishes the fields with which the fluid and any suspended particles interact.

Relative to the overall scheme of transport in porous media, the experimental subject of this dissertation, namely, the diffusion of flexible polymers in random rigid porous materials, is in some ways simple, but in other ways complex. It is simple insofar as only diffusion, without convection or chemical reaction, is present. Furthermore, it is diffusion in a system at macroscopic equilibrium, with no macroscopic concentration gradients present. However, certain features of the system introduce complexity. First, the size of the diffusant--that is, the polymer--is comparable to the size of the pores. The diffusion of a Brownian particle near a wall is slowed due to hydrodynamic interactions with that wall.<sup>4-9</sup> Since diffusing polymer coils are closely surrounded by walls, these hydrodynamic interactions are significant. Second, for flexible polymers, in contrast to rigid Brownian particles, the overall hydrodynamics may be further complicated by changes in intra-chain hydrodynamic interactions as

caused by changes of polymer configuration inside pores.<sup>10-12</sup> Lastly, the pore space is relatively random, with geometrical features perhaps difficult to capture in a mathematical model, thereby preventing accurate *a priori* prediction of diffusion behavior.

The experimental system--porous medium, polymer, and solvent--studied in this dissertation is as follows. As porous medium, three porous glasses, of different porosity and pore size, were used. As polymer, various flexible, nearly monodisperse polystyrenes were used, chosen to span as wide a molecular weight range as experimentally feasible. The solvent was chosen to be thermodynamically good for the polymers and to match the refractive index of the glasses. Dynamic light scattering<sup>13-15</sup> was the technique used to investigate the diffusion of these polymers, dissolved in dilute solution, in these porous glasses.

These experiments were motivated by the following considerations. First, dynamic light scattering is more "direct" than many other techniques. Previous experiments on diffusion in porous materials,<sup>7,16-37</sup> whether of polymers or of small molecules, and whether in geometrically regular or random pore spaces, have with some exceptions<sup>38-45</sup> been phenomenological measurements, in the sense that microscopic diffusion behavior has been inferred, using various theories and assumptions, from macroscopic flux measurements, say across a membrane or into a chunk of porous material. In contrast, dynamic light scattering measurements directly reflect the Brownian motion of the scatterers,<sup>15,46,47</sup> allowing relatively straightforward conclusions about microscopic diffusion behavior. A second motivation was provided by the unbelievable (at least to me) conclusions about the mole-

cular weight dependence of the diffusion coefficient of flexible polymers in porous glasses (essentially the same as the system studied in this work) which had been reached in previous phenomenological investigations.<sup>16,17,34</sup> I saw no reason to expect that the hindrance to diffusion for flexible polymers in random porous materials should be qualitatively different than hindrance to diffusion in ideal pore geometries, the latter as has been established by theory<sup>10-12</sup> and experiment.<sup>29-32</sup>

The work of this dissertation can be placed in a more specific context by considering previous experiments on the diffusion of polymers and colloids in porous materials. Those experiments can be divided into those in which the pores have well defined geometry, and those in which the pore space is relatively random. Prime examples are diffusion across track-etched membranes,<sup>7,27-32</sup> and transient diffusion into pieces of porous glass.<sup>16,17</sup> A central goal has been to relate the results of these phenomenological measurements to the microscopic parameters characterizing the polymer and porous material. For the membrane transport experiments (pores of well defined geometry) this goal has been met fairly successfully using theories based on low Reynolds number hydrodynamics<sup>6-9,28</sup> (colloids and rigid polymers) and scaling concepts<sup>10-12</sup> (flexible polymers). In contrast, the results and conclusions<sup>16,17,34</sup> of previous experiments for diffusion of polymers, especially flexible polymers, in random porous materials present a confused and conflicting picture. This dissertation attacks the problem of polymer diffusion in random porous materials by applying for the first time the technique of dynamic light scattering.

The potential advantages offered by dynamic light scattering as a tool to study diffusion in porous materials are summarized as follows. First, it is a measurement made directly within the porous material, as opposed to indirectly in a surrounding fluid reservoir, so that results are directly related to the Brownian motion of the diffusing polymer inside the pores. Second, it is a measurement which can be made entirely at equilibrium, without possible nonequilibrium complications as might be encountered in relaxation of macroscopic concentration gradients. Lastly, in contrast to most other (i.e., phenomenological) approaches, light scattering experiments can be designed so that the equilibrium partitioning coefficient<sup>48-59</sup> of solute between unbounded solution and pore space does not have to be known. This coefficient, just as the diffusion behavior, depends on the nature of the diffusant and the geometry of the pore space. The technique of dynamic light scattering has in fact been used to advantage in previous studies of Brownian motion in confined geometries, as was learned near the completion of my work. Heterodyne spectroscopy has been used to study the hindered diffusion of colloids between parallel glass plates;<sup>43,44</sup> and scattering from an evanescent wave has been used to investigate fundamental aspects of Brownian motion near a reflecting wall.<sup>45</sup>

Having outlined these potential advantages of dynamic light scattering in studying diffusion in porous materials, it is necessary to point out general obstacles to the application of this technique. Trivially, the diffusant must be relatively large: to scatter enough light, and to diffuse slowly enough. A more important obstacle follows. As mentioned above, the solvent was chosen to match the refractive index of the porous glass. Now

normally, if a porous material (e.g., with pores of a size suitable for studying hindered diffusion of polymers) is not index matched, it will scatter light very strongly--far more strongly than a dilute solution of polymer. This makes it next to impossible to extract the signal due to polymer diffusion, among other problems. If, however, the porous material is index matched, its scattering is greatly decreased, making it possible to extract the desired signal. Although this trick of index matching has commonly been used to make a polymer matrix invisible in studies of probe diffusion (e.g., see<sup>60</sup> for references to use of this trick), it apparently has never before been used for studying diffusion in a rigid macroporous material. The initial idea for these experiments sprang from the realization that, at least in principle, this index matching trick should work for a rigid macroporous matrix, as well as for concentrated polymer solutions or polymer gels.

Starting with this simple idea, the initial research objective was to see if such experiments were feasible; and, if so, to investigate the diffusion of flexible polymers in porous glasses. Although the general feasibility was quickly demonstrated, it was obvious that a number of experimental improvements would be required in order to make accurate measurements. Therefore, early work focused on improving the light scattering apparatus, finding more suitable porous materials, eliminating polymer adsorption on porous glass, and developing satisfactory data analysis methods. As work on these improvements proceeded, it became possible to formulate more specific scientific objectives. An initial goal was to examine the dependence of results on scattering wavevector--the inverse of the wavevector roughly corresponds to the distance over which diffusion is being examined. This

wavevector dependence was found to be complicated; however, at low wavevector, corresponding to diffusion over large distances, a limiting "macroscopic" diffusion behavior was found.

This discovery led to the primary objective of this dissertation: to examine and try to understand the dependence of the macroscopic diffusion coefficient on parameters characterizing the polymers and porous materials which were used. All experiments were with linear polymers, so the primary polymer variable was the molecular weight. Experiments were performed with three porous glasses, each with a different porosity and pore size. Secondary objectives were pursued to a lesser extent; for example, to see whether or not the glasses have fractal pore spaces, and to examine limiting early and long time diffusive behaviors.

With regard to the above primary objective, the results reported in this dissertation argue that the diffusion of flexible polymers in random porous materials is in no way unusual. The results can be understood in light of a combination of existing theories: phenomenological theories for macroscopic diffusion of point particles in random porous materials;<sup>1-3,61-70</sup> and microscopic theories for diffusion of rigid Brownian particles and of flexible polymers in pores of comparable size.<sup>4-12</sup> The former theories incorporate the effects of random structure; the latter incorporate hydrodynamic polymer-wall interactions. In terms of intra-chain hydrodynamics, a transition is seen from essentially hard sphere, non-free draining behavior at low molecular weight, to free draining behavior at high molecular weight, as predicted by scaling theories.<sup>10-12</sup> With regard to the secondary objectives, the glasses used here do not appear to have fractal pore spaces; but

experimental difficulties preclude significant conclusions about limiting diffusive behavior at short and long times. As an unanticipated result, it has proved possible to obtain values of a fundamental material parameter of the porous glasses. This parameter, which is variously known as the tortuosity or intrinsic conductivity or formation factor,<sup>1-3,61-68</sup> is related to transport (e.g., diffusion or conduction) of point particles in porous materials.

The remainder of this chapter describes the content of this dissertation.

Chapter II presents selected theoretical and experimental background material on partitioning and diffusion in porous materials. Results that are directly related to the work of this dissertation are emphasized. The presentation anticipates, and is thus tailored to understanding, my results. In outline, Chapter II includes discussion of theories on the equilibrium partitioning of flexible and rigid polymers between a bulk solution and pore space, microscopic theories for the diffusion of a flexible or rigid polymers in geometrically simple pores of comparable size, macroscopic theories for the diffusion of point particles in porous materials, and previous experimental results for diffusion of polymers in porous materials.

The rationale underlying the presentation of Chapter II is as follows. As mentioned above, the primary objective of this dissertation is to understand the molecular weight dependence of the macroscopic diffusion coefficient of flexible polymers in random porous materials. This requires making connections between historically and philosophically different approaches to diffusion in porous materials. On the one hand, a number of theories have been developed which take into account hydrodynamic inter-

actions, between a polymer and pore walls, and between different segments on the same polymer, for the diffusion of rigid and flexible polymers in geometrically simple and comparably sized pores. Although these theories are not expected to be directly applicable to diffusion in "random" pore spaces, they nonetheless provide the essential physics needed to understand the hydrodynamic interactions. On the other hand, a number of theories have been developed dealing with macroscopic diffusion in all sorts of more complicated porous materials: for example, networks of cylindrical pores; solid spheres, disks, or rods randomly embedded in space; and fractal pore networks. Invariably, however, the diffusant in these theories is implicitly assumed to be negligibly small; that is, hydrodynamic interactions are not considered. In Chapter II, these two classes of theories are first presented independently. A heuristic synthesis of these theories is then attempted, in order to modify the theories for macroscopic diffusion of point particles in random porous materials to take into account the effects due to tangibly finite diffusant size, not only hydrodynamic interactions, but also partitioning effects.

Throughout the presentation of Chapter II, the connection between theory and experiment is emphasized. Generally, diffusion measurements in porous materials yield some effective diffusion coefficient, which is shown to be related to the experimental method which is used. Previous experimental results are reviewed critically and in sufficient detail to allow substantive comparison to my results, although the actual comparison is deferred to Chapter VII. The theoretical framework of Chapter II is also used to point out errors which have been made in interpreting effective diffusion coef-

ficients, such errors arising from neglect of the effects of finite size, such as partitioning and hydrodynamic interactions, or from improper understanding of the phenomenology of diffusion in porous materials.

Chapter III presents those aspects of the theory of dynamic light scattering which are relevant to my experiments, introduces the notation which is used in this dissertation, and establishes the connection between light scattering theory and the theory for diffusion in porous materials as presented Chapter II. In these experiments, the intensity autocorrelation function is measured; the relation of this function to the scattered electric field autocorrelation function, which is also known as the dynamic structure factor, is shown. Alternative ways to view light scattering, as scattering either from individual molecules or from fluctuations in a dielectric continuum, are compared. Subsequently, the connection between the dynamic structure factor and Brownian motion is established. Since dynamic light scattering measurements are made in Fourier space, but Brownian motion is usually considered in real space, understanding this connection aids in understanding, at least qualitatively, how the wavevector dependence of the dynamic structure factor is related to Brownian motion and diffusion. The connection of dynamic light scattering to the phenomenology of diffusion is then considered, starting with diffusion in unbounded solution, then turning to diffusion in porous materials. Of prime importance is establishing the nature of the effective diffusion coefficient which is measured using dynamic light scattering. A few specialized aspects of dynamic light scattering theory, with direct bearing on these experiments, are also presented.

Chapter IV describes the materials--polymers, solvents, and porous glasses--which were used in the experiments, and the preparation of samples for light scattering. Molecular weights of the polymers are given, as are molecular weight-property relationships which are useful in planning experiments. General requirements for choosing a suitable solvent, and the properties of the solvent used (2-fluorotoluene), are given. Characteristics of the porous glasses are tabulated; however, since the measurement of those characteristics is not entirely straightforward, a substantial discussion is devoted to considering what qualitative and quantitative conclusions can be drawn about the actual structure of the porous glasses. Since surface treatment of porous glasses is important and necessary, in order to prevent undesired polymer adsorption, the testing of the efficacy of various treatments is discussed in detail sufficient to demonstrate that adsorption is negligible using the treatment which was chosen for actual use. Lastly, the section on sample preparation provides a few useful tips peculiar to these experiments.

Chapter V is devoted to details of experimental techniques and data analysis methods. The new light scattering apparatus which was constructed for these experiments is described. Experimental considerations peculiar to these dynamic light scattering experiments in porous materials are discussed: how to control the refractive index match, how to ensure operation in the heterodyne signal limit, and how to focus on a single fragment of porous glass. A number of technical problems with these experiments are also discussed from both theoretical and experimental standpoints: the mixing of local oscillator and scattered electric fields;

divergence of the incident beam within a porous material; and difficulty in accurately determining the baseline of the intensity autocorrelation function in these heterodyne experiments. These problems in turn strongly influence the approach which must be taken in order to analyze data properly. After a brief review of the numerous methods which have previously been used to analyze dynamic light scattering data, the methods which are used in this dissertation are presented, and their suitability is discussed.

Chapters VI and VII deal with the experimental results and discussion thereof. Chapter VI is restricted to a straightforward, mainly descriptive, exposition of certain general features which are largely independent of molecular weight and pore size, and to a consideration of the uncertainty in results which is imposed by experimental problems and the resultant difficulties in data analysis. The results on molecular weight dependence of the macroscopic diffusion coefficient, and further discussion of both general features and the molecular weight dependence, are deferred to Chapter VII.

Chapter VI starts with an overview of the experiments, that is, the range which was investigated of important parameters such as molecular weight, bulk solution diffusion coefficient, scattering angle, scattering wavevector, relative size of polymer hydrodynamic radius to pore radius, and relative size of pore radius to inverse wavevector. The wavevector dependence of the results is shown. Three regimes are identified, which show different wavevector dependence of both the effective diffusion coefficient and the deviation of the autocorrelation function from a single exponential. It is shown how data from the simpler of these regimes (at low wavevector),

where the effective diffusion coefficient is constant and the autocorrelation functions are single exponential, can be used to extract macroscopic diffusion coefficients. Chapter VI concludes with a discussion of the effects of experimental uncertainties and the choice of data analysis method on the values obtained for the effective diffusion coefficient and the deviation from single exponentiality. This includes consideration of the potential error in diffusion coefficients due to making measurements at only a single concentration and sample time, which is contrary to the preferred practice of extrapolating to zero concentration and zero sample time.

Chapter VII starts with a presentation of the principal experimental results of this dissertation, namely, the molecular weight dependence of the macroscopic diffusion coefficient of flexible polymers in three different porous glasses. These results are interpreted in light of the theories presented in Chapters II and III, and compared to previous experimental results; the implications of my results with regard to the structure of the porous glasses are also considered. (See the Abstract for a summary of all the principal conclusions.) The wavevector dependence is discussed further, focusing in particular on the transition to macroscopic diffusion behavior at low wavevector. Practical implications of the results, for example, with regard to peak broadening in size exclusion chromatography, are mentioned. Chapter VII concludes with a number of suggestions for the extension of the dynamic light scattering technique to other studies of polymer transport in porous media, and for the application of related techniques which could complement dynamic light scattering measurements on such systems.

## **CHAPTER II**

### **PARTITIONING AND DIFFUSION IN POROUS MATERIALS: THEORY AND BACKGROUND**

This chapter provides the background required to understand the experimental results of this dissertation. The first section reviews theories for the equilibrium partitioning of flexible and rigid polymers between a bulk solution and pore spaces; although perhaps not obvious, such equilibrium partitioning effects generally are intimately related to dynamics (e.g., diffusion) in porous materials. The second section reviews theories for the hindered diffusion of flexible polymers and hard spheres in comparably sized pores of simple geometry--between parallel walls, and in cylindrical tubes. This hindrance to diffusion arises from hydrodynamic interactions between the Brownian particle and the pore walls. The third section treats the general phenomenology of diffusion in porous materials, starting with consideration of appropriate macroscopic forms of Fick's law for diffusion of point particles in random porous materials, and ending with a discussion of modifications to such theories as required to account for the effects of finite diffusant size (i.e., equilibrium partitioning and hydrodynamic interactions). Throughout this section, the connection with experiment is emphasized. The fourth section presents miscellaneous diffusion theories of interest. The last section critically reviews previous related experimental work, to provide a basis for eventual comparison with my results.

### Equilibrium Partitioning of Polymers

The equilibrium partitioning coefficient  $K_D$  for a macromolecular solution in contact with a porous material<sup>48-59</sup> is defined as the ratio of polymer concentration inside the porous material  $c_p$  to the polymer concentration in the contacting bulk solution  $c_0$ :

$$K_D = c_p/c_0 \quad (2.1)$$

(Strictly,  $K_D$  is the ratio of activities, corresponding to the ratio of concentrations in the limit of dilute solution.) As discussed subsequently in this chapter, knowledge of some *macroscopic*  $K_D$  is often required in order to obtain a value for the effective diffusion coefficient inside a porous material; this is, however, not the case for the dynamic light scattering experiments of this dissertation. Despite this, partitioning effects are nonetheless manifested in diffusion coefficients<sup>33</sup> (e.g., from dynamic light scattering): first, due to *microscopic* partitioning between differently dimensioned regions of the pore space, which in turn determines the weighting of hydrodynamic interactions in the overall measured diffusion coefficient; and second, since microscopic partitioning in and of itself constitutes an energetic hindrance to diffusion. (These effects are absent only for perfectly monodisperse uniform pore systems.) Hence, theories for equilibrium partitioning of polymers in porous materials are presented here in order to be able later to examine the influence of partitioning on effective diffusion coefficients. These theories will also be used to justify the claim that, for the experimental systems examined in this dissertation, these effects are relatively negligible.

The partitioning coefficient can also be defined, using statistical thermodynamics, as a ratio of configurational integrals, that is, as a ratio of the partition function in the porous material to the partition function in unbounded solution:<sup>48-55</sup>

$$K_D = \frac{\int d\Omega_1 \exp[-\epsilon_{PM}(\Omega_1, \Omega_2)/kT]}{\int d\Omega_1 \exp[-\epsilon_0(\Omega_1)/kT]} \quad (2.2)$$

where  $\epsilon_{PM}$  and  $\epsilon_0$ , the energies in the porous material and unbounded solution, are functions of the coordinates (in general configuration space) of the macromolecules ( $\Omega_1$ ) and, for  $\epsilon_{PM}$ , also of the porous material ( $\Omega_2$ ). Here the limits of integration are to be chosen large enough such that the porous material can be considered homogeneous. These limits of integration can be defined either with regard to unit *void* volume or with regard to unit *total* volume (i.e., including the solid matrix); the latter partitioning coefficient is a factor of the porosity  $\Phi$  times the former. These correspond to different definitions of  $c_p$  in equation (2.1), either with respect to void volume or to total volume.

Simplifying assumptions, valid for particular cases, have been used by various workers to derive explicit expressions for  $K_D$  as a function of parameters characterizing the polymer and the porous material. All such expressions, even those which follow from very simple arguments, are ultimately derivable from equation (2.2). Historically, the interest in theories for  $K_D$  stems from a desire to understand the separation of all sorts of macromolecules in all sorts of porous materials using size exclusion chromatography (SEC), since, as has been well established, SEC is primarily

an equilibrium process, with peak positions determined by equilibrium partitioning.<sup>49,50</sup>

Returning to equation (2.2), it is usually assumed that  $\epsilon_0$  can be written as a sum of terms due to intramolecular and intermolecular interactions, and that  $\epsilon_{PM}$  is given likewise, with an additional term due to interactions between macromolecules and the porous material. The general coordinates  $\Omega_1$  of the macromolecule are its center of mass position, orientation, and conformation (i.e., internal degrees of freedom). In any case,  $K_D$  is determined by the excluded volume in this generalized coordinate space.<sup>49,50,53</sup> Many common situations allow for simplification, for example: intermolecular interactions can be neglected in very dilute solution; if the only interaction between polymer and porous material is that of "hard" repulsion (i.e.,  $\epsilon=\infty$  for overlapping configurations,  $\epsilon=0$  otherwise), then the Boltzmann factor for interaction between polymer and porous material is simply either 1 (allowed configurations) or 0 (disallowed); and for rigid particles there are no internal degrees of freedom, and for hard spheres the orientation also need not be considered.

Various results for partitioning of polymers in porous materials are now reviewed. All expressions for  $K_D$  are, unless otherwise noted, for dilute solutions and for concentration in the porous material defined with respect to void volume only.

The simplest case is for rigid spheres in uniform pores of ideal geometry,<sup>50</sup> where the sphere-wall potential is hard repulsive. Considering pores between infinite parallel plates ("slit-like" pores), infinitely long pores

of circular cross section ("cylindrical" pores), and spherical pores, the results can be summarized as:

$$K_D = \{1 - (R_S/x_p)\}^m = \{1 - \lambda_S\}^m \quad (2.3)$$

where  $R_S$  is the sphere radius and  $x_p$  is some pore dimension, and where  $\lambda_S = R_S/x_p$ . For slit-like pores,  $m=1$  and  $x_p$  is the slit half-width; for cylindrical pores,  $m=2$  and  $x_p$  is the pore radius; and for spherical cavities,  $m=3$  and  $x_p$  is the sphere radius. The expression for cylindrical pores was given long ago by Ferry.<sup>18</sup> For hard spheres,  $K_D$  can be seen simply as the ratio of the volume inside pores which is accessible to sphere centers, to the total pore volume.

Equation (2.3) can be alternatively expressed<sup>50</sup> as:

$$K_D = \{1 - (\sigma R_S/m)\}^m \quad (2.4)$$

Here the parameter  $\sigma$  is the ratio of pore surface area to pore volume; this is the inverse of what is commonly known as the "hydraulic radius".<sup>1,3</sup> This quantity  $\sigma$  can be experimentally measured for any porous material, regardless of how random, and can thus be used as a dimension to characterize both regular and random pore spaces. Giddings et al.<sup>50</sup> have pointed out that, since the loss of entropy for macromolecules confined to pores spaces is primarily a surface effect, the quantity  $\sigma$ , which is a measure of surface area per pore volume, is perhaps the most nearly "universal", hence useful, pore size parameter. Remaining results will be given either in terms of  $\sigma$  or more usual pore dimensions such as the radius.

Giddings et al.<sup>50</sup> have given the most complete treatment for the partitioning of rigid macromolecules in inert porous media. They have given results for spheres in slit-like pores, spherical pores, and infinite cylindrical pores with circular, elliptical, and rectangular cross sections; their results thus include equation (2.4). They also developed expressions for molecules with rotational symmetry (e.g., rods, capsules) in cylindrical pores. In recognition of the nature of most porous materials, they discussed ways to introduce non-uniformity and randomness: either by assuming a distribution of size and shape (of ideal uniform pores), or by creating more truly random models. For the partitioning of arbitrarily shaped rigid molecules in an isotropic network of randomly inserted plane surfaces, they obtained the simple result:

$$K_D = \exp(-\sigma L_p/2) \quad (2.5)$$

with  $L_p$ , the mean external length, being the average maximum lineal projection of the molecule on the plane surfaces. Similarly, for arbitrarily shaped rigid molecules in an isotropic network of randomly placed fibers, they obtained:

$$K_D = (1/\Phi) \exp(-h A_p) \quad (2.6)$$

where  $A_p$  is the average areal projection of the molecule on planes normal to fiber axes and  $h$  is the fiber concentration in length per volume; the factor  $(1/\Phi)$  accounts for finite fiber dimensions. This equation includes a result which had been obtained previously by others<sup>71,72</sup> for spheres (diameter  $D_s$ ) in a bed of fibers (diameter  $D_f$ ):

$$K_D = (1/\Phi) \exp\{-\pi h(D_S + D_F)^2/4\} \quad (2.7)$$

Calculations of the partitioning of flexible polymers in porous materials<sup>48,49,51-55</sup> are generally more involved than the above mentioned calculations for rigid molecules, because of the large number of internal coordinates, required to specify the configuration of a flexible polymer, which must be considered. Nonetheless, various limiting cases of interest have been rigorously treated. Obviously, results for the partitioning of flexible polymers are of more relevance to the work of this dissertation than results for partitioning of rigid molecules.

Casassa was first to treat the partitioning of linear flexible chains in uniform, ideal pores.<sup>48,49</sup> Results are given here in terms of the parameter  $\sigma$ --see following equation (2.4)--but these results could be cast in terms of more common geometrical parameters  $x_p$ --compare equations (2.3) and (2.4). For slit-like, cylindrical, and spherical pores respectively:

$$K_D = (8/\pi^2) \sum_{n(\text{odd})=1}^{\infty} (1/n^2) \exp\{-\langle R_G^2 \rangle \sigma^2 \pi^2 n^2/4\} \quad (2.8a)$$

$$K_D = 4 \sum_{n=1}^{\infty} (1/\beta_n^2) \exp\{-\langle R_G^2 \rangle \sigma^2 \beta_n^2/4\} \quad (2.8b)$$

$$K_D = (6/\pi^2) \sum_{n=1}^{\infty} (1/n^2) \exp\{-\langle R_G^2 \rangle \sigma^2 \pi^2 n^2/9\} \quad (2.8c)$$

where  $\langle R_G^2 \rangle$  is the mean square radius of gyration in unbounded solution and  $\beta_n$  are the roots of the Bessel function of the first kind of order zero,  $J_0(\beta)=0$ .

Casassa and Tagami extended these results to regular star branched mole-

cules (i.e., the Zimm-Stockmayer<sup>73</sup> model,  $f$  arms of equal length from a single branch point). Their results correspond to the physical situation of very dilute polymer solutions at the theta-temperature (Gaussian chain statistics), with polymer adsorption absent, and with no alteration of polymer-solvent interactions in the pores. The assumption of Gaussian chain statistics made possible the enumeration of allowed chain configurations using the diffusion equation with absorbing boundary conditions on the pore surfaces (actually, by analogy to heat conduction with the surface at zero temperature). They discussed the implications of their results for both static partitioning and size exclusion chromatography, in particular, what dimensionless parameters (incorporating the size and architecture of both polymer and pores) might best be used to correlate  $K_D$  values from such experiments.

Using the method of reflections, Gaylord and Lohse<sup>51,52</sup> have developed expressions for the configurational statistics of polymer chains confined by any number of orthogonal planes (e.g., single wall, parallel plates, rectangular cylinder or box). They claim that their results are applicable to *any* end to end distance distribution function, not just Gaussian, for an unbounded chain. Implicit assumptions are again that the polymer not interact with the walls, and that polymer-solvent interactions are unaltered in the pores. In practice, there can be difficulties with convergence over some portions of the range of the relative size (i.e., polymer to pore) parameter using this method; nonetheless, their results in principle provide a means of enumerating chain statistics, hence calculating

$K_D$ , for polymers with excluded volume in ideal pores of rectangular geometry (this latter not a significant limitation).

Partitioning of flexible Gaussian chains in random porous media has been considered by Doi.<sup>53</sup> His model for a random porous medium is that of randomly embedded spheres of radius  $R_S$  at concentration  $c_S$  (number per total volume of porous material). For this model, the porosity is given as:

$$\Phi = \exp(-4\pi c_S R_S^3/3) \quad (2.9)$$

The following approximate result was obtained for  $K_D$ , given the assumptions of Gaussian chains, dilute solution, and no interaction with the porous material:

$$K_D = \exp\{-(4 \langle R_G^2 \rangle \sigma^2 / \pi)^{1/2} - (\langle R_G^2 \rangle \sigma^2 / 4\pi c_S R_S^3)\} \quad (2.10)$$

Doi has pointed out that both equations (2.8) and (2.10) approach:

$$K_D = 1 - \{4 \langle R_G^2 \rangle \sigma^2 / \pi\}^{1/2} \quad (2.11)$$

in the limit of small  $\langle R_G^2 \rangle \sigma^2$  and that both have the asymptotic form:

$$K_D \propto \exp\{-a_1 \langle R_G^2 \rangle \sigma^2\} \quad (2.12)$$

in the limit of large  $\langle R_G^2 \rangle \sigma^2$ . (These asymptotic behaviors had been previously noted by Casassa<sup>49</sup> for his results. N. B. Doi's equations<sup>46</sup> (39a), (39c), and (41) are in error--see Casassa for correct expressions.<sup>48,49</sup>) This led Doi to propose the following general form for partitioning of Gaussian chains in random media:

$$K_D = \exp\{-(4 \langle R_G^2 \rangle \sigma^2 / \pi)^{1/2} - a_2 \langle R_G^2 \rangle \sigma^2\} \quad (2.13)$$

with  $a_2$  some constant dependent on the shape of the pore space. (For example, for the randomly embedded sphere model,  $a_2 = 1/(4\pi c_s R_s^3) - 1/(-3 \ln \Phi)$ .)

The partitioning of strongly confined flexible polymers in good solvents, that is, with excluded volume, in ideal pore geometries has also been considered.<sup>54,55,58</sup> By strongly confined is meant that the polymer end to end distance in unbounded solution ( $R_F$ ) is much greater than the typical pore dimension ( $x_p$ ). Daoud and de Gennes<sup>54</sup> applied scaling arguments to obtain the following dilute solution result, for both slit-like and cylindrical pores:

$$K_D = a_3 \exp\{-a_4 \lambda_F^{5/3}\} = a_3 \exp\{-a_4 [\langle R_G^2 \rangle \sigma^2]^{5/6}\} \quad (2.14)$$

where  $\lambda_F \equiv R_F/x_p$  (here  $x_p$  is the slit half width or cylinder radius), and where  $a_4$  depends on the pore geometry (slit vs cylinder) and  $a_3$  depends weakly on  $\lambda_F$  in addition to the pore geometry. (Their result has also been rewritten here in terms of  $\langle R_G^2 \rangle \sigma^2$ .) This scaling prediction has recently been rigorously derived by Chen and Muthukumar.<sup>58</sup> Daoud and de Gennes<sup>54</sup> also discussed partitioning of flexible chains in semi-dilute solution, using the same scaling approach. Various regimes, in terms of the pore dimension, the chain end to end distance, and the correlation length were identified; extensions to these theories were later made by Brochard and de Gennes<sup>56</sup> (concentrated solutions and melts in pores), and by Turban<sup>57</sup> (cross-over from slit-like to capillary pore). As this dissertation is concerned with diffusion in dilute solution, the results for semi-dilute and concentrated solutions, although interesting, are not discussed here.

Comparison of equations (2.12) and (2.14), for the behavior of  $K_D$  in the limit of large  $\langle R_G^2 \rangle \sigma^2$  (i.e., large  $\lambda_F$ ) for linear Gaussian chains (theta-solvent) and linear chains with excluded volume (good solvent), indicates the general result:

$$K_D \propto \exp(-a_5 \lambda_F^{1/v}) \propto \exp(-a_5 [\langle R_G^2 \rangle \sigma^2]^{1/2v}) \quad (2.15)$$

where  $a_5$  is dependent on the structure of the porous material and  $v$  is the exponent in the dependence of the end to end distance  $R_F$  on the degree of polymerization  $N$ :

$$\langle R_F^2 \rangle \propto N^{2v} \quad (2.16)$$

(For linear polymers,  $\langle R_G^2 \rangle$  should have nearly the same dependence.) In a theta-solvent,  $v = 1/2$ ; in a good solvent,  $v \approx 3/5$ . Perhaps this observation could also be extended to polymers in good solvents strongly confined in fractal pore spaces,<sup>59</sup> with  $v = 3/(d_F + d_w) \geq 3/5$ , where  $d_F$  is the fractal exponent of the pore space and  $d_w$  is the fractal exponent for a particle diffusing in that pore space,  $\langle R(t)^2 \rangle \propto t^{2d_w}$ .

Partitioning of spheres in cylindrical pores, with inclusion of Coulombic and van der Waals interactions, has been considered by Malone and Anderson.<sup>7,28</sup> As discussed in the next section, continuum mechanics approaches to transport of spheres in porous materials have often been formulated including some general interaction potential; but when actually evaluated, the potential has usually been simply hard repulsive.

A few comments from a practical or experimental viewpoint are in order. Many experiments (e.g., those of this dissertation) are in good

solvents and in porous materials with pores of irregular geometry. The only expression for good solvents--equation (2.14)--lacks numerical factors and is only valid for strongly confined chains. In fact, for strongly confined chains,  $K_D$  is on the order of 0.01 or less, so there is very little polymer in the pores; and if, in order to increase the concentration in the pores, the concentration in the surrounding solution is raised to where the static correlation length is less than the pore size, then  $K_D$  is no longer even given by these dilute solution theories.<sup>54-56</sup> Dilute solution experiments that depend upon polymer for "signal" (e.g., light scattering) thus may in practice be restricted to smaller relative sizes (i.e.,  $\langle R_G^2 \rangle \sigma^2$  or  $\lambda_F$ ) where this scaling theory does not apply.

Experimental results<sup>16,74</sup> for polystyrene in good solvents in controlled pore glasses can be used to provide an estimate of  $K_D$  at smaller relative size. These results are in reasonable agreement with the theories for Gaussian chains (e.g., Casassa and Doi), using as a relative size parameter the radius of gyration (theory, for Gaussian chains; and experiment, for chains in a good solvent) divided by the hydraulic radius  $\sigma^{-1}$ . This indicates that from a practical standpoint the theories of Casassa<sup>48,49</sup> and Doi<sup>53</sup> can be used to estimate  $K_D$ , even for chains in good solvents, at these smaller values of  $\langle R_G^2 \rangle \sigma^2$ . It is reasonable to expect that these theories for Gaussian chains provide a lower limit for chains in a good solvent, when both chains have equivalent  $R_G$ , based on the observation (see equation (2.15)) that  $K_D$  for Gaussian chains shows a stronger asymptotic dependence on  $\langle R_G^2 \rangle \sigma^2$  at high  $\langle R_G^2 \rangle \sigma^2$  than does  $K_D$  for chains in a good solvent (i.e., a similarly stronger dependence is expected at lower  $\langle R_G^2 \rangle \sigma^2$  for Gaussian chains).

Some of these theoretical results have been plotted in Figure 1. This plot will be used subsequently to estimate  $K_D$  for our experiments. The results have been plotted in terms of the relative size parameter  $\lambda_H \equiv R_H/R_p$ , where *for good solvents*  $R_H$  can be related to  $R_G$  as given by equation (2.20a), and where  $R_p = 2\sigma^{-1}$  is the pore radius as would be obtained by mercury intrusion porosimetry (see Chapter IV, section 2). Note that all the Gaussian chain curves nearly superimpose for  $\lambda_H < 0.1$ ; that  $K_D$  is nearly zero for  $\lambda_H > 0.7$  for all geometries; and that a flexible chain has a lower  $K_D$  than a hard sphere with radius equal to the radius of gyration.

### Diffusion in Single Pores of Simple Geometry

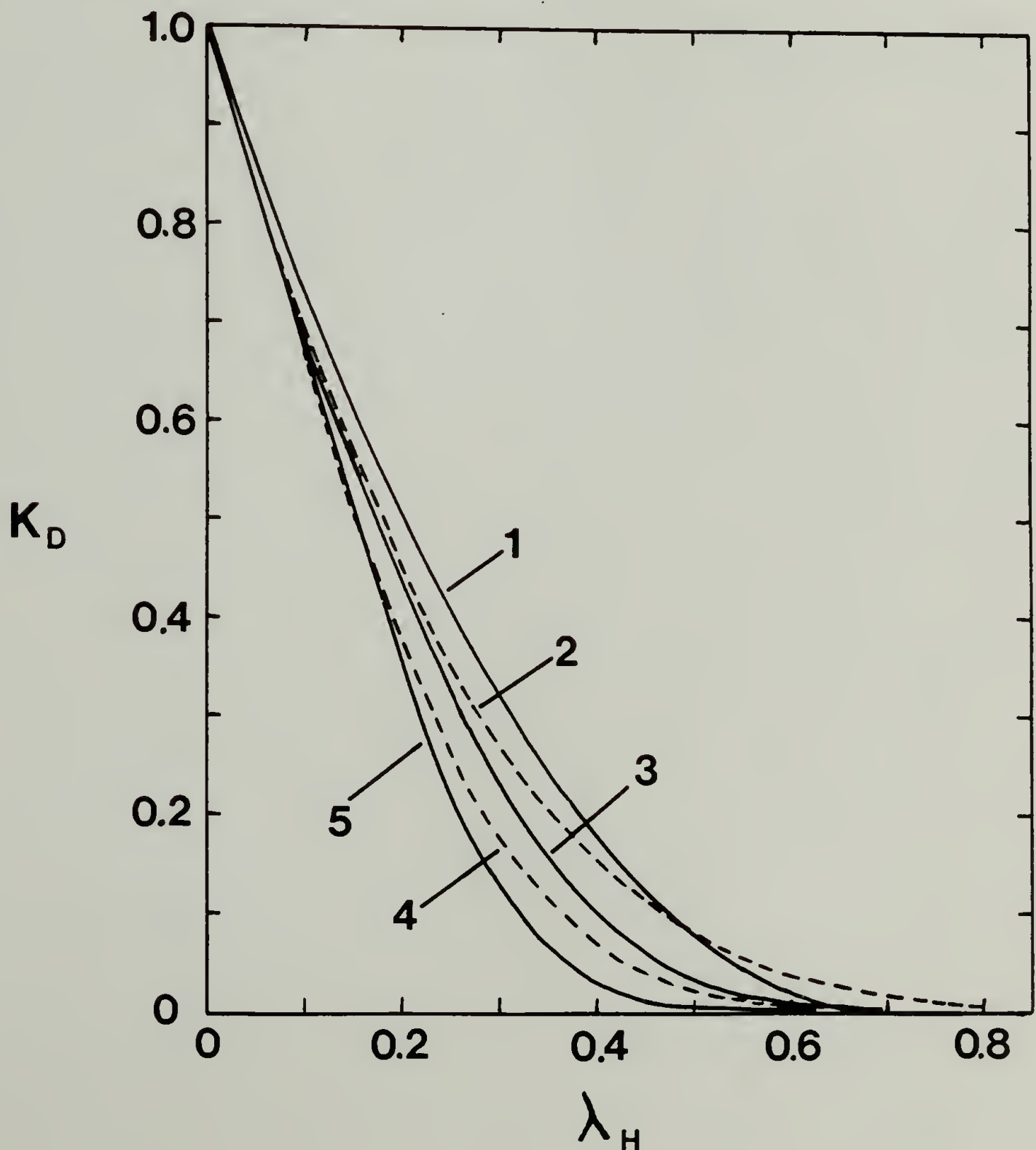
As part of the attempt to understand the convective and diffusive transport of solutes through porous materials (especially membranes), a number of workers have considered the transport of solute through a single pore of simple geometry, in particular, through a cylindrical pore with circular cross section.<sup>5-12,22,28,75</sup> These models are reviewed here, with the presentation being simplified by the consideration of diffusion alone (i.e., in the absence of convection) as corresponds to the phenomenon being examined in our experiments, namely, the Brownian motion of polymers in a quiescent fluid inside pores. The original references can be consulted for the results for the more general case of both diffusion and convection.

The models to be discussed here are all concerned with the situation where a neutrally buoyant diffusing particle, either hard sphere or flexible polymer, is of a size comparable to that of the pore but much larger than that of the solvent molecules, yet still small enough to undergo

Figure 1.

Equilibrium partitioning coefficient  $K_D$  vs relative size parameter  $\lambda_H$ .

The parameter  $\lambda_H \equiv R_H/R_p$  can be related to  $R_G \cong 1.45 R_H$  and  $\sigma = 2/R_p$ , with  $R_p$  the nominal pore radius from mercury intrusion porosimetry. Casassa's results for Gaussian chains in cylindrical (curve 3, equation (2.8b)) and slit-like (curve 5, equation (2.8a)) pores are plotted, as are Doi's results for Gaussian chains in a randomly embedded sphere porous medium (equations (2.10) and (2.9)) with porosity  $\Phi = 0.46$  (curve 2) and  $\Phi = 0.72$  (curve 4). Also shown is the result for a hard sphere ( $R_S = R_G$ ) in a cylindrical pore (equation (2.4), with  $m=2$ ).



Brownian motion. In addition to the equilibrium partitioning effects discussed in the preceding section, the dynamics of the polymer are significantly affected by the proximity of the pore walls. For this situation, the dynamics can be treated in terms of the hydrodynamics of a particle immersed in a fluid continuum which is bounded by the pore walls. The interaction potential between the diffusing particle and the pore walls also affects the dynamics insofar as it affects the configurational distribution (i.e., of position, orientation, and conformation) of the particles in the pore.

The various approaches to this problem can be grouped into two categories, based on the type of particle considered: either a hard sphere,<sup>5-9,28</sup> or a flexible polymer chain.<sup>10-12,75</sup> For either hard sphere or flexible polymer, the particle interacts hydrodynamically with the pore walls: this is manifested as increased drag. For a flexible polymer, one must also consider the intramolecular hydrodynamic interactions, which depend on the polymer conformation and which will thus be different for a polymer in a pore as compared to in unbounded solution. The questions of the suitability of hard sphere models for flexible polymers, and the general applicability of any of these models for diffusion in ideal cylindrical pores to the experimental situation of diffusion in random porous materials, are addressed later: the latter question, with regards to phenomenological theories for diffusion in porous materials (later this chapter); and both questions, with regard to my experimental results (Chapters VI and VII). It is also important to note that all of the following results are for axial diffusion only; and that partitioning effects *per se* are not included. For example, for diffusion across a membrane with cylindrical pores, or a

membrane merely modeled as such, the membrane diffusion coefficient is given as:<sup>7</sup>

$$D_M' = \Phi K_D D_{P, \parallel} \quad (2.17a)$$

or, more commonly (factoring out the porosity):

$$D_M = K_D D_{P, \parallel} \quad (2.17b)$$

where  $\Phi$  is the porosity,  $K_D$  the partitioning coefficient, and  $D_{P, \parallel}$  the averaged axial diffusion coefficient inside the pores. It is the quantity  $D_{P, \parallel}$ , which is related to the axial mobility of the Brownian particle by the Einstein relation,<sup>7,8</sup> that is considered here. It should be noted that for a Brownian particle in a confined space, the diffusivity will generally be anisotropic due to hydrodynamic and nonhydrodynamic interactions with the walls; hence the diffusion coefficient will be a spatially dependent tensorial quantity.<sup>8,9</sup> In cylindrical geometries, it is the axial component  $D_{P, \parallel}$  of this tensor which has been calculated.

Results are given as ratios of  $D_{P, \parallel}$  to the diffusion coefficient in unbounded solution  $D_0$ ; or alternatively as the ratio of the friction coefficient in unbounded solution  $f_0$  to the appropriately averaged (see below) axial friction coefficient in the pores  $f_{P, \parallel}$ :

$$f(\lambda) = (D_{P, \parallel} / D_0) = (f_0 / f_{P, \parallel}) \quad (2.18)$$

where  $f$  is the shorthand notation for this ratio. This ratio is expressed as a function of some appropriate ratio  $\lambda$  of particle size to pore radius. For a hard sphere of radius  $R_S$ , one has:

$$\lambda_S = R_S/R_P \quad (2.19a)$$

For flexible polymers, one has:

$$\lambda_H = R_H/R_P \quad (2.19b)$$

$$\lambda_G = R_G/R_P \quad (2.19c)$$

$$\lambda_F = R_F/R_P \quad (2.19d)$$

where  $R_H$ ,  $R_G$ , and  $R_F$  are chain dimensions in unbounded solution--the hydrodynamic radius, the root mean square radius of gyration, and the root mean square end to end distance (the Flory radius). Only  $R_H$  and  $R_G$  have meaning for chains with other than linear topology (e.g., star or branched polymers). For linear polymers,

$$R_H \equiv k_1 R_G \quad (2.20a)$$

$$R_G \equiv k_2 R_F \quad (2.20b)$$

where  $k_1$  and  $k_2$  are numerical constants ( $k_2 = 1/6^{1/2}$ ; and, e.g.,  $k_1 = 1/1.45$  for polystyrene in the good solvent toluene<sup>77</sup>); hence an expression given as a function of one of the  $\lambda$ 's can be rewritten as a function of either of the others. In addition, there are relations for various branched polymer models:

$$R_H \equiv k_3 R_G \quad (2.20c)$$

where  $k_3$  depends on the topology.<sup>78</sup>

The determination of  $f(\lambda_S)$  for a sphere in a cylindrical pore involves evaluating the integral:<sup>6-9,28</sup>

$$f(\lambda_S) = \frac{D_{p, \parallel}}{D_0} = \frac{\int_0^{R_p} \{f_0/f_{p, \parallel}(\lambda_S, r)\} \exp \{-\epsilon(r)/kT\} r \, dr}{\int_0^{R_p} \exp \{-\epsilon(r)/kT\} r \, dr} \quad (2.21)$$

where  $r$  is the radial position of the sphere and  $\epsilon(r)$  is the cylindrically symmetric sphere-wall interaction potential. Results of low Reynolds number hydrodynamics,<sup>4</sup> at various levels of approximation, are used to give the integrand  $\{f_0/f_{p, \parallel}(\lambda_S, r)\}$ . Of course,  $f_0 = 6\pi\eta_S R_S$ .

The simplest cases are for a "hard sphere" repulsive potential,

$$\epsilon(r) = 0, \quad \beta \leq 1 - \lambda_S \quad (2.22a)$$

$$\epsilon(r) = \infty, \quad \beta > 1 - \lambda_S \quad (2.22b)$$

where  $\beta \equiv r/R_p$  is the dimensionless radial position. Equation (2.21) then reduces to<sup>28</sup>

$$f(\lambda_S) = \frac{D_{p, \parallel}}{D_0} = \frac{2 \int_0^{1-\lambda_S} \{f_0/f_{p, \parallel}(\lambda_S, \beta)\} \beta \, d\beta}{(1 - \lambda_S)^2} \quad (2.23)$$

where  $(1 - \lambda_S)^2$  is the partitioning coefficient  $K_D$ .

The crudest approximation (the centerline approximation) is to assume:

$$f_{p, \parallel}(\lambda_S, \beta) = f_{p, \parallel}(\lambda_S, 0) \quad (2.24)$$

in which case equation (2.23) reduces to:

$$f_{CL}(\lambda_S) = (f_0/f_{p, \parallel}(\lambda_S, 0)) \quad (2.25)$$

where the subscript CL denotes centerline approximation. Equation (2.25) was first applied to membrane transport by Renkin,<sup>22</sup> who used Faxén's result<sup>143</sup> for the drag on a sphere moving along the centerline of a cylinder filled with stagnant fluid, a problem which has no analytic solution. Since then, workers have improved on the numerical calculation of the centerline friction,<sup>80</sup> culminating in the work of Paine and Scherr,<sup>81</sup> who have tabulated  $(f_{p, \parallel}(\lambda_S, 0)/f_0)$  for  $\lambda_S$  up to 0.90. An analytical expression due to Bohlin,<sup>82</sup> which extended Faxén's result to higher order, and which is useful for  $0 < \lambda_S \leq 0.6$ , is:

$$\begin{aligned} f_{CL}(\lambda_S) = & 1 - 2.10444 \lambda_S + 2.08877 \lambda_S^3 - 0.94813 \lambda_S^5 \\ & - 1.372 \lambda_S^6 + 3.87 \lambda_S^8 - 4.19 \lambda_S^{10} + \dots \end{aligned} \quad (2.26)$$

A more precise result to still higher order, due to Haberman and Sayre,<sup>83</sup> is:

$$f_{CL}(\lambda_S) = \frac{1 - 2.1050 \lambda_S + 2.0865 \lambda_S^5 + 0.72603 \lambda_S^6}{1 - 0.75857 \lambda_S^5} \quad (2.27)$$

The Renkin equation, which is equation (2.26) or one of its numerical variants multiplied by the steric partitioning factor  $(1 - \lambda_S)^2$ , has been much applied to diffusion across membranes.<sup>24,81</sup> Reviews of the development of the centerline approximation have been given by Bean,<sup>5</sup> Happel and Brenner,<sup>4</sup> and by Paine and Scherr.<sup>81</sup>

No matter how precise the calculation of the centerline friction  $f_{p,\parallel}(\lambda_S, 0)$ , equation (2.25) is expected to be a good approximation only if the position of the sphere is constrained to be on the axis ( $\beta = 0$ ), or if  $f_{p,\parallel}(\lambda_S, \beta)$  were to be nearly constant regardless of position  $\beta$ . Although the former condition would be realized for a strongly confining potential (e.g.,  $\epsilon(r) = 0$  for  $\beta = 0$  and  $\epsilon(r) = \infty$  for  $\beta > 0$ ), in most situations of interest, for example, the potential given by equation (2.22), this is not the case. The results of low Reynolds number hydrodynamics indicate that the latter condition is certainly not true. Famularo<sup>84</sup> has calculated the leading term (hence, his results are valid for  $\lambda_S \ll 1 - \beta$ ) in  $f_{p,\parallel}(\lambda_S, \beta)$  as a function of  $\beta$ . For  $\beta \leq 0.6$ , the coefficient is relatively constant ( $\approx 2$ ), but as  $\beta$  approaches one, the coefficient increases sharply, reflecting the increased drag near the wall. Therefore the centerline approximation underestimates the average friction factor and hence the hindrance to diffusion.

More precise calculation of the hindrance to diffusion  $f(\lambda_S)$  requires evaluation of the integral given by equation (2.23), properly taking into account the radial dependence of  $f_{p,\parallel}(\lambda_S, \beta)$ . Unfortunately this is only possible for  $\lambda_S \ll 1$ , given the hydrodynamics results currently available. Two locally valid solutions for axial motion of spheres in cylinders are for:

$$1 - \beta \gg \lambda_S \quad (2.28a)$$

$$1 - \beta = O(\lambda_S) \quad (2.28b)$$

Equation (2.28a) corresponds to a sphere relatively far from the wall; in this core region, the method of reflections<sup>4</sup> can be used to give  $f_{p,\parallel}(\lambda_S, \beta)$ .

Equation (2.28b) corresponds to a sphere close to the wall, where lubrication

theory<sup>4</sup> applies. If  $\lambda_S \ll 1$ , it is possible to asymptotically match these locally valid solutions to obtain a uniformly valid composite solution.

This was first done by Anderson and Quinn,<sup>6</sup> who applied the reflection method results of Famularo,<sup>84</sup> for motion in the core region of a cylinder, with the lubrication theory results of Goldman et al.,<sup>85</sup> for motion near a wall. Although Anderson and Quinn did not arrive at an analytical expression, the plot of their integration of equation (2.23) clearly showed significant reduction in  $f(\lambda_S)$  compared to the result using the centerline approximation. More recently, Brenner and Gajdos<sup>8,9</sup> have more carefully evaluated the integral (2.23), obtaining a result only slightly different than that of Anderson and Quinn:

$$f_{BG}(\lambda_S) = \frac{1 + (9/8)\lambda_S \ln \lambda_S - 1.539 \lambda_S + O(\lambda_S)}{(1 - \lambda_S)^2} \quad (2.29)$$

Based on the assumptions involved, it is emphasized that this expression is only expected to be valid for  $\lambda_S \ll 1$ , say for  $\lambda_S \leq 0.1$ . It is significant to note that this more exact result, as compared to the centerline result, has a term logarithmic in  $\lambda_S$ . (This term arises from  $f_{p,||}(\lambda_S, \beta)$  as  $\beta \rightarrow 1$ , that is, this logarithmic term arises from contributions of particles near the walls.) As an aside, to illustrate the significant effect of the walls on reducing diffusivity compared to unbounded solution, for  $\lambda_S = 0.01$ , corresponding to relative cross sectional area of sphere to tube of 0.01%, the diffusion coefficient is reduced by 5%.

Malone and Anderson<sup>7,28</sup> have discussed approximate approaches to extend equation (2.29) to the case of spheres electrostatically interacting

with the pore walls. Brenner and Gajdos<sup>8,9</sup> have discussed the general framework required to extend their work to nonspherical particles, more general boundary shapes, and other than "hard sphere" potentials. Although conceptually simple (i.e., integral formulations such as equation (2.23)), such extensions in general require substantial numerical effort and as yet unknown solutions to various problems in low Reynolds number hydrodynamics.

Turning to the diffusion of flexible polymers in slit-like and cylindrical pores, the picture is complicated due to the large number of conformations which a flexible polymer can assume. Equation (2.21) could be rewritten as:

$$\frac{D_{p,\parallel}}{D_0} = \frac{\iint \{f_0/f_{p,\parallel}(\Omega_1, \mathbf{r})\} \exp \{-\epsilon(\Omega_1, \mathbf{r})/kT\} d\mathbf{r} d\Omega_1}{\iint \exp \{-\epsilon(\Omega_1, \mathbf{r})/kT\} d\mathbf{r} d\Omega_1} \quad (2.30)$$

where  $\mathbf{r}$  is the position of the polymer center of mass and where the  $\Omega_1$  are the internal coordinates of the chain. The denominator is the usual partitioning coefficient  $K_D$ . General evaluation of these integrals is difficult.

Perhaps the simplest situation, which has been considered using scaling arguments, is that of a strongly confined chain dissolved in a good solvent.<sup>54,10-12</sup> The "strongly confined" condition has been given in these treatments as:

$$R_F > 2 R_p \quad (2.31)$$

where  $R_F$  is the root mean square end to end distance in unbounded solution and  $2R_p$  is the gap width (slit-like pores) or the diameter (cylindrical pores).

Cast in terms of equation (2.30), the scaling approach has been to calculate an averaged configuration of the confined polymer in terms of  $R_F$  and  $R_p$ , then to calculate the axial mobility (cylinders) or mobility parallel to the walls (slit) for that averaged polymer configuration. Hence the calculation of  $D_{p,\parallel}/D_0$  reduces to:

$$f(\lambda_F) = \frac{D_{p,\parallel}}{D_0} = \frac{f_0}{f_{p,\parallel}(R_F/R_p)} \quad (2.32)$$

where  $f_{p,\parallel}$  is the friction coefficient for the confined chain, expressed as a function of  $\lambda_F \equiv R_F/R_p$ .

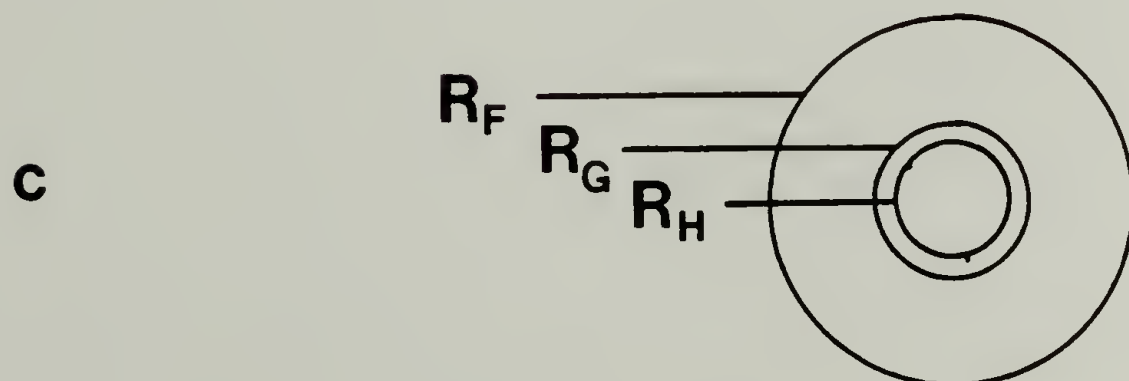
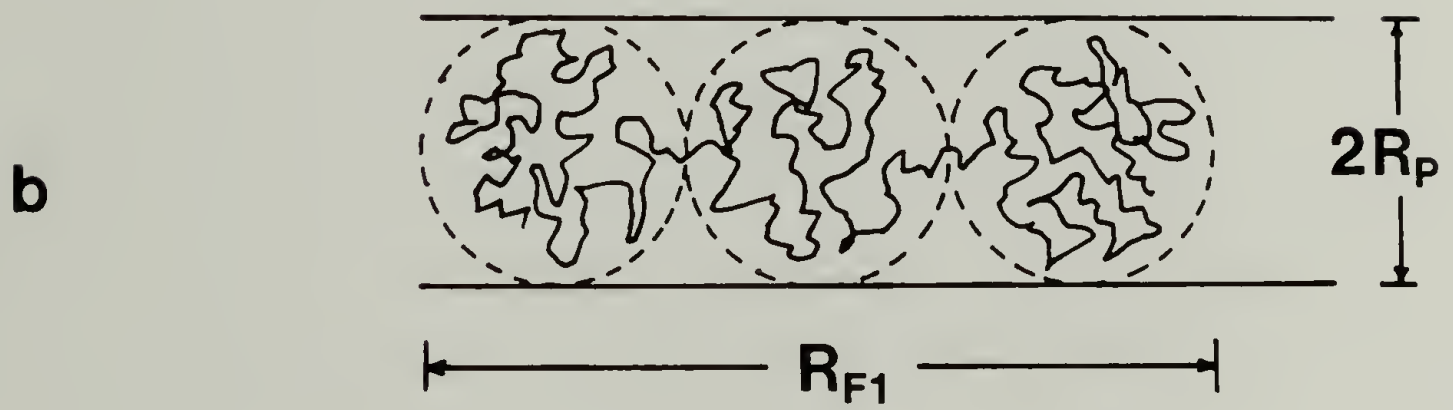
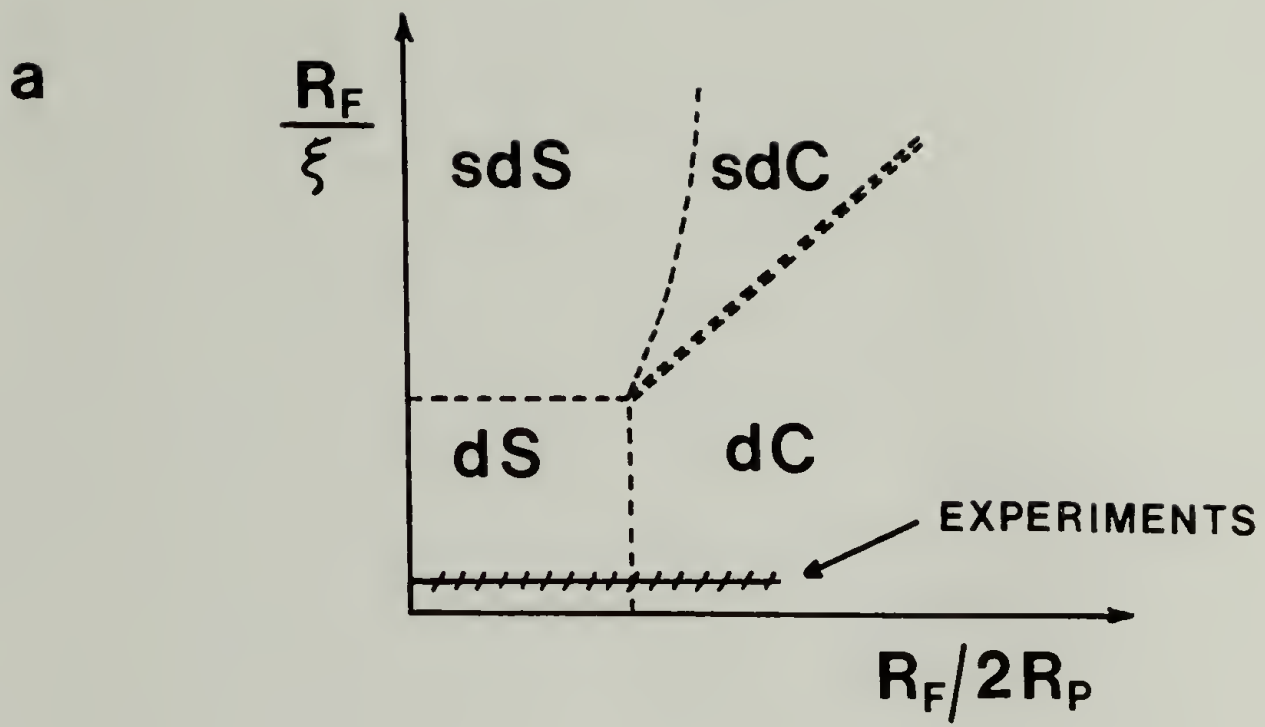
The statics of polymer chains in good solvents confined in slit-like and cylindrical pores has been treated by Daoud and de Gennes<sup>54,12</sup> using a scaling approach; this gives the averaged configuration in the pores. Different regimes are identified in Figure 2. Pursuant to the experiments of this dissertation, consideration is restricted here to the dilute 2-D (slit) and 1-D (cylinder) regimes. In a slit, a chain with  $N$  monomers becomes a "pancake" of thickness  $2R_p$  and (two dimensional) end to end distance  $R_{F2}$ ; likewise, in a cylinder, a "cigar" of diameter  $2R_p$  and (one dimensional) end to end distance  $R_{F1}$ . The confined chains are regarded as reduced dimensional self-avoiding walks with elementary units, not of monomers of size  $a$ , but of blobs of size  $2R_p$  each containing  $g$  monomers (Figure 2), where the blobs are strongly repulsive (i.e., self-avoiding). Inside each blob, the chain is a three dimensional self-avoiding walk (i.e., normal excluded volume):

$$2R_p = a g^{3/5} \quad (2.33)$$

Figure 2.

## Flexible polymers in pores.

- (a) Different regimes for polymer solutions in a cylindrical pore as a function of relative size parameters:  $(R_F/2R_p) \rightarrow$  ratio of bulk solution end to end distance to pore diameter;  $(R_F/\xi) \rightarrow$  ratio of bulk solution end to end distance to correlation length. This figure is taken from Ref. 54; a similar figure is shown there for slit-like pores. Regimes are denoted by the following codes: d  $\rightarrow$  dilute, sd  $\rightarrow$  semi-dilute; and S  $\rightarrow$  spherical conformation, C  $\rightarrow$  "cigar-like" conformation. The experiments of this dissertation are given by the hatched line, that is, the relative size parameter  $(R_F/2R_p)$  was varied while keeping the reduced concentration,  $c/c^*$ , approximately constant and dilute ( $c/c^* \approx 1/8$ ). The locations and sharpness of transitions are not known precisely.
- (b) Strongly confined chain in dilute solution in a cylindrical pore. (see text for description)
- (c) Different spherically averaged dimensions for an unconfined linear polymer in a good solvent. These are shown to scale, assuming  $R_G \approx 1.45 R_H$  and  $R_F \approx 6^{1/2} \cdot R_G$ . The radius of a hydrodynamically equivalent hard sphere is  $R_H$ , which is clearly smaller than the total domain pervaded by the coil.



Hence, for a chain in a slit ( $v_{2D} = 3/4$ ),

$$R_{F2} = 2R_p (N/g)^{3/4} \quad (2.34a)$$

and for a chain in a cylinder ( $v_{1D} = 1$ ),

$$R_{F1} = 2R_p (N/g) \quad (2.34b)$$

Equations (2.34a) and (2.34b) can be rewritten solely in terms of the pore size  $R_p$  and the three dimensional Flory radius  $R_F = a N^{3/5}$  as:

$$R_{F2} \cong 2R_p (R_F/2R_p)^{5/4} \quad (2.35a)$$

$$R_{F1} \cong 2R_p (R_F/2R_p)^{5/3} \quad (2.35b)$$

The dynamics of these strongly confined chains has been considered by Brochard and de Gennes,<sup>10-12</sup> again using a scaling approach. The same simple scaling result is obtained for the chain friction coefficient  $f_{p, \parallel}$ , for chains in *either* slit-like or cylindrical pores:

$$f_{p, \parallel} \propto 6 \pi \eta_s R_p (N/g) \quad (2.36)$$

This result for the overall chain friction is  $N/g$  times the friction coefficient for a single blob (of radius  $R_p$ ); that is, the blobs are hydrodynamically uncorrelated. The essential arguments underlying this result are that there are large fluctuations in the concentration (of order unity) over the size of a blob; and that the range of the Oseen tensor  $T_{nm}(\mathbf{r})$  ( $\mathbf{r} = \mathbf{r}_n - \mathbf{r}_m$ ) describing hydrodynamic interactions between the  $n^{\text{th}}$  and  $m^{\text{th}}$  monomers has a cutoff for distances greater than  $2R_p$ , due to the presence of the walls. For distances  $r < 2R_p$  (i.e., within a blob) one has the usual situation,  $T \propto 1/r$ , but

for larger distances  $r \gg 2R_p$ ,  $T(r)$  decreases more rapidly, approximately exponentially  $T \propto \exp(-\pi r/2R_p)$ . (This hydrodynamic screening has been explained,<sup>10-12</sup> using the method of reflections,<sup>4</sup> as due to the approximate cancellation, for distances  $r \gg 2R_p$ , of image disturbances.)

Using the Einstein relation, equation (2.36) can be used to write the diffusion coefficients  $D_{p,\parallel}$  for slit-like and cylindrical pores (using also the preceding static results):

$$D_{p,\parallel} = k_{\text{SLIT}} (kT/6\pi\eta_S)(2R_p/R_{F2})^{1/3} (1/R_{F2}) \quad (\text{slit}) \quad (2.37a)$$

$$D_{p,\parallel} = k_{\text{CYL}} (kT/6\pi\eta_S)(1/R_{F1}) \quad (\text{cylinder}) \quad (2.37b)$$

where  $k_{\text{SLIT}}$  and  $k_{\text{CYL}}$  are constants not given by the scaling analysis. More useful for our purposes, these results can also be written solely in terms of  $R_F$  and  $R_p$ , which gives the same result for slit-like and cylindrical pores:

$$D_{p,\parallel} = k_4 (kT/6\pi\eta_S) (2R_p/R_F)^{5/3} (1/2R_p) \quad (2.38)$$

or in terms of the ratio  $\lambda_F \equiv R_F/R_p$  as:

$$f_S(\lambda_F) = \frac{D_{p,\parallel}}{D_0} = k_5 (R_F/R_p)^{-2/3} = k_5 \lambda_F^{-2/3} \quad (2.39)$$

Although the constants  $k_4$  and  $k_5$ , which are not given by the scaling analysis, are expected to differ for slits versus tubes, it is important to note the identical functional dependence for  $D_{p,\parallel}/D_0$  on  $\lambda_F$ . Just as was the case for  $K_D$  for strongly confined chains,<sup>54</sup> only various constants are geometry dependent; this implies that measurements of  $K_D$  or  $D_{p,\parallel}$  might not provide

much information about pore space geometry. It is also remarked that explicit in the scaling analysis is the significant assumption that the pores are uniform or only gradually tapered.

The internal mode structure has also been predicted,<sup>10-11</sup> again following from the blob concept,<sup>54,12</sup> by equating the elastic free energy of deformation to the frictional force for these reduced dimensional self-avoiding chains of blobs. Several regimes, as given by the scattering wavevector  $q$  and the polymer dimensions, are of interest. (Implicitly,  $q$  is assumed parallel to  $R_{F2}$  or  $R_{F1}$ .)

- (1)  $qR_{F1} < 1$ ,  $qR_{F2} < 1$  : diffusion of the entire chain ( $D_{p, \parallel}$ )
- (2)  $qR_{F1} = 1$ ,  $qR_{F2} = 1$  : terminal relaxation time of confined chain ( $\tau_1$ )
- (3)  $qR_{F1} > 1$ ,  $qR_{F2} > 1$  : relaxation times of internal modes ( $\tau_q$ )
  - (a)  $2qR_p < 1$  : modes of reduced dimensional "blob chain"
  - (b)  $2qR_p > 1$  : modes of three-dimensional chain (i.e., inside a blob)

Simply citing the scaling results<sup>10,11</sup> (those for  $D_{p, \parallel}$  have already been given), one has:

$$(1/\tau_1) = k_6 (kT/6\pi\eta_S)(2R_p/R_{F2})^{1/3} (1/R_{F2})^3 \quad (\text{slit}) \quad (2.40a)$$

$$(R_{F2} = q^{-1})$$

$$(1/\tau_1) = k_7 (kT/6\pi\eta_S)(1/2R_p) (1/R_{F1})^2 \quad (\text{cylinder}) \quad (2.40b)$$

$$(R_{F1} = q^{-1})$$

$$(1/\tau_q) = k_8 (kT/6\pi\eta_S)(2R_p)^{1/3} q^{10/3} \quad (\text{slit}) \quad (2.40c)$$

$$(R_{F2} > q^{-1} > 2R_p)$$

$$(1/\tau_q) = k_9 (kT/6\pi\eta_S)(1/2R_p) q^2 \quad (\text{cylinder}) \quad (2.40d)$$

$$(R_{F1} > q^{-1} > 2R_p)$$

$$(1/\tau_q) = k_{10} (kT/6\pi\eta_S) q^3 \quad (\text{both}) \quad (2.40e)$$

$$(q^{-1} < 2R_p)$$

The amplitudes of these internal modes and other numerical prefactors are not given by the scaling analysis. Note that the relaxation frequencies associated with the slower internal modes are predicted to have different scaling behavior for the different geometries:  $q^{10/3}$  for slits, but  $q^2$  for cylinders. This stands in contrast to the geometry-independent scaling behavior for entire chain diffusion. It has been pointed out<sup>11</sup> that there is not a smooth crossover between diffusion and the internal modes at  $qR_{F1} = 1$  or  $qR_{F2} = 1$ , because the chain moves in the pores by a reptation-like process. Equation (2.40e) is the high frequency, short wavelength limit for Zimm chains<sup>12</sup> (i.e., chains in a good solvent with excluded volume).

To summarize the scaling results,<sup>54,10-12</sup> flexible polymers in good solvents strongly confined in pores statistically behave as two-dimensional (slit) or one-dimensional (cylinder) self-avoiding walks, if they are considered as chains of blobs with diameter equal to the pore dimension. Because of hydrodynamic screening by the pore walls, these strongly confined polymers dynamically behave *analogously* to Rouse chains, that is, the blob "monomer" units are hydrodynamically uncorrelated. The ratio  $D_{p,\parallel}/D_0$  is predicted to scale as  $\lambda_F^{-2/3} q^0$ , and the relaxation frequencies  $1/\tau_q$  of slower internal modes as  $q^{10/3}$  (slit) or  $q^2$  (cylinder); this latter  $q^2$  behavior is also *analogous* to the mode structure of Rouse chains.

Various extensions of these theories are mentioned for completeness. Kremer and Binder<sup>75</sup> have given a similar, but more detailed and thorough, treatment of confined Rouse chains (versus the results that have been given here for confined Zimm chains), including Monte Carlo simulations. Turban<sup>57</sup> has considered the statics of the crossover from slit to capillary, results that could be useful for understanding dynamics in intermediate geometries. The statics<sup>54,57</sup> and dynamics<sup>10-12</sup> of semi-dilute and concentrated solutions, even melts,<sup>56</sup> trapped in pores have also been considered using a scaling approach, as has the aspiration of chains into tapered pores.<sup>55,11,12</sup>

### **General Phenomenology of Diffusion in Porous Materials**

Although the phenomenology of diffusion and conduction in porous materials is for the most part relatively straightforward,<sup>1-3,65-68</sup> some confusion nonetheless exists in the literature. What follows is an attempt to briefly summarize the essentials of this phenomenology. Apology is made for lack of mathematical rigor, which has been sacrificed for the sake of emphasizing certain major points. This exposition is aimed at clearly distinguishing the different "effective diffusion coefficients" which are measured in different sorts of experiments, thereby laying the groundwork for establishing the connection between this phenomenology and dynamic light scattering measurements of polymer diffusion in porous materials.

The starting point is the description of particle diffusion on a microscopic level. For a point particle with a constant and spatially independent diffusivity  $D_0$  in the pores, one has:

$$\mathbf{J} = -D_0 \nabla c \quad (2.41a)$$

$$\nabla \cdot \mathbf{J} + \partial c / \partial t = 0 \quad (2.41b)$$

$$\partial c / \partial t = -D_0 \nabla^2 c \quad (2.41c)$$

$$\mathbf{J} \cdot \mathbf{n}_S = 0 \quad \text{on pore surfaces} \quad (2.41d)$$

where  $\mathbf{J}$  and  $c$  are the flux and concentration fields in the pore fluid and  $\mathbf{n}_S$  is the surface normal. These equations are, respectively, Fick's first law, the continuity equation, Fick's second law, and a no flux boundary condition (i.e., adsorption or reaction at the walls is absent). For the more general situation of a particle with a spatially dependent diffusivity in the pores  $\mathbf{D}_p$  (e.g., because of hydrodynamic interactions with the walls), and which interacts with external forces  $\mathbf{F}$ , represented by the potential  $\mathbf{F}/kT = -\nabla E$ , the flux is:<sup>8</sup>

$$\mathbf{J} = -\mathbf{D}_p \cdot (\nabla P + P \nabla E) = -e^{-E} \mathbf{D}_p \cdot \nabla (P e^E) \quad (2.42a)$$

where  $P = P(\mathbf{R}, t | \mathbf{R}', 0)$  is the probability density that a particle lies at  $\mathbf{R}$  at time  $t$  given a position  $\mathbf{R}'$  at time  $t=0$ . This more general case has been written in terms of  $P$ , as opposed to  $c$ , to emphasize the equivalence of these two commonly used approaches, either considering diffusion in a dilute solution (concentration  $c$ ) or the Brownian motion of a single particle (probability density  $P$ ). The corresponding continuity equation is:

$$\nabla \cdot \mathbf{J} + \partial P / \partial t = \delta(\mathbf{R} - \mathbf{R}') \delta(t) \quad (2.42b)$$

giving a Fick's second law type result:

$$\partial P / \partial t = \nabla \cdot [e^{-E} \mathbf{D}_p \cdot \nabla (P e^E)] + \delta(\mathbf{R} - \mathbf{R}') \delta(t) \quad (2.42c)$$

Assuming no adsorption, the no flux boundary condition (2.41d) again applies. This surface boundary condition, through which the structure of the possibly complex porous material enters into the microscopic description, is of course what presents general difficulties, both in solving these equations on a microscopic level and in establishing the relation between microscopic and macroscopic descriptions of diffusion. A spatially dependent diffusion coefficient makes this task even more difficult.

It is now assumed that it is possible to develop a phenomenological description for diffusion over large distances in the porous material (using macroscopic forms of Fick's laws) from this microscopic description of diffusion. Such an assumption is not always justified. Lehner has pointed out that this requires that diffusion must be approximately "quasi-steady" on a pore scale.<sup>68</sup> This can be expressed by the condition that the time associated with a change of the average concentration be much greater than the time required for diffusion across a pore,

$$|c_p/(\partial c_p/\partial t)| \gg (2R_p)^2/D_0 \quad (2.43)$$

where  $c_p$  is the average concentration at some point in a porous material with pore diameter  $2R_p$ . The implications of this condition with regard to the results of dynamic light scattering experiments are discussed in Chapter III. Suffice it to say at present, that it is believed that such a condition is indeed satisfied in our dynamic light scattering experiments *at low wavevector*. However, for transient diffusion experiments such as those discussed later in this chapter, large concentration gradients may exist, with associated rapid changes in average concentration at a given point, and such an assumption

may well *not* be valid. (An additional condition established by Lehner is that any interphase mass transfer, for example, adsorption or reaction with the pore walls, must either be absent or depend at most linearly on concentration.)

The development that follows is for diffusion of point particles (in a dilute solution) in a porous material.<sup>2,3,67,68</sup> The particular approach follows that of Lehner.<sup>68</sup> In what follows, fluxes and concentrations, with respect to the fluid alone, and with respect to the saturated porous medium (i.e., fluid phase plus solid matrix), will be denoted by subscripts P and PM respectively. These particles have a constant diffusivity  $D_0$ , both in bulk solution and in the pores, and are vanishingly small ( $K_D=1$ ) compared to the dimensions of the pore space. Adsorption is assumed absent. The porous material is characterized by a porosity  $\Phi$  and an "intrinsic conductivity"  $\mathbf{X}$ . The introduction of  $\mathbf{X}$  (a symmetric second rank tensor) in what follows is justified later, at which time different definitions of intrinsic conductivity and the related concept "tortuosity" will be discussed in an attempt to clarify their physical basis.

The macroscopic diffusive mass flux is most reasonably defined (particularly for random porous materials) per unit cross section of the entire porous material ( $\mathbf{J}_{PM}$ ). A macroscopic form of Fick's first law in a porous material can be written as:<sup>68</sup>

$$\mathbf{J}_{PM} = -\Phi D_0 \mathbf{X} \cdot \nabla c_P \quad (2.44)$$

where  $c_P$  ( $\langle c \rangle^f$  in Lehner's notation) is the average concentration (the intrinsic phase average over a representative elementary volume<sup>66-68</sup>) in the

fluid-filled pore space. The quantity  $\Phi \mathbf{X}$  which appears in equation (2.44) is defined by the linear vector transformation:<sup>7</sup>

$$\langle \nabla c \rangle_{PM} = \Phi \mathbf{X} \cdot \nabla c_p \quad (2.45)$$

where the left hand side of equation (2.45) is the phase average<sup>66-68</sup> of the microscopic concentration gradient  $\nabla c$  over the entire porous material.

Loosely, the porosity accounts for the reduction in driving force due to the presence of the solid matrix (essentially a concentration renormalization,  $c_{PM} = \Phi c_p$ ); whereas the intrinsic conductivity tensor relates (in an average sense) the microscopic and macroscopic lines of flux. The corresponding continuity equation is:<sup>68</sup>

$$\nabla \cdot \mathbf{J}_{PM} + \partial(\Phi c_p)/\partial t = 0 \quad (2.46a)$$

$$\nabla \cdot \mathbf{J}_{PM} + \Phi \partial c_p/\partial t = 0 \quad (2.46b)$$

The porosity enters as above, to renormalize the concentration; and equation (2.46b) follows from (2.46a) on the assumption that the porous medium is stationary. Combining equations (2.44) and (2.46b) gives a macroscopic Fick's second law:<sup>68</sup>

$$\partial c_p/\partial t = \nabla \cdot D_0 \mathbf{X} \cdot \nabla c_p \quad (2.47)$$

As can be seen, given the assumption of a macroscopically homogeneous and stationary porous medium, the porosity cancels.

Analogous developments could be carried out for electrical conduction and heat conduction in porous materials (where the matrix itself is

non-conducting). For example, the electrical conduction analog of equation (2.44), for a porous material filled with a conducting electrolyte solution, is:

$$i_{pM} = -\Phi \sigma_0 \mathbf{X} \cdot \nabla E_p \quad (2.48)$$

where  $i_{pM}$  is the current (per unit cross section of porous material),  $\sigma_0$  is the conductivity in bulk solution, and  $\nabla E_p$  is the electric potential gradient.

These equations can be cast in forms more directly analogous to Fick's laws, Ohm's law, etc. by introducing *effective* transport coefficients (subscript EFF), which are related to the transport coefficients in bulk solution (subscript 0). For example, the effective diffusion coefficient  $D_{EFF}$  from equation (2.44) is (writing  $D_{EFF}$  and  $\mathbf{X}$  as a scalars for simplicity):

$$D_{EFF} = \Phi X D_0 \quad (2.49)$$

whereas that from equation (2.47) is:

$$D_{EFF} = X D_0 \quad (2.50)$$

Similarly, the effective conductivity from equation (2.48) is:

$$\sigma_{EFF} = \Phi X \sigma_0 \quad (2.51)$$

which is the analog of equation (2.49).

An important distinction should be obvious, namely, that effective transport coefficients from flux laws (e.g., Fick's first law, Ohm's law) are related to the bulk transport coefficients by the proportionality constant  $\Phi X$ ; whereas effective transport coefficients from the related second order partial differential equations (e.g., Fick's second law) are instead related to

the bulk transport coefficients by a different constant  $X$ . (Properly, as shown in the original development of equations (2.44) to (2.47), these are not constants but tensors.<sup>2,68</sup>)

Different measurements will thus yield effective transport coefficients which are related to bulk transport coefficients in different ways. Experiments that measure flux directly--for example, the current flow through a porous material saturated with electrolyte solution, or the diffusive flux of a radioactively labeled species across a membrane separating two solutions of equal concentration (and other "steady state" diffusion experiments)--give one type of effective transport coefficient (factor  $\Phi X$ ). Experiments where the effective transport coefficient is obtained by using a second order partial differential equation (e.g., Fick's second law) to relate the measured rate of change of some transported quantity (e.g.,  $\partial c/\partial t$ ) to the driving force (e.g.,  $\nabla c$ ) yield a second type of effective transport coefficient (factor  $X$ ). This distinction should be borne in mind when interpreting experimental results. In Chapter III (section 2) it will be shown that dynamic light scattering and forced Rayleigh scattering experiments yield an effective diffusion coefficient as given by equation (2.50).

It is also important to point out a further distinction. Many experiments aimed at looking at diffusion in porous materials--for example, the transient diffusion experiments discussed later in this chapter--would seem to fall into the second category above, insofar as effective diffusion coefficients are obtained from measurements of  $\partial c/\partial t$  (i.e., in reservoirs of bulk solution) and solution of Fick's second law with appropriate boundary

conditions. *However, these boundary conditions essentially require that one know the flux  $J_{PM}$  (i.e., equation (2.44)) at one or more surfaces.* Hence, even in these experiments, the porosity  $\Phi$  enters into the phenomenological description. This requirement of knowing the flux also leads to further complications when the effects of finite size and hindered diffusion are considered.

Essentially, the measurement itself must be made directly within the porous material to be able to obtain the "simpler" effective diffusion coefficient given by equation (2.50). A related but different point is that, in order to avoid having an admixture of the bulk diffusion coefficient and the diffusion coefficient given by equation (2.50), one must perform measurements of this type entirely within a single piece of the porous material.

In the preceding development, a quantity  $X$ , called the intrinsic conductivity, was introduced. Before proceeding further, it is worthwhile to examine in some detail this useful but perhaps somewhat muddy concept. As is evident, for example, from equations (2.49) and (2.50), this quantity is in some way reflected in effective transport coefficients, regardless of how measured.

This discussion starts with consideration of what is called the "formation factor"<sup>2,3</sup>  $F$  of a porous material, defined as the ratio of the resistivity of the porous material saturated with an electrolyte solution ( $\rho_{EFF}$ ) to the resistivity in bulk of that same solution ( $\rho_0$ ):

$$F \equiv \rho_{EFF}/\rho_0 = \sigma_0/\sigma_{EFF} \quad (2.52)$$

Here  $F$  has been written equivalently in terms of the bulk and effective conductivities,  $\sigma_0$  and  $\sigma_{\text{EFF}}$ . The formation factor has long been used in petroleum reservoir engineering to characterize porous rock strata. It is a "fundamental" property of a porous material insofar as it is *unambiguously defined* by equation (2.52) and as it can be *measured straightforwardly*, at least in principle. It can be seen that it is basically a measure of how difficult it is for transport to occur between two widely separated points, and as such, it must be related in some way to a number of characteristics of the pore space, for example, the porosity. Problems and ambiguities arise in trying to define these relationships.<sup>2,3</sup> Indeed, much of understanding transport of small particles in porous materials reduces to understanding how this formation factor is related to the structure of the porous material. A comparison of equation (2.52) and (2.51) gives:

$$F = 1/\Phi X \quad (2.53)$$

as the relation between the formation factor, porosity, and intrinsic conductivity.

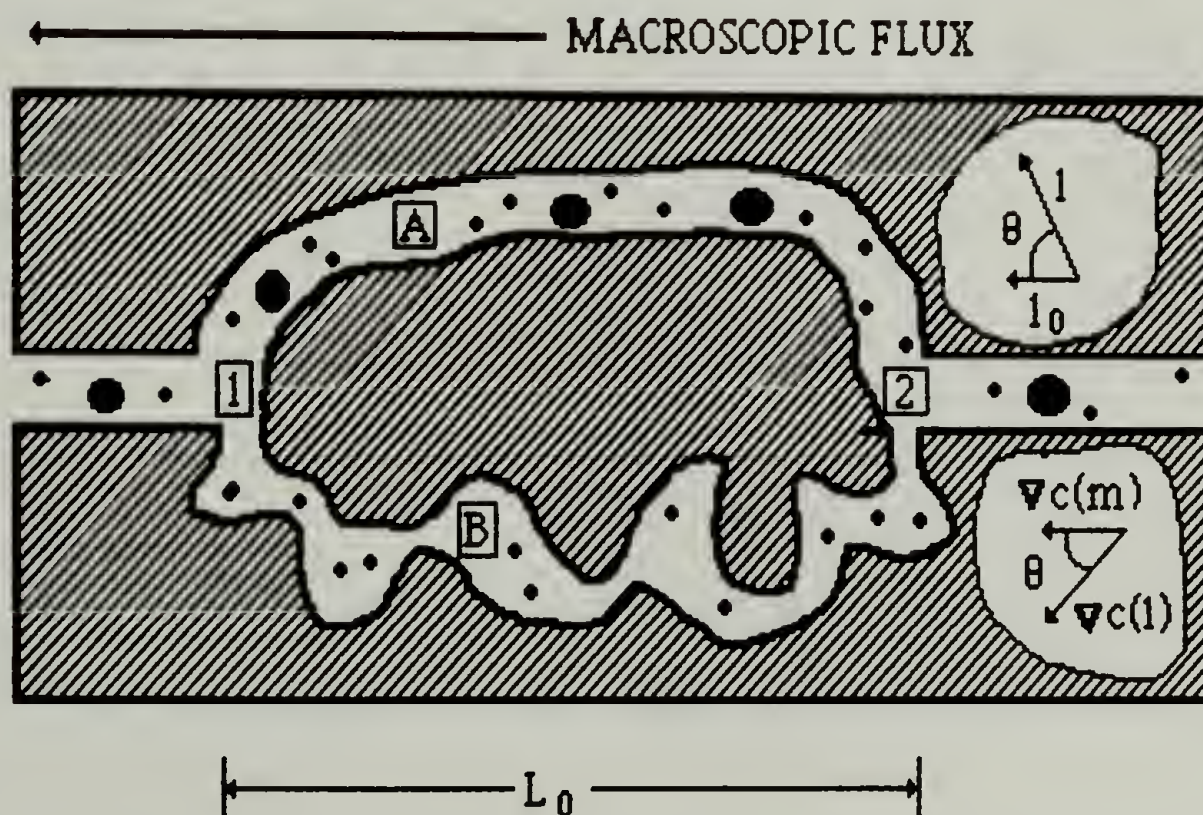
Some idea of the physical significance of the intrinsic conductivity  $X$  can be gained by considering the "tortuosity"<sup>2,3,62,63,65</sup>  $T$ , which is essentially the inverse of  $X$ . An intuitive definition of tortuosity<sup>3,61,62</sup> has existed for a number of years, based on the relation between microscopic and macroscopic lines of flux. Illustrated in Figure 3 is a "tortuous" pore (pore A) connecting two points which lie on the same macroscopic line of flux; this line of flux is normal to planes of macroscopic isopotential. In the absence of the porous material, transport would be along this macroscopic line of flux; the distance

$L_0$  traveled would be given by the path integral along that line of flux. However, in the presence of the porous material, there are two related effects on the *effective* flux along that macroscopic flux line. First, since the actual distance traveled along the pore  $L_p$  exceeds the projected distance  $L_0$  along the macroscopic line of flux, the effective macroscopic flux will be reduced by the factor  $L_0/L_p$ . Second, since the microscopic flux along the pore is driven only by the component of the macroscopic field gradient projected along the actual direction of travel, the effective field gradient, and hence the effective macroscopic flux, will be reduced by a second factor  $L_0/L_p$ . Thus, the overall flux (i.e., conductivity) is reduced by the factor

Figure 3.

Schematic of tortuous and constricted pores.

Tortuous pore (A), and tortuous and constricted pore (B). For a particle diffusing from node 2 to node 1, the macroscopic distance ( $L_0$ ) traveled will be the same regardless of pore. Tortuosity leads to a reduction in the macroscopic flux: both because the actual distance ( $l$ ) traveled is greater than the projected distance ( $l_0$ ), that is,  $l_0 = l \cos \theta$ ; and because the local driving force is less than the macroscopic concentration gradient, that is,  $\nabla c(\text{local}) = \nabla c(\text{macroscopic}) \cdot \cos \theta$ . Larger particles are less likely to pass through the constricted pore, or are even unable if large enough. Hence constrictions lead to a size dependent tortuosity.



$(L_0/L_p)^2$ ; alternatively, the resistivity increases by the factor  $(L_p/L_0)^2$ .

Comparison with, for example, the analog of equation (2.44) for a single pore (i.e., no factor of  $\Phi$ ) indicates:

$$X = (L_0/L_p)^2 \quad (2.54)$$

and

$$T = 1/X = (L_p/L_0)^2 \quad (2.55)$$

thereby defining the intrinsic conductivity and tortuosity *for this simple case*. (In this simple case,  $X = \cos^2\theta$ , where  $\theta$  is the angle between microscopic and macroscopic lines of flux; by an appropriate averaging procedure, some "average" intrinsic conductivity can be defined.)

As an aside on notation, it should be pointed out that tortuosity has also been defined as  $(L_p/L_0)$ ,  $(L_0/L_p)$ , and  $(L_0/L_p)^2$ --the square root, inverse square root, and inverse of the definition in equation (2.55)! In this dissertation, intrinsic conductivity and tortuosity are to be considered according to the *sense* of equations (2.54) and (2.55). This goes also for the related tensorial quantities.

In the preceding discussion, intrinsic conductivity and tortuosity have sometimes been written as scalars. However, as discussed amply by Bear,<sup>2</sup> and pointed out by Lehner,<sup>68</sup> among others, the macroscopic flux is related to the macroscopic potential gradient via a symmetric second rank tensor, not a scalar. Equation (2.45) presented a formal definition of this tensor  $\mathbf{X}$ , which can be compared with the intuitive ideas just discussed. As has been mentioned, this tensor is obtained from the appropriate average

over a "representative elementary volume" of the porous material; references can be consulted for details.<sup>66-68</sup> This tensor corresponds to  $X$ , or alternatively  $1/T$ , in the scalar notation which has been used. The terminology of Lehner,<sup>68</sup> who identifies this tensor as the "intrinsic conductivity" of the porous medium, is to be preferred to that of Bear,<sup>2</sup> who identifies it as the "tortuosity". (Intuitively, an increase in "tortuosity" is associated with an increase in "resistivity", whereas an increase in this tensorial quantity is in fact associated with an increase in "conductivity".) This quantity has also been called the "obstruction factor" by Giddings.<sup>62</sup> The relation of this quantity to the formation factor and porosity has been given in equation (2.53).

In an actual measurement, one essentially obtains a scalar quantity which presumably is one third of the trace of the tensor, at least for an isotropic porous material. Thus, under the assumption of isotropy, the tensorial nature of the intrinsic conductivity will henceforth be ignored unless relevant.

In the arguments leading to equation (2.54) and (2.55), the pores were implicitly considered to be of uniform diameter. However, in most real porous materials, there are divergent and convergent areas in the pores (e.g., pore B of Figure 3). Divergence and convergence will also affect how the macroscopic flux is related to the macroscopic potential gradient, that is, it will affect the intrinsic conductivity.<sup>2,3,62,63,65</sup> Hence,  $X$  and  $T$  are in general related not only to "geometrical tortuosity" effects, as embodied in equation (2.54) and (2.55), but also to the "constrictedness" of the pores. The effects of dead end pores<sup>86</sup> will also be included in  $X$ . Attempts have been made to

separate and calculate these factors for a number of models of porous materials; for example, see Dullien,<sup>3</sup> Giddings,<sup>62</sup> Pismen,<sup>65</sup> and van Brakel and Heertjes.<sup>63</sup> In these approaches, the "overall tortuosity"  $T$  is written as the product of a "geometric tortuosity"  $T_G$  (this corresponds to equation (2.55)) and a "constrictedness" factor  $C$ :

$$T = T_G C \quad (2.56)$$

Giddings<sup>62</sup> relates  $C$  to different averages of the pore cross section area  $A$ :

$$C = \langle A \rangle \langle 1/A \rangle \quad (2.57)$$

In a similar vein, Dullien<sup>3</sup> has suggested that  $C$  is related to somewhat different averages of  $A$ . The continuum mechanical approach,<sup>8,9</sup> which is perhaps more fundamentally appealing, will of course automatically include both these effects. Actually, neither approach is very practical for calculating the intrinsic conductivity, except for relatively simple models of porous materials. (For extensive compilations of such models, consult Dullien<sup>3</sup> or van Brakel.<sup>64</sup>) Hence some motivation remains for performing experiments!

Dullien<sup>3</sup> discusses the relation between "electrical" and "hydraulic" tortuosity, the latter as might be obtained from capillary transport experiments, for example, from the specific permeability in Darcy's law.<sup>1-3</sup> However, general correlations are not expected, as these are fundamentally different quantities; that is, the rate of viscous dissipation, which governs capillary transport phenomena, will depend on different structural features

of porous materials than will diffusive type transport phenomena such as molecular diffusion and ionic conduction.

Some remark should be made on the applicability of this intrinsic conductivity phenomenology to materials with fractal pore spaces. Since real fractal materials must have some lower and upper cutoff lengths associated with the fractal structure, it is argued here that this phenomenology should still apply, if in the averaging procedure necessary to achieve a "macroscopization" of transport phenomena, the "representative elementary volume"<sup>66,67</sup> is chosen sufficiently large with respect to the upper cutoff dimension of the fractal pore space.

A somewhat different definition of tortuosity has been made by Gray.<sup>67</sup> His tortuosity *vector*  $\tau$  can be related to the intrinsic conductivity tensor  $\mathbf{X}$  and the concentration gradient in the pore space fluid  $\nabla c_p$  as:

$$\tau = -(\mathbf{I} - \mathbf{X}) \cdot \nabla c_p \quad (2.58)$$

where  $\mathbf{I}$  is the idemfactor. It can be seen that this tortuosity vector opposes the diffusive flux.<sup>68</sup>

To summarize, the physical significance of the intrinsic conductivity factor  $X$ , or alternatively the tortuosity factor  $T$ , lies in the geometrical tortuosity and constrictedness of the pore space. This factor provides the relation between the macroscopic flux and macroscopic potential gradient. In this dissertation, it shall generally be referred to as the intrinsic conductivity rather than the tortuosity.

Earlier in this chapter, the effects of finite particle size upon equilibrium partitioning and transport in pores were discussed. It is important to

show now how these considerations are related to the general phenomenology for diffusion of point particles as has been developed thus far.

It is again necessary to consider the general relation between effective diffusion coefficients and measurements. For a porous body in contact with a surrounding solution of concentration  $c_0$ , the concentration  $c_p$  with respect to the *total* pore volume will be less because of partitioning,  $c_p = K_D c_0$ . Nonetheless, from a macroscopic point of view, the preceding development given by equations (2.44) through (2.47) remains valid, neglecting for the moment finite size effects on the quantity  $\bar{X}D_0$ . Thus the partitioning coefficient  $K_D$  does not *explicitly* enter into the macroscopic phenomenological equations (or therefore the effective diffusion coefficients) when the driving force, that is, the concentration gradient, is given in terms of the concentration  $c_p$  inside the pores. From an experimental standpoint, this implies that if one makes a measurement, either flux ( $J_{PM}$ ) or second law type ( $\partial(\Phi c_p)/\partial t$ ), directly within the porous material, then the partitioning coefficient does not explicitly enter the effective diffusion coefficients and need not be known. As before, the porosity  $\Phi$ --*not* an effective porosity, i.e.,  $\Phi$  as reduced by  $K_D$ --enters the effective diffusion coefficients for flux measurements *within* a porous material.

Historically, measurement *within* a porous material has been the exception not the rule. Instead, for typical experiments such as membrane transport or transient diffusion, the change in concentration of a *surrounding* reservoir ( $\partial c_0/\partial t$ ) is measured; therefore,  $K_D$  enters the phenomenological equations in addition to  $\Phi$ . This is seen by rewriting equation (2.44) in terms

of  $c_0$  for a finite sized particle ( $K_D < 1$ ), still neglecting changes in  $\mathbf{X}D_0$ , and assuming  $\Phi$  and  $K_D$  constants:

$$\mathbf{J}_{PM} = -\Phi K_D \mathbf{X} D_0 \cdot \nabla c_0 \quad (2.59)$$

This equation is appropriate for flux at the bounding surface between a porous body and a surrounding solution; the effective diffusion coefficient for this boundary flux is:

$$D_{EFF} = K_D \Phi \mathbf{X} D_0 \quad (2.60)$$

This can be compared to equations (2.17) for the "membrane" diffusion coefficient, in which case, since the pores were modeled as straight,  $\mathbf{X}=1$ .

Conclusions about the general relationships between effective diffusion coefficients and experiment are as follows. In experiments where equation (2.47) or an analog applies directly (e.g., dynamic light scattering and forced Rayleigh scattering), that is, for Fick's second law type measurements within a porous material, only the intrinsic conductivity of the porous medium and the diffusivity of the particle are included in  $D_{EFF}$ ; neither  $K_D$  nor  $\Phi$  enters explicitly. This is true not only for point particles but for finite sized particles as well. In experiments where equation (2.44) is applicable--flux of point particles across or within a porous body, or flux of finite sized particles within a porous body--the effective diffusion coefficient includes the porosity and intrinsic conductivity of the porous material and the diffusivity of the particle. In experiments where equation (2.59) is applicable--involving flux of finite sized particles across the surface of a porous body (e.g., membrane transport, transient diffusion)--the effective diffusion

coefficient includes the porosity and intrinsic conductivity of the porous material, the diffusivity of the particle, and the partitioning coefficient of the particle in the porous material.

In principle, the difference amongst these various effective diffusion coefficients is trivial, inasmuch as  $\Phi$  and  $K_D$  are both measurable quantities; furthermore, these overall mass transfer coefficients are often of direct interest. However, measurements of  $\Phi$  and  $K_D$  can sometimes be difficult if not impossible (e.g., thin membranes, non-rigid porous materials); and even if possible, substantial uncertainty can be involved. Obviously, if one is interested in the effects of hindered diffusion and intrinsic conductivity alone, Fick's second law type measurements are preferred.

Some workers have "directly" obtained effective diffusion coefficients such as that given by equation (2.50) (i.e., without  $\Phi$  or  $K_D$ ) from flux and transient diffusion measurements. It is nonetheless clear that this can only be done by *assuming or by knowing accurately* the conditions governing the flux at interfaces between porous material and bulk fluid. When previous experiments on diffusion in porous materials are discussed later in this chapter, difficulties in prescribing this flux will be made evident.

The concept of diffusivity in a porous material is now clarified. At any given point in a pore space, the diffusivity of a Brownian particle is related to its hydrodynamic resistance by the generalized Einstein relation.<sup>76</sup> Effective diffusion coefficients, which are clearly to be regarded as phenomenological coefficients which arise in macroscopic descriptions of diffusion in porous media, are related to this true diffusivity (e.g.,  $D_0$  in unbounded solution,  $D_p$  in pores) by various flux-related quantities (e.g.,  $\Phi$ ,  $K_D$ ,  $\mathbf{X}$ ). The

definition of the true diffusivity, which is independent of flux considerations, differs from the definition of "diffusivity" that arises in the usual global irreversible thermodynamic treatments<sup>5,6,87</sup> of membrane transport. This latter diffusivity is a factor of  $K_D$  times the former, and is properly regarded as an effective diffusion coefficient. This duality disappears for point particles ( $\lambda \rightarrow 0$ ), that is, for  $K_D = 1$ . Brenner and Gajdos<sup>8,9</sup> have pointed out that this global irreversible thermodynamic approach is fundamentally incorrect from the standpoint of continuum mechanics, and they further argue that such an approach, wherein separate transport and partitioning factors are combined, can lead to ambiguities when particles are irregularly shaped or when the particle-wall potential is other than hard repulsive. Most importantly, they have clearly shown<sup>8</sup> (as has Lehner<sup>68</sup> using a different approach) that the driving force in a proper macroscopic continuum mechanical formulation is the concentration inside the pores with respect to the *total* pore volume; this corresponds to  $\nabla c_p$  in the notation used here (e.g., equations (2.44) through (2.47)). This has been compared<sup>8</sup> to the alternative approach of defining the concentration (hence the driving force) with respect to the "effectively accessible" pore volume ( $\nabla c_0$ ,  $c_0 \equiv c_p/K_D$ ); potential ambiguities arise in non-equilibrium or non-steady state situations, and also insofar as  $K_D$  does not always have a simple geometrical basis (e.g., as it does for hard spheres).

Turning now to the question of the effects of finite size on " $\chi D_0$ ", the situation is complicated. It is clear from the earlier discussion of hindered diffusion in simple pores, that  $D_0$  in equation (2.47) must be replaced in some way by a different intrapore diffusion coefficient which takes into

account hydrodynamic (and non-hydrodynamic) particle-wall interactions. In addition, the intrinsic conductivity  $\mathbf{X}$ , heretofore held to be simply a material property of the porous medium, indeed is in the most general case also dependent on the size of the diffusant.

The following discussion is confined to emphasizing in a general way the qualitative features which are expected to be important. The absolute and relative importance of these different features will depend in any case on the detailed structure of the porous material; on the nature of the diffusing species (e.g., polymer versus small molecule, flexible polymer versus colloid); and on the relative size of the diffusant to the structural features of the porous material. This discussion is broken into two parts: first, a brief consideration of formal aspects of the diffusion of particles of size comparable to pore dimensions in random porous media; and second, presentation of approximate *ad hoc* expressions that will be used in interpreting my experimental results.

Formal consideration is based loosely on extension of the ideas of Lehner<sup>68</sup> (point particles, random media) and of Brenner and Gajdos<sup>8,9</sup> (diffusivity of Brownian particles in confined spaces). Equation (2.45), which defines the intrinsic conductivity for diffusion of point particles, was obtained from a reciprocity relation for two distinct diffusive fluxes of the same chemical substance in a porous material.<sup>68</sup> In that development, the molecular diffusivity  $D_0$  was assumed constant. Extending that treatment here to the situation where the translational diffusivity is a spatially dependent tensor  $\mathbf{D}_p$ , one obtains the reciprocity relation:

$$\langle \mathbf{D}_p \cdot \nabla c_1 \rangle_{PM} \cdot \nabla c_{p,2} = \langle \mathbf{D}_p \cdot \nabla c_2 \rangle_{PM} \cdot \nabla c_{p,1} \quad (2.61)$$

where the  $c_i$  are the concentration fields, and the  $\mathbf{D}_p \cdot \nabla c_i$  ( $= \mathbf{J}_i$ ) are the associated flux vector fields. As before,  $\langle \dots \rangle_{PM}$  refers to the phase average (entire porous material) and subscript P to the intrinsic phase average (fluid alone); the usual averaging procedure<sup>66-68</sup> would have to be extended, following Brenner and Gajdos,<sup>8,9</sup> to the product  $\mathbf{D}_p \cdot \nabla c$ . Since equation (2.61) holds for arbitrary pairs of vector fields, then the vectors  $\langle \mathbf{D}_p \cdot \nabla c \rangle_{PM}$  and  $\nabla c_p$  must be related by a linear transformation, giving the macroscopic flux:

$$\mathbf{J}_{PM} = - \langle \mathbf{D}_p \cdot \nabla c \rangle_{PM} = - \Phi \mathbf{D}_\infty \cdot \nabla c_p \quad (2.62)$$

where  $\mathbf{D}_\infty$  is a macroscopic *effective* diffusivity tensor which relates the appropriate macroscopic gradient  $\nabla c_p$  to the averaged microscopic quantity  $\mathbf{D}_p \cdot \nabla c$ . For equation (2.62) to hold,  $\mathbf{D}_\infty$  must be symmetric. Comparison of equation (2.62) with (2.45) shows that the tensor  $\mathbf{D}_\infty$  includes, *in an intimately linked fashion*, both hindered diffusion and intrinsic conductivity effects. Hence, in the most general case, when the species diffusing in a porous material has a spatially dependent diffusivity (e.g., from hydrodynamic particle-wall interactions), these effects are not separable. Evaluation of  $\langle \mathbf{D}_p \cdot \nabla c \rangle_{PM}$  would appear quite formidable for finite sized particles even in porous media with relatively simple (not to mention more complex) structures.

It is now argued that the essential prerequisite, in terms of the structure of the porous material, for the hindered diffusion and intrinsic conductivity to be separable is a narrow pore size distribution; and to the contrary, that these effects will be fundamentally inseparable if there is a significant distribution of pore sizes (e.g., as would be the case for a fractal

pore space), or even if there are just a number of severe constrictions in the pore space. With reference to the intuitive concepts of "geometrical tortuosity" and "constrictedness", it is clear that these factors will in general depend on the size of the diffusant when there is a significant distribution of pore sizes or very many constrictions. Such constrictions present a size dependent energetic hindrance to diffusion; as one increases the size of the diffusant in a given porous material, the relative "constrictedness" along a given path increases and molecules will also on the average take more "geometrically tortuous" paths. (As noted before, viewing these separately is not generally justified, which is particularly true for diffusants of size comparable to the pore.)

To put these arguments somewhat more precisely, consider the diffusion of spheres (radius  $R_s$ ) in a straight pore (i.e., no geometrical tortuosity) with a variable circular cross section (radius  $R_p$  and cross sectional area  $A_p$  at a given point). Since  $\lambda_s = R_s/R_p$  varies along the pore, the partitioning coefficient  $K_D$  and parallel diffusivity  $D_{p, \parallel}$ , both functions of  $\lambda_s$ , also vary. The effective intrapore diffusion coefficient for transport through such a pore (say between two reservoirs) will be:

$$D_{\text{EFF}} = \langle K_D A_p \rangle^{-1} \langle 1 / K_D A_p D_{p, \parallel} \rangle^{-1} \quad (2.63)$$

where  $\langle \dots \rangle$  refers to an average over the length of the pore. Equation (2.63) follows from the argument that the effective conductivity of a channel will be inversely proportional to the averaged effective cross sectional area  $\langle K_D A_p \rangle$  (i.e., the factor  $K_D$  gives the "effective" area), and also inversely proportional to the averaged "resistance" of the channel  $\langle 1 / K_D A_p D_{p, \parallel} \rangle$ .

Analogous arguments for the case  $K_D = 1$  and  $D_{p, \parallel} = D_0$  were used to derive<sup>61</sup> equation (2.57) for the "constrictedness" factor  $C = \langle A \rangle \langle 1/A \rangle$ , and also by Giddings et al.<sup>33</sup> for the case  $K_D < 1$  (but still assuming  $D_{p, \parallel} = D_0$ ) to give the following result for  $C$ :

$$C = \langle K_D A_p \rangle \langle 1/K_D A_p \rangle \quad (2.64)$$

Equation (2.63) provides a prescription for calculating  $D_{\text{EFF}}$  given knowledge of the size distribution  $A_p$  and the dependence of  $K_D$  and  $D_{p, \parallel}$  on  $\lambda_s$ . This equation again shows the general inseparability of intrinsic conductivity (in this case, "constrictedness") and hindered diffusion. Except for the case of constant radius, where  $K_D A_p = \text{constant}$  and  $D_{\text{EFF}} = D_{p, \parallel}$ ,  $D_{\text{EFF}}$  is given by a complex average.

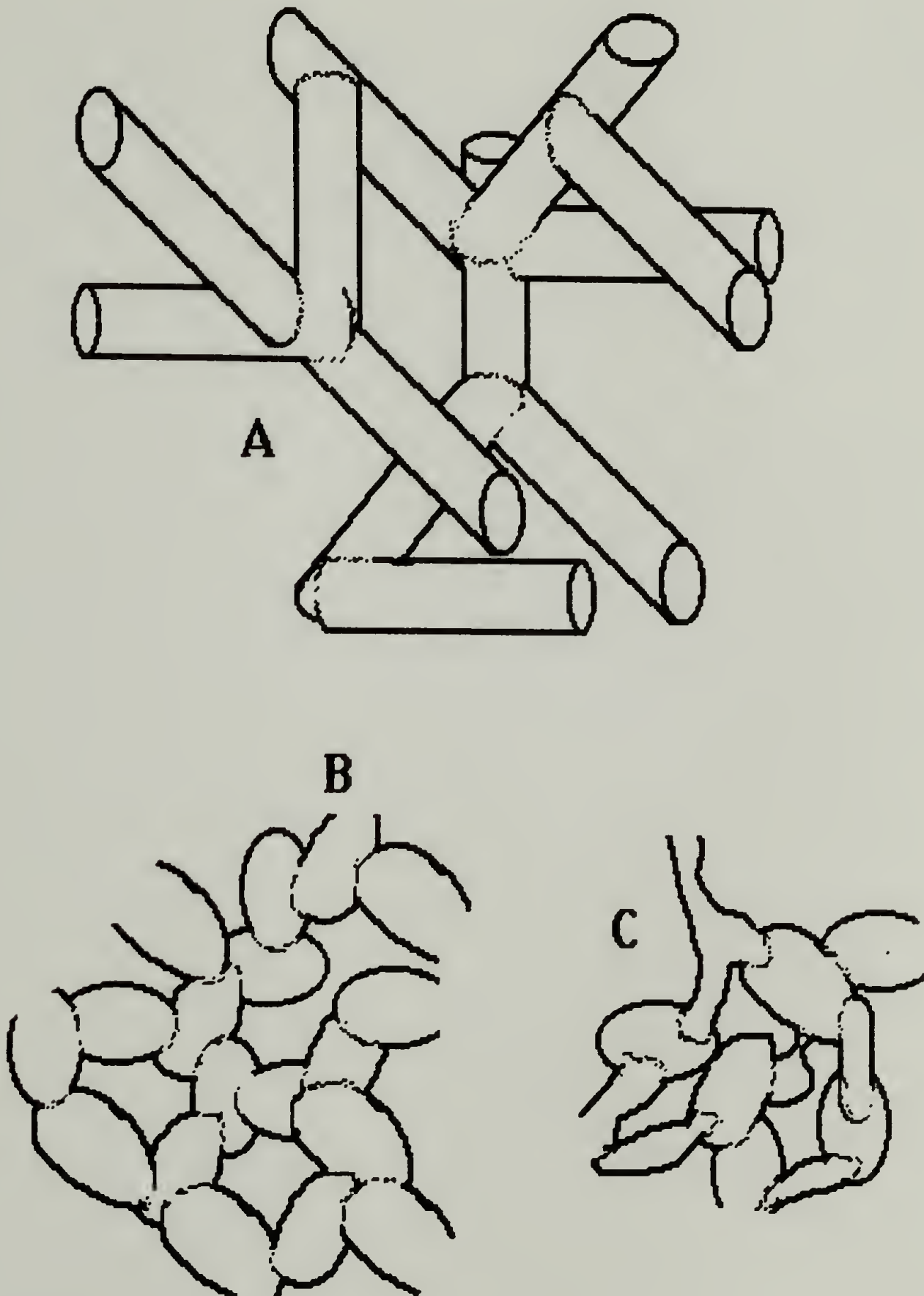
Consider now the extension of these arguments to three-dimensional pore spaces where the geometrical tortuosity is no longer unity. Take first a network of long cylindrical pores, each with the same constant cross section, and with the nodal regions, which obviously must have a different geometry than the pores, comprising only a small fraction of the total pore volume (Figure 4). By extension of the above single pore result, constriction effects are negligible, even for the diffusion of finite sized particles, in such a network. Thus, to a first approximation, the various effective diffusion coefficients for diffusion in such a pore space can be written as:

$$D_{\text{EFF}} = X_0 D_{p, \parallel} = X_0 D_0 f(\lambda) \quad (2.65)$$

$$D_{\text{EFF}} = \Phi X_0 D_{p, \parallel} = \Phi X_0 D_0 f(\lambda) \quad (2.66)$$

Figure 4.

Schematics of well-connected (A, B) and non-well-connected (C) pore spaces.



$$D_{\text{EFF}} = \Phi K_D X_0 D_{P,\parallel} = \Phi K_D(\lambda) X_0 D_0 f(\lambda) \quad (2.67)$$

$$D_M = K_D X_0 D_{P,\parallel} = K_D(\lambda) X_0 D_0 f(\lambda) \quad (2.68)$$

where  $X_0$  is the intrinsic conductivity ( $= 1/T_0$ , with  $T_0$  the tortuosity) for diffusion of point particles (subscript 0) in the same network, and where  $D_{P,\parallel}$  is the parallel diffusivity in each of the identical pores. The size dependence of the factors  $K_D$  and  $f$  is explicitly noted. When constrictions are negligible, the intrinsic conductivity is essentially related only to the "geometrical tortuosity". The above equations correspond, respectively, to equations (2.50), (2.49), (2.60), and (2.17b), which are the results given previously for diffusion of point particles of constant diffusivity. These different results correspond, as before, to effective diffusion coefficients that would be obtained in different types of experiments.

The simple relationships proposed in equation (2.65) to (2.68) are only expected to be a reasonable approximation for "well-connected" pore spaces. Attempting to define well-connected, I propose that such a pore space should be comprised of geometrically and dimensionally similar basic elements ("pores"), with the basic elements joined in such a way as to avoid the introduction of dissimilar geometric elements, for example, large nodes or severe constrictions. The network model given earlier (i.e., with long cylinders as the basic elements), although well-connected, is undoubtedly a poor model for any real porous material. Shown in Figure 4 are schematic diagrams: that model; another perhaps more realistic looking well-connected pore space; and a counterexample, that is, a pore space where these simple relationships would not be useful.

It is reemphasized that in the most general case of diffusion of particles of size comparable to the pores, the effects of hindered diffusion and intrinsic conductivity--tortuosity, constrictions--are not separable (i.e., as would be given by equations (2.65) to (2.68)) but are instead intimately interrelated (i.e., as given by equation (2.62)). The only situation where such separation is approximately justified is for well-connected pore spaces. This development has shown that when the microscopic diffusivity in a porous material is significantly size (i.e., relative size) dependent, for whatever reason, then the treatment of hindered diffusion in terms of equations such as (2.65) through (2.68) must be justified. This justification is required because these equations, which are essentially *ad hoc* modifications to the phenomenology for diffusion of point particles, are only valid in certain limited circumstances. Despite this, it is noted that these types of equations have to my knowledge always been used without any justification (either phenomenologically or in terms of pore structure) to analyze the results of hindered diffusion experiments.<sup>16,35-37</sup> Similarly, diffusion of molecules of size comparable to pores has sometimes been made solely in terms of point particle phenomenology.<sup>40</sup> It is clear that either approach can result in misleading or wrong conclusions about the underlying causes (e.g., porous material structure, partitioning, diffusant size, etc.) of an overall hindrance to diffusion.

### **Miscellaneous Diffusion Theories**

Two theories are presented in this section: a mode-coupling theory for macroscopic diffusion;<sup>69,70</sup> and the theory for diffusion on a fractal.<sup>88-93</sup> Both these theories deal with departures from "ordinary" diffusion (i.e., where the mean squared displacement  $\langle R^2(t) \rangle$  varies linearly with time, and where the distribution of displacements is Gaussian). As these theories are implicitly for the diffusion of point particles, brief mention will be made of their possible applicability to particles of finite size.

In the mode-coupling analysis,<sup>69,70</sup> calculations are based on a coarse-grained or macroscopic diffusion equation, valid for length scales  $L$  much greater than the range of spatial correlations  $l_2$  in the random medium, that is, valid in the long-time or low frequency limit. This diffusion equation is rewritten in terms of the Fourier components of certain fluctuating quantities, namely, the concentration, the diffusion tensor, and the local free volume fraction (the integral of which over the total volume is the porosity). In this diffusion equation, the concentration fluctuations are thus coupled to stationary "modes" (i.e., the Fourier components of fluctuations in the diffusion tensor and free volume) which are determined by the complex statistical nature of the random medium. The calculation focuses on the autocorrelation function of the concentration fluctuations (i.e.,  $g_s^{(1)}(\mathbf{q}, t)$ , which is given by equation (3.24) in section 1 of Chapter III); therefore, the result is readily related to the dynamic light scattering experiment, as will be given in section 2 of Chapter III. The primary result of the mode coupling analysis is that disorder in the porous material leads to long time

dynamical correlations. At long times, the memory kernel for diffusion shows an algebraic decay, like  $t^{-5/2}$  (in three dimensions).

As an aside, it is noted that the results of a perhaps more conventional treatment of diffusion in a random porous medium<sup>65</sup> would appear consistent with this mode-coupling analysis, in that the particle displacement distribution function is non-Gaussian, with non-zero higher order moments. Although this treatment<sup>65</sup> does not give a power law decay, the degree of deviation from Gaussian behavior, as in the mode-coupling theory, is related to the degree of randomness in the structure of the porous material. Both types of analysis indicate that, the more random a structure, the greater the deviation from "normal" (i.e., Gaussian) macroscopic diffusion behavior (e.g., the amplitude of the power law term in the mode-coupling theory).

Diffusion and conduction on (or for a porous material, in) a fractal structure have been considered relatively recently,<sup>88-93</sup> often in connection with the conductivity of percolation networks. Most real materials, if fractal, will only be so over some range of length scales,  $l_1 < L < l_2$ . The lower cutoff length  $l_1$  is associated with some elementary structural building block, for example, a lattice spacing, or minimum sized pore. The upper cutoff length  $l_2$  is that above which dilational symmetry is lost (i.e., density will again scale with Euclidean dimensionality). For  $L > l_2$ , transport coefficients (e.g., specific conductivity, effective diffusion coefficients) are independent of  $L$ ; however, for  $l_1 < L < l_2$ , anomalous transport will be observed.

Only the results are cited here; the references<sup>88-93</sup> can be consulted for details. (The relation of these results to dynamic light scattering experiments is given in Chapter III, section 2.) For the anomalous diffusion regime

( $l_1 < L < l_2$ ), O'Shaughnessy and Procaccia<sup>93</sup> have recently given an analytical solution  $P(\mathbf{R}, t | 0, 0)$  to the diffusion equation, with the result for the mean square displacement:

$$\langle R^2(t) \rangle = \beta t^{2/d_w} \quad (2.69)$$

where

$$\beta = (D_0 d_w^2)^{2/d_w} \Gamma((d_f + 2)/d_w) / \Gamma(d_f/d_w) \quad (2.70)$$

Here  $d_w$  is the dynamical fractal walk exponent,<sup>89-93</sup> which characterizes the diffusion of a random walker on a particular fractal structure. It is related to the fractal dimensionality of the object,  $d_f$ , and to the spectral (fracton) dimension,<sup>89,91</sup>  $d_s$ , as:

$$d_s = 2 d_f / d_w \quad (2.71)$$

For ordinary Fickian diffusion,  $d_w = 2$ ; but for diffusion on a fractal,  $d_w > 2$ . Also, for  $l_1 < L < l_2$ , the effective diffusion coefficient  $D_{\text{EFF}}$  should be independent of  $l_2$  and a function of  $L$  only,<sup>88,90</sup> with  $D_{\text{EFF}} \propto L^{2-d_w}$ . Crossover arguments indicate that for macroscopic diffusion ( $L \gg l_2$ ), the effective diffusion coefficient is:<sup>90,94,40</sup>

$$D_\infty = D_0 (l_1/l_2)^{d_w-2} \quad (2.72)$$

The intrinsic conductivity for this fractal model is thus identified as:

$$X_0 = (l_1/l_2)^{d_w-2} \quad (2.73)$$

(N. B. The exponent  $\Theta = d_w - 2$  is called the exponent of anomalous diffusion; see<sup>90</sup> for example for the relation of  $\Theta$  to various critical exponents for percolation clusters.<sup>88-91</sup>) For a fractal porous material, the porosity can also be given in terms of  $l_1$ ,  $l_2$ , and  $d_f$  as:<sup>94</sup>

$$\Phi = A (l_1/l_2)^{3-d_f} \quad (2.74)$$

with  $A$  a constant of order unity. Combination of equations (2.73) and (2.74) gives the relationship between the intrinsic conductivity and porosity of a fractal material.

Regardless of whether a pore space is fractal or not,  $D_\infty$  will be less than  $D_0$ , so that there is some crossover between diffusion on a microscopic level (characterized by  $D_0$ , for lengths of order  $l_1$ ) to diffusion on a macroscopic level (characterized by  $D_\infty$ , for lengths greater than  $l_2$ ). Even classical models (see for example, Pismen<sup>65</sup>) thus show an "anomalous diffusion" regime for some distances  $l_1 < L < l_2$ . Even in cases where the porous material is not fractal in any usual sense, it *may* be possible to consider this anomalous diffusion in terms of some "effective fractal" behavior. For classical models of fairly regular pore spaces,  $1/3 \leq X_0 \leq 1$ . In terms of a fractal picture, such relatively high  $X_0$  imply  $l_2/l_1$  of order unity and  $d_w$  relatively close to 2 (or  $\Theta$  of about zero; compare versus  $\Theta=1.5$  for percolation clusters in three dimensions<sup>90</sup>).

A last comment concerns the application of these "miscellaneous" theories to the diffusion of particles of size comparable to the pores. First, since the power law term in the mode coupling analysis is a direct consequence of randomness in the structure of the porous material, it presumably

would be expected regardless of the size of the diffusing species relative to the size of the pores. Second, as pointed out in the previous section of this chapter, for diffusion in a structure with widely varying pore sizes (e.g., in a fractal), the macroscopic diffusion coefficient will include in a linked fashion not only specific hindrances to diffusion, such as hydrodynamic interactions, but also partitioning effects (see equation (2.62) and the heuristic equation (2.63)). As a consequence of this fundamental inseparability of hydrodynamic interactions and structural effects, the relation of  $D_\infty$  to  $D_0$  will no longer be given by a simple equation such as (2.72).

### **Experimental Background**

This section is a selected and critical review of experiments which have focused on partitioning and transport in porous materials. This discussion emphasizes, but is not confined to, experiments dealing with the diffusion of flexible polymers or with diffusion in porous glasses, since those areas are the most relevant to the work of this thesis. Of particular interest are values which have been obtained for the ratio of the diffusion coefficient inside a porous material to the diffusion coefficient in bulk solution, and how that ratio has been observed to depend on the parameters which characterize the diffusant and the porous material. Past experimental results are presented here in some detail in order to allow substantive comparison with the results of our dynamic light scattering experiments.

In this thesis research, the diffusion of polystyrene in dilute solution in a good solvent in porous glasses has been investigated. Two groups had previously investigated just this system using transient diffusion

techniques. Colton et al.<sup>16</sup> added polystyrene solution to solvent-saturated cubes of porous glass, then monitored the change in the concentration of the bulk solution over time by UV absorbance. Tennikov et al.<sup>17</sup> introduced a solution of anthracene labeled polystyrene under slow flow (0.002 - 0.02 cm<sup>3</sup>/min) into a closed loop containing a segment packed with porous glass fragments, then monitored the change in fluorescent intensity (i.e., concentration) in the packed bed. In principle, in either experiment, partitioning coefficients  $K_D$  could be calculated from the concentration reached at long times, and effective diffusion coefficients  $D_{EFF}$  could be extracted from the data for approach to equilibrium.

Colton et al.<sup>16</sup> observed no systematic decrease in  $D_{EFF}/D_0$  for a given pore size with an increase in molecular weight, in contrast to expectations of hindered diffusion theories. Their conclusion was that  $D_{EFF}/D_0$  was a constant, independent of molecular weight, for a given pore size; and that the value of this constant ratio was not monotonically related to either pore size or porosity. The average values of  $D_{EFF}/D_0$  for each glass ranged from 0.22 to 0.43. (For rigid proteins--with adsorption present, however--they did see a reduction in  $D_{EFF}/D_0$  with increasing  $\lambda_G$ .) Tennikov et al.<sup>17</sup> observed a minimum in the dependence of  $D_{EFF}/D_0$  as a function of molecular weight for each pore size glass, and values of  $D_{EFF}/D_0$  exceeding unity at higher molecular weights. Correcting for an obvious error in their data, they obtained values of  $D_{EFF}/D_0 \approx 0.5$  for three similar glasses, with the lowest molecular weight polystyrene ( $\lambda_H \approx 0.2$ ).

Colton et al.<sup>16</sup> came to further conclusions from their data. The  $D_{EFF}$  which they obtained was claimed to be that of equation (2.65). Based on the

apparent lack of molecular weight dependence, they *assumed* that  $f(\lambda)=1$  in all cases. They then calculated a tortuosity  $T_j$  for each pore size glass as:

$$T_j = \left[ \sum_{i=1}^{N_j} (D_{\text{EFF}}/D_0)_i \right] / N_j \quad (2.75)$$

where  $N_j$  was the number of measurements for the  $j^{\text{th}}$  glass. They then took these values of  $T_j$  and calculated  $T_j D_{\text{EFF}}/D_0$  for each data point. All these values, for all porous glasses, were averaged to "determine"  $[f(\lambda)]_{\text{AVG}} = 1.00 \pm 0.27$ , thereby recovering their assumption. (That is, based on this procedure,  $[f(\lambda)]_{\text{AVG}} = 1.00000 \dots$ ) Having thus "proved" the absence of hindered diffusion, they then further concluded that polystyrene is "free draining" inside pores, thereby coining a new definition for "free draining" as meaning no hindered diffusivity in pores. Actually, since  $D_0 \propto M^{-a}$  ( $a = 0.55$  and  $0.58$  for the two solvents they used), if  $D_{\text{EFF}}/D_0$  is constant, that is,  $D_{\text{EFF}}/D_0 \propto M^0$ , then  $D_{\text{EFF}}$  must also be proportional to  $M^{-a}$ . This is certainly different than the usual definition of free draining, which gives  $D \propto M^{-1}$ .

Turning aside these obvious errors in interpretation by Colton et al., it is difficult to even qualitatively reconcile the results of either of these transient diffusion experiments<sup>16,17</sup> with the predictions of theories of hindered diffusion or with the results of membrane transport experiments which are discussed below (or, to foreshadow, with our dynamic light scattering results). One can speculate as to why the results of these conceptually and technically simple experiments are so anomalous. The finger would seem to point at the methods of data analysis (and related assumptions) which were used to extract  $D_{\text{EFF}}$  values. At the outset, it is

unclear whether the condition<sup>68</sup> given by equation (2.43) would have been met in either experiment, hence, whether or not it was valid to use macroscopic forms of Fick's laws. Secondly, in both these experiments, the boundary layer resistance was assumed negligible. (This is often a poor assumption in membrane transport experiments.<sup>7,28,95</sup>) Lastly, in neither paper was any real detail given of how  $D_{\text{EFF}}$  values were obtained from raw data.

Colton et al.<sup>16</sup> claim to have solved equation (2.47) subject to the initial conditions of concentration inside and outside the glass and subject to the boundary condition (which introduces the need to know  $K_D$  and  $\Phi$ ) which prescribes the flux at the surfaces (again, boundary layer resistance is neglected):

$$V_B \partial c_0 / \partial t = - 2 D_{\text{EFF}} \Phi A \nabla c_p |_{\text{at cube surface}} \quad (2.76)$$

where  $V_B$  is the volume of solution outside the glass cube,  $c_p$  is the concentration inside the pores,  $c_0$  is the concentration in the bulk solution (they assumed  $c_p = K_D c_0$  at the cube surface), and  $A$  is the area of a single cube face. This boundary condition is essentially that of equation (2.59).

One can infer from their paper that they were attempting to solve "directly" for a  $D_{\text{EFF}}$  such as given by equation (2.65) (i.e.,  $D_{\text{EFF}} = X_0 D_0 f(\lambda)$ ), of course in essence by correcting a  $D_{\text{EFF}}$  as given by equation (2.67) (i.e.,  $D_{\text{EFF}} = K_D \Phi X_0 D_0 f(\lambda)$ ) using measured values of  $K_D$  and  $\Phi$ . However, in their paper, they failed to give the actual approximate solution which they obtained and used. Although the problem appears to have been properly formulated, it is perhaps possible that a trivial error was made in the

solution, such that their reported  $D_{\text{EFF}}$  values were not  $(X_0 D_0 f(\lambda))$  but actually  $(X_0 D_0 f(\lambda)/K_D)$ , or even  $(X_0 D_0 f(\lambda)/K_D \Phi)$ , etc. (Such an error would roughly account for the observed discrepancies.) Tennikov et al.<sup>17</sup> gave the equation which they used, but provided no real information as to the differential equation and boundary conditions to which it was a solution; hence, no judgment can be made as to whether it was a reasonable solution, and which type of  $D_{\text{EFF}}$  they obtained. It is noted here that their reported  $D_0$  values, which they did not measure but only calculated from a literature correlation, undoubtedly are about twice as large as the true  $D_0$  values, with corresponding reported  $R_H$  values about half the true values.

Turning to another type of experiment, it is known that the broadening of peaks in steric exclusion chromatography (SEC), or any other type of chromatography employing porous packings, is related in part to diffusional transport within the pores of the column packing material.<sup>62</sup> Various workers<sup>33,34,61</sup> have attempted to exploit this connection in order to extract information on diffusion in porous materials. Now the overall broadening in SEC is a combination of dispersion in the mobile phase (i.e., the interstitial volume between packings) and in the stationary phase (i.e., inside the pores). At flow rates usually employed in SEC, the broadening due to dispersion in the mobile phase is independent of flow rate, that is, longitudinal dispersion in the usual sense is negligible.<sup>34</sup> The broadening due to dispersion in the stationary phase is superimposed on this flow rate independent mobile phase dispersion.

In general, the dispersion in the pore space is proportional to the flow rate and is related both to diffusion and to any adsorption which might

be occurring.<sup>62</sup> In general, these two mass transfer processes are coupled. However, in the absence of significant adsorption, the following simple expression has been obtained,<sup>62,34</sup> giving the portion of the variance which is due to dispersion in the stationary phase ( $\mu_{2s}$ ):

$$\mu_{2s} = Q_V (q_p d_p^2 K_C V_i / D_{EFF}) \quad (2.77)$$

where  $Q_V$  is the volume flow rate,  $q_p$  is a form factor related to the packing shape,  $d_p$  is some characteristic dimension of the packing,  $K_C$  is the chromatographic partitioning coefficient,  $V_i$  is the total internal pore volume, and  $D_{EFF}$  is the effective diffusion coefficient. (The quantity  $K_C V_i$  is related to the elution volume  $V_e$  and column interstitial volume  $V_0$  as  $V_e = V_0 + K_C V_i$ .)

Thus  $D_{EFF}$  can in principle be obtained from the slope of plots of total variance  $\mu_2$  versus the flow rate  $Q_V$ , with the intercept being the flow rate independent contribution  $\mu_{2m}$ . Aside from questions about the adequacy of the simple dispersion theory embodied in equation (2.77), there are certain difficulties associated with obtaining accurate values for  $D_{EFF}$ . First, one must be able to accurately determine the total variance; this is especially difficult for skewed peak shapes. Second, many packings are irregularly shaped, and nearly all have a distribution of sizes; usually, however, the packings are assumed monodisperse (single effective diameter  $d_p$ ) and spherical (form factor  $q_p = 1/30$ ). Of course, in a series of measurements with the same packing material, even if uncertainty in  $d_p$  and  $q_p$  leads to uncertainty in absolute values of  $D_{EFF}$ , those values should still bear the correct relative relationship. Other form factors can differ significantly;<sup>62</sup> for example, for rod shaped porous packings,  $q_p = 1/8$ . Giddings<sup>62</sup> has pointed

out that the proper average of  $q_p d_p^2$  should be volume weighted. Since  $D_{\text{EFF}} \propto d_p^2$ , choice of the characteristic dimension is also particularly critical.

Lastly, adsorption if present will also contribute to the variance.

As was the case for the transient diffusion experiments discussed previously, the theory for chromatographic broadening as formulated should "directly" provide a  $D_{\text{EFF}}$  as given by equation (2.65). In fact, the effects of partitioning and porosity enter equation (2.77) through the factors  $K_C$  and  $V_i$  respectively. In the development of this theory, the flux between mobile (bulk) phase and stationary (pore) phase is assumed to be governed by the chromatographic partitioning coefficient  $K_C$ , which is usually assumed to be equal to the equilibrium partitioning coefficient  $K_D$ . This assumption is in turn based on the established consensus that SEC is essentially an equilibrium process.<sup>49,50</sup> However, remark is made of experiments by Haller wherein  $K_C \neq K_D$  was found,<sup>96</sup> and further that very few experimental tests of this critical assumption have been made. No other resistance to mass transfer between bulk and pores (e.g., boundary layer) is included. In the original theory,<sup>62</sup> no explicit account was taken of size dependence, except for implicit effects on  $K_C$ ; that is, the factor  $f(\lambda)$  was assumed equal to unity. Obviously, this might or might not<sup>34</sup> be a good assumption for any particular experiment.

Results for  $D_{\text{EFF}}/D_0$  from a few selected and disparate band broadening experiments are mentioned briefly. Gas chromatographic experiments of Knox and McLaren<sup>61</sup> for the diffusant ethylene in columns of non-porous spheres, and "loose" and "dense" diatomaceous earth gave  $D_{\text{EFF}}/D_0 = 0.60$ , 0.74, and 0.46 respectively. Longitudinal dispersion in convective-diffusive

flow of single component fluids through packed beds of non-porous spheres gives  $D_{\text{EFF}}/D_0 \approx 0.67$ ; this is the "average" of a number of values obtained by various workers, collected by Pfannkuch, and cited in Dullien<sup>3</sup> and Bear.<sup>2</sup> (This value was obtained from data at low Reynolds number, where the convective-diffusive picture is relatively simple.) In these first two cases, the assumption  $f(\lambda) = 1$  is probably reasonable.

Of perhaps more relevance to the work of this thesis, two groups have also looked at the diffusive broadening for polystyrene eluting through SEC columns packed with porous glasses.<sup>33,34</sup> Giddings et al.<sup>33</sup> used a very small pore size glass ( $R_p \approx 20 \text{ \AA}$ ); hence, although they used low molecular weights of oligostyrene (600 and 4000), their assumption that the "obstruction factor"  $D_{\text{EFF}}/D_0$  should be independent of molecular weight is doubtful, based on my estimate of  $\lambda_G$  values. With this assumption, they obtained an "average" value for  $D_{\text{EFF}}/D_0 \approx 0.17$  from the slope of a plot of reduced plate height versus reduced flow velocity data for two molecular weights of polystyrene in two solvents, also for toluene. Actually, the scatter in their data indicated *greater* hindrance to diffusion for toluene and the M-600 oligostyrene than for the M-4000 polystyrene.

Klein and Grüneberg<sup>34</sup> performed more extensive experiments, looking at elution of polystyrene through columns packed with porous glasses and with macroporous crosslinked polystyrene beads. They presented their results in terms of  $D_{\text{EFF}}/D_0$  as a function of  $K_C$ , which is in turn some function of the relative size of polymer to pore (e.g., of  $\lambda_G$ ). These authors found  $D_{\text{EFF}}/D_0$  in the range 0.10-0.25 for the different porous glasses, and 0.01-0.20 for the macroporous polystyrene beads. For  $K_C > 0.35$

(i.e., relatively small  $\lambda_G$ ) they observed  $D_{\text{EFF}}/D_0$  to be independent of  $K_C$ , that is, independent of molecular weight, for both the porous glass and porous polystyrene packings. They did not attempt to explain this observation, but noted that it was in agreement with the work of Colton et al.<sup>16</sup> (although they did not expect such behavior). Again, it is difficult to reconcile this result with the predictions of hindered diffusion theories or the results of membrane experiments. For  $K_C < 0.35$  (i.e., relatively large  $\lambda_G$ ) they observed a decrease in  $D_{\text{EFF}}/D_0$  with decreasing  $K_C$ , that is, with increasing molecular weight. The only experiments with  $K_C < 0.35$  were in the macroporous polystyrene beads. They concluded that there was some indication of a decrease in  $D_{\text{EFF}}/D_0$  with decrease in porosity, but it is questionable whether their data support such a conclusion. They noted that their values of  $D_{\text{EFF}}/D_0$  were about 50% lower than those of Colton et al.<sup>16</sup> at similar porosities, and suggested that this could be due in part to difficulty in estimating  $q_p$  and  $d_p$  in equation (2.77). Lastly, they noted that the obstruction to diffusion in the macroporous polystyrene was higher than in glasses of similar porosity, and suggested that this could be due to much wider pore size distributions in the macroporous polystyrene packings.

This review turns now from those experiments most closely related to the system of this dissertation (i.e., flexible polymers in porous glass) to those experiments most closely related to theories for hindered diffusion in simple pore geometries, namely, membrane transport experiments. In this type of experiment, a membrane separates two solutions of initially different concentration. Allowing diffusion to proceed, the changes in concentration over time in one or both chambers are monitored by absorbance, differential

refractive index, assay of radiolabeled solute, or the like. These concentration changes are easily related to the total resistance  $R_{TOTAL}$  of the membrane, for example:<sup>31</sup>

$$\frac{[c(\infty) - c(t)]}{[c(\infty) - c(0)]} = \exp \{- 2 A_M t / R_{TOTAL} V\} \quad (2.78)$$

corresponds to measurements in the downstream (i.e., low concentration) chamber of volume  $V$ , where  $c(0)$ ,  $c(\infty)$ , and  $c(t)$  are the initial, equilibrium, and transient concentration and  $A_M$  is the exposed membrane area. The total membrane resistance is given by:<sup>7,28,95</sup>

$$R_{TOTAL} = R_M + R_B + R_E \quad (2.79)$$

where  $R_M$  is the intrapore membrane resistance,  $R_B$  is the boundary layer resistance, and  $R_E$  is a pore end resistance. These details are given here as they arise in any critical discussion of the results of such experiments, since, although  $R_E$  is usually negligible,  $R_B$  can often be a significant fraction (e.g., 20%) of  $R_{TOTAL}$  and must therefore be corrected for. The intrapore membrane resistance  $R_M$  is related to the membrane diffusion coefficients  $D_M' = \Phi K_D D_{p,\parallel}$  or  $D_M = K_D D_{p,\parallel}$  (given in equations (2.17)) by:

$$R_p = \frac{L_M}{D_M'} = \frac{L_M}{n_p \pi R_p^2 D_M} \quad (2.80)$$

where  $L_M$  is the pore length and where the second version (with  $n_p$ -number of pores per unit area) has been written to indicate more transparently the connection to cylindrical pore geometry. It is the quantity  $D_M$ , which

combines partitioning ( $K_D$ ) and hindered diffusivity ( $D_{p,||}$ ), that is most frequently compared directly to theoretical predictions.

Systematic investigation of the diffusion of molecules of size comparable to the pores through membranes dates to the early work of Ferry,<sup>18,19</sup> Papenheimer et al.,<sup>20</sup> Renkin,<sup>22</sup> and Papenheimer.<sup>21</sup> The principal outcome of that work, the Renkin equation, wherein the membrane diffusion coefficient  $D_M$  is given as the product of a factor due to hydrodynamic drag times a steric partitioning coefficient, continues to be used extensively as a model for membrane transport. Combining equations (2.3) and (2.26) gives this Renkin equation:

$$D_M/D_0 = (1 - \lambda_S)^2 \{1 - 2.104 \lambda_S + 2.089 \lambda_S^3 + \dots\} \quad (2.81)$$

where as before  $\lambda_S = R_S/R_P$  is the ratio of sphere to pore radii and  $D_M = K_D D_{p,||}$  is an effective membrane diffusion coefficient. Solomon<sup>24</sup> and Paine and Scherr<sup>81</sup> have reviewed applications of this equation. Given that the structure of membranes is often poorly known, this model has in fact been used to provide equivalent pore radii by fitting data to the Renkin equation; but such agreement of data to the Renkin equation, with the radius as an adjustable parameter (e.g., Ref. 23), is certainly no proof of the quantitative validity of that equation. In fact, by ignoring the intrinsic conductivity (tortuosity) of complex membranes, such an approach gives a misleading idea of membrane structure, for example, by underestimating the pore dimensions.

While not denying the empirical utility of the above approach for complex systems, more fundamental studies of membrane transport have

concentrated on better characterized systems, either membrane, solute, or both. An early attempt in this regard was by Uzelac and Cussler,<sup>25</sup> who examined diffusion of monodisperse polystyrene latex through Millipore® filters (nominal pore radii, 0.22  $\mu\text{m}$  to 1.2  $\mu\text{m}$ ) and found, surprisingly,  $D_M/D_0 \approx 10$  in the limit  $\lambda_S \rightarrow 0$ , a result which they attributed to charge effects. The search for ideal systems received a boost with the advent of track-etched membranes, which have relatively monodisperse parallel pores of reasonably well defined geometry. Conlon and Craven,<sup>26</sup> who examined the diffusion of polystyrene latex through Nuclepore® track-etch membranes (i.e., a system closely akin, excepting charge effects, to hard sphere-cylinder models), found less hindrance to diffusion than predicted even by the Renkin equation and also  $D_M/D_0 > 1$  in the limit  $\lambda_S \rightarrow 0$ , results attributed to electrostatic interactions between latex and membrane. (Also, as noted by Malone,<sup>28</sup> the boundary layer resistance, which they neglected, was probably comparable to the intramembrane resistance for this system.)

Beck and Schultz<sup>27</sup> examined the diffusion of relatively small molecules through track-etched mica membranes ( $0 < \lambda_S < 0.2$ ) in a careful and extensive study in which they used non-charged solutes and corrected for the boundary layer resistance. Their results for  $D_M/D_0$ , the first and still perhaps the best data on a well-defined system closely corresponding to the hard sphere-cylindrical pore model, clearly showed greater hindrance than predicted by the Renkin equation (but less than predicted by the as yet undeveloped Brenner-Gajdos theory<sup>8,9</sup>), thereby indicating the qualitative correctness but quantitative failings of the centerline approximation theory.

Malone and Anderson<sup>7,28</sup> measured the membrane diffusion coefficient for polystyrene latex spheres through track-etched mica membranes as a function of pore size ( $\lambda_s \leq 0.2$ ) and ionic strength. The observed ratio  $D_M/D_0$  was significantly less (i.e., greater hindrance) than predicted by all the hard sphere theories, but could be reconciled with theory by accounting for electrostatic (i.e., non-hydrodynamic) interactions, osmotic backflow, and the rhombic pore cross section. Lower ionic strength showed greater hindrance to diffusion.

These workers<sup>7,28</sup> and others<sup>27,95</sup> have discussed potential sources of error in membrane transport experiments. As given by equation (2.79), the total membrane resistance includes the intrapore resistance, end effects, and boundary layer resistance. The boundary layer resistance varies with stirring speed and particle size, and can be a significant fraction of the total resistance. Very importantly, the *relative* importance can change significantly with porosity, molecular size, and stirring speed; but while Malone and Anderson<sup>28</sup> imply that  $R_B$  increases with increase in porosity, Bohrer found the opposite.<sup>95</sup> To accurately make the necessary corrections in order to extract  $D_M$ , and to be able to calculate  $\lambda$  values, requires accurate independent measurement of the pore radius. Lastly, osmotic backflow can cause substantial error in  $D_M$ .<sup>7,28</sup> this can, however, be experimentally eliminated.<sup>29</sup> Overall, the typical uncertainty in  $D_M$  might be 10-20%; and further, as these analyses of potential sources of error indicate, this error would probably be systematic. Referring back to equations (2.79) and (2.80), it can be seen that a given fractional error in the estimate of the intramembrane resistance (e.g., as caused by error in correcting for

extramembrane resistance) would lead to a similar fractional error in the value of  $D_M$ .

More recently, and of more relevance to the work of this dissertation, several groups have looked at the diffusion of flexible chain polymers through these relatively ideal track-etched membranes.<sup>29-32,97</sup> (Similarly, convective transport has also been the subject of recent investigations--see references cited in Ref. 29.) The scaling theory analog of the Renkin equation is:

$$D_M/D_0 = \kappa_1 (\kappa_2 \lambda_H)^{-2/3} \exp\{-(\kappa_2 \lambda_H)^{5/3}\} \quad (2.82)$$

This result is a combination of equations (2.14) and (2.39) and as such it is valid for diffusion of dilute, strongly-confined chains in slit-like or cylindrical or other regular pores, with only the constants dependent on the geometry. It has been written in terms of perhaps the most experimentally accessible relative size parameter  $\lambda_H$ .

Cannell and Rondelez<sup>30</sup> examined the diffusion of linear polystyrenes in dilute solution through cylindrical pores ( $0.06 < \lambda_H < 0.72$ ), and concluded that their results could be described equally well by the Renkin equation (with  $\lambda_S = 1.45 \lambda_H$ ) or by the scaling equation (with  $\kappa_1 = 0.379$  and  $\kappa_2 = 4$ ). They also performed a single run at a higher semi-dilute concentration and observed the higher effective diffusion coefficient predicted by scaling theory (because of an increase in  $K_D$ ). Some experimental notes: they did not correct for boundary layer resistance, having estimated it at less than 20% of the total; initial concentrations were the same for all molecular weights save one; and they did notice a 5-10% decrease in  $R_H$  for

polymer having diffused through the membrane (but was this extrapolated to  $c=0$  as the initial  $R_H$  values were?).

This work was extended by Guillot, Léger, and Rondelez,<sup>29,97</sup> principally focusing on diffusion of semi-dilute solutions, but rechecking dilute solution diffusion. Again, dilute solution data for  $D_M/D_0$  could be fit equally well by the Renkin equation or the scaling theory. However, a somewhat different fitting approach was taken: lacking knowledge of  $n_p$  in equation (2.80), they estimated the membrane constant by force-fitting (at  $\lambda_H = 0.1$ ) to the Renkin equation (2.81) (assuming  $\lambda_S = \lambda_H$ ?). Also, they reported  $\kappa_1=0.32$  and  $\kappa_2=2.5$ , claiming that  $\kappa_2$  is the same (it would appear to differ) as Cannell and Rondelez;<sup>30</sup> perhaps their reported  $\kappa_1$  and  $\kappa_2$  were actually for equation (2.82) with  $\lambda_H$  replaced by  $1.45 \lambda_H$ . Their work also confirmed qualitatively the scaling predictions for enhanced diffusion in semi-dilute solution due to higher  $K_D$  values as the correlation length decreases (e.g.,  $D_M/D_0$  for  $\lambda_H \approx 1$  is about 100 times higher than the hard sphere  $D_M/D_0$ ); this is also in accord with the semi-dilute partitioning experiments of Satterfield et al.<sup>74</sup> The boundary layer resistance, estimated to be less than 20%, was not corrected for in these experiments.

In order to address the question as to the "proper" polymer radius to use in these theories, Deen, Bohrer, and Epstein,<sup>31</sup> and Bohrer, Patterson, and Carroll<sup>32</sup> have compared the diffusion of short-chain branched (essentially linear) dextrans to that of ficoll, a very highly crosslinked and compact polysaccharide. The initial study by Deen et al.<sup>31</sup> clearly showed less hindrance to diffusion for linear dextran versus compact ficoll at equivalent  $\lambda_H$  values. However, certain methodological problems, i.e., diffusion of highly

polydisperse samples with diffusion of each fraction being calculated by deconvoluting a SEC chromatogram, prevented firm conclusions. In fact, the observation (not noted by them) that the extrapolation of their  $D_M/D_0$  data to  $\lambda_H = 0$  would give  $D_M/D_0$  significantly greater than unity for *both* ficoll and dextran indicates systematic error and prevents quantitative comparison with theory. Bohrer et al.<sup>32</sup> performed a similar comparative study of ficoll ( $\lambda_H = 0.01-0.66$ ) and dextran ( $\lambda_H = 0.01-1.00$ ) using relatively monodisperse fractions, and again observed significantly less hindrance to diffusion for dextran than for ficoll. The  $D_M/D_0$  data for ficoll were fit well, even up to  $\lambda_H = 0.66$ , using the Paine and Scherr (sophisticated centerline) version of the Renkin equation, whereas  $D_M/D_0$  data for dextran were consistently higher than values for ficoll at the same  $\lambda_H$  (e.g., even for  $\lambda_H = 1$ ,  $D_M/D_0 \approx 0.04$ ). Again, the  $D_M/D_0$  data (for dextran only) appear to extrapolate to a value exceeding unity at  $\lambda_H = 0$ . In both experiments,<sup>31,32</sup> the only explanation offered for the difference between ficoll and dextran was the greater ability of flexible dextrans to "change configuration" in the pores. (The peculiar "free-draining" concept of Colton et al.<sup>16</sup> was mentioned but not embraced.)

This review of membrane transport experiments has not been but comprehensive, but sufficient to give the most significant and relevant results; references to other experimental work somewhat arbitrarily not included can be found in the papers cited. Closing with a summary, the results of experiment, especially using track-etched membranes, are in fundamental agreement with theories for diffusion through simple pores. Nonetheless, questions remain as to the extent of quantitative agreement; this is especially so for flexible polymers. Ultimately, the comparison of

experiment to theory rests on how well certain difficulties, such as determination of porosity, pore radius, and boundary layer resistance, can be resolved. A perhaps unfortunate aspect of membrane experiments is that the effective diffusion coefficient includes both partitioning and hindered diffusivity effects.

The technique of dynamic light scattering has been used previously to study Brownian dynamics in confined geometries,<sup>43-45,98</sup> as was learned near the completion of this work. These previous studies have demonstrated the utility of dynamic light scattering in studying hindered diffusivity (due to hydrodynamic particle-wall interactions<sup>43,44</sup>), and in studying other fundamental aspects of Brownian motion near a bounding surface.<sup>45</sup> Independently, two groups have investigated the diffusion of polystyrene latex spheres (radius  $R_p$ ) between parallel plates (spacing  $L$ ) as a function of  $R_p/L$  ( $0.01 < R_p/L < 0.25$ ) using heterodyne techniques.<sup>43,44</sup> By proper alignment, the scattering wavevector in these studies was constrained to lie parallel to the walls, giving the parallel diffusivity. The results of these somewhat different experiments--a dilute solution with supporting electrolyte (i.e., non-interacting)<sup>44</sup> versus concentrated suspensions<sup>43</sup>--were in good agreement with Faxén's results<sup>4,43,44</sup> for the motion of a sphere between parallel plates, a result that is similar to that given earlier for cylindrical pores, i.e., equations (2.26) and (2.27).

Other researchers have looked at dynamic light scattering from evanescent waves--illuminated regions, having a (variable) thickness about the wavelength of light, and lying parallel to a flat surface--to examine Brownian motion near a bounding surface.<sup>45,98</sup> The non-exponential

correlation functions observed for spheres near a reflecting wall can be explained completely on the basis of the theory for Brownian motion near a wall.<sup>45</sup> Although the system was such that hydrodynamic interactions between spheres and wall could be neglected, work is reported underway to probe those effects.<sup>45</sup>

Having reviewed experiments measuring fluxes (transient diffusion, membrane transport) and ensemble averaged Brownian motion (light scattering), it should be mentioned that, in the spirit of the classical experiments of Perrin, the Brownian motion of single particles ( $\approx 1 \mu\text{m}$ ) in tubes ( $\approx 150 \mu\text{m}$  diameter) has been examined directly using a microscope equipped with a movie camera.<sup>38,39</sup> These experiments have not been aimed at measuring hindered diffusion; a possible complication would be sedimentation and limited range of relative size parameter.

Lastly, several miscellaneous experiments on diffusion in porous materials are mentioned to illustrate points of interest. A number of groups have studied diffusion of liquids in porous aluminas (e.g., see<sup>35-37</sup>). For these materials with small pore sizes: (1) the solute may be of comparable size to the solvent, hence not excluded by steric partitioning;<sup>35</sup> (2) partitioning may depend largely on preferential adsorption;<sup>35</sup> (3) pore sizes are often quite non-uniform; and (4) treating small solutes as massive bodies (i.e., continuum hydrodynamics), although perhaps a reasonable approximation in unbounded solution, might not be a good approach in pores. For all these reasons, interpretation of hindered diffusion on the basis of the Renkin equation, or various other *ad hoc* functions of the relative size  $\lambda$ , is dubious.

Other studies are noted to call attention to techniques which unambiguously measure self-diffusion. Since the nature of the systems to which these techniques have been applied obviates interpretation on the basis of steric partitioning and continuum hydrodynamics, the results are not detailed. Pulsed field gradient spin echo NMR has been used to look at the diffusion of neat liquids in porous sandstones<sup>41</sup> and crosslinked polystyrene packings,<sup>42</sup> and of *adsorbed* liquids in porous glasses,<sup>99</sup> aluminas, etc. A  $D_{\text{EFF}}$  is extracted from the time constant of the spin echo signal attenuation envelope. Practically, the interpretation is often clouded by the necessity to separate a contribution from diffusion in bulk liquid (i.e., interstitial regions) from that inside pores; or clouded due to presence of strong interactions of liquid with surfaces, although this is often the phenomenon of primary interest. Forced Rayleigh scattering<sup>100</sup> has been used to study the diffusion of a dye in porous Vycor glass.<sup>40</sup> This technique monitors the decrease in intensity diffracted from a photochemically induced transient optical grating, said intensity proportional to the square of the concentration of optically excited species. Diffusion of the dye in the presence and absence of adsorption was compared; a single exponential decay was observed only for surface treated glass. Their interpretation was made solely in terms of the geometry of the glass (i.e., tortuosity and porosity), despite a relative size parameter of about 1/5; the models they used, both classical and fractal, are for the diffusion of point particles. (The  $D_{\text{EFF}}$  measured in these forced Rayleigh experiments does not include a factor of the porosity, contrary to the assumption of these authors.)

## CHAPTER III

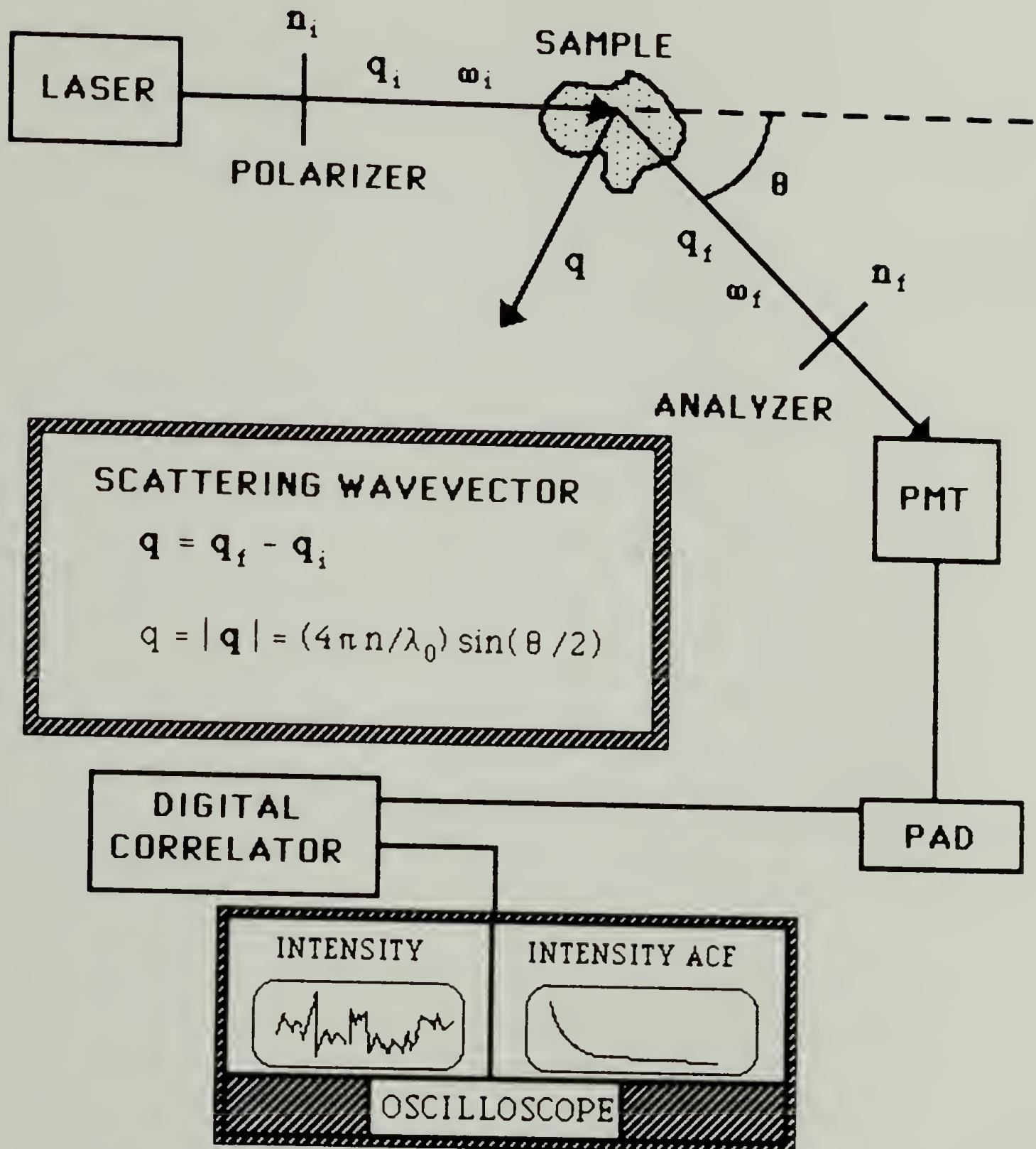
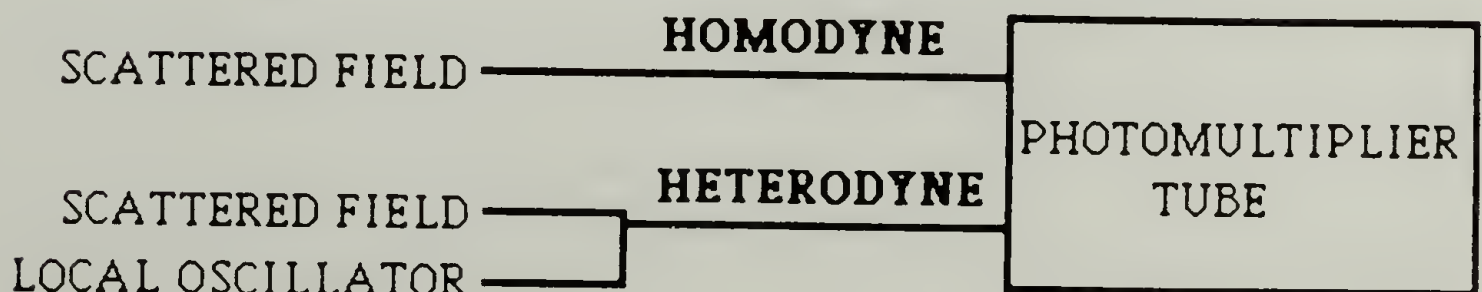
### DYNAMIC LIGHT SCATTERING: THEORY

#### Basics

The scattering of light can provide useful information on the structure, dynamics, and thermodynamics of a wide variety of systems. Basic light scattering theory, and its historical development and applications, have been presented in a number of excellent monographs: the scattering from particles small (Rayleigh-Debye scattering) and large (Mie scattering) compared to the wavelength of light;<sup>101,102</sup> the scattering from polymer solutions,<sup>15,102-104</sup> including a collection of the classical papers;<sup>105</sup> and light scattering as a tool to study the dynamics of a variety of systems.<sup>13-15,106</sup> This section summarizes those aspects of light scattering theory relevant to the work of this dissertation, and introduces the notation to be used in presenting and discussing dynamic light scattering data.

The basic light scattering experiment is shown schematically in Figure 5. Incident light (subscript i) with polarization  $\mathbf{n}_i$ , frequency  $\omega_i$ , and propagating wavevector  $\mathbf{q}_i$  impinges on a sample, thereby inducing oscillating dipoles in the scattering medium. These oscillating dipoles in turn re-radiate light, giving rise to some generally complex pattern of scattered light. In the experiment, one measures the intensity of scattered light (subscript f) with some propagating wavevector  $\mathbf{q}_f$  as defined by the scattering angle  $\theta$ , frequency  $\omega_f$ , and polarization  $\mathbf{n}_f$ . This intensity is deter-

Figure 5. Dynamic Light Scattering

COMMON EXPERIMENTAL OPTIONS:

mined by the amplitude and phase relationships of the components of the scattered electric field, in turn determined by the configuration of the molecules in the sample. In a gas or liquid, that configuration changes with time due to molecular motions, giving rise to fluctuations in intensity.

In a dynamic light scattering experiment, one examines the time correlations in this fluctuating intensity. The intensity autocorrelation function (ACF), to be denoted by  $G^{(2)}(\mathbf{q}, t)$ , is the experimentally measurable time correlation function of these fluctuations, and is defined as:

$$\begin{aligned} G^{(2)}(\mathbf{q}, t) &= \langle I(\mathbf{q}, 0) I(\mathbf{q}, t) \rangle \\ &= \lim_{T \rightarrow \infty} \frac{1}{2T} \int_{-T}^T I(\mathbf{q}, \tau) I(\mathbf{q}, \tau + t) d\tau \end{aligned} \quad (3.1)$$

where  $t$  is the delay time and  $\mathbf{q}$  is the scattering wavevector, which is defined as:

$$\mathbf{q} = \mathbf{q}_i - \mathbf{q}_f \quad (3.2)$$

Since the scattering is nearly elastic,  $|\mathbf{q}_i| \cong |\mathbf{q}_f|$ , giving by simple geometry the magnitude of  $\mathbf{q}$ :

$$q = |\mathbf{q}| = (4\pi n/\lambda_0) \sin(\theta/2) \quad (3.3)$$

where  $n$  is the sample refractive index and  $\lambda_0$  the wavelength in vacuo. The intensity ACF is a measure of the correlation between the molecular configuration at a given time, as reflected in the intensity at that time, to the configuration at some later time  $t$ , again, as reflected in the intensity; as

such, the intensity ACF is related to dynamical processes in the scattering medium.

These dynamical processes can also be related to the spectrum of the scattered light. Although the scattering process is very nearly elastic, in that there is a large change in momentum ( $h\mathbf{q}/2\pi$ ) but very little change in energy (e.g., 1 part in  $10^{10}$ ), there are nonetheless very small frequency shifts  $\omega = \omega_i - \omega_f$ , essentially Doppler shifts, that are caused by time dependent fluctuations in the scattering medium. The goal is to relate the spectrum of scattered light, or alternatively, the intensity ACF given by equation (3.1), to the underlying dynamics.<sup>13-15,106</sup> Of particular interest here is showing the relationship between the intensity ACF of light scattered from a polymer solution and the Brownian motion of the polymer molecules in that solution.<sup>15,46,47</sup>

Unfortunately, it is not the intensity ACF, but instead the scattered electric field ACF, that is fundamentally related to the dynamics of the scattering medium. The scattered electric field ACF, to be denoted by  $G_s^{(1)}(\mathbf{q},t)$ , is defined as:

$$\begin{aligned} G_s^{(1)}(\mathbf{q},t) &= \langle E_s^*(\mathbf{q},0) E_s(\mathbf{q},t) \rangle \\ &= \lim_{T \rightarrow \infty} \frac{1}{2T} \int_{-T}^T E_s^*(\mathbf{q},\tau) E_s(\mathbf{q},\tau+t) d\tau \end{aligned} \quad (3.4)$$

Normalized intensity and electric field ACFs are introduced as:

$$g^{(2)}(\mathbf{q},t) = \frac{\langle I(\mathbf{q},0) I(\mathbf{q},t) \rangle}{\langle I(\mathbf{q},0) I(\mathbf{q},0) \rangle} \quad (3.5)$$

$$g_s^{(1)}(\mathbf{q}, t) = \frac{\langle E_s^*(\mathbf{q}, 0) E_s(\mathbf{q}, t) \rangle}{\langle E_s^*(\mathbf{q}, 0) E_s(\mathbf{q}, 0) \rangle} \quad (3.6)$$

These normalized ACFs are often more convenient to use, as they decrease from one to zero for scattering from random thermal fluctuations.

It can be shown<sup>13,15</sup> that  $g_s^{(1)}(\mathbf{q}, t)$  is proportional to the ACF of the  $\mathbf{q}^{\text{th}}$  Fourier component of dielectric constant fluctuations in the scattering medium:

$$g_s^{(1)}(\mathbf{q}, t) \propto \langle \delta \epsilon_{if}^*(\mathbf{q}, 0) \delta \epsilon_{if}(\mathbf{q}, t) \rangle \quad (3.7)$$

where

$$\delta \epsilon_{if}(\mathbf{q}, t) = \mathbf{n}_f \cdot \delta \underline{\epsilon}(\mathbf{q}, t) \cdot \mathbf{n}_i \quad (3.8)$$

is the component of the dielectric constant fluctuation tensor along the initial and final polarization directions, and where

$$\delta \underline{\epsilon}(\mathbf{q}, t) = \int d\mathbf{r} \exp(i\mathbf{q} \cdot \mathbf{r}) \delta \underline{\epsilon}(\mathbf{r}, t) \quad (3.9)$$

is the Fourier transform of the spatial dielectric fluctuations. This continuum approach (i.e., in terms of the dielectric constant) to light scattering is perhaps the most general, and shows that the frequency-integrated intensity is proportional to  $\langle \delta \epsilon_{if}^*(\mathbf{q}) \delta \epsilon_{if}(\mathbf{q}) \rangle$ , that is, to the square of the  $\mathbf{q}^{\text{th}}$  dielectric fluctuation projected onto the polarization directions. At a given wavevector  $\mathbf{q}$ , as fixed by the experimental geometry, the scattering which is seen is scattering from dielectric fluctuations for which the Bragg condition is satisfied, that is, it is scattering from fluctuations of spacing  $\mathbf{q}$  in reciprocal

space. It should be noted that, by the Wiener-Khintchine theorem, the spectral density of the scattered light is proportional to the Fourier transform of  $\langle E_s^*(\mathbf{q},0) E_s(\mathbf{q},t) \rangle$ , or alternatively,  $\langle \delta\epsilon_{if}^*(\mathbf{q},0) \delta\epsilon_{if}(\mathbf{q},t) \rangle$ .<sup>13,15</sup> Aside from remarking that the width of the power spectrum is related to the decay time of the corresponding ACFs,<sup>13,15</sup> all further discussion of the frequency domain will be shunned in favor of the time domain, where the measurements of this dissertation reside.

The molecular approach to light scattering,<sup>15</sup> to be considered now, is intuitively useful in considering Brownian motion (e.g., in a porous material), but nonetheless involves some approximation with regard to the proper phenomenology of diffusion. Despite some such limitations, this approach has been quite useful in modeling the scattering from dilute solutions of macromolecules. For a dilute solution of monodisperse isotropic scatterers (polarizability  $\alpha$ ), small compared to the wavelength of light, the scattered electric field can be written as:

$$E_s(\mathbf{q},t) = \sum_i \alpha \exp i \mathbf{q} \cdot \mathbf{r}_i(t) \quad (3.10)$$

where  $\mathbf{r}_i(t)$  is the center of mass position of the  $i^{\text{th}}$  particle at time  $t$  and the sum is over particles in the scattering volume. Using this result with equation (3.6), the normalized scattered electric field ACF can be written:

$$g_s^{(1)}(\mathbf{q},t) = \frac{S(\mathbf{q},t)}{S(\mathbf{q},0)} = \frac{\langle \sum_i \sum_j \exp i \mathbf{q} \cdot (\mathbf{r}_j(t) - \mathbf{r}_i(0)) \rangle}{\langle \sum_i \sum_j \exp i \mathbf{q} \cdot (\mathbf{r}_j(0) - \mathbf{r}_i(0)) \rangle} \quad (3.11)$$

thereby defining the static and dynamic structure factors,  $S(\mathbf{q},0) = S(\mathbf{q})$  and  $S(\mathbf{q},t)$ . Under the assumption of statistically independent particles,<sup>15</sup> this reduces to:

$$g_s^{(1)}(\mathbf{q},t) = (1/\langle N \rangle) \langle \sum \exp i\mathbf{q} \cdot \Delta \mathbf{R}_i(t) \rangle \quad (3.12)$$

where  $\Delta \mathbf{R}_i(t) = \mathbf{r}_i(t) - \mathbf{r}_i(0)$  is the displacement of the  $i^{\text{th}}$  particle in time  $t$  and  $\langle N \rangle$  is the average number of particles in the scattering volume.

Equations (3.11) and (3.12) have been written so as to emphasize the nature of the averaging which is inherent in time correlation functions from light scattering, namely, the time-average of a property which is in turn a function of the generalized coordinates of the ensemble of particles in the scattering volume. This is contrasted to theoretical calculations, where usually an ensemble-averaged time correlation function is computed; for example, the theoretical calculation for equation (3.12) would be for the ensemble-averaged quantity  $\langle \exp i\mathbf{q} \cdot \Delta \mathbf{R}_i(t) \rangle$ . Under the assumption that the system is ergodic, these averages will be the same; this usual assumption will be presumed.<sup>15</sup>

Returning to equation (3.11), it is seen that  $g_s^{(1)}(\mathbf{q},t)$  can be predicted from a model prescribing the time dependence of the quantity  $(\mathbf{r}_j(t) - \mathbf{r}_i(0))$ . Considering only the case of statistically independent particles, as is often a reasonable approximation for dilute solutions of macromolecules, and assuming equivalence of time and ensemble averages, evaluation of equation (3.12) reduces to calculating the self-intermediate scattering function<sup>15</sup>  $F_s(\mathbf{q},t)$ , that is, for this simple case:

$$g_s^{(1)}(\mathbf{q},t) = F_s(\mathbf{q},t) \quad (3.13)$$

with  $F_S(\mathbf{q}, t)$  defined as

$$F_S(\mathbf{q}, t) = \langle \exp i\mathbf{q} \cdot \Delta\mathbf{R}_i(t) \rangle \quad (3.14)$$

$F_S(\mathbf{q}, t)$  is the characteristic function of the Green's function  $P(\mathbf{R}, t | \mathbf{R}', 0)$ , which is the probability for a particle to undergo a displacement from  $\mathbf{R}'$  to  $\mathbf{R}$  in time  $t$ :

$$P(\mathbf{R}, t | \mathbf{R}', 0) = \langle \delta((\mathbf{R} - \mathbf{R}') - \Delta\mathbf{R}_i(t)) \rangle \quad (3.15)$$

The functions  $F_S(\mathbf{q}, t)$  and  $P(\mathbf{R}, t | \mathbf{R}', 0)$  are a Fourier transform pair, a relation which holds regardless of the dynamic model for  $\Delta\mathbf{R}_i(t)$ .

For scattering from a non-interacting dilute polymer solution, there are two alternative but equivalent models<sup>15</sup> to consider for  $P(\mathbf{R}, t | \mathbf{R}', 0)$ , in terms of either diffusion or Brownian motion. For times long compared to the velocity correlations (which die rapidly for massive particles),  $P(\mathbf{R}, t | \mathbf{R}', 0)$  is the solution to the diffusion equation

$$\partial P / \partial t = D_S \nabla^2 P \quad (3.16)$$

subject to the initial condition ( $t = 0$ )

$$P(\mathbf{R}, 0 | \mathbf{R}', 0) = \langle \delta(\mathbf{R} - \mathbf{R}') \rangle = \delta(\mathbf{R} - \mathbf{R}') \quad (3.17)$$

with  $D_S$  the self-diffusion coefficient. These equations can be transformed to give:

$$\partial F_S / \partial t = -q^2 D_S F_S \quad (3.18)$$

$$F_S(\mathbf{q}, 0) = 1 \quad (3.19)$$

solution of which yields

$$F_s(\mathbf{q}, t) = \exp(-q^2 D_s t) = \exp(-\Gamma t) \quad (3.20)$$

with the relaxation rate

$$\Gamma = D_s q^2 \quad (3.21)$$

The alternative approach is to directly consider this diffusion in terms of Brownian motion. For relatively long times, the distribution of displacements,  $\Delta \mathbf{R} = \mathbf{R} - \mathbf{R}'$ , is a Gaussian:

$$P(\mathbf{R}, t | \mathbf{R}', 0) = \{(2\pi \langle \Delta R^2(t) \rangle / 3)\}^{-3/2} \exp\{-3(\Delta \mathbf{R})^2 / 2 \langle \Delta R^2(t) \rangle\} \quad (3.22)$$

with  $\langle \Delta R^2(t) \rangle$  the mean square displacement in time  $t$ . The transform of this Gaussian gives:

$$F_s(\mathbf{q}, t) = \exp(-q^2 \langle \Delta R^2(t) \rangle / 6) \quad (3.23)$$

which can be compared with equation (3.20).

The extension of these results to diffusion and Brownian motion in confined spaces (e.g., a porous material), where one must add reflecting boundary conditions to the solution of equation (3.16) or equation (3.18), is discussed in the second section of this chapter.

The major assumption of the preceding development, that each particle behaves independently, implies that the results will strictly be valid only for non-interacting macromolecular solutions in the limit of infinite dilution. In a light scattering experiment (at finite concentration), one obtains not the self-diffusion coefficient  $D_s$  (i.e., the "true diffusivity" in the

language of Chapter II, section 3), but the mutual diffusion coefficient  $D_C$ , which corresponds to  $D_S$  only in this limit.<sup>15,107-109</sup> The fundamental difference between  $D_C$  and  $D_S$ , and the demonstration that it is  $D_C$  not  $D_S$  that is measured by dynamic light scattering, is made clear by comparing the results of non-equilibrium thermodynamics<sup>87,15</sup> (applied to binary diffusion) to the light scattering formalism developed thus far.

It can be shown<sup>15</sup> that the scattered electric field  $E_s(\mathbf{q},t)$  (e.g., equation (3.10)) is proportional to the  $\mathbf{q}^{\text{th}}$  Fourier component of the number density fluctuations  $\delta\rho(\mathbf{q},t)$  or, equivalently, of the concentration fluctuations  $\delta c(\mathbf{q},t)$ . Hence, using equation (3.6), the scattered electric field ACF could be written as:

$$g_s^{(1)}(\mathbf{q},t) = \frac{\langle \delta c^*(\mathbf{q},0) \delta c(\mathbf{q},t) \rangle}{\langle |\delta c(\mathbf{q},0)|^2 \rangle} \quad (3.24)$$

This corresponds to equation (3.11), *not* (3.12), given previously. From non-equilibrium thermodynamics, the flux of solute (component 1) in a laboratory-fixed coordinate system is:<sup>87,15</sup>

$$\mathbf{J}_1 = - D_C \nabla c_1 \quad (3.25)$$

with  $D_C$  the (laboratory-fixed) mutual diffusion coefficient, and  $c_1$  the solute concentration. Combined with the continuity equation, this gives

$$\partial c_1 / \partial t = D_C \nabla^2 c_1 \quad (3.26)$$

Equation (3.26) can be rewritten by substituting  $c_1 = \langle c_1 \rangle + \delta c$ , yielding the diffusion equation for the fluctuations:

$$\partial \delta c(\mathbf{r},t)/\partial t = D_C \nabla^2(\delta c(\mathbf{r},t)) \quad (3.27)$$

Solution<sup>110</sup> of the transform of equation (3.27) for  $\delta c(\mathbf{q},t)$  results in the following ACF for the concentration fluctuations:

$$\langle \delta c^*(\mathbf{q},0) \delta c(\mathbf{q},t) \rangle = \langle |\delta c(\mathbf{q},0)|^2 \rangle \exp(-q^2 D_C t) \quad (3.28)$$

Comparison with equation (3.24) indicates that

$$g_s^{(1)}(\mathbf{q},t) = \exp(-q^2 D_C t) \quad (3.29)$$

hence that the diffusion coefficient measured by light scattering is identified as the mutual diffusion coefficient. The phenomenology of non-equilibrium thermodynamics gives  $D_C$  as:<sup>87,15,109</sup>

$$D_C = \frac{(1 - \phi_1) c_1}{N_A f_1} \cdot (\partial \mu_1 / \partial c_1)_{T,P} \quad (3.30a)$$

or as<sup>107-109</sup>

$$D_C = \frac{(1 - \phi_1) c_1}{N_A f_1} \cdot (\partial \mu_1 / \partial c_1)_{T,\mu_0} \quad (3.30b)$$

where  $\phi_1$ ,  $f_1$ , and  $\mu_1$  are the volume fraction, mutual friction coefficient, and chemical potential of the solute,  $N_A$  is Avogadro's number, and  $\mu_0$  is the chemical potential of the solvent. It is claimed<sup>109</sup> that  $D_C$  given by equation (3.30b) is that appropriate for dynamic light scattering (random Brownian motion at thermal equilibrium,  $\mu_0$  constant) whereas the  $D_C$  of equation (3.30a) is appropriate for conventional gradient experiments. Regardless, in

either case, one sees in the limit of infinite dilution, that  $1 - \phi_1 \equiv 1$  and  $(1/N_A)(\partial\mu_1/\partial c_1)_{T,x} \approx kT/c_1$  and  $f_1 \equiv \zeta_1$  where  $\zeta_1$  is the friction coefficient at infinite dilution, hence

$$\lim_{c_1 \rightarrow 0} D_C = \frac{kT}{\zeta_1} = D_S \quad (3.31)$$

It is also clearly seen that the diffusion coefficient  $D_C$  measured by light scattering (i.e., equation (3.30)) is fundamentally different than the self-diffusion coefficient  $D_S$  given by the Einstein relation (i.e., equation (3.31)).

The diffusion coefficient from light scattering is often used to calculate a hydrodynamic radius  $R_H$  by means of the Stokes-Einstein relation:

$$D_C = \frac{kT}{6\pi\eta_s R_H} \quad (3.32)$$

where  $\eta_s$  is the solvent viscosity. Two features of  $R_H$  as so *defined* are that, by equations (3.30) and (3.31), it only acquires a purely frictional interpretation in the limit of infinite dilution (i.e., equation (3.32) is strictly valid only for  $D_C = D_S$ ); and that, for non-spherical particles (e.g., flexible polymers or rods), even in the  $c = 0$  limit,  $R_H$  has the interpretation of being the radius of a hydrodynamically equivalent sphere.

This review of light scattering theory turns now to somewhat more practical aspects. Most of the discussion thus far has centered on the scattered electric field ACF,  $g_s^{(1)}(\mathbf{q}, t)$ , which is fundamentally related to dynamical processes in the scattering medium. However, it is not  $g_s^{(1)}(\mathbf{q}, t)$ , but instead the intensity ACF,  $g^{(2)}(\mathbf{q}, t)$ , that is measured experimentally,

insofar as photon detectors (e.g., photomultipliers) have a response that is proportional to the square of the incident electric field, not to the electric field itself.

The relation of  $g^{(2)}(\mathbf{q}, t)$  to  $g_s^{(1)}(\mathbf{q}, t)$  depends on the experimental arrangement, two of which are common (Figure 5). In the homodyne (self-beating) method, only light scattered from the sample hits the detector. In the heterodyne technique, a coherent local oscillator field ( $E_{LO}$ ) is mixed with the scattered field ( $E_s$ ) on the photocathode. For the homodyne experiment, the intensity ACF is:

$$G^{(2)}(t) = \langle I(0) I(t) \rangle = \langle |E_s(0)|^2 |E_s(t)|^2 \rangle \quad (3.33)$$

and for the heterodyne experiment

$$G^{(2)}(t) = \langle I(0) I(t) \rangle = \langle |E_s(0) + E_{LO}(0)|^2 |E_s(t) + E_{LO}(t)|^2 \rangle \quad (3.34)$$

Actually, what is correlated in an actual experiment is the photomultiplier (PM) output, either an analog current, or most commonly single photon pulses; however, this PM output is proportional to  $I(t)$ , and the correlated PM output to  $\langle I(0) I(t) \rangle$ . Two excellent review of optical mixing techniques have been given, by Chu<sup>13</sup> and by Pike and Jakeman,<sup>111</sup> discussing with much greater precision and detail the material to follow; a less elaborate presentation has been given by Berne and Pecora.<sup>15</sup>

For the homodyne experiment, if the scattered electric field  $E_s$  is a Gaussianly distributed random variable (the "Gaussian approximation"), then the relation between  $G_s^{(2)}$  and  $G_s^{(1)}$  (or  $g_s^{(2)}$  and  $g_s^{(1)}$ ) is given by the Siegert relation:<sup>13,15,111</sup>

$$G_s^{(2)}(\mathbf{q}, t) = |G_s^{(1)}(\mathbf{q}, 0)|^2 + |G_s^{(1)}(\mathbf{q}, t)|^2 \quad (3.35a)$$

$$g_s^{(2)}(\mathbf{q}, t) = 1 + |g_s^{(1)}(\mathbf{q}, t)|^2 \quad (3.35b)$$

where the subscript  $s$  signifies homodyne ACFs.

For the heterodyne experiment,<sup>13,15,111</sup> expansion of equation (3.34) leads to a complicated expression with sixteen terms. To simplify this expression, two assumptions are usually made: (1) fluctuations in  $E_{LO}$  are negligible; and (2) fluctuations of  $E_{LO}$  and  $E_s$  are uncorrelated. With these assumptions,

$$g^{(2)}(t) = 1 + \{\langle I_s \rangle \langle I_{LO} \rangle / \langle I \rangle^2\} \{e^{i\omega t} g_s^{(1)}(t) + e^{-i\omega t} g_s^{(1)*}(t)\} + \{\langle I_s \rangle^2 / \langle I \rangle^2\} \{g_s^{(2)}(t) - 1\} \quad (3.36)$$

where  $\langle I \rangle = \langle |E_s + E_{LO}|^2 \rangle$ ,  $\omega = \omega_{LO} - \omega_s$ , and  $g_s^{(2)}$  and  $g_s^{(1)}$  are as previously defined. Equation (3.36) often admits to further simplification. Usually, the local oscillator frequency is the same as that of the scattered light, so that  $\omega=0$  (i.e., "homodyne" heterodyne). In the absence of directed motion (e.g., electrophoresis),  $g_s^{(1)}(\mathbf{q}, t)$  is real and even. Lastly, if the experiment is in the "strong heterodyne" limit, then  $\langle I_{LO} \rangle \gg \langle I_s \rangle$ . With these stipulations, equation (3.36) reduces to:

$$g^{(2)}(\mathbf{q}, t) = 1 + \frac{2\langle I_s \rangle \langle I_{LO} \rangle}{\langle I \rangle^2} \text{Re}\{g_s^{(1)}(\mathbf{q}, t)\} \quad (3.37)$$

Due to the "peculiar" nature of the local oscillator employed in the experiments of this dissertation, namely, scattering from the stationary porous

material, these assumptions, particularly (1) and (2) above, will be examined critically in Chapter V.

Spatial coherence considerations<sup>13,15,111</sup> (i.e., the coherence of  $E_S$ , or of  $E_S + E_{LO}$  over the illuminated PM cathode area) demand that the above equations be modified. Introducing the coherence function  $f_C$ , equations (3.35b) and (3.37) read:

$$g_S^{(2)}(\mathbf{q}, t) - 1 = f_C |g_S^{(1)}(\mathbf{q}, t)|^2 \quad (3.38)$$

$$g^{(2)}(\mathbf{q}, t) - 1 = f_C \frac{2\langle I_S \rangle \langle I_{LO} \rangle}{\langle I \rangle^2} \text{Re}\{g_S^{(1)}(\mathbf{q}, t)\} \quad (3.39a)$$

$$g^{(2)}(\mathbf{q}, t) - 1 = f_C^+ \text{Re}\{g_S^{(1)}(\mathbf{q}, t)\} \quad (3.39b)$$

The coherence function  $f_C$  depends for the most part on the optical arrangement, and additionally for heterodyne experiments on the efficiency of mixing (wave front matching) of  $E_S$  and  $E_{LO}$ . For the sample times employed, temporal coherence effects<sup>111</sup> can be ignored.

For a solution of monodisperse isotropic scatterers, substitution of the result for  $g_S^{(1)}(\mathbf{q}, t)$  given by equation (3.29) into equations (3.38) and (3.39b) gives the desired expressions relating the measured intensity ACF to the mutual diffusion coefficient, wavevector, and delay time:

$$g_S^{(2)}(\mathbf{q}, t) - 1 = f_C \exp(-2 q^2 D_C t) \quad (3.40)$$

$$g^{(2)}(\mathbf{q}, t) - 1 = f_C^+ \exp(-q^2 D_C t) \quad (3.41)$$

for homodyne (Gaussian approximation) and heterodyne experiments respectively. Now equation (3.29), on which these results are based, relies

on several assumptions which are rarely, if ever, all valid for real polymer solutions. Polymer samples are generally polydisperse, each fraction having a different scattering power and diffusion coefficient. In addition, the light scattered by a polymer will generally depend not only on its position, but also on its orientation and conformation, so that rotational diffusion and internal motions affect the fluctuations in scattered intensity.

A general form for  $g_s^{(1)}(\mathbf{q}, t)$  can be written taking into account this multiplicity of relaxation processes:

$$g_s^{(1)}(\mathbf{q}, t) = \int_0^\infty G(\Gamma, \mathbf{q}) \exp(-\Gamma t) d\Gamma \quad (3.42)$$

where  $G(\Gamma, \mathbf{q})$  is the distribution of amplitudes of the generalized relaxation modes with relaxation rates  $\Gamma$ . It is implicitly assumed that the relaxation processes all satisfy "normal" diffusion equations, that is, relaxing exponentially with  $t$ . Formally, this excludes fractal diffusion, and diffusion with an additional power law decay term (e.g., see Chapter II, section 4). Practically, a decomposition into *apparent* relaxation rates as given by equation (3.42) can still provide some useful information even when the use of this equation is not strictly valid.

Any general expression for  $g_s^{(1)}(\mathbf{q}, t)$  can of course be substituted into equations (3.38) and (3.39b) to give expressions for the homodyne and heterodyne intensity ACFs. For example, using equation (3.42) for a polydisperse collection of small (form factor  $\approx 1$ ) isotropic scatterers, where only translational diffusion need be considered, one would have:

$$g_s^{(1)}(\mathbf{q}, t) = \int_0^\infty G(D_C) \exp(-D_C q^2 t) dD_C \quad (3.43)$$

Here the amplitude distribution function is assumed independent of angle, with the scattering intensity (i.e.,  $G(D_C) dD_C$ ) for a given species proportional to the weight concentration of that species times its molecular weight (or alternatively, the number of molecules times the square of the polarizability, or the number times the square of the molecular weight). Hence the average diffusion coefficient is a z-average,  $\langle D_C \rangle_z$ . Returning to equation (3.32) for the hydrodynamic radius, this shows that for a polydisperse sample, the hydrodynamic radius by dynamic light scattering is:

$$R_H \equiv \langle 1/R_H \rangle_z^{-1} \quad (3.44)$$

This equation, together with equation (3.32), provides the operational definition for the hydrodynamic radius which is to be used in this dissertation; it will be denoted simply as  $R_H$ .

### **Applications to Diffusion in Porous Materials**

Although dynamic light scattering has usually been used to study polymer diffusion in unbounded solutions, it also has been used to study diffusion in various sorts of bounded systems and in systems with obstacles: for example, diffusion in strongly interacting colloidal suspensions, where a particle may be "trapped" by its neighbors;<sup>47</sup> diffusion in very small scattering volumes, where "number fluctuations" are seen as a result of particles crossing boundaries;<sup>15</sup> diffusion of probe particles through semi-dilute and concentrated solutions (for a review, see<sup>60</sup>) and gels; and diffusion

inside biological cells.<sup>106</sup> However, only a few light scattering studies have been concerned with Brownian motion and diffusion in bounded systems similar to that of this dissertation, that is, diffusion in close proximity to an impenetrable surface. These previous studies have been on simple systems: diffusion of hard spheres parallel to and between two essentially infinite plane surfaces;<sup>43,44</sup> and diffusion of hard spheres near a single wall.<sup>45</sup> In the first case, a complete expression for  $g_s^{(1)}(\mathbf{q},t)$  was calculated<sup>44</sup> (for  $\mathbf{q}$  parallel to the walls, hence two-dimensional diffusion) using low Reynolds number hydrodynamics results for  $D_{p,\parallel}$  as a function of sphere radius and gap width. In the second case,  $g_s^{(1)}(\mathbf{q},t)$  was calculated from the expression for Brownian motion near a single reflecting wall, taking into account the small scattering volume, but neglecting hydrodynamic interactions.<sup>45</sup>

Although specific expressions for  $g_s^{(1)}(\mathbf{q},t)$  for particles diffusing in random porous media have not been previously derived, the preceding section and the above examples have demonstrated the simple connection that exists between the Green's function solution to the diffusion equation and the scattered electric field ACF. The purpose of this section is to establish along these lines the general connection between the basic light scattering theory presented earlier in this chapter and the phenomenology of diffusion in random porous materials as presented in Chapter II. Since appropriate and exact expressions for  $P(\mathbf{R},t|\mathbf{R}',0)$  are lacking, it is not possible to calculate an exact result for  $g_s^{(1)}(\mathbf{q},t)$ . However, it is possible to establish a correspondence between  $g_s^{(1)}(\mathbf{q},t)$ , in the low wavevector limit, and the macroscopic diffusion phenomenology of Chapter II. The application of dynamic light scattering theory to diffusion in porous materials is further

discussed in Chapters V, VI, and VII, in connection with experimental procedures, data analysis, and results.

The formulation of the relevant diffusion problem has already been given (Chapter II, section 3, equations (2.42) and (2.41d)) and will not be repeated here. That presentation was in terms of  $P(\mathbf{R}, t | \mathbf{R}', 0)$ , corresponding to a molecular approach to light scattering in the infinite dilution limit; however, it could as well have been made in terms of the concentration or concentration fluctuations. If the particle-wall interaction potential is presumed to be "hard sphere" repulsive (i.e.,  $E = 0$  for all allowed molecular configurations), then the diffusion problem to be solved is:

$$\partial P / \partial t = \nabla \cdot \mathbf{D}_p \cdot \nabla P + \delta(\mathbf{R} - \mathbf{R}') \delta(t) \quad (3.45a)$$

subject to the reflecting walls boundary condition

$$(\nabla \cdot \mathbf{D}_p) \cdot \mathbf{n}_s = 0 \quad \text{on pore surfaces} \quad (3.45b)$$

Significant obstacles to solution of these equations in the case of random porous media are posed by the spatially dependent diffusivity  $\mathbf{D}_p$  and the boundary condition (3.45b), since: (1) complete results for  $\mathbf{D}_p$  are available only for particles of simple shapes and limited values of relative size diffusing in simple geometries; and (2) the surface geometry is generally complex, hence a specification of  $\mathbf{n}_s$  over the pore surface is impossible.

The general solution for  $P$  in the presence of reflecting walls could perhaps, at least formally, be written as a sum of terms. For instance, for a particle diffusing near a single wall, the well known result is:<sup>112</sup>

$$P(z,t|0,0) = \frac{1}{(4\pi D t)^{1/2}} \{ \exp(-z^2/4Dt) + \exp(-[2z_0-z]^2/4Dt) \} \quad (3.46)$$

where  $P$  is the probability for a particle initially at the origin to be at  $z$  at time  $t$ , given a reflecting wall at  $z = z_0$ . The second image term is not Gaussian in the actual displacement  $z$  but in the displacement from the imaginary source,  $(2z_0-z)$ . More complicated bounding surfaces lead to additional such terms, to satisfy the no-flux boundary condition. Typically such solutions are expressible as infinite sums of such terms.

A few general comments can be made about the behavior, in certain limits, of  $P(\mathbf{R},t|\mathbf{R}',0)$  and its spatial Fourier transform, the self-intermediate scattering function  $F_S(\mathbf{q},t)$ . Because of image source terms, attributable to reflecting walls, the distribution function  $P(\mathbf{R},t|\mathbf{R}',0)$  is fundamentally non-Gaussian in terms of the actual particle displacement, at least for relatively small displacements and short times; hence the transform of  $P$  (i.e.,  $F_S(\mathbf{q},t)$ ) is not generally expected to be a single exponential. The transform of image source terms leads naturally to complex variables (e.g., see<sup>45</sup>); the complete behavior of the resulting  $F_S(\mathbf{q},t)$  as a function of  $\mathbf{q}$  and  $t$  is complicated (e.g., even for reflection from a *single* wall<sup>45</sup>). Qualitatively, one expects that for times very long relative to the average time between collisions with the walls, or alternatively, for very large displacements relative to the dimensions of a pore, that the distribution should again become Gaussian, *at least to first approximation*. (However, see<sup>65,69</sup> as examples of approaches towards considering deviations from Gaussian behavior.)

Now some of the macroscopic (i.e., the long time and large displacement limit) diffusion results from Chapter II are simply rewritten in terms of the distribution  $P$ . For axial motion down a cylindrical tube, one has:

$$P(z,t|0,0) = \frac{1}{(4\pi D_{p,\parallel} t)^{1/2}} \{ \exp(-z^2/4 D_{p,\parallel} t) \} \quad (3.47)$$

with  $D_{p,\parallel}$  the axial diffusivity, either that for hard spheres<sup>8,9</sup> (equation (2.29)) or flexible polymers<sup>10-12</sup> (equation (2.38)). The corresponding result for a random porous material is:

$$P(R,t|0,0) = \frac{1}{(4\pi D_{\infty} t)^{3/2}} \{ \exp(-R^2/4 D_{\infty} t) \} \quad (3.48)$$

with  $D_{\infty}$  the scalar diffusivity (i.e., isotropic porous material assumed) corresponding to the definition of equation (2.62). The spatial Fourier transforms of these Gaussian distributions are of course single exponentials. For diffusion in a cylinder, one has:

$$F_S(\mathbf{q},t) = \exp(-D_{p,\parallel} q_z^2 t) \quad (3.49)$$

with  $q_z$  the component of  $\mathbf{q}$  along the tube axis; and for diffusion in a random porous material:

$$F_S(\mathbf{q},t) = \exp(-D_{\infty} q^2 t) \quad (3.50)$$

It is important to consider at what limit of  $q$  and  $t$  such simple behavior is expected. Brenner and Gajdos<sup>8</sup> give the "long-time" limit, for which equation (3.47) would be valid, as

$$(D_0 t/R_p^2) \gg 1 \quad (3.51)$$

with  $R_p$  the pore radius (or just some characteristic pore dimension) and  $D_0$  the bulk diffusivity. This can be rewritten as:

$$t \gg t_{\text{WALL}} \quad (3.52)$$

defining

$$t_{\text{WALL}} \equiv R_p^2/D_0 \quad (3.53)$$

as the time to diffuse into contact with a wall (neglecting numeric factors). Essentially this condition states that the time be long enough for particles to lose "memory" of their initial radial positions. Perhaps more precise is Lehner's requirement<sup>68</sup> (see Chapter II, section 3) that diffusion must be "quasi-steady" on a pore scale in order to use macroscopic forms of Fick's laws, which of course assume a Gaussian probability distribution function. His result was:

$$|c_p / (\partial c_p / \partial t)| \gg (2R_p)^2/D_0 \quad (3.54)$$

Recognizing that in a light scattering experiment, one is looking not at transient diffusion, as was considered by Lehner,<sup>68</sup> but at relaxation of concentration fluctuations of wavevector  $q$ , this condition (3.54) can be rewritten more clearly after appropriate substitutions, which follow from equation (3.28):

$$c_p \rightarrow \delta c(q,0)$$

$$(\partial c_p / \partial t) \rightarrow (\Delta \delta c / \Delta t) \approx \delta c(q, 0) \cdot \{1 - (1 - D_\infty q^2 t)\} / t$$

This gives as a criterion for macroscopic diffusion

$$(D_\infty q^2)^{-1} \gg t_{\text{WALL}} \quad (3.55)$$

Applied to light scattering, this macroscopic diffusion criterion can be stated as the requirement that the characteristic time associated with the relaxation of a fluctuation of wavevector  $q$  be much longer than the time between wall collisions. It is a requirement that the longitudinal relaxation rate be much slower than the transverse relaxation rate. This criterion will be discussed further in later chapters with regard to our experimental results.

Since  $D_\infty$  and  $t_{\text{WALL}}$  are fixed for a given polymer and porous material, the macroscopic diffusion regime is seen to correspond to the low wavevector limit. This is of course what is expected, with equation (3.55) simply providing a semi-quantitative estimate of this limit.

If the above criterion (3.55) is not satisfied, the "non-Gaussian" effects, which can be attributed to the reflecting walls, are expected to be seen in the correlation function. As mentioned previously, it is clear that the dynamic structure factor will be a function of complex variables. Whether this leads to any "unusual" behavior at higher wavevector (e.g., exponentially damped cosine ACFs) is not known. It is emphasized that theory is lacking for even a firm qualitative understanding of light scattering results at higher  $q$  where such non-Gaussian effects are expected to be important.

One other limit should be noted: for  $t \ll t_{\text{WALL}}$ , such non-Gaussian effects should be negligible, and the corresponding diffusion coefficient should be the true diffusivity  $D_p$ , that is,  $D_0$  as modified by hydrodynamic

interactions with the walls; this differs from the macroscopic diffusivities  $D_{p,\parallel}$  and  $D_\infty$ . (N.B. The non-Gaussian effects referred to here do not imply that the "Gaussian approximation"<sup>13,15</sup> with regard to the scattered electric field does not hold.)

The results for the dynamic structure factor corresponding to the miscellaneous theories mentioned in Chapter II, section 4--the mode-coupling theory for macroscopic diffusion, and the theory for diffusion in a fractal pore space--are given now. For diffusion in a fractal pore space, if  $l_2 \ll q^{-1}$ , with  $l_2$  the upper cutoff length scale of the fractal, one again has the macroscopic diffusion result of equation (3.50), with  $D_\infty$  given by equation (2.72). However, for  $l_1 < q^{-1} < l_2$ , the fractal nature of the pore space should be evident, with:<sup>113</sup>

$$F_S(\mathbf{q}, t) = \exp(- D_{\text{EFF}} q^2 t^{2/d_w}) \quad (3.56)$$

where  $d_w$  is the dynamic fractal walk exponent and  $D_{\text{EFF}}$  is the effective diffusion coefficient. For the mode-coupling theory, an algebraic long time tail is predicted, in addition to the exponential decay:<sup>114</sup>

$$F_S(\mathbf{q}, t) = \exp(- D_\infty q^2 t) + A q^{-2} D_\infty^{-5/2} t^{-5/2} \quad (3.57)$$

where the amplitude  $A$  is related in a complicated way to the degree of disorder in the porous material. The power law term should dominate at sufficiently long times.

The significant results of this section are the expressions given for macroscopic diffusion in cylindrical pores and in a random porous material, equations (3.49) and (3.50). A rough criterion for the applicability of these

results is given as  $(D_{\infty} q^2)^{-1} \gg t_{\text{WALL}}$  or  $(D_{p,\parallel} q_z^2)^{-1} \gg t_{\text{WALL}}$ ; simply put, these macroscopic diffusion results are expected to be approximately valid in the low wavevector limit. At higher wavevector, the behavior of the correlation functions is not known even qualitatively, other than the obvious conclusion that the ACFs are not expected to be single exponential.

As a last point, it is important to note that the porosity does not enter into the effective diffusion coefficients from dynamic light scattering. As shown in Chapter II, the porosity in effect cancels in the macroscopic formulation of Fick's second law. Even if one were to keep in the factor of the porosity and solve for  $\Phi_{cp}$  (or in terms of fluctuations,  $\delta(\Phi_{cp})$ ), it can be seen, by reference to equation (3.24), that the factor of the porosity cancels in the normalized field ACF,  $g_s^{(1)}(\mathbf{q}, t)$ . That is,

$$g_s^{(1)}(\mathbf{q}, t) = \frac{\langle \delta \Phi_c^*(\mathbf{q}, 0) \delta \Phi_c(\mathbf{q}, t) \rangle}{\langle |\delta \Phi_c(\mathbf{q}, 0)|^2 \rangle} \quad (3.58)$$

which for a stationary and macroscopically homogeneous porous material reduces to equation (3.24).

Similar arguments can be advanced for forced Rayleigh scattering and pulsed field gradient NMR experiments, which involve similar correlation functions. Hence these experiments all measure the "simpler" effective diffusion coefficients (i.e., only including intrinsic conductivity and hindered diffusion, but not porosity or partitioning), as given for example by equation (2.50) (point particles) and equation (2.65) (finite size particles in a well-connected pore space).

## CHAPTER IV

### MATERIALS

#### Polymers and Solvents

A number of linear polystyrenes, with narrow molecular weight distributions, were used in these experiments, spanning two decades of molecular weight ( $2 \times 10^4$  to  $2 \times 10^6$ ). Polystyrene has of course been used in countless studies as the prototypical flexible polymer. This popularity is due largely to the ready commercial availability of relatively monodisperse (since they are made by living anionic polymerization) samples of many different molecular weights. The samples in this work were used as received, without fractionation.

Characteristics of these linear polystyrenes are given in Table 1: different average molecular weights, the estimated overlap concentration, and the measured diffusion coefficient in bulk solution. (These latter two quantities are in the solvent 2-fluorotoluene.) These samples were obtained from Pressure Chemical (P2-P9) and Polymer Laboratories (P14-P17). Molecular weights (except  $M_D$  -- see below) are those given by the suppliers: number average,  $M_n$ , from membrane osmometry; weight average,  $M_w$ , from light scattering; viscosity average,  $M_v$ , from capillary viscometry; and peak molecular weight,  $M_p$ , from size exclusion chromatography (SEC). Obviously, these suppliers' values are not extremely accurate, as they are not even always internally consistent (e.g., proper ordering should be  $M_n < M_v < M_w$ ).

TABLE 1  
Characteristics of Linear Polystyrene Samples<sup>†</sup>

Code (Lot)	10 <sup>-3</sup> · Molecular Weight					PD	c*	10 <sup>7</sup> · D <sub>0</sub>
	M <sub>p</sub>	M <sub>n</sub>	M <sub>v</sub>	M <sub>w</sub>	M <sub>D</sub>			
P3 (41220)	17.5	15.1	17.4	20.4	21.3	1.06	59.0	14.4
P4 (80317)	35	34.1	36.2	-	33.1	1.06	43.0	11.2
P5 (60917)	50	51.2	47.4	53.7	53.2	1.06	30.6	8.55
P6 (70111)	100	92.6	98.7	93.1	102	1.06	19.2	5.92
P7 (30126)	170	156	-	169	181	1.06	12.7	4.26
P8 (00507)	300	243	281	293	401	1.06	7.21	2.71
P2 (3b)	390	350	383	392	406	1.06	7.14	2.69
P9 (30121)	575	573	586	591	583	1.06	5.51	2.19
P15	1030	-	-	-	1050	1.06	3.62	1.56
P16	1400	-	-	-	1380	1.05	2.98	1.34
P17	2050	-	-	-	2120	1.06	2.19	1.05

<sup>†</sup> PD = M<sub>w</sub>/M<sub>n</sub>

c\* = overlap concentration (mg/ml); calculated from equation (4.2) using M<sub>D</sub>  
D<sub>0</sub> = diffusion coefficient (cm<sup>2</sup>/s) at T=42.6°C, η = 0.00523 poise and c ≈ c\*/8

The  $M_p$  values from SEC are presumed to be the most reliable, due to error compensation inherent in calibration of SEC columns. The  $M_v$  values should also be relatively reliable, since viscometry is a simple technique and the Mark-Houwink equation for polystyrene is well established. The  $M_n$  and  $M_w$  values are probably less reliable due to the greater error associated with osmometry and light scattering measurements. Values given for  $M_w/M_n$  are upper limits, obtained from SEC data, as quoted by the suppliers; obviously, these do not correspond to ratios of independently measured  $M_n$  and  $M_w$  values.

The overlap concentration  $c^*$  is the concentration at which coils in solution start to interpenetrate.<sup>12</sup> Various theories for  $c^*$  can be expressed as:<sup>115</sup>

$$c^* = C_1/[\eta] \quad (4.1)$$

where  $[\eta]$  is the intrinsic viscosity and  $C_1$  is a constant depending on the coil packing model; for example,  $C_1=1.08$  for hexagonal close packing, and  $C_1=0.77$  for random close packing. In order to obtain the  $c^*$  values in Table 1,  $C_1=1$  was chosen, and the  $[\eta]$ - $M_v$  relation from Pressure Chemical for polystyrene in toluene (*not* 2-fluorotoluene) was used:

$$[\eta] = (1.35 \times 10^{-4}) M_v^{0.716} \text{ dl/g} \quad (4.2)$$

The molecular weights used to estimate  $c^*$  were  $M_D$  (see below). For the purpose of estimating  $c^*$  in 2-fluorotoluene, the use of this expression for  $[\eta]$  (for the different solvent toluene) is reasonable. First, the Mark-Houwink exponents for 2-fluorotoluene and toluene are similar (*vide infra*), even if

the prefactors might differ. Second,  $c^*$  is by no means a precisely defined quantity. The main value of the  $c^*$  concept is that it allows one to consistently and semi-quantitatively define how "dilute" or "concentrated" a solution is. In fact, these  $c^*$  estimates were used so that all solutions could be prepared at the same dilute reduced concentration,  $c/c^* \approx 1/8$ .

The diffusion coefficients in bulk solution ( $D_0$ ) are used with the molecular weight data to determine the  $D_0$ - $M$  scaling relationship for polystyrene in the solvent 2-fluorotoluene. Strictly, these are only estimates of  $D_0$ , for the following reasons. First, these measurements were made at various temperatures between 41.7°C and 45.3°C, and corrected to a common temperature and viscosity (42.6°C, 0.00523 poise). Such a correction assumes that changes in coil expansion, hence frictional properties, as a function of temperature are negligible over this range; that is, that  $\partial R_H/\partial T \approx 0$ , where  $R_H$  is the polymer hydrodynamic radius. (This is supported by results of  $R_H$  vs  $T$ --see Chapter VII.) Second, these values were measured at a single finite concentration ( $c \approx c^*/8$ ), not extrapolated to  $c = 0$ . This involves some error, as discussed in Chapter VI; the values in Table 1 thus exceed true values of  $D_0$  by some factor close to unity.

Figure 6 is a double logarithmic plot of  $D_0$  versus  $M_p$ , the latter chosen as the most reliable, or at least internally consistent, molecular weights available. The  $M_p$  values for samples P3 and P8 are clearly anomalous. A fit of the remaining data to the form,  $\log D_0 = A + \alpha \log M_p$ , gives the power law:

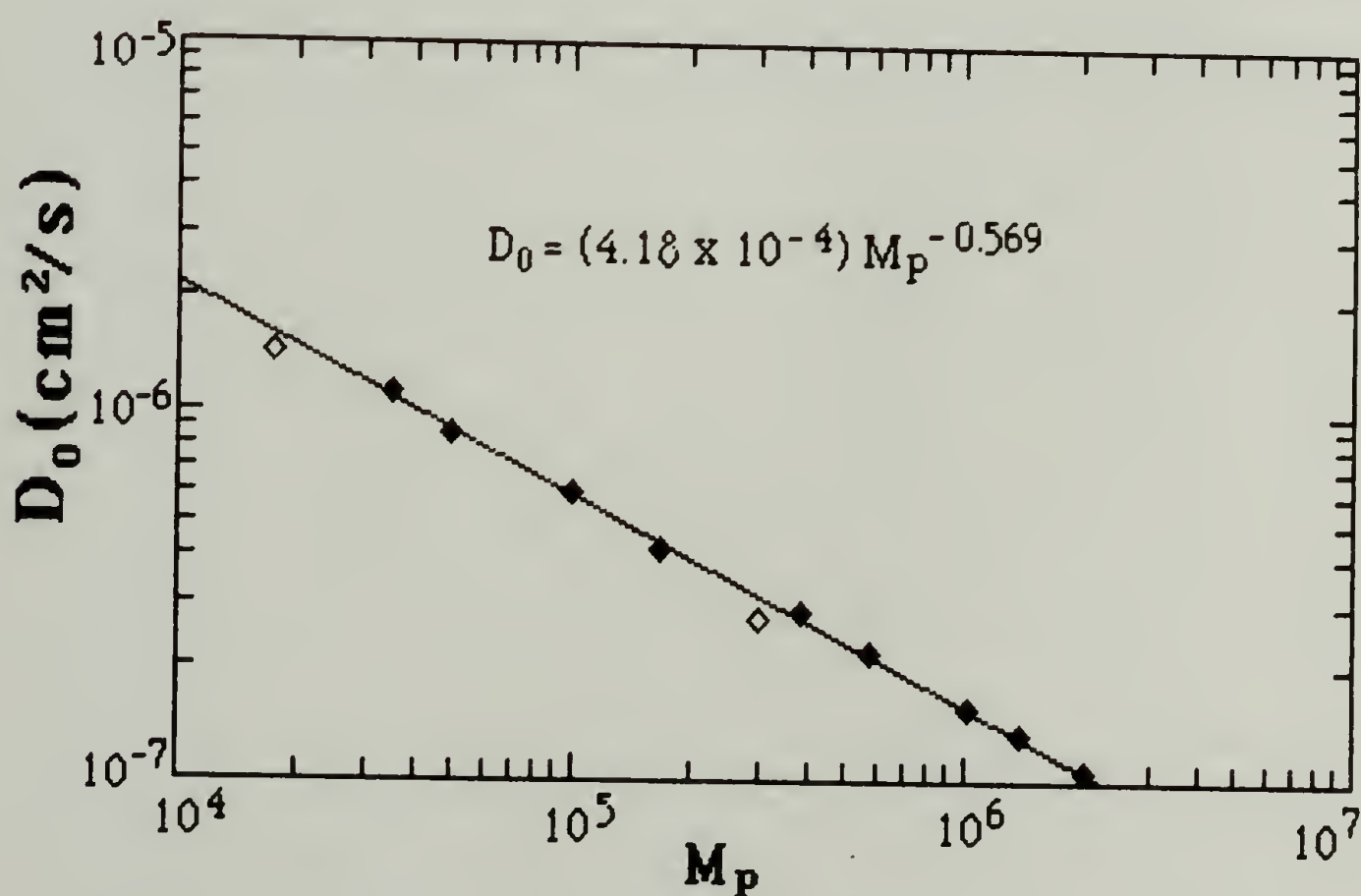
$$D_0 (42.6^\circ\text{C}, 0.00523 \text{ poise}) =$$

$$(4.18 \times 10^{-4}) M_p^{-0.569} \text{ cm}^2/\text{s} \quad (4.3)$$

Figure 6.

Bulk solution diffusion coefficient  $D_0$  vs molecular weight for linear polystyrenes in 2-fluorotoluene.

Double logarithmic plot of  $D_0$  versus  $M_p$  for linear polystyrene dissolved in 2-fluorotoluene.  $D_0$  is the diffusion coefficient in unbounded solution, measured at a finite concentration  $c$  (i.e., not extrapolated to  $c = 0$ ), with  $c \approx c^*/10$ , where  $c^*$  is the overlap concentration. All values are corrected to  $T = 42.6^\circ\text{C}$ ,  $\eta = 0.00523$  poise.  $M_p$  is the peak molecular weight from size exclusion chromatography, as quoted by the suppliers. The solid line is the fit to the data assuming a power law relationship. Unfilled pips were excluded from this fit.



with error in the scaling exponent,  $\alpha = -0.569 \pm 0.007$ . This  $\alpha$  corresponds to a Mark-Houwink exponent of 0.707; compare this with equation (4.2). This result for  $\alpha$  shows that 2-fluorotoluene is a thermodynamically good solvent for polystyrene.

Since  $D_0$  from light scattering is a z-average, but  $M_p$  is some other average, this fit is strictly not correct. However, since  $M_w/M_n$  is nearly constant for these samples, then by implication  $M_z/M_p$  should also be nearly constant, making this fit in fact reasonable. (Furthermore, error in  $M_z/M_p$  is expected to be random, leading to little bias in the determination of the scaling exponent.) The corresponding scaling law for the hydrodynamic radius, obtained using the Stokes-Einstein relationship, equation (3.32), is:

$$R_H (42.6^\circ\text{C}, 0.00523 \text{ poise}) = (0.106) M_p^{0.569} \text{ \AA} \quad (4.4)$$

The power law given in equation (4.3) was used to back-calculate "diffusion" molecular weights,  $M_D$  (Table 1). It can be seen that these correspond to size exclusion chromatography (SEC) peak molecular weights,  $M_p$ . I believe this set of  $M_D$  values to be the best set of molecular weights in Table 1.

How is the peak molecular weight  $M_p$  related to more common molecular weight averages? The peak molecular weight in SEC (using weight sensitive detectors) is the molecular weight for which the weight distribution is a maximum. Thus the relation of  $M_p$  to other averages depends on the type of molecular weight distribution. For these anionic linear polystyrenes, the molecular weight distribution is perhaps well approximated as log normal,<sup>116</sup> for which it can be shown that:

$$M_p = (M_n \cdot M_w)^{1/2} \quad (4.5)$$

It should be noted that, in order for  $M_D$  back-calculated from  $D_0$  using equation (4.3) to actually correspond to the molecular weight average given by equation (4.5), it is required that the  $M_p$  values (Table 1) which were used to determine equation (4.3) be correct in *absolute* terms; that is, it is required that the SEC columns were correctly calibrated.

As hinted in the preceding, the primary solvent used in this work was 2-fluorotoluene (2FT), which is a good solvent for polystyrene, and which provides a satisfactory refractive index match with porous silica. The 2FT was used as received (Aldrich, 99+% pure). The two other isomeric fluorotoluenes also meet the requirements of solvent goodness and of refractive index match, but are only available commercially in lower purity than 2FT, making 2FT the more desirable. Following is a brief history explaining my arrival at 2FT as the solvent of choice, which, in addition to a small amount of information on other solvents which has been collected in Appendix A, might be useful in planning other light scattering experiments in porous media.

The initial light scattering experiments in porous glasses used a mixed solvent, 80/20 (w/w) chloroform ( $n_D^{20} = 1.4460$ ) and 1,2-dichlorobenzene ( $n_D^{20} = 1.5504$ ). By adjusting the solvent ratio, it was possible to change the refractive index to match the glass. By this means, the glass refractive index was found to be about 1.47. It was then decided to find a single component solvent, to avoid problems such as preferential solvency, lack of knowledge of solvent properties, and difficulty of maintaining constant solvent composition during solution preparation and filtering.

The next solvent chosen was trans-decahydronaphthalene (TD). The viscosity and refractive index of TD are known (Appendix A). Also, TD has a relatively high viscosity, which is advantageous for looking at low molecular weight polymers. Furthermore, TD is a well-known theta-solvent for polystyrene, with the theta-temperature ( $\Theta$ ) about 18.2-23.8°C.<sup>117</sup> (It was felt that it could be useful to have Gaussian chain statistics.) However, the use of TD was abandoned, because of persistent problems with polymer adsorption (see below), and because TD is not a theta-solvent at the temperatures required to index match the glass. (Expansion of PS in TD for  $T > \Theta$  is significant.<sup>118</sup>) It was finally decided to find a single, thermodynamically good solvent to use in these experiments, principally to eliminate adsorption. 2-Fluorotoluene was the solvent ultimately chosen.

The viscosity of 2FT as a function of temperature had to be determined, both to allow the calculation of polymer hydrodynamic radii, and to be able to approximately correct values of the diffusion coefficient measured at a given temperature to the corresponding value at some other temperature. The viscometer (Ubbelohde type, Cannon model 25-A494) was chosen such that efflux times were sufficiently long to be able to neglect end effect and inertial corrections. Efflux times  $t$  were converted to kinematic viscosities  $\nu$  (stokes) as:

$$\nu = a t \quad (4.6)$$

where  $a$ , the viscometer constant, was determined by calibration using water ( $a = 1.987 \pm 0.001 \times 10^{-5}$  stokes/s). Measurements were made between 38 and 49°C, which includes the range of most light scattering

measurements. Approximate correction of kinematic viscosity to viscosity  $\eta$  (poise) was made as:

$$\eta = \nu \rho_4^T \quad (4.7)$$

where  $\rho_4^T$  was estimated by *linear* extrapolation from literature values ( $\rho_4^{13} = 1.0041$  119 and  $\rho_4^{20} = 1.001$  120):

$$\rho_4^T \approx 1.001 - (4.43 \times 10^{-4}) (T - 20) \quad (4.8)$$

where  $T$  is the temperature ( $^{\circ}\text{C}$ ). Data were fit to the form

$$\ln \eta = \ln A + (\Delta E_{\eta} / RT) \quad (4.9)$$

which is based on the assumption of an Arrhenius relation  $\eta = A \exp(\Delta E_{\eta} / RT)$  for the viscosity temperature dependence, where  $A$  is a prefactor,  $\Delta E_{\eta}$  is the viscosity activation energy, and  $R$  is the gas constant. The expression obtained was:

$$\eta \text{ (poise)} = (2.033 \times 10^{-4}) \exp(1025/T) \quad (4.10)$$

Error in  $\eta$  using this expression over the temperature range of light scattering experiments is estimated to be  $< 0.5\%$ .

Other properties of 2-fluorotoluene are as follows. The boiling point is  $114^{\circ}\text{C}$ , well above the temperature required for light scattering experiments ( $40 \pm 5^{\circ}\text{C}$ ). The refractive index of 2FT at  $40.7^{\circ}\text{C}$  (the temperature of optimum match with glass B7) was estimated as  $n=1.471$ , by comparison to the optimum match results for TD, a solvent for which the wavelength and temperature dependence of  $n$  is known (see Appendix A). The wavelength,

temperature, and concentration dependence of  $n$  for 2FT was not measured. For calculating the scattering wavevector  $q$  by equation (3.3), a value of  $n=1.467$  was always used, regardless of temperature or solution concentration. However, for  $dn/dT \approx -4 \times 10^{-4}$  RIU/ $^{\circ}\text{C}$ , with  $T = 40 \pm 5^{\circ}\text{C}$ , the error in refractive index is  $\Delta n \leq 2 \times 10^{-3}$  RIU; and for  $dn/dc \approx 0.1$  cm<sup>3</sup>/g, with  $c \leq 1 \times 10^{-2}$  g/cm<sup>3</sup>,  $\Delta n \leq 1 \times 10^{-3}$  RIU. Hence error in  $q^2$  by neglect of  $c$  and  $T$  dependence of  $n$  is estimated at  $< 0.5\%$ .

### Porous Glass Characterization

Since, as discussed in Chapter II, transport properties depend significantly on the structure of the porous medium, some space will now be devoted to the structure of the porous glasses used in this work: which glasses were used; how porous glasses are made (which has implications with regard to their structure); qualitative structural features; and quantitative properties of the glasses used, including how they were characterized.

The porous materials used in this work were various "controlled pore" glasses (CPGs), which constitute one of several classes of commercially available porous glasses. Vycor glasses (Corning) are readily available in variety of fabricated geometries, but these glasses have relatively small pores (typically, the average pore radius  $R_p$  is about 30 Å), and were thus deemed unsuitable for use in studying hindered diffusion of polymers. The CPGs, which are available from Electro-Nucleonics in a variety of pore sizes but which are unfortunately sold as relatively small crushed fragments, have larger pores ( $80 \text{ Å} \leq R_p \leq 1500 \text{ Å}$ ) and relatively narrow pore size distri-

butions. Sol-gel glasses can also be made having a variety of pore sizes, but the pore size distributions tend to be relatively broad.

Several steps are involved in the production of CPG<sup>121-124</sup> or Vycor<sup>125,126</sup> type porous glasses. Certain sodium borosilicate glasses, which are miscible in the melt, will phase separate upon heat treatment below the liquidus temperature. The nascent structure produced upon phase separation of these ternary (i.e.,  $\text{Na}_2\text{O}-\text{B}_2\text{O}_3-\text{SiO}_2$ ) glasses which are used to make CPGs and Vycors depends on both thermodynamic (e.g., composition, temperature) and kinetic (e.g., time, temperature) factors, some discussion of which can be found in a number of references.<sup>122,127-129</sup> It is by varying these factors that glasses with different properties, for example, pore size and porosity, can be made. Effects that can lead to non-uniform pore structure, such as surface crystallization and inhomogeneous cooling, must be controlled.<sup>124</sup> The phase rich in sodium and boron, which in fact may further separate into two phases<sup>122</sup> (i.e.,  $\text{Na}_2\text{O}$  and  $\text{B}_2\text{O}_3$ ), can be etched out using  $\text{HCl}$ , leaving behind a porous skeleton of the silica rich phase, which is typically 96%  $\text{SiO}_2$ . Colloidal silica, which comes from  $\text{SiO}_2$  initially present in the  $\text{Na}_2\text{O}-\text{B}_2\text{O}_3$  rich phase and which is deposited in the pores during the acid leaching treatment, can be removed by controlled etching with  $\text{NaOH}$ .<sup>121,122</sup> The microstructure of the pore space which is ultimately produced depends not only on the phase separation process but also on the etching procedure, in particular, whether or not the colloidal silica deposits, which give a superimposed fine structure, are removed. All CPGs undergo this second etching step, whereas Vycors don't.<sup>122,124</sup>

Phase separation in CPGs has been interpreted as occurring either by a nucleation and growth<sup>122,128</sup> or by a spinodal<sup>130</sup> mechanism; the mechanism has a bearing on ultimate structure. Observation of spherical domains at early times supports a nucleation and growth mechanism.<sup>124,128</sup> Haller and Macedo attribute the relatively uniform pore size in CPGs to a high nucleation density achieved by quenching the miscible glass melt to room temperature before reheating to cause phase separation.<sup>128</sup> The initial composition used by Haller ( $\text{SiO}_2$ :  $\text{B}_2\text{O}_3$ :  $\text{Na}_2\text{O}$  = 67:25:7 wt %) gives a final volume ratio of the two phases of about 1:1, or a porosity for the leached glass of about 0.50, regardless of pore size.<sup>121,122,128</sup> Most glasses from Electro-Nucleonics have a higher porosity, indicating a different starting composition or etching process. Aside from differences in details, I believe that the proprietary Electro-Nucleonics process is fundamentally similar<sup>123</sup> to that of Haller and thus yields similar glasses.

A qualitative idea of the structural features of these CPGs is best obtained pictorially. Scanning electron micrographs (Figure 7) show certain features which are typical of these CPGs. First, the pore space is highly interconnected, as is the glass matrix. Since the pore space is made by etching, one can conclude that all pores must be accessible by some path, however tortuous, originating on the outside surface of the macroscopic piece. This, together with the observations that nearly all the  $\text{Na}_2\text{O}$ - $\text{B}_2\text{O}_3$  phase is removed and that the remaining silica skeleton is rigid, proves that the two phases, glass and pores, are bicontinuous.<sup>122</sup> Second, at least in a loose sense, the structures appear random. To what degree actual structures might correspond to various mathematical models of randomness--for

Figure 7.

Scanning electron micrographs of porous glasses.

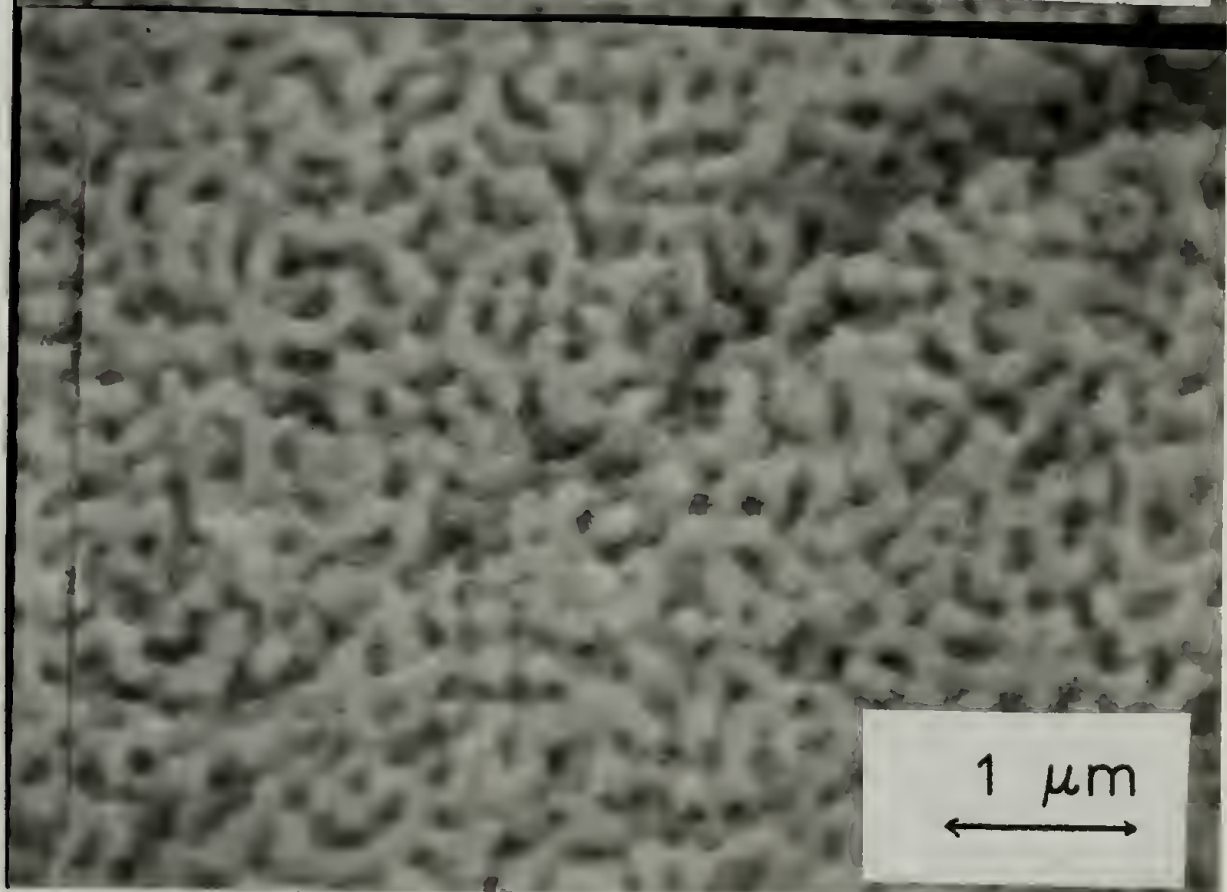
(a) Glass B5,  $R_p = 1866 \text{ \AA}$ ,  $\Phi = 0.62$ , Magnification = 10K

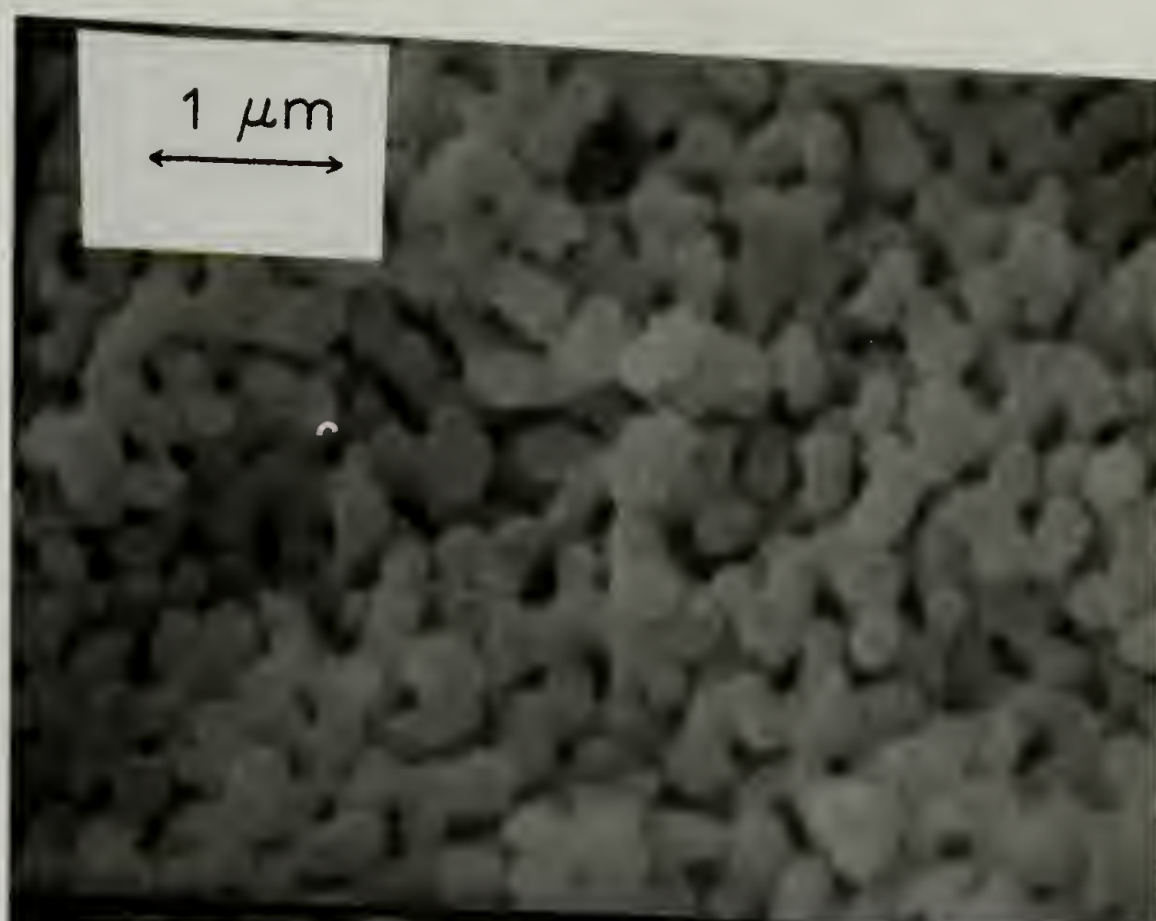
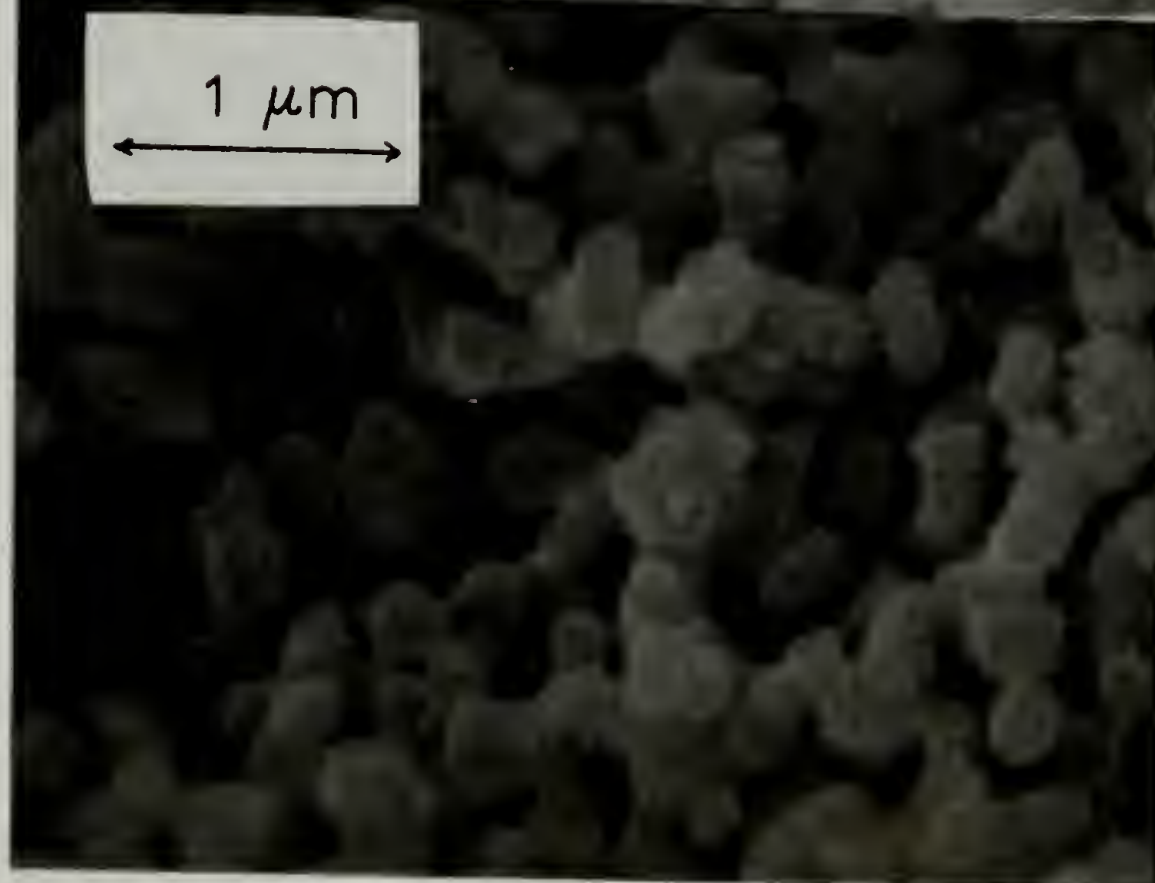
(b) Glass B7,  $R_p = 893 \text{ \AA}$ ,  $\Phi = 0.72$ , Magnification = 20K

(c) Glass B13,  $R_p = 703 \text{ \AA}$ ,  $\Phi = 0.46$ , Magnification = 20K

(d) Glass B13, Magnification = 30K

All samples were shadowed with about 100-200  $\text{\AA}$  of gold. The magnifications in (a)-(c) are roughly proportional to  $1/R_p$ , which allows a relatively direct structural comparison. Glasses B5 and B7--(a) and (b)--look qualitatively similar. However, glass B13 looks qualitatively quite different than either glass B5 or B7.

**a****b**

**c****d**

example, to the Debye-Bueche model often used to model scattering from random two phase systems,<sup>131</sup> or to some sort of percolation model, or to some sort of fractal model as might be suggested from studies of porous sandstones<sup>94</sup> or Vycor glass<sup>132</sup>--is unknown. (Implications of diffusion measurements with regard to structure are discussed in Chapter VII.)

Inspection of micrographs shows that most features, for example, cross sections of either matrix or pores, are of *relatively* uniform size. This conclusion is based not so much on the scanning electron micrographs of these CPGs (Figure 7) as on published transmission electron micrographs of other CPGs made by the same basic process. (See Figure 1 in Refs. 121, 122, and 128; compare also Figures 1 and 4 in Ref. 128 to see the effect that heat treatment conditions can have on pore uniformity.)

These CPGs were characterized in terms of an overall porosity  $\Phi$  and a nominal pore radius  $R_p$  (*vide infra*). Perhaps a weakness of this work has been the limited investigation of the structure of the porous glasses, since, as discussed in Chapter II, transport properties depend significantly on the structure of the porous medium. However, it should be noted that "simply" determining the structure of porous materials continues to be a challenging and active area of research, so that it was by no means clear how much useful or unambiguous information would have been gained by more detailed structural investigations.

The parameters characterizing the glasses used in this work are summarized in Table 2. The CPG0350 (B1), CPG1400 (B7), and CPG3000 (B5) glasses were obtained commercially as irregularly shaped fragments. The fragments of B1 were very small (80/120 mesh, 125-177  $\mu\text{m}$ ) and were

TABLE 2  
Porous Glass Characteristics: Specific Pore Volume  $v_p$ ,  
Porosity  $\Phi$ , and Nominal Pore Radius  $R_p$

Glass Code (Description)	$v_p$ (cm <sup>3</sup> /g)	$\Phi$ <sup>a</sup>	$R_p$ (Å)				Notes
			Median	Average	Mode		
B1 (Electro-Nucleonics, CPG0350, Lot 05A03)	0.92	0.67	211	---	---		<u>b</u> , <u>e</u> , <u>f</u>
			(174)	---	---		<u>b</u> , <u>d</u> , <u>f</u>
B7 (Electro-Nucleonics, CPG1400, Lot 09D02)	1.16	0.72	908	---	---		<u>b</u> , <u>e</u> , <u>f</u>
			(745)	---	---		<u>b</u> , <u>d</u> , <u>f</u>
	1.17	0.72	893	998	862		<u>c</u> , <u>e</u> , <u>f</u>
			893	863	847		<u>c</u> , <u>e</u> , <u>h</u>
B5 (Electro-Nucleonics, CPG3000, Lot 11D10)	0.69	0.60	1905	---	---		<u>b</u> , <u>e</u> , <u>f</u>
			(1563)	---	---		<u>b</u> , <u>d</u> , <u>f</u>
	0.75	0.62	1866	1824	1848		<u>c</u> , <u>e</u> , <u>f</u>
			1848	1778	1848		<u>c</u> , <u>e</u> , <u>h</u>
B13 (Dr. W. Haller)	0.37	0.45	703	---	---		<u>m</u> , <u>e</u>
	0.38	0.46	(620)	---	---		<u>i</u> , <u>k</u>
RA (Dr. W. Haller)	0.26	0.37	125	---	---		<u>i</u> , <u>k</u>
RB (Dr. W. Haller)	0.20	0.30	250	---	---		<u>i</u> , <u>k</u>

<sup>a</sup> Calculated from  $v_p$  using equation (4.11)

b, c From mercury intrusion: Electro-Nucleonics (b) or Quantachrome (c)

d  $\gamma_{Hg} = 469$  dynes/cm,  $\theta_A = 130^\circ$

e  $\gamma_{Hg} = 480$  dynes/cm,  $\theta_A = 140^\circ$ ,

f, h Volume (f) or surface area (h) distribution

i Estimated pore size, Dr. W. Haller

k  $v_p$  and  $\Phi$  from weight and volume measurements

m  $v_p$  and  $\Phi$  from solvent imbibition; see text for  $R_p$  estimate

used only for testing surface treatments to prevent adsorption. Fragments of B7 and B5 were larger (20/80 mesh, 177-840  $\mu\text{m}$ ) and were sorted by hand to obtain fragments of large enough size to be individually mounted. The other three glasses were generously provided by Dr. Wolfgang Haller, of the National Bureau of Standards. Haller was the first to make CPGs<sup>121,122</sup> and is perhaps the world expert with regard to the arts involved. These latter glasses were supplied as macroscopic pieces of cylindrical (RA, RB) or rectangular (B13) geometry, but in too small amounts to be as extensively characterized as the commercial CPGs. Following are some details and comments about the characterization of all these glasses.

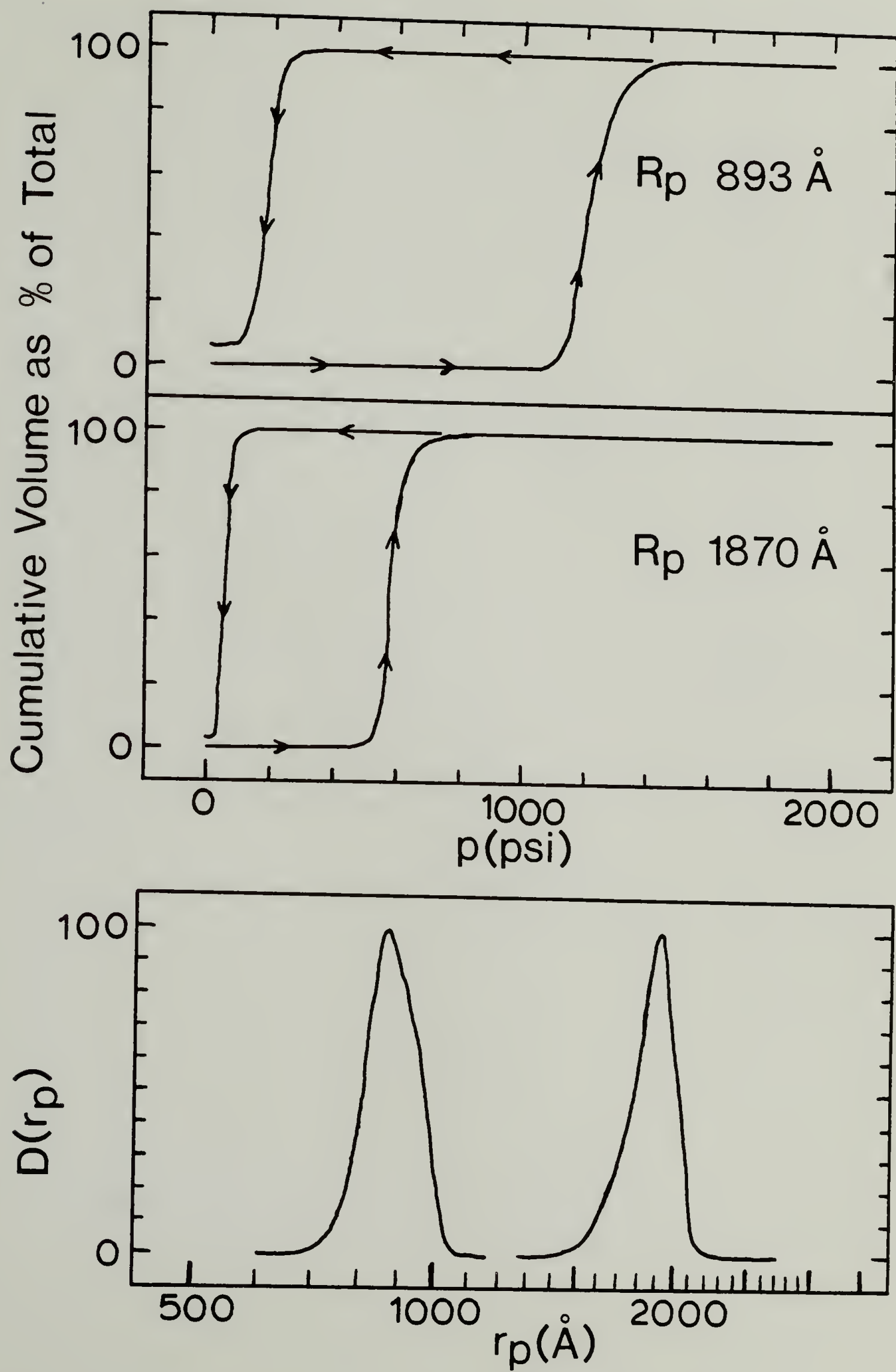
Mercury porosimetry<sup>133-139</sup> was used to characterize the commercial porous glasses B5 and B7. Although the experimental technique is straightforward, the interpretation of the raw data is much less so. The following discussion is intended to show how porosity and pore "radius" values are obtained from such measurements, and to point out what inferences can (and cannot) be made with respect to the actual structure of the porous glasses.

To make these measurements, a weighed amount of porous glass is placed in a mercury filled dilatometer. The pressure  $p$  is then gradually increased, forcing mercury, which is non-wetting, into successively smaller pores. One ends up with a curve of the cumulative volume  $V$  of penetrated pore space as a function of pressure. Similarly, by reducing the pressure, mercury will be extruded from successively larger pores. Mercury intrusion and extrusion curves for B5 and B7 are shown in Figure 8. Most of the

Figure 8.

Mercury porosimetry results for controlled pore glasses B7 (893 Å) and B5 (1866 Å).

The dual upper plot shows the raw data (from Quantachrome) of cumulative intruded volume vs pressure. The bottom plot shows the corresponding volume pore radius distributions, in arbitrary units, vs nominal pore radius. These distributions are derived from the intrusion (increasing pressure) branches of the curves in the upper plots, as given by equation (4.15a). The curves in the upper plots are identified by the median  $R_p$  values obtained from these volume radius distributions. The text discusses the detailed interpretation of these results.



hysteresis is attributed to differences between the advancing and receding mercury contact angles.<sup>133-139</sup>

The specific pore volume  $v_p$  is simply the total volume of intruded mercury per gram of porous glass. Porosity  $\Phi$  is calculated from  $v_p$  using the known density of silica,  $\rho_G = 2.2 \text{ g/cm}^3$ :

$$\Phi = v_p / (v_p + (1/\rho_G)) \quad (4.11)$$

All pore space measured by this technique is accessible from the outside of the glass. It is reasonable to assume that this pore space is identical to that which is filled when the porous glasses are immersed in polymer solutions, which wet the glass. Since the  $V$  versus  $p$  curves for these glasses are flat at the highest pressures, it is also unlikely that there is any additional pore space, connected through small pores, that would be accessible to polymer solutions but not to mercury. Hence it is concluded that mercury intrusion measurements of  $\Phi$  correctly give the porosity of these CPGs with respect to polymer solutions.

Interpretation of the data to determine a pore "radius" distribution<sup>140</sup> starts with the Laplace equation, which gives the relation between the capillary pressure  $p$ , the surface tension of mercury  $\gamma_{Hg}$ , and the principal radii of curvature ( $r_1$  and  $r_2$ ) of the mercury meniscus:

$$p = \gamma_{Hg} (1/r_1 + 1/r_2) \quad (4.12)$$

Given the complicated and generally unknown geometry of most pore spaces, the quantity  $(1/r_1 + 1/r_2)$  is usually replaced by the corresponding quantity for cylindrical pores of radius  $r_p$ , giving:

$$p = (2 \gamma_{\text{Hg}} \cos \theta_c) / r_p \quad (4.13)$$

Here  $\theta_c$  is the contact angle, either advancing ( $\theta_c = \theta_A$ ) or receding ( $\theta_c = \theta_R$ ) for mercury intrusion and extrusion respectively. For a conical pore with taper angle  $\theta_T$ ,  $\theta_c$  must be replaced by  $\theta_c \pm \theta_T$  as appropriate. Figure 9 illustrates the geometry of mercury intrusion. The quantity  $r_p$  is the radius of a cylindrical pore which would be penetrated at the same  $p$  as the actual pore, hence, a nominal pore radius. Equation (4.13) is then used to convert  $V$  vs  $p$  curves to  $V$  vs  $r_p$  curves. In general, only the intrusion branch of the data is analyzed to obtain pore size information; this is the case for this dissertation also.

In order to obtain some single value of the nominal pore radius to represent the distribution, one proceeds as follows. Volume and surface area pore size distributions,  $V_p(r_p)$  and  $S_p(r_p)$ , can be defined as:

$$dV = - V_p(r_p) dr_p \quad (4.14a)$$

$$dA = - S_p(r_p) dr_p \quad (4.14b)$$

where  $dV$  and  $dA$  are the volume and surface area associated with pores with radii between  $r_p$  and  $r_p - dr_p$ . Using the differential form of the Laplace equation,  $p dr_p + r_p dp = 0$ , plus equation (4.14a), gives:

$$V_p(r_p) = (p/r_p)(dV/dp) = (- dV/dr_p) \quad (4.15a)$$

and, plus equation (4.14b), and continuing the assumption of cylindrical pores,

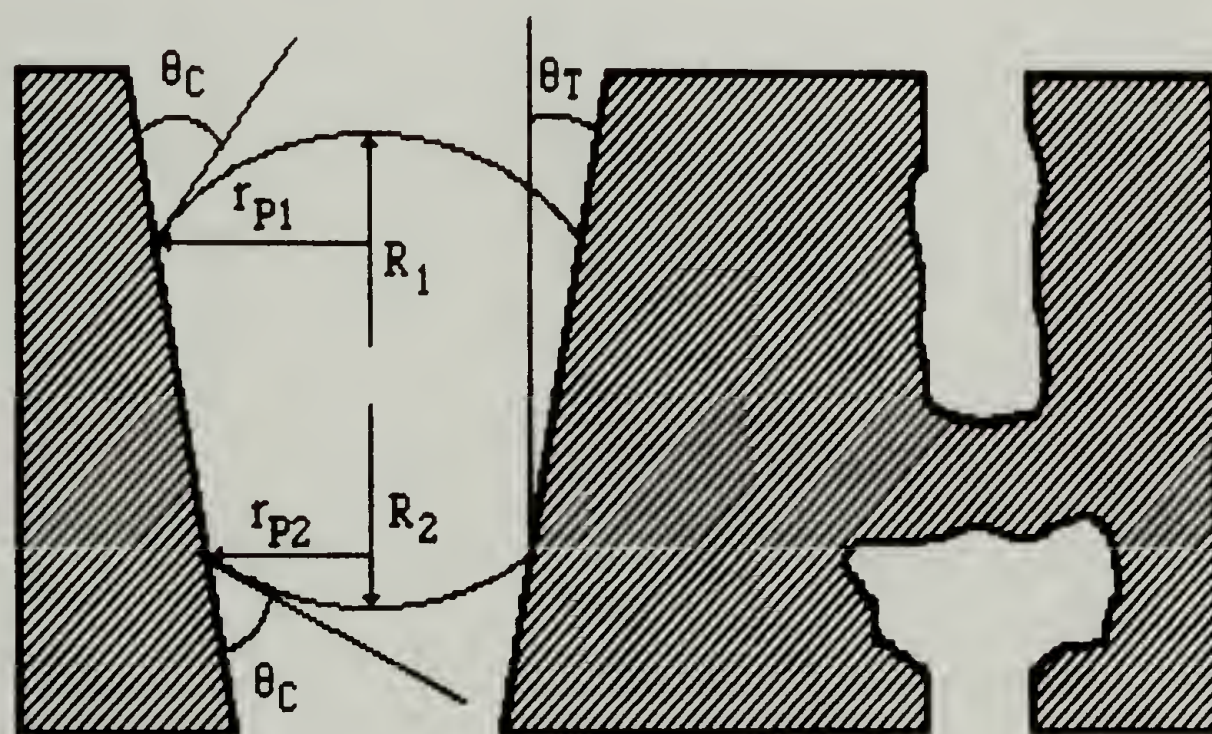
Figure 9.

## Mercury porosimetry: geometry and ink bottle pores

This figure shows the relation of the radius of curvature  $R$  of a mercury meniscus to the geometry of a conical pore, with circular cross section of radius  $r_p$  and taper angle  $\theta_T$ . The contact angle is  $\theta_C$ .

This figure also illustrates "ink bottle" pores. The pores shown on the right have the same entry diameter and thus would be penetrated at the same pressure. Despite the difference in actual radii, mercury porosimetry would give the same radius for both.

$$R_1 = r_{p1} / \cos(\theta_C - \theta_T)$$



$$R_2 = r_{p2} / \cos(\theta_C + \theta_T)$$

$$S_p(r_p) = 2 V_p(r_p)/r_p = (2/r_p)(-dV/dr_p) \quad (4.15b)$$

These distributions can be calculated from the  $V$  vs  $r_p$  curves by numerical differentiation. Average, mode, and median (with respect to either distribution) nominal pore radii can then be calculated as:

$$(R_p)_{\text{AVERAGE}} = (1/X_{\text{TOTAL}}) \int_0^\infty r_p X_p(r_p) dr_p \quad (4.16a)$$

$$(R_p)_{\text{MODE}} = r_p \text{ for which } dX_p/dr_p = 0 \text{ and } d^2X_p/dr_p^2 < 0 \quad (4.16b)$$

$$(R_p)_{\text{MEDIAN}} = r, \text{ where } \int_0^r X_p(r_p) dr_p = 0.5 \quad (4.16c)$$

where  $X_{\text{TOTAL}}$  is the total volume or surface area, and where  $X_p(r_p)$  represents either  $V_p(r_p)$  or  $S_p(r_p)$ . The median  $R_p$ , obtained using the volume distribution, is often called the "50% intrusion" radius, and even, incorrectly, the average radius.

The values for  $R_p$  in Table 2 merit discussion. Glasses B1, B5, and B7 were supplied with values of "average"  $R_p$ , actually median (volume)  $R_p$  values. (These  $R_p$  values from Electro-Nucleonics are tabulated in parentheses.) Glasses B5 and B7 were also submitted for independent testing (Quantachrome Corporation), in order to check the Electro-Nucleonics results, and to allow the determination of average, median, and mode  $R_p$  values from both volume and surface area distributions.

Values of median (volume)  $R_p$  from Electro-Nucleonics and Quantachrome are quite different. These differences are attributable to different values of  $\gamma_{\text{Hg}}$  and  $\theta_A$  being used in equation (4.13). Electro-Nucleonics uses  $\gamma_{\text{Hg}} = 469$  dynes/cm and  $\theta_A = 130^\circ$ , while Quantachrome

uses  $\gamma_{\text{Hg}} = 480$  dynes/cm and  $\theta_A = 140^\circ$ . This gives a 22% difference in  $(-\gamma_{\text{Hg}} \cos \theta_A)$ : 301.7 vs 367.7 dynes/cm. If the median (volume)  $R_p$  values of Electro-Nucleonics are corrected for this difference, they are in good agreement with the Quantachrome results.

This leads to the question, what are the best values to use for  $\gamma_{\text{Hg}}$  and  $\theta_A$ ? Literature values for these quantities show considerable variation. There appears to be reasonable consensus<sup>136,140</sup> that  $\gamma_{\text{Hg}} = 485$  dynes/cm.<sup>141</sup> However, the proper contact angle to use is more controversial. Most commonly,  $\theta_A$  is chosen between  $130^\circ$  and  $140^\circ$ .<sup>133-139</sup> However, it has been argued<sup>136,139</sup> that  $\theta_A$  is *effectively*  $180^\circ$  in most porous materials due to "surface roughness". I feel little qualified to evaluate these conflicting claims, and only make the following points.

First, the  $R_p$  values in this dissertation (Table 2), which will be used to calculate relative size parameters, are obtained using  $\gamma_{\text{Hg}} = 480$  dynes/cm and  $\theta_A = 140^\circ$ . Having clearly stated the values which I am using (contrary to much literature), it becomes a simple matter to recalculate  $R_p$  values for different  $\gamma_{\text{Hg}}$  and  $\theta_A$  if desired. Second, uncertainty in  $\theta_A$  causes greater uncertainty in  $R_p$  than does uncertainty in  $\gamma_{\text{Hg}}$ . The relative difference in  $R_p$  over the range of  $\gamma_{\text{Hg}}$  (469-485 dynes/cm) is only 3.4%, but over the range of  $\theta_A$  ( $130^\circ$ - $180^\circ$ ), the relative difference is 56%, even 19% on going from  $130^\circ$  to  $140^\circ$ . Third, any error in  $R_p$  values, hence relative size parameters, will be subsumed in the experimentally determined prefactors of theories for hindered diffusion. Since complexities of pore geometry preclude exact foreknowledge of these prefactors for these porous glasses, ambiguities arise in making quantitative comparison of experiment and theory. The desire to

make this comparison as "absolutely" as possible is in fact the reason behind this digression on correct  $\gamma_{\text{Hg}}$  and  $\theta_A$ . Lastly, given more fundamental problems with mercury porosimetry, to be discussed now, this question is in some ways trivial.

There are difficulties in establishing a correspondence between such nominal  $R_p$  values and the actual pore space geometry, and in comparing  $R_p$  values for different porous materials.  $R_p$  values ultimately follow from equation (4.13), which assumes non-tapered pores with circular cross section. These values can be related to the actual geometry of different simple cross sections, but in practice, since cross section geometry is usually complicated and unknown, no such correction can be made. As two examples, consider a slit-like pore (width  $d_s$ ) or an elliptical pore (semi-axes  $a_e$  and  $b_e$ ); for these cases, equation (4.12) yields results which can be compared to equation (4.13) to show how  $R_p$  is related to these geometries:

$$p = (2 \gamma_{\text{Hg}} \cos \theta_c) / d_s \quad (4.17)$$

$$p = \gamma_{\text{Hg}} \cos \theta_c (1/a_e + 1/b_e) \quad (4.18)$$

Similarly, pore taper (as it affects the contact angle) can in principle, but rarely in practice, be corrected for. These considerations lead to the conclusions that for different size pores with geometrically identical cross sections, regardless of the exact geometry,  $R_p$  values will accurately reflect the *relative* size of the pores; but that comparing  $R_p$  values for pores with geometrically dissimilar cross sections can be misleading.

It should be noted that for most simple geometries (e.g., slit, cylinder) the quantity  $(1/r_1 + 1/r_2)^{-1}$  of equation (4.12) is equal (or very nearly so) to the so-called hydraulic radius, defined as the ratio of pore volume to surface area. Thus  $(1/r_1 + 1/r_2)$  from mercury intrusion should in principle directly give the quantity  $\sigma$  introduced in Chapter II with regard to partitioning theories *if the pore distribution is narrow*. This hydraulic radius can be estimated in another way for glasses B7 and B5, using the specific pore volume  $v_p$  from mercury intrusion, plus the specific surface area  $a_p$  from nitrogen adsorption (BET, Electro-Nucleonics):

$$\sigma^{-1} = v_p/a_p \quad (4.19)$$

For B7 ( $v_p = 1.16 \text{ cm}^3/\text{g}$ ,  $a_p = 17.6 \text{ m}^2/\text{g}$ ),  $\sigma^{-1} = 659 \text{ \AA}$ ; and for B5, ( $v_p = 0.69 \text{ cm}^3/\text{g}$ ,  $a_p = 6.36 \text{ m}^2/\text{g}$ ),  $\sigma^{-1} = 1085 \text{ \AA}$ . For *monodisperse* pores of *any* geometry, the *nominal*  $R_p$  from mercury intrusion should be twice  $\sigma^{-1}$ . For B7 and B5,  $2\sigma^{-1}$  is 1318  $\text{\AA}$  and 2170  $\text{\AA}$  respectively. The ratio of  $2\sigma^{-1}$  to nominal  $R_p$  is about 1.45 (B7) and 1.15 (B5) using the median (volume)  $R_p$  values of Quantachrome. These results indicate that the pore size from mercury intrusion is too low.

The question of pore uniformity and connectivity is now considered. Mercury intrusion analysis in essence assumes a bundle of different sized capillaries, each accessible through pores of the same size or larger. However, in practice there may be some larger pores accessible only through smaller pores ("ink bottles"), as illustrated schematically in Figure 9. The two pores shown would be intruded at the same  $R_p$  value; clearly, however, the pore sizes differ. This effect can cause underestimation (potentially

severe) of the average pore size, and of the breadth of the pore size distribution. To get an idea of the range in pore radius consistent with the values of  $(2\sigma - 1/R_p)$  for B7 and B5 given above, consider a network of cylindrical pores of two different radii ( $R_2 = 2 R_1$ ), with equal volume associated with each pore radius, but with all volume *accessible* only through the smaller size pore (i.e., the radius as measured by mercury intrusion  $R_p = R_1$ ). For this model,  $(2\sigma - 1/R_p) = 4/3$ ; hence, a significant size variation (say a factor of 2 or even more) is not inconsistent with the characterization data on these glasses. One can further comment that usually some mercury remains trapped in the porous material even after complete depressurization during mercury extrusion. Since one cause of this trapping, among several,<sup>136,138</sup> is the presence of "ink bottle" pores, the amount of trapped mercury provides a crude estimate of an *upper limit* to the number of *severe* constrictions which form the necks of such pores.

From all these considerations, the following conclusions can be made about glasses B7 and B5. First, judging from the scanning electron micrographs (Figure 7), the glasses B7 and B5, so by implication the pore spaces also, appear geometrically similar. Hence, nominal  $R_p$  values should accurately reflect the relative pore sizes of these two glasses. Second, from these micrographs, and also based on an *assumed* similarity of these glasses to those in published transmission electron micrographs,<sup>121,122,128</sup> it is concluded that pore cross sections are for the most part roughly circular, or elliptical with modest axial ratio. In the published micrographs, one sees variation in pore sizes of up to a factor of about 2 or 3. Hence, in absolute terms,  $R_p$  values should be relatively close (i.e., by a factor of 2 to 3) to the

actual pore dimensions, subject to whatever uncertainty exists due to lack of knowledge of the correct values of  $\gamma_{\text{Hg}}$  and  $\theta_{\text{A}}$  and of the distribution of pore sizes. Lastly, the relatively small amount of trapped mercury upon depressurization (5.5% for B7 and 3.6% for B5--see Figure 8), in addition to the narrow ranges of pressure over which intrusion and extrusion occur, indicates that the pore space cross sections are remarkably uniform, with relatively few severe constrictions, and hence that the nominal  $R_p$  values probably don't *seriously* (i.e., by an order of magnitude) underestimate the actual pore dimensions.

This relative pore uniformity and lack of severe constrictions is also supported both by the aforementioned microscopy results and by a previous study, in which mercury porosimetry ( $\gamma_{\text{Hg}}=474$  dynes/cm;  $\theta_{\text{A}}$  not given, perhaps  $130^\circ$ ) and electron microscopy measurements of  $R_p$  for other CPGs from Electro-Nucleonics were compared.<sup>137</sup> Those workers found good correlation between the two techniques, further supporting the conclusion about  $R_p$  values being close to absolute pore dimensions (insofar as microscopy can be considered an "absolute" technique, and insofar as they used the "correct" values of  $\gamma_{\text{Hg}}$  and  $\theta_{\text{A}}$ ). They also observed narrow pore size distributions. Their "quality of cylindrical pore model" parameter,  $(2v_p/a_p R_p)$ , which was close to unity, also indicated the pore distribution to be relatively narrow; however, it does not, despite their claim, prove that the pores are cylindrical. The volume pore size distributions for glasses B5 and B7, obtained from the raw data of Figure 8 using equation (4.15a), are also shown in Figure 8; indeed, these distributions are relatively narrow.

Glasses provided by Haller could not be characterized by mercury porosimetry because of insufficient quantity. Values of  $v_p$  and  $\Phi$  were determined as follows. A micrometer was used to measure the sample dimensions, from which the macroscopic volume  $V_G$  was calculated. (To avoid damaging the glass pieces, the micrometer wasn't tightened extremely snug. This could lead to a slight overestimation of  $V_G$ , hence also  $v_p$  and  $\Phi$ , on the order of 2-3%.) Together with the weight of the glass  $w_G$ , and assuming the density  $\rho_G$  of the glass to be  $2.2 \text{ g/cm}^3$ , the specific pore volume  $v_p$  was calculated as:

$$v_p = (V_G - w_G/\rho_G)/w_G \quad (4.20)$$

and the porosity  $\Phi$  was calculated from this  $v_p$  using equation (4.11). For B13, the porosity was also determined by weighing the glass pieces before and after the imbibition of a wetting solvent, dimethylsulfoxide. From weights and densities of glass ( $w_G, \rho_G$ ) and solvent ( $w_S, \rho_S$ ),  $\Phi$  was calculated as:

$$\Phi = (w_S/\rho_S)/(w_S/\rho_S + w_G/\rho_G) \quad (4.21)$$

This value was in good agreement with the value from macroscopic volume measurements.

Pore sizes of the Haller glasses could not be measured. However, based on his past experience relating mercury intrusion pore size to heat treatment and etching conditions, Haller provided estimates of the median (volume)  $R_p$  values for these glasses. For glass B13, Haller gave  $R_p = 620 \text{ \AA}$ . From previously published mercury intrusion curves by Haller (for a glass

with  $R_p = 620 \text{ \AA}$ , perhaps the same glass),<sup>96</sup> it was deduced that he used  $(-\gamma_{\text{Hg}} \cos \theta_A) \approx 324 \text{ dynes/cm}$ . For consistency with  $R_p$  values for glasses B7 and B5 (i.e., with  $\gamma_{\text{Hg}} = 480 \text{ dynes/cm}$ ,  $\theta_A = 140^\circ$ ,  $-\gamma_{\text{Hg}} \cos \theta_A = 367.7 \text{ dynes/cm}$ ), the pore radius used in this work for glass B13 was corrected to  $R_p = 703 \text{ \AA}$ . Comparing micrographs of B13 with those of B7 and B5 (Figure 7) certainly indicates that it has a lower porosity, but little can be concluded about the pore size, particularly as compared to B7, which has  $R_p$  about 27% above that estimated for B13. The pore structure of B13 is believed to be similar to that seen in published micrographs<sup>121,122,128</sup> of other Haller glasses--roughly circular or elliptical pore cross sections, relatively uniform pore size, and few significant constrictions.

Glasses RA and RB were not used to any great extent in this work, for the reasons that follow. This information is included to point out possible pitfalls to avoid if future experiments are planned with these glasses. The porosities are quite low, which, in conjunction with the small pore sizes (which requires relatively low molecular weight polymers), leads to very low signal to noise levels. Furthermore, these rods became discolored (purple) in 2-fluorotoluene. This color absorbs light, reducing incident and scattered intensities; and becomes "burned in" by the laser, at least at 514.5 nm, creating a circular aperture which diffracts the laser beam (Airy disk). Lastly, micrographs of RB show the outer surface of the cylinder to be mainly covered with an apparently non-porous skin; only scattered pits, which cover about 10-20% of the surface, are porous. It is unknown whether the entire rod has this heterogeneous morphology.

### **Glass Pretreatment and Adsorption Testing**

The surfaces of these porous glasses were chemically treated to prevent adsorption of polymer. Quite early in this work it became apparent, as evidenced by reduced polymer concentration in supernatant solutions above packed beds of untreated fragments, that polystyrene would adsorb under some conditions. Furthermore, in comparison to results in the absence of adsorption, correlation functions would show contributions from the dynamics of adsorbed chains, manifested in slower average decay rates and higher polydispersities (i.e., broader distributions of decay rates). It was thus imperative to develop a means to prevent adsorption.

One of the easiest ways to inactivate glass or silica surfaces (e.g., towards adsorption) is by silanization.<sup>142,143</sup> Silanization generally involves pretreatment of the glass, thorough drying, reaction with the silanizing reagent, workup, and a final postcure. Several silanization procedures were evaluated for their efficacy in preventing adsorption. Following are details of these procedures, the results of adsorption tests, and the conclusions drawn therefrom.

Pretreatment consisted of several steps. The glass was heated overnight at 90°C in concentrated HNO<sub>3</sub>, rinsed thoroughly with deionized water until neutral, soaked overnight at room temperature in concentrated HCl, rinsed until neutral, and dried in a convection oven at 90°C for 24 hours. (Temperature was kept below boiling to avoid damage to the glass.) Pretreatment serves to remove organic impurities (HNO<sub>3</sub>) and metal ion contaminants (HCl), and also to activate the silica surface towards silanization.<sup>142</sup>

Silanization reactions were carried out in a Schlenk tube, which had an o-ring joint and Teflon/o-ring stopcocks, to avoid any possibility of grease contamination. Samples of about 1.5 g of glass were dried for >3.5 hours at 210 - 240°C under vacuum (0.01 torr) then allowed to cool to room temperature under vacuum. The silanizing solution was added to the Schlenk tube while sparging through the sidearm with dry nitrogen. The Schlenk tube was then capped under nitrogen flow and sealed for the duration of the reaction. The amount of silanizing reagent was in large excess. For example, the lowest concentration solutions had 25 millimoles of reagent, compared to, for example, 1.7 millimoles of silanol (which would correspond to a rather high density of one silanol per 10 Å<sup>2</sup>). Some of the specific treatments attempted are outlined in Table 3. Reactions were quenched by addition of dry filtered methanol, which was also used to wash the fragments until the filtrate was neutral. Samples were then dried in a convection oven at 50°C overnight, then finally dried for 1 hour at 135-210°C under vacuum prior to use. The final heat treatment serves to further convert the silanized layer.

The protocol to test for presence or absence of adsorption was as follows. The porous glass chosen (B1) had a relatively small pore size ( $R_p = 174$  Å, as reported by Electro-Nucleonics, or 211 Å, using better values for contact angle and surface tension) with a correspondingly high surface area (68.4 m<sup>2</sup>/g), in order to *maximize* the possibility for adsorption. (Given the concentration and amount of polystyrene added in these tests, the surface area per polystyrene monomer unit is estimated to have been relatively high, about 60 Å<sup>2</sup>.) The polystyrene chosen was of relatively low molecular

TABLE 3  
Silanization Treatments

Code	Time	T(°C)	Silanizing Reagent
B1-NO	-----	-----	None (control)
B1-7	70 hr	25	1M CTMS <sup>†</sup> in hexane
B1-8	48 hr	25	1M DCDMS <sup>††</sup> in hexane
B1-9	19 hr	25	1M CTMS <sup>†</sup> in toluene
B1-10	72 hr	95	2M CTMS <sup>†</sup> in toluene
B1-11	7 day	100	2M HMDS <sup>†††</sup> in toluene

<sup>†</sup> CTMS = chlorotrimethylsilane,  $\text{ClSi}(\text{CH}_3)_3$

<sup>††</sup> DCDMS = dichlorodimethylsilane,  $\text{Cl}_2\text{Si}(\text{CH}_3)_2$

<sup>†††</sup> HMDS = hexamethyl disilazane,  $(\text{CH}_3)_3\text{Si}-\text{N}=\text{N}-\text{Si}(\text{CH}_3)_3$

weight ( $M = 35,000$ ), so that, in accordance with partitioning predictions, a substantial amount could penetrate the pores. All treatments were tested with solutions of polystyrene in both 2-fluorotoluene (2FT) and trans-decahydronaphthalene (TD). About 1 g of dilute (5 mg/ml) polystyrene solution was added to 0.25 g of glass fragments in a test tube, which was then securely capped, vortex mixed, and equilibrated for 2 weeks at room temperature.

Tests for adsorption were then made by comparing the total intensity of light scattered from supernatant solutions (i.e., above beads) to that from control solutions (i.e., no beads), as follows. At fixed angle, for a given polymer, the excess Rayleigh ratio  $\mathfrak{R}_E$ , defined as the difference between the Rayleigh ratios for solution ( $\mathfrak{R}_2$ ) and solvent ( $\mathfrak{R}_1$ ), is to first order proportional to the polymer concentration  $c$ :

$$\mathfrak{R}_E = \mathfrak{R}_2 - \mathfrak{R}_1 \propto c \quad (4.22)$$

In practice, ratios between scattered intensity (at  $90^\circ$ ) and the intensity of a deflected portion of the incident beam were used in place of Rayleigh ratios. By this means, ratios of concentration in the supernatant ( $c_0^+$ ) to the initial concentration of solution added ( $c_0$ ) were obtained and compared to theoretical ratios estimated using partitioning theories. Theoretical ratios  $c_0^+/c_0$  were estimated as:

$$(c_0^+/c_0) = 1 / \{1 - x(1 - K_D)\} \quad (4.23)$$

with the partitioning coefficient  $K_D$  being defined as the ratio of the concentration inside the pores to out ( $K_D = c_p/c_0^+$ ), and  $x$  being the solution volume fraction inside the pores. The quantity  $x$  was calculated as:

$$x = w_G v_p \rho_2 / w_2 \quad (4.24)$$

with  $w_G$  and  $w_2$  being the weights of glass fragments and solution respectively,  $v_p$  the specific pore volume of the glass ( $0.92 \text{ cm}^3/\text{g}$ ), and  $\rho_2$  the density of the solution (2FT,  $1.001 \text{ g/cm}^3$ ; TD,  $0.870 \text{ g/cm}^3$ ).

Evaluation of equation (4.23) requires a value for  $K_D$  in addition to the experimental quantity  $x$ . The partitioning coefficient  $K_D$  was estimated to lie in the range 0.45 to 0.69. The lower value  $K_D = 0.45$  was obtained from Figure 1 (Chapter II) for  $\lambda_H = R_H/R_p \approx 0.19$ , using  $R_H$  of 40 Å (2FT) and 39 Å (TD), and  $R_p$  of 211 Å (revised from manufacturer's value, see Table 2);  $K_D = 0.45$  is about the middle of the range of theoretical values for Gaussian chains with  $\lambda_H = 0.19$  in different pore geometries. The upper value  $K_D = 0.69$  was obtained from Figure 1 for  $(\lambda_H/1.8) \approx 0.10$ . This factor 1.8 was empirically found to bring partitioning data for polystyrenes in good solvents in similar controlled pore glasses into agreement with theories for  $K_D$  for Gaussian chains.<sup>16,74</sup> (A value  $K_D \approx 0.55$ , for  $(\lambda_H/1.28) \approx 0.145$ , is in the middle of this range; the factor 1.28 is the ratio of  $2\sigma^{-1}/R_p$  for glass B1.)

Values of measured and calculated ratios  $c_0^+/c_0$  for various treatments are given in Table 4. The ratio of measured to calculated values is an estimate of how much polymer is *not* adsorbed. An upper limit on adsorption is provided from the lowest estimate of  $K_D \approx 0.45$ . A lower limit on adsorption is provided from the highest estimate of  $K_D \approx 0.69$ . In light of

TABLE 4  
Tests of Silanized Glasses for Polystyrene Adsorption

Code	2-Fluorotoluene $c_0^+/c_0^{\dagger}$			t-Decalin $c_0^+/c_0^{\dagger}$		
	meas.	calc.	Ratio(%)	meas.	calc.	Ratio(%)
B1-NO	0.714	1.050 (1.094)	68.0 (65.3)	0.002	1.077 (1.145)	0.2 (0.2)
B1-7	1.047	1.056 (1.105)	99.2 (94.8)	-0.002	1.082 (1.155)	-0.2 (-0.2)
B1-8	1.052	1.064 (1.122)	98.8 (93.8)	0.066	1.087 (1.165)	6.1 (5.7)
B1-9	1.061	1.064 (1.120)	99.8 (94.7)	0.195	1.075 (1.141)	18.1 (17.1)
B1-10	1.059	1.055 (1.103)	100.4 (96.0)	0.216	1.083 (1.158)	19.9 (18.7)
B1-11	1.064	1.072 (1.137)	99.2 (93.5)	1.010	1.089 (1.169)	92.7 (86.4)

<sup>†</sup> Ratio of concentration in the solution above glass to the concentration of solution originally added. The ratio of measured to calculated  $c_0^+/c_0$  gives an estimate of the amount *not* adsorbed. The first values are the best estimates of the amount adsorbed, while the values in parentheses are a conservative estimate of the greatest amount adsorbed (see text).

the discussion of equilibrium partitioning in Chapter II, I would emphasize that the *upper* estimate of adsorption, which follows from the *lowest* estimate of  $K_D$ , is believed to be an "extreme" estimate; that is, all reasonable theories, and also experimental data, would indicate  $K_D$  greater than that lowest estimate (i.e.,  $K_D > 0.45$ ).

For 2FT solutions, all treatments were largely successful in preventing adsorption. For TD solutions, however, only treatment B1-11 (hexamethyldisilazane) was reasonably effective. It should be pointed out that TD solutions were equilibrated at room temperature, which is perilously close to the theta-temperature ( $\Theta$ ) for polystyrene in TD ( $\Theta \approx 18.2-23.8^\circ\text{C}$ );<sup>117</sup> hence this was a quite stringent test. For TD solutions maintained at  $T > \Theta$ , treatments B1-9 and B1-10 were also relatively effective.

In 2FT, the amount adsorbed is estimated to lie between zero and 7%. (For another porous glass, molecular weight, and concentration, exact results might differ somewhat.) Uncertainty in estimating  $K_D$  and hence the expected values of  $c_0^+/c_0$ , not in measuring the actual ratios  $c_0^+/c_0$ , prevents me from concluding that adsorption of polystyrene from 2FT solutions is *totally* absent. However, such a conclusion is not unreasonable, based on the observations that: (1) adsorption from 2FT is not excessive, even for untreated glass; (2) 2FT is highly polar and would be expected to adsorb at least as strongly as polystyrene, if not more so; (3) 2FT is a good solvent for polystyrene; and (4) the better estimates of  $K_D$  and  $c_0^+/c_0$  (based on experimental results<sup>16,74</sup> for partitioning of polystyrene in good solvents in controlled pore glasses), when compared with results, indicate essentially zero adsorption for treated glasses. At the worst, if adsorption does occur,

these measurements provide an upper limit on the amount adsorbed, and hence on the contribution of adsorbed chain dynamics to correlation functions, of about 7%. Any such contribution of adsorbed polymer dynamics *might* be well separated temporally. (A better way to test for adsorption might be to look for residual fluorescence after thorough solvent washing of glasses which had been previously exposed to solutions of fluorescently labeled polystyrene.<sup>29)</sup>

Those factors mitigating against adsorption from 2FT solutions, namely solvent quality and polarity, are lacking for TD, evidenced by substantial amounts of polymer adsorption in these tests. Even if the glass were to be silanized using one of the better treatments (e.g., B1-9, B1-10, or B1-11) and solutions were kept at  $T > \Theta$  (e.g.,  $> 30^{\circ}\text{C}$ ), it is doubtful that adsorption could be totally eliminated, hence the decision not to pursue a parallel study of diffusion in the poorer solvent TD. If such a study were to be undertaken in the future, B1-11 would be the recommended treatment.

### **Sample Preparation**

All glass fragments used in the experiments reported in this dissertation were silanized using treatment B1-10 (2M chlorotrimethylsilane in toluene at  $95^{\circ}\text{C}$  for 3 days) or a minor variation thereof. The results of adsorption testing as reported above provide reasonable assurance that adsorption of polystyrene from 2FT is absent or negligible for glass treated in this way.

Solutions for light scattering were prepared by weighing the desired amount of polymer into a volumetric flask, then adding solvent. The

only agitation was by occasional inversion of the flasks. Solutions were not used immediately but allowed to sit to ensure complete dissolution: at least 2 days for lower molecular weights, or 2 weeks for the highest molecular weights. Solutions in t-decahydronaphthalene were maintained above the theta-temperature.

These solutions were filtered to remove dust. First, the filter assembly, consisting of 13 mm stainless steel Swinnex housing, Teflon o-ring and gasket, stainless steel support screen, and Fluoropore membrane filter (Millipore), was rinsed with dust free water and filtered acetone, then oven dried. After drying, about 50 ml of solvent was passed through until the filtrate was dust free. Next, the syringe and filter assembly were rinsed with about 3 ml of polymer solution. Finally, the polymer solution was filtered directly into dust free cells, one with no porous glass to serve as a control, and one or more containing porous glass. The cutoff size of the filter membranes (0.2 or 0.5  $\mu\text{m}$ ) was chosen as required to avoid removal of polymer from solution. Filtered samples were examined in the laser beam under low power magnification to ensure the absence of dust. Samples without porous glass which were prepared in this fashion typically showed no dust events even upon several minutes viewing. However, samples containing porous glass fragments would invariably show some slight dust contamination because of inability to insert the mounting assemblies in a totally dust free manner. It has been assumed that any such dust would be incapable of penetrating the porous glass and thereby incapable of affecting measurements inside the fragments.

Sample cells were generally standard 10 mm O.D. test tubes, sorted to remove those which were significantly scratched. Test tubes were made dust free by exhaustive washing with "super water", i.e., the deionized, doubly distilled, and dust free water available from the still apparatus in our laboratory. It was found that silane pretreatment of the test tubes, in order to deactivate the glass surface, greatly aided in obtaining dust free cells. Cells were soaked 8 hours in dilute (3% w/v) chlorotrimethylsilane in toluene, then rinsed with methanol prior to water washing. Super water cleaned cells were oven dried with slip-on caps of Teflon tubing. These tubing caps were sealed on one end and had several pinpricks, allowing water to escape but preventing entry of dust.

Filled sample cells were capped with Teflon stoppers (rinsed with super water and dried). The ends to be inserted into the test tubes were machined to a diameter ( $0.305 \pm 0.005$ " ) smaller than the I.D. of the test tubes. A tight seal was made by an o-ring inserted in an annular groove (width =  $0.105 \pm 0.010$ ", diameter =  $0.199 \pm 0.003$ " ) cut in the inserted end of the stoppers; this groove was designed for standard AS-568-008 o-rings. Either Viton or FETFE (a Viton/Teflon compound from Ace Glass) o-rings were used. These materials and the Teflon stopper are neither attacked nor leached by 2-fluorotoluene or t-decahydronaphthalene. (Different o-ring materials might be required for other solvents.) Samples sealed in this way lost negligible ( $<1\%$ ) solvent by evaporation, even on storage for months at room temperature, including some periods at the higher temperatures (about  $40^{\circ}\text{C}$ ) required for light scattering. Nonetheless, as a precaution, samples were always weighed to allow solvent loss, hence concentration, to be

monitored. This also allowed for the later possibility of in-situ dilution or concentration of samples.

Pieces of porous glass were held in assemblies that could be slid into the standard 10 x 75 mm test tube cells. The main Teflon insert blocks had the following features: inertness to 2FT (and most other solvents); low coefficient of friction for easy insertion; deformability, allowing them to be machined slightly oversize (diameter =  $0.314 \pm 0.002$ " ) to snugly fit the somewhat variable I.D. of the test tubes; and low dust affinity for easy cleaning. These inserts had channels cut along the sides to allow solvent to pass.

Subassemblies holding the glass fragments were inserted into centered holes (diameter =  $0.045 +0 - 0.002$ " ) in these main Teflon inserts. The smaller commercial fragments (B5, B7) were mounted by cold working a piece of standard wall Teflon spaghetti insulation (AWG#24) to enlarge the I.D., carefully placing the fragment in the enlarged end, then shrinking the tubing back with a heat gun to firmly hold the fragment. The larger glass pieces from Haller were mounted by attaching them to stepped stainless steel adapter posts (insert end diameter =  $0.045 +0.001 -0$ " , shrink tube end diameter =  $0.059 +0.002 -0$ " ) using Korvex 1.3X shrink tubing (AWG#18; Chemplast). All tubing used in mounting fragments was fluorocarbon plastic and totally inert to 2FT.

Fragment assemblies were rinsed with filtered acetone, oven dried, and inserted into test tubes prior to addition of polymer solutions. Care was taken during mounting to try to center fragments as well as possible in the tubing subassemblies. Nonetheless, the "centers" of completely mounted

fragments in test tubes were as much as 0.015" off center with respect to the vat center. Much of this is due to the varying and irregular shape of the fragments, which makes precise centering difficult. Resultant alignment problems are discussed in Chapter V.

## CHAPTER V

### DYNAMIC LIGHT SCATTERING EXPERIMENTS IN POROUS MATERIALS

#### Light Scattering Apparatus and General Procedure

The general objective of these experiments was to compare the effective diffusion coefficient  $D_{\text{EFF}}$  for a polymer inside a porous glass to the diffusion coefficient  $D_0$  of that same polymer in unbounded (i.e., bulk) solution, with said diffusion coefficients obtained from the autocorrelation functions (ACFs) of the intensity of scattered light. This section describes the apparatus and experimental procedure that was used to obtain these intensity ACFs.

As discussed in Chapter III, there are two basic experimental arrangements--homodyne and heterodyne--in dynamic light scattering. Both of these arrangements were used in these experiments: homodyne for bulk solution measurements, and heterodyne for measurements in the porous glass. The heterodyne arrangement, which involves the mixing of a local oscillator field with the field of light scattered by the solution at the photomultiplier cathode, is generally more complicated experimentally than the homodyne arrangement because of the requirement that the local oscillator and scattered wavefronts be "matched" at the photocathode; also because a small amount of drift or fluctuation in the local oscillator may overwhelm the relatively weak experimental signal. Hence, the simpler

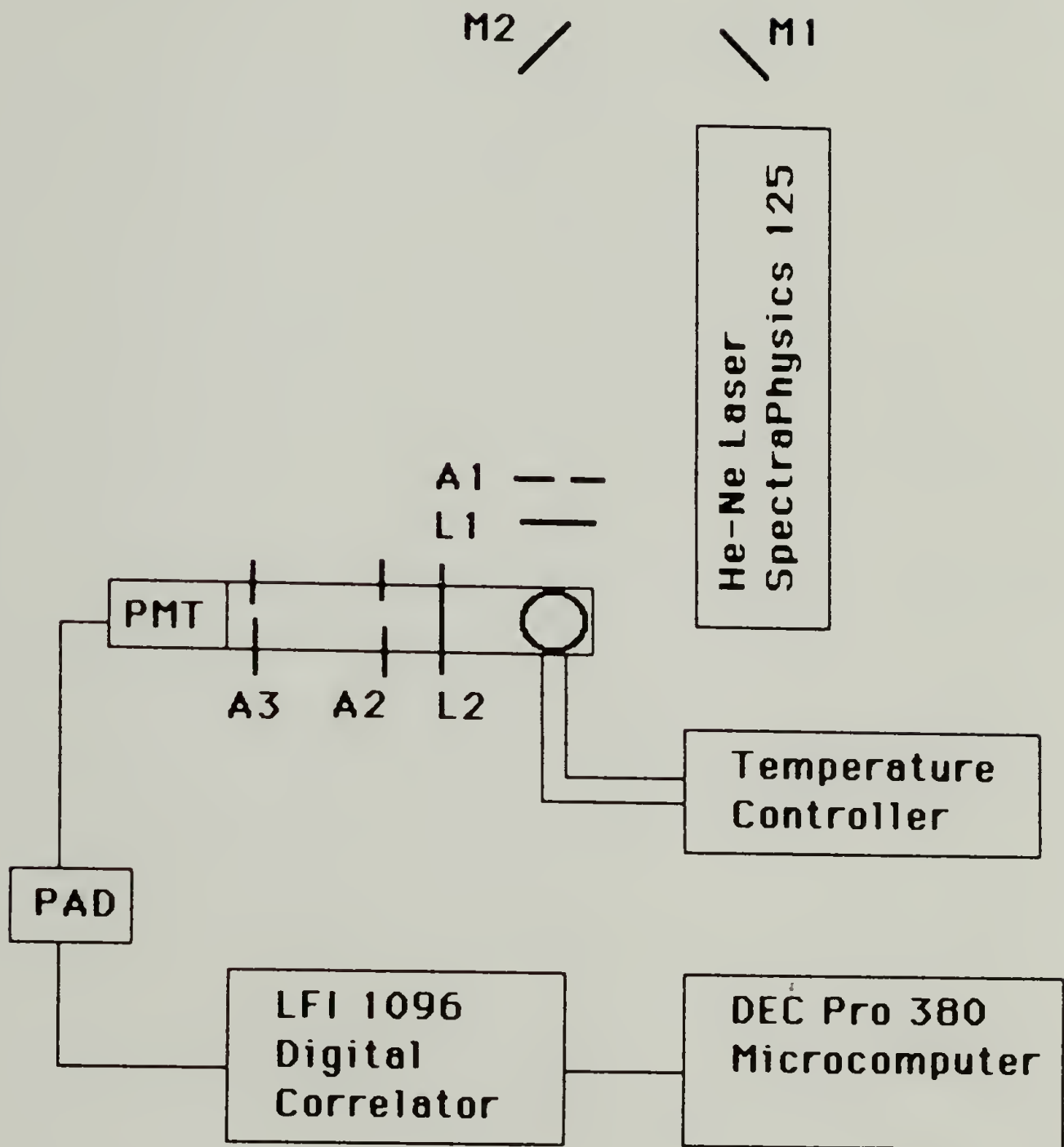
homodyne arrangement is usually used for making measurements with polymer solutions, as it was in this work.

Despite these comments, the heterodyne arrangement which was used for making measurements in the porous glass was actually fairly simple (at least in some ways). The basic idea was to use light scattered from the porous glass as a local oscillator. Since this light comes from the same spatial region (the scattering volume) as the light scattered by the polymer solution, the local oscillator and scattered fields are well matched. This technique relies on the glass being stationary, so that the light scattered by the glass is not frequency shifted. The amount of scattering, that is, the local oscillator strength, was controlled by appropriately adjusting the refractive index of the solution. This involved choosing a solvent with a refractive index nearly matching but slightly higher than that of the glass at room temperature, thereby reducing scattering from the glass to a basically tolerable level. (In air, porous glasses with these relatively large pore sizes scatter light so strongly that they are opaque.) Final control of the scattering strength involved raising the temperature, hence lowering the solution refractive index, to achieve an optimum match ( $dn/dT < 0$ , and  $|dn/dT|_{\text{SOLUTION}} \gg |dn/dT|_{\text{GLASS}}$ ). More detail on this local oscillator scheme is given in this and the following sections of this chapter.

A fairly standard light scattering spectrometer, shown schematically in Figure 10, was used in these experiments. The scattering cell, containing polymer solution either with or without glass, is situated in a temperature controlled vat. The light scattered by the sample from a sharply focused incident laser beam is detected by a photomultiplier

Figure 10.

Dynamic light scattering apparatus.



mounted on the end of the movable scattering arm. The scattering angle  $\theta$  is fixed by the rotation of this arm from the forward beam direction. The lens on the arm serves to focus an image of the scattering volume on the pinhole, while the aperture and pinhole, along with the diameter of the incident beam, serve to define this scattering volume. The pulse amplifier discriminator transforms the photomultiplier output into standard logic pulses acceptable by the digital correlator, ideally providing one pulse per detected photon.

The digital correlator takes these photon pulses (i.e., the intensity) and computes the photon count ACF, which is closely related to the intensity ACF discussed in Chapter III:

$$\frac{\langle n(\tau) n(\tau + t) \rangle}{\langle n \rangle^2} = g^{(2)}(t) + \langle n \rangle \delta(t) \quad (5.1)$$

Aside from a shot noise term at  $t=0$  ( $\delta(t)$  is a delta function), the normalized ACFs are the same. Actually, what is computed by the correlator is not a continuously varying function, but an approximation at discrete values of  $t=j\Delta t$ ,  $j=1, 2, 3, \dots$ , where  $\Delta t$  is the sample time, which can be set on the correlator. This function  $C(j\Delta t)$  is defined as:

$$C(j\Delta t) = \sum_{i=0}^{N-1} n(i\Delta t) \tilde{n}([i+j]\Delta t) \quad (5.2)$$

where  $N$  is the total number of sample times over the duration of the experiment,  $n(i\Delta t)$  is the *total* number of pulses arriving in the  $i^{\text{th}}$  sample time interval, and  $\tilde{n}([i+j]\Delta t)$  is the number of *prescaled* pulses arriving in the

$(i+j)^{\text{th}}$  sample time interval. Roughly speaking,  $\tilde{n}=n/2^m$ , where the prescaling factor  $2^m$  can be set on the correlator.

The function  $C$ , which is experimentally measured, is a reasonably good approximation to the exact photon count correlation function  $\langle n(0)n(t) \rangle$ , and hence, by equation (5.1), to  $G^{(2)}(t)$ , when the departure of the correlation function from linearity over an interval  $\Delta t$  is small. (N. B. The function  $C$  is of course  $N$  times the photon count ACF  $\langle n(0)n(t) \rangle$ , hence also a factor of  $N$  times  $G^{(2)}(t)$ .) Following this assumption, for the remainder of this dissertation discussion is in terms of  $G^{(2)}(t)$ , not  $C$ ; but it should be kept in mind, as has been amply discussed in a number of references (e.g., see<sup>144</sup>), that  $C$  is indeed a *biased* estimate of  $G^{(2)}(t)$ . (Some comment is made on this in Chapter VI.)

Of great importance in analyzing exponential decays, as are expected for random thermal diffusion, is knowing the baseline, that is, the value of  $G^{(2)}(\mathbf{q}, t)$  for  $t \rightarrow \infty$ . From the correlator, two estimates of this baseline can be obtained. The first, which will be called the " $p^2/N$ " baseline, or  $B_p$ , is the square of the average intensity, or in the photon counting implementation (i.e., for the function  $C$ ),

$$B_p = P \cdot P_S / N \quad (5.3a)$$

where

$$P = \sum_{i=0}^{N-1} n(i\Delta t), \quad P_S = \sum_{i=0}^{N-1} \tilde{n}(i\Delta t) \quad (5.3b)$$

The second baseline, which will be called the "last channels" or "delayed" baseline or  $B_L$ , is simply the average of the last  $Y$  channels, out of a total of  $X$  channels, of the correlator. Generally, these last  $Y$  channels can be delayed by some time interval  $Q\Delta t$  from the first  $X$ - $Y$  channels so as to provide an estimate of  $G^{(2)}(\infty)$ . The critical question of baseline determination for the heterodyne experiments (i.e., with the porous glass) is discussed in the second section of this chapter.

Having given an outline of the dynamic light scattering experiments and the apparatus, these subjects will now be covered again, in reverse order and in more detail. The purpose here is to adequately describe the significant details of the apparatus and procedure, for although dynamic light scattering experiments are simple--put in a sample, scatter light, and obtain a correlation function--the reliability of parameters derived by analyzing those correlation functions ultimately depends on the experiment having been performed properly (and, as in the third section of this chapter, analyzed properly). (Good comprehensive reviews of experimental aspects of dynamic light scattering, which emphasize the interrelationship of apparatus, procedure, and analysis, have been given by Oliver,<sup>144</sup> Ford,<sup>145</sup> and Chu.<sup>13</sup>)

Successful execution of these experiments required the design and construction of a new light scattering spectrometer. The old spectrometer, although quite suitable for homodyne (bulk solution) measurements, was found to be unsuitable for the heterodyne experiments. The primary problem was that of "vibrations": in a heterodyne experiment, relative motion (on the order of the wavelength of light) of the laser relative to the

sample is manifested as periodic or random contributions to the correlation functions. The cause or causes of these vibrations, which were nearly always apparent when using the old spectrometer, were never isolated. However, possible causes were identified as a guide towards constructing the new apparatus: vibrations from the argon laser cooling water supply or from the circulating water bath (connected to the sample holder) which was used for temperature control; or building vibrations, picked up by the apparatus, which was situated on a non-vibration isolated table; or vibrations of the sample holder (possibly driven acoustically), mounted in a relatively non-massive block at the end of a post.

The new apparatus, although not particularly elaborate, was designed with the primary goal of eliminating vibrations, the presence of which makes any analysis quite uncertain; and with a secondary goal of reducing sources of baseline drift, particularly critical for heterodyne experiments. (Some references to light scattering apparatus design can be consulted for general information.<sup>13,144,145</sup> Specific apparatus designs have been detailed and give some idea of tests for proper apparatus functioning.<sup>77,146</sup> A design idea not considered, but which perhaps might be useful in experiments on diffusion in porous materials, uses a microscope to focus and position the incident beam,<sup>147,148</sup> e.g., in a biological cell.)

The apparatus was constructed entirely on a massive 4' x 6' x 1' two-ton granite table supported on four inflatable vibration dampening legs; when inflated, the table floats suspended, largely decoupled from building vibrations. (The apparatus is located on the 5th floor of the wind-encircled

Graduate Research Center high-rise, with powerful 3-phase air-circulating blowers just down the hall.)

The laser is a 50 mW Spectra-Physics Model 125 helium-neon laser with Model 250 power supply, operated with the RF exciter near maximum power to suppress the 135 kHz plasma oscillation. The laser and power supply are enclosed in wire mesh to shield the 45 MHz RF output. Two low attenuation (power drop to  $\approx 40$  mW) "helium-neon" laser mirrors (Edmund Scientific) bring the laser beam across the center of the spectrometer and parallel to the table. (The mirrors are attached near the centers of rotation of the adjustable faces of the mounting assemblies, the wholes of which are bolted to the table.) The beam then passes through a 3mm pinhole, which serves as a very crude spatial filter (mostly removing extraneous reflections from the mirrors).

The beam is focused into the sample cell by a coated plano-convex lens ( $f = 80$  mm). The beam diameter ( $1/e^2$  intensity) is about 2 mm (unfocused) and  $50\text{ }\mu\text{m}$  (focused). Claimed beam divergence is about 0.7 milliradians ( $\approx 0.04^\circ$ ). The lens is mounted on a massive x-y-z translator, epoxied to the table.

The vat, in some ways the heart of the apparatus, serves the functions of holding the sample cell and of temperature control. Two cutaway views are shown (Figures 11 and 12), parallel and perpendicular to the table. The beam enters and exits through flat windows whose axes are parallel to the table. The scattering windows ( $15^\circ$ ,  $35^\circ$ ,  $65^\circ$ ,  $90^\circ$ ,  $115^\circ$ , and  $155^\circ$  on one side;  $25^\circ$  on the opposite side--see Figure 11) are tilted  $5^\circ$  down from the horizontal. The critical windows (entrance, exit,  $15^\circ$ ,  $25^\circ$ , and  $35^\circ$ ) are high

Figure 11.

Light scattering apparatus: cutaway view of vat parallel to table.

This figure shows the locations of the vat windows and two of the heater cartridges. The optic axes of the entrance ( $180^\circ$ ) and exit ( $0^\circ$ ) windows lie in this plane; the optic axes of the other windows are tilted down by  $5^\circ$ , and are coincident with the center of the vat at the  $0^\circ$ - $180^\circ$  beam line. Scale is 1:1.

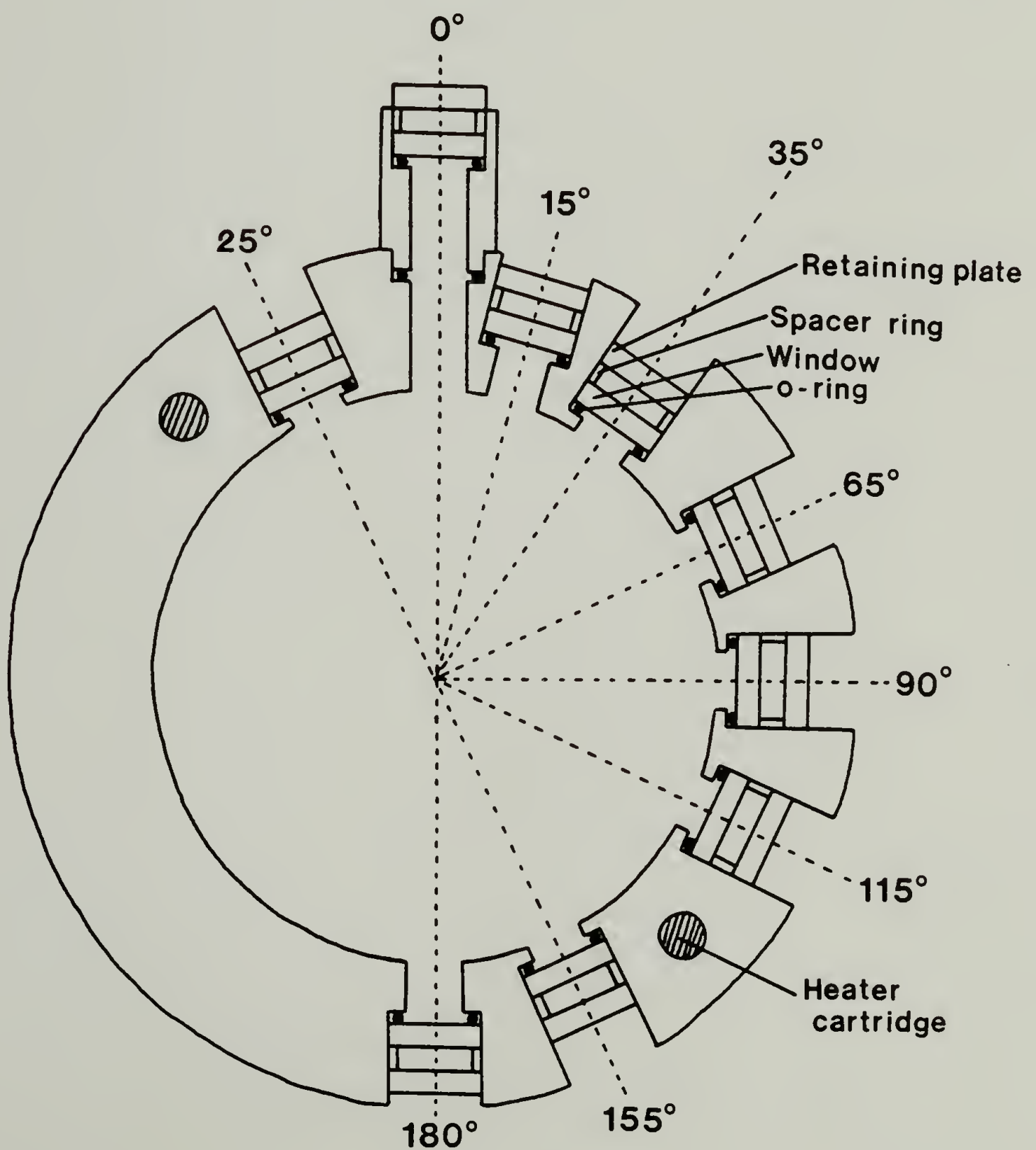
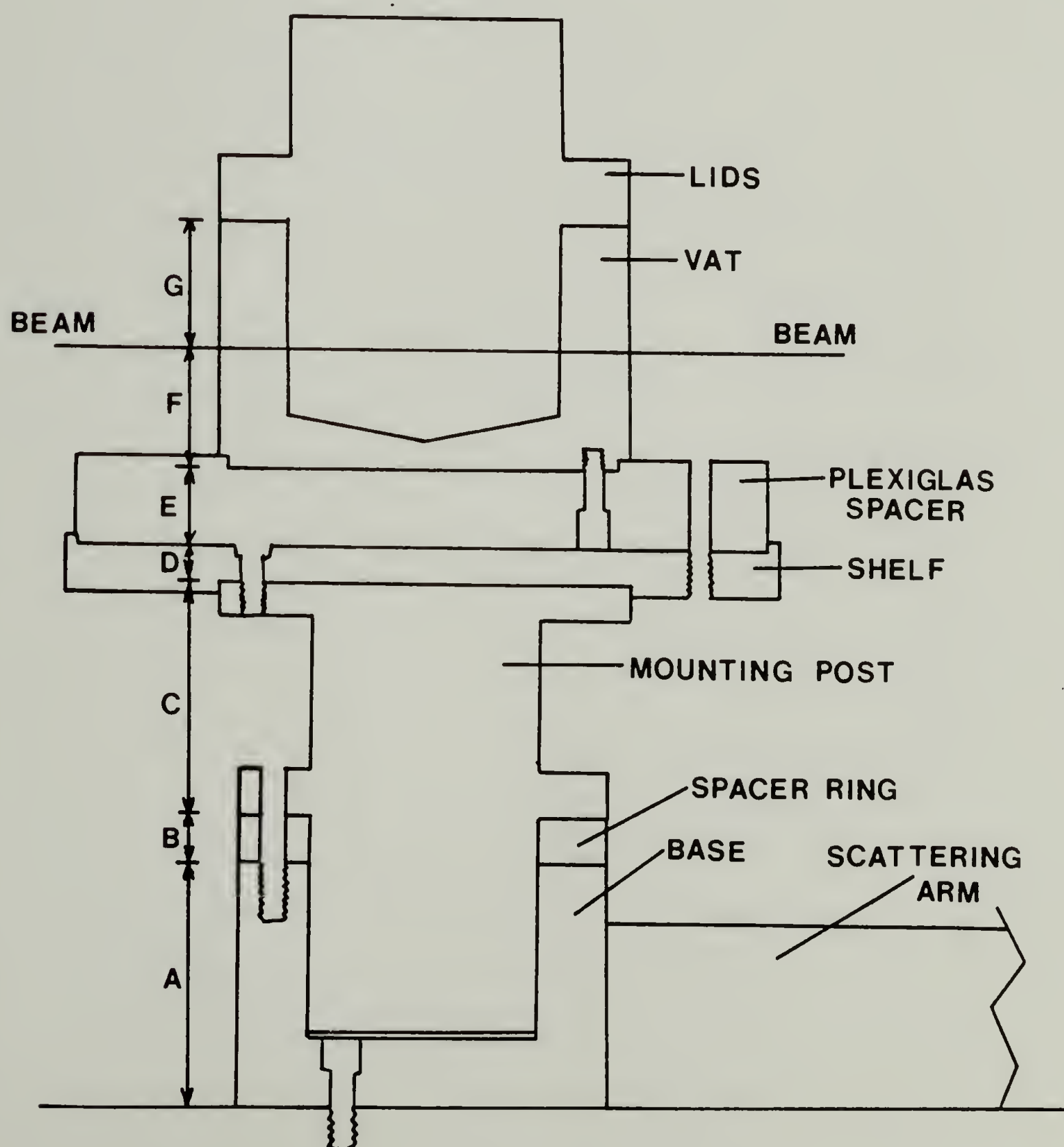


Figure 12.

Light scattering apparatus: cutaway view perpendicular to table.

This figure shows the mounting assembly by which the vat is held to the table, and about which the scattering arm rotates. Dimensions:  $A=2.625''$ ,  $B=0.50''$ ,  $C=2.375''$ ,  $D=0.375''$ ,  $E=0.875''$ ,  $F=1.25''$ , and  $G=1.375''$ . The height of the beam above the table is  $8.00''$ . Scale is 1:2.



quality ( $\lambda/20$  flatness, 1 sec parallelism) uncoated fused silica ( $n \approx 1.457$ ) windows (Oriel). The other windows, where wavefront distortion is less critical, are of lower quality, still fused silica (Continental Optics). Windows are mounted in counterbored holes, pressed lightly against o-rings to make a solvent-tight seal. The entire vat, constructed of aluminum, is black anodized, with all interior surfaces roughened before anodizing by glass peening. The vat is filled with trans-decalin, which nearly exactly matches the refractive index ( $n \approx 1.47$ ) of the solvent used in these experiments (2-fluorotoluene), and which matches the refractive index of the silica windows fairly well. Perhaps because of the tapered bottom, dust settles out of the vat fluid remarkably well. The apparatus is designed for use with interchangeable cell holders: one for 10.0 mm O.D. cylindrical cells, the other for 12.5 mm square cells. The cell holders allow for vertical adjustment but have very little and poorly controlled x-y adjustment capability. The vat has a bolt-on o-ring sealed lid, preventing rapid vat fluid evaporation.

The entire vat assembly (Figure 12) is mounted on a post which can be rotated to align the beam with the  $0^\circ$ - $180^\circ$  axis of the vat, then clamped in place. Separating the vat from this metal post is an insulating plexiglas plate. The vat assembly (aside from the windows) is insulated on the sides and top by 1" thick foam. The temperature control was designed with these particular experiments in mind (i.e., for above room temperature operation). Heating is by resistive electric cartridge elements, symmetrically positioned, with two parallel to the table and two perpendicular. The heaters are positioned such that any temperature gradient established will oppose convection in the vat fluid. The total heat load is selectable by a switching

box. Temperature control is via an Omega Series 6000 Microprocessor Controller equipped with a sheathed platinum RTD probe which is inserted vertically into the vat body; temperature control was to within  $\pm 0.1^\circ\text{C}$  over the course of a day, sufficient for these experiments.

The scattering arm rotates about a cylindrical base which is firmly bolted and epoxied to the table and to which the vat assembly is bolted. The optical subassembly slides on a  $5^\circ$  incline which is machined in the scattering arm and which was of course designed so that the optic axis of the detector arm intersects the  $0^\circ$ - $180^\circ$  beam axis. The entire scattering arm can optionally be clamped firmly to the table surface by application of vacuum; otherwise, it rests slightly raised on o-rings which provide the vacuum seal.

The optics of the detector arm are as follows. A lens ( $f = 80\text{ mm}$ ) serves to focus the scattering volume on the pinhole; the focus is adjusted by sliding the optic subassembly along the scattering arm and bolting it in place. The illuminated sample can be viewed through a low power microscope upon insertion of a reflex mirror in the path of the scattered beam; this feature is immensely useful in these experiments. Along the optic axis, between the lens and the photomultiplier tube, are two (variable) apertures. The aperture closest to the PMT (selectable as 50, 84, 155, or  $250\text{ }\mu\text{m}$  diameter) largely determines the size of the cross section of intersection with the beam (i.e., the scattering volume); given the  $\approx 2.5\times$  magnification, these correspond to dimensions in the sample of about 20, 34, 62, and  $100\text{ }\mu\text{m}$ . The front aperture, closest to the lens, which is selectable at 1, 2, or 3 mm, determines the scattering solid angle accepted by the detector.

The photon counting electronics consist of an ITT FW-130 end-on photomultiplier tube (dark counts  $\approx 7/\text{sec}$  at  $20^\circ\text{C}$ ), operated at 2000 V. The PMT is connected by a short 6" BNC cable to a Langley-Ford Instruments Model PAD-1 pulse amplifier-discriminator. This PAD provides TTL output pulses as required by the correlators.

Two different Langley-Ford Instruments digital correlators were used. The 1096 Model, which was used most often, under normal single-block operation has 256 contiguous channels plus 16 channels reserved for measuring a last channels baseline. If these last channels are delayed, the gap between the contiguous channels and the baseline is  $1024 \Delta t$  ( $= 4$  times the contiguous channel span of  $256 \Delta t$ ). The DC-64 Model, used less often, has 56 contiguous channels plus an 8 channel baseline, with a delay of  $64 \Delta t$  ( $\approx$  one times the contiguous channel span of  $56 \Delta t$ ). Aside from the greater delay of the baseline, the primary advantages of the 1096 over the DC-64 which proved important for these experiments are: greater memory capacity in each channel; sample time settable to 2 significant figures (versus only multiples of 1, 2, or 5 for the DC-64); and four times better resolution in the contiguous channel range, making  $C(j \Delta t)$  a less biased estimate of  $G^{(2)}(t)$  over a given range of  $t$ . Both of these correlators were interfaced to a Digital Equipment Corporation Professional 380 microcomputer (the 1096 by IEEE-488, the DC-64 by RS-232) for automated data acquisition, cumulants analysis, and data plotting. The comprehensive computer program QLSCUM was written to perform these tasks. This microcomputer was also used to transfer data to a mainframe for more sophisticated analyses.

To summarize, successful execution of the heterodyne experiments was only made possible by the construction of this new light scattering spectrometer. First and foremost, the vibration problem was eliminated. Very importantly, the range of  $q^2$  was extended downward by about a factor of ten; in fact, only this made it possible to examine macroscopic diffusion. The large thermal inertia and better insulation of the new vat improved baseline stability. The more advanced correlator (i.e., the LFI 1096), as noted above, provided features useful for these experiments. However, as discussed in connection with the experiments, the apparatus as it currently exists suffers from small problems with alignment and angular measurement.

Having described the apparatus, the experimental procedure for collecting the raw data (i.e., the correlation functions) is now given; discussion of data analysis (i.e., the extraction of diffusion coefficients) is deferred to later this chapter, and to Chapter VI.

Cylindrical tubes containing the samples, that is, polymer solution with or without porous glass, were inserted in the vat and allowed to equilibrate for at least 30 minutes before starting data collection. Experiments were run in the temperature range 32-46°C, with measurements made at the same temperature for corresponding bulk and porous glass samples. The temperature was chosen to provide a suitable refractive index match for each particular porous glass sample (more below).

The assertion that the dynamic light scattering measurements were made on samples "at equilibrium" relies on an implicit, but untested, assumption; namely, that the change in temperature (i.e., from room temper-

ature to the slightly elevated temperature of the experiment) does not induce a significant flow of polymer either into or out of the porous glass. Such a flow could result from a change in the equilibrium partitioning coefficient with temperature. This seems unlikely, based on the observation that  $R_H$  for  $M_D = 1.05 \times 10^6$  polystyrene remains essentially unchanged, at about 283 Å, on going from 32.8°C to 45.5°C; similar insensitivity of  $R_H$  to temperature is seen for other molecular weights (see Chapter VII for various examples). Since the partitioning coefficient  $K_D$  is a function of molecular size, this result argues that  $K_D$  is not strongly temperature dependent, hence that a significant directed flow is not expected.

Bulk solutions were run in the homodyne mode. Sample times were chosen such that the contiguous channels spanned about 10 exponential time constants (about four base 10 logarithmic decades), that is,  $2 \langle T \rangle N_{\text{LAST}} \Delta t \approx 10$ , with  $\langle T \rangle$  the average relaxation rate and  $N_{\text{LAST}}$  the number of the last contiguous channel. Experiment durations were chosen to provide  $> 1 \times 10^7$  counts above baseline. This total duration was broken into 10-15 individual runs, each with greater than  $\approx 1 \times 10^6$  counts above baseline, in order to allow the discarding of "dusty" runs; however, due to care in sample preparation,  $< 1\%$  of runs ever had to be discarded, even at  $\theta = 15^\circ$ . For these bulk solution measurements, prescaling was never used, and the last channels were always delayed. The last channels baseline was always within 0.1% of the  $p^2/N$  baseline for these nearly monodisperse samples. Values of the coherence function  $f_c$  ranged from 0.15 to 0.6, depending primarily on the aperture settings but also on the polymer molecular weight. An estimate of the noise to signal ( $N/S$ ) for these homodyne experiments is:

$$N/S = \frac{\{ (1 + f_C) B \}^{1/2}}{f_C B} \quad (5.4)$$

where B is the baseline. (This expression assumes relatively low light levels and Poisson statistics.) Given the usual level of counts above baseline (i.e.,  $f_C B$ ) and the range of  $f_C$ , the N/S was less than  $\approx 8 \times 10^{-4}$  (total summed run) and less than  $\approx 3 \times 10^{-3}$  (each individual run) for these bulk solution measurements.

The experiments looking at scattering from a polymer solution inside a piece of porous glass were far less routine. Primary difficulties centered on: (1) ensuring that the scattering volume lay entirely within the porous glass fragment; and (2) obtaining an optimum level--neither too high nor too low--of scattering from the glass (i.e., the local oscillator) compared to scattering from the polymer solution.

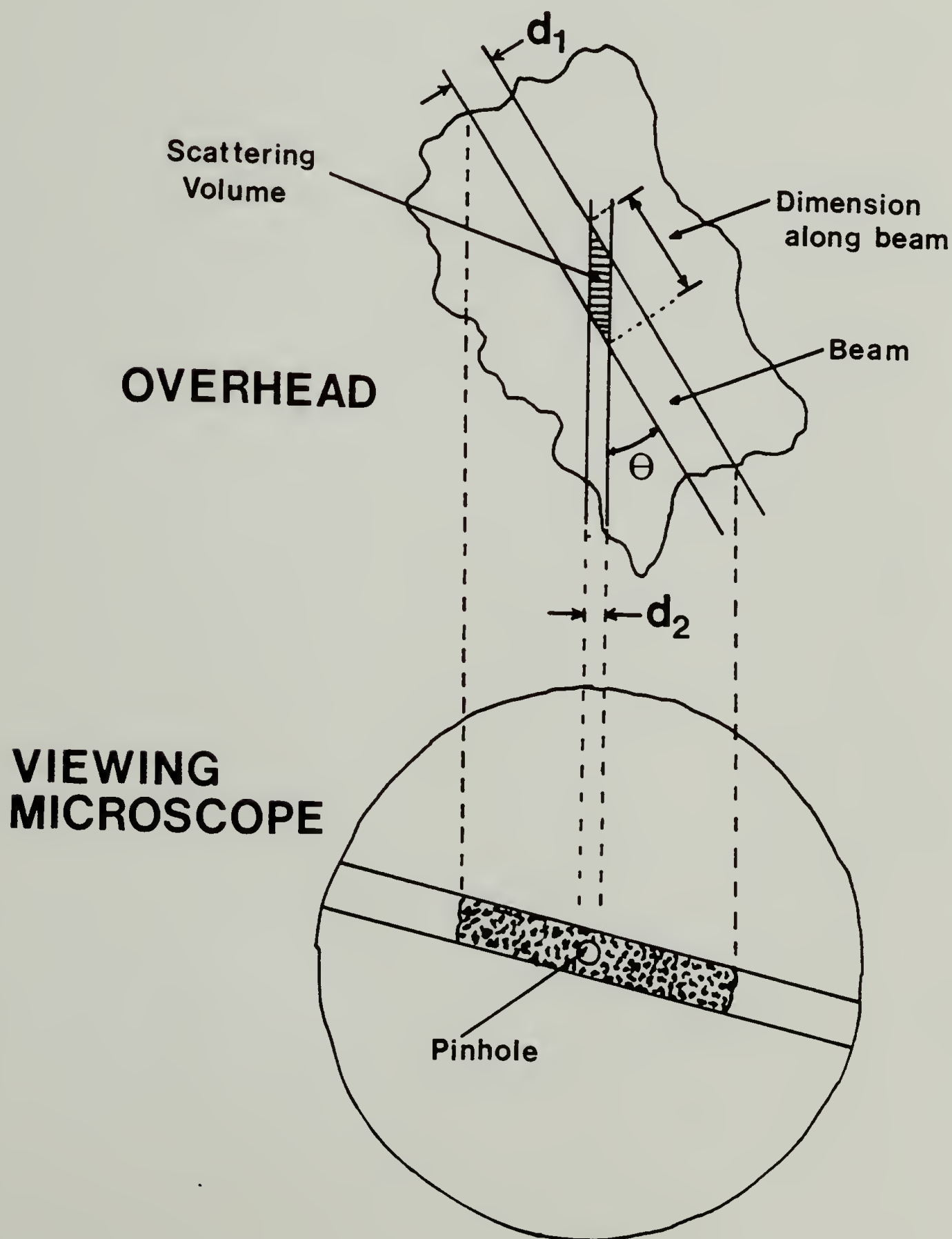
The first problem only existed because of the small size of most of the fragments that had to be used. The admittedly less than ideal procedure to deal with this problem is as follows. As a first step, the sample cell was carefully adjusted to align the major fragment dimension parallel to the beam. As a second step, the beam was centered between the fragment edges. Figure 13 shows the intersection of the thus aligned beam with a fragment, both an overhead view, and as it appears through the viewing microscope.

The "less than ideal" nature of this procedure is that the beam was centered in fragments by *shifting the beam off the  $0^\circ$ - $180^\circ$  axis of the spectrometer* by moving the focusing lens sideways. Typically, a shift of 0.010"-0.020" (250-500  $\mu\text{m}$ ) was required, resulting in a deflection of the

Figure 13.

Situation of the scattering volume in porous glass fragments.

This figure shows the relationship (not accurately drawn to scale) between the speckle pattern of an illuminated fragment, as seen through the viewing microscope on the detector arm, and an overhead view of the fragment. Equation (5.5) gives the dimension along the beam in terms of  $d_1$ ,  $d_2$ , and  $\theta$ .



beam in the forward direction of about  $0.25^\circ$ - $0.50^\circ$  (5-10 milliradians). Although this deflection could be approximately corrected for in calculating  $q$ , it is obviously less than ideal. It was initially believed that this was due to problems in precisely centering fragments during mounting (which is indeed a problem); however, as evidence accumulated, it pointed to an error in design of the stationary cell holder jaw, or the location of the fastening holes for the jaw. (The jaw is apparently about 0.020" too far away from the beam, along the  $135^\circ$  line on "25° window" side of the vat.)

This off-center holder was only a problem because of the small fragment dimensions transverse to the beam: typically 0.015"-0.025" (300-500  $\mu\text{m}$ ) for B7 and B5, and about 0.040" (800  $\mu\text{m}$ ) for B13. It should be noted that, because of the excellent refractive index match of the vat fluid with 2-fluorotoluene, this small amount of off-center cell location caused *no noticeable deviation* upon insertion of cylindrical cells (e.g., for bulk solution measurements).

The other difficulty in ensuring that the scattering volume lie entirely within the fragment is seen by reference to Figure 13. The scattering volume is defined by the intersection of the cylindrical beam (diameter  $d_1$ ) with the cylinder defined by the detection optics (diameter  $d_2$ ). The y-dimension (along the beam) is given by:

$$\text{y-dimension} = \{d_1/\tan \theta\} + \{d_2/\sin \theta\} \quad (5.5)$$

For our apparatus,  $d_1 \cong 50 \mu\text{m}$ ,  $\theta_{\text{MIN}} \cong 14^\circ$ , and  $d_2$  is roughly the diameter of the back aperture divided by the magnification ( $M \cong 2.5$ ). For back

apertures of 50, 84, and 155  $\mu\text{m}$ , this gives a maximum y-dimensions of 285, 340, and 460  $\mu\text{m}$ .

Although the back aperture was usually set at 50  $\mu\text{m}$  (sometimes 84  $\mu\text{m}$ ) for these experiments (thereby giving relatively shorter y-dimensions), the fragment dimensions along the beam were small enough as to require careful positioning of the scattering arm. Experimentally, this required moving the scattering arm to put the pinhole about midway (or slightly in the forward direction) between the illuminated fragment edges. Typical fragment dimensions along the beam were:  $\approx 800 \mu\text{m}$  (B13),  $\approx 500$ - $1000 \mu\text{m}$  (B7), and  $\approx 400$ - $700 \mu\text{m}$  (B5). Misalignment could often be detected as an anomalously high diffusion coefficient, due to contributions from diffusion in bulk solution. However, following the above alignment procedure, such misalignment was rarely seen except for the smallest fragments at the smallest angles. Obviously, at angles less oblique to the beam, the problem is less critical.

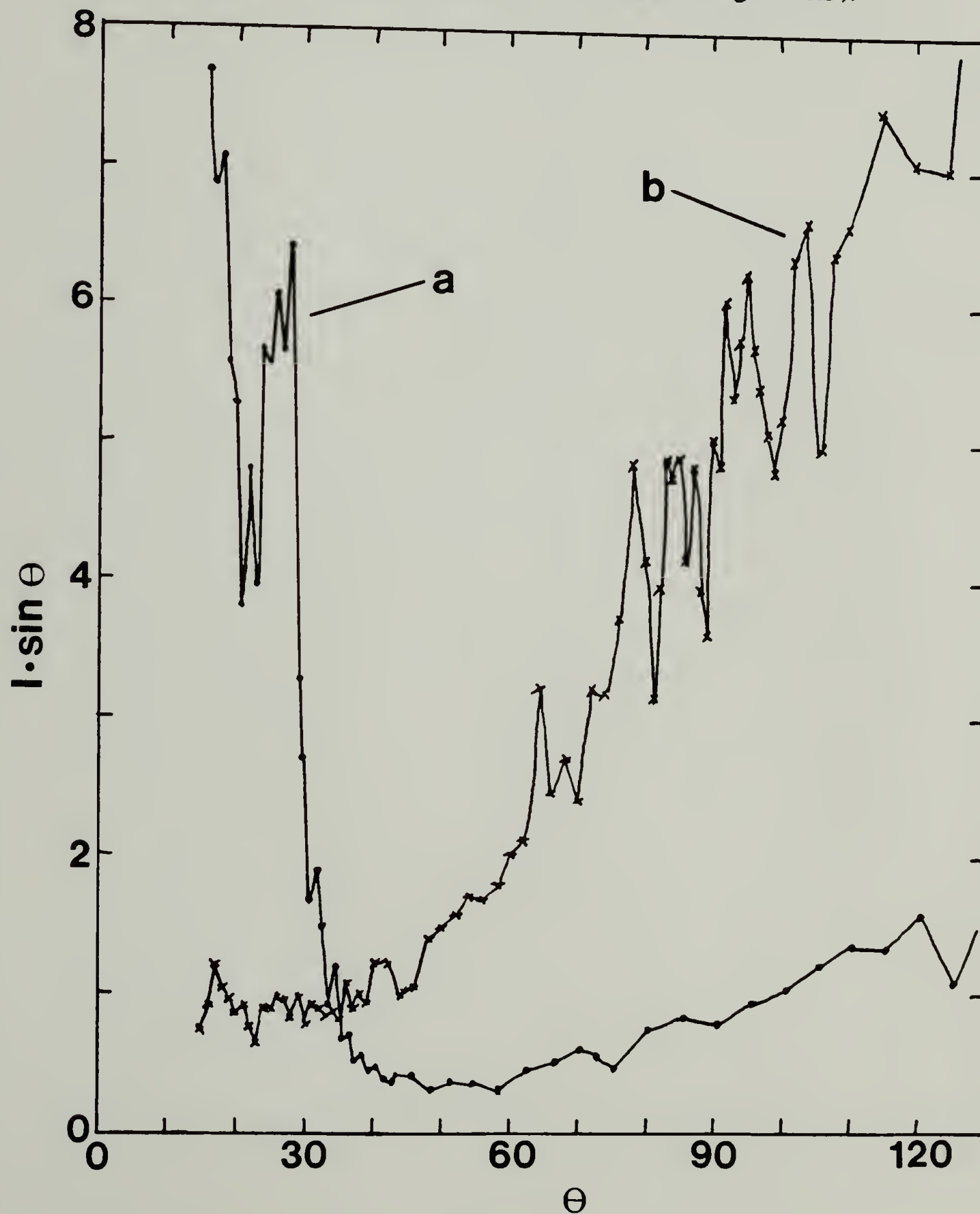
The problem of controlling the strength of the local oscillator can be understood by reference to Figure 14. The intensity of scattering from the porous glass shows not only relatively sharp local variation, but also more gradual variation, as a function of scattering angle. Interference of the largely coherent light scattered by the stationary "fluctuations" in the solution-filled porous glass produces the speckle pattern (i.e., the local variation). The more gradual variation is determined by the structure factor of the glass; that is, it is related to the characteristic length scale (the correlation length) of the porous glass. The location of maxima and minima in this

Figure 14.

Angular variation of intensity of light scattered by porous glass fragments.

Plots of  $I \cdot \sin \theta$  (intensity  $I$  in arbitrary units;  $\sin \theta$  corrects for variation in scattering volume size) vs scattering angle  $\theta$  for typical porous glasses, in 2-fluorotoluene, at temperatures about  $0.5^\circ\text{C}$  off optimum match.

(a)  $R_p = 577 \text{ \AA}$ ,  $\Phi = 0.70$ ; and (b)  $R_p = 250 \text{ \AA}$ ,  $\Phi = 0.30$  (glass RB).



overall structure factor is influenced by the temperature, as that affects the refractive index mismatch between glass and solution.

Given this "macro" and "micro" variation of intensity as a function of  $\theta$ , the adjustment of the temperature was aimed first at achieving the best compromise in terms of the macro intensity variation over the desired range of  $\theta$ . The micro intensity variation was then used to fine-tune the intensity in the desired direction, either down in generally high intensity regions, or up in generally low intensity regions. Practically, this fine-tuning was performed by either slight movement of the scattering arm, or by a slight shift in the incident beam; both of these serve to shift the speckle pattern relative to the pinhole.

Although the apparent coherence function  $f_c^+$  ranged from about 0.001 up to 0.06 for these experiments, it was generally attempted to maintain  $f_c^+$  in the range 0.01-0.02. Such a choice provides a reasonable compromise between homodyne "contamination" on the one hand, and the ability to accurately determine the baseline and to obtain a reasonable signal to noise level in a reasonable amount of time on the other hand. (The local oscillator is discussed quantitatively with regard to the "strong heterodyne" limit, in the second section of this chapter.) For these experiments, overall run times were chosen to give noise to signal (N/S) of about  $3 \times 10^{-3}$ , with N/S estimated as

$$N/S \approx (f_c^+ (2^m B)^{1/2})^{-1} \quad (5.6)$$

where  $2^m$  is the prescaling factor. In practice,  $N/S$  ranged from about  $8 \times 10^{-4}$  to  $1 \times 10^{-2}$ , but was generally near target; typically overall run times were about 1 hour.

In these experiments, the agreement between the last channels and  $p^2/N$  baselines was usually  $< 1\%$  for the overall summed run, and  $< 0.1\%$  for individual runs. Although the last channels were usually delayed, they sometimes were not. (Baseline determination is discussed in the next section.) Often prescaling was used; by equation (5.6), for a given  $f_c^*$  and nominal baseline,  $N/S$  is lower with prescaling. Occasionally, if the scattered intensity was excessive, neutral optical density filters were used to attenuate the incident beam rather than using very high prescaling. Prescaling when used was "continuous" in the sense that the shift register counter was not cleared at the end of each sample time; this is generally preferable to the "reset" alternative. As for the homodyne experiments, sample times  $\Delta t$  were chosen to have the contiguous channels span about 10 decay times (about 4 decades); or in other words,  $\langle T \rangle N_{\text{LAST}} \Delta t \approx 10$ .

All experiments were run with "raw" polarization: no polarizer preceding the vat (although the incident beam is highly vertically polarized); and with no analyzer preceding the detector. Due to the  $5^\circ$  tilt of the detector arm, a full consideration of the polarization of the scattered light is complicated. It has been assumed that the polarized intensity ( $I_{VV}$ ) was much greater than the depolarized intensity ( $I_{VH}$ ) in these experiments, hence that the decay of the  $I_{VV}$  intensity autocorrelation function is primarily that due to translational diffusion. (Strictly, of course, the situation is more complicated; since the detector is tilted, intensities are

neither UV, VV, or HV.) This assumption should be viewed with some skepticism for strongly confined chains, whose conformation is non-spherical; in such a case, it is possible that the  $I_{UV}$  intensity ACF has a significant depolarized contribution.

### Technical Details

This section treats the following topics: divergence of the incident wavevector in the porous glass; the suitability of the assumptions that are usually made in relating  $g^{(2)}(\mathbf{q}, t)$  to  $g_s^{(1)}(\mathbf{q}, t)$  for heterodyne experiments; causes of baseline drift; misnormalization of correlation functions as related to baseline error and the coherence function  $f_c^+$ ; and estimation of the homodyne to heterodyne ratio.

Divergence of the incident wavevector  $\mathbf{q}_i$  can lead to spectral broadening, since decay rates  $\Gamma$  (for translational diffusion) are proportional to  $q^2 = |\mathbf{q}_f - \mathbf{q}_i|^2$ . In addition, since the divergence in  $\mathbf{q}_i$  is expected to be symmetric about  $\theta = 0^\circ$  and since  $q^2$  is proportional to  $\sin^2(\theta/2)$ , then  $\langle \sin^2(\theta/2) \rangle < \sin^2(\theta_{\text{NOM}}/2)$ , implying that the average decay rate  $\langle \Gamma \rangle$  will be slightly less than  $Dq_{\text{NOM}}^2$ . (This assumes divergence mainly in the near-forward direction.) Lastly, any back-reflected light (effective incident wavevector of  $-\mathbf{q}_i$ ) will lead to complementary scattering, that is,  $\theta_{\text{EFF}} = \pi - \theta_{\text{NOM}}$ .

Of course, divergence in the final wavevector  $\mathbf{q}_f$  also causes spectral broadening. Since this divergence is determined by the detector optics--the solid angle subtended by the detector (e.g., the front aperture in our spectrometer)--it will be present in both homodyne and heterodyne experiments to

the same extent. (The relative amount of spectral broadening increases as  $q$  decreases, with aperture fixed; it can be significant, especially at low angles.) The discussion here focuses on *additional* spectral broadening as might be caused by the divergence of  $\mathbf{q}_i$  inside a porous material.

In considering these effects, attention is focused on both the expected causes of such divergence, and on experimental observations. The major cause of divergence is due to scattering by the porous glass, and is not due to reflection or refraction in the conventional sense. This conclusion follows from two observations. First, the interfaces between glass and solution (in the interior of fragments) are highly curved over distances less than the wavelength of light; these are not macroscopic interfaces at which reflection and refraction can occur. Second, the relative refractive index  $m \equiv (n_{\text{GLASS}}/n_{\text{SOLUTION}})$  is very close to unity. In this case, even the scattering, not to mention reflection and refraction, is relatively weak. This latter observation is also important, because if scattering from the glass were quite strong, then this scattered light could itself serve as a source of light (with wavevector different from that of the incident beam) to be scattered by the polymer solution ("multiple scattering").

Experimental observations support the conclusion that divergence of the incident wavevector is relatively unimportant; however, the necessary measurements to estimate quantitatively the extent of this divergence were not performed.

There is no noticeable broadening of the beam (as judged by the diameter in the forward direction) on passage through a solution with a single glass fragment, as compared to a solution without one. Viewing of the

beam through the microscope on the detector arm also shows no significant divergence for single fragments, as judged by comparison of the size of the beam image inside and outside of a fragment. The path length through single glass fragments was less than 1 mm. However, in earlier experiments on packed beds of fragments (8 mm total path length; 4 mm path prior to the scattering volume) some divergence was seen, evidenced by broadening of the beam in the forward direction and broadening of the beam image in the microscope.

If divergence in the forward direction (from whatever cause) were significant, it would lead to more spectral broadening at low  $q$ . This is counter to the observed trend, where the normalized variance  $\mu_2/\langle I \rangle^2$  actually decreases and then levels off at low  $qR_p$  (see Chapter VI, section 2). Further, since this variance is similar in magnitude to that in bulk solution, it implies that any divergence-caused broadening cannot be large. (N. B. This is not to rule out the possibility that such divergence might become important at angles still lower than those accessible with the current apparatus.)

Significant divergence as might be caused by scattering by the solution, from light initially scattered by the glass, is unlikely. The scattering from the glass ("concentration"  $\approx 1000$  mg/ml) was generally only about 50-200 times greater than that from dilute ( $\approx 0.1$ -10 mg/ml) polymer solutions. Nearly index matched fragments do not evince the typical multiple scattering appearance of diffuse illumination; the beam remains clearly defined and there is no "noticeable" attenuation of the beam in the sample. (However, turbidity was never actually measured.) Given the dimensions of the scattering volume (50  $\mu\text{m}$  transverse, 500  $\mu\text{m}$  maximum along the beam)

any such "multiple scattering" divergence would be expected to be more significant at low  $q$ , which as mentioned above is not seen.

Back-reflection, which could lead to complementary scattering, is also not expected to be significant. The interfaces are not flat over the wavelength of light, hence reflection as such should be absent. Given the quality of the refractive index match, even if reflection did occur the reflectivity  $r$  for normal incidence would only be  $r \approx (n_1 - n_2)^2 / (n_1 + n_2)^2 \approx 5 \times 10^{-7}$ . Trends in the average relaxation rate  $\langle \Gamma \rangle$  and the variance  $\mu_2 / \langle \Gamma \rangle^2$  versus  $q^2$  (Chapter VI, section 2) do not support there being significant divergence due to back-reflection.

To close, however, it should be mentioned that macroscopic reflection and refraction perhaps cannot be totally ruled out. Occasionally, viewing of the beam showed localized bright spots of very strong scattering, sometimes at the edges, and sometimes in the interior of fragments. Presumably such spots are due to heterogeneities (e.g., non-porous regions) in the porous glasses. As it is not possible to rule out reflection, refraction, and "multiple scattering" effects from such relatively large heterogeneities, every attempt was made to adjust the beam and sample positions to give a beam image, as viewed through the microscope, free of such bright spots.

Starting from equation (3.34), the derivation of equations (3.36) and (3.37), both expressions for the heterodyne intensity autocorrelation function, involved several assumptions:<sup>13,15</sup> (1) that fluctuations in the local oscillator field  $E_{LO}$  are negligible; (2) that fluctuations of  $E_{LO}$  and the scattered field  $E_S$  are uncorrelated; and (3) that  $\langle I_{LO} \rangle \gg \langle I_S \rangle$ . The first two assumptions are considered now in light of the nature of the local oscillator,

namely, scattering from the porous glass; the last assumption will be considered separately.

From a practical standpoint, these assumptions could be restated as requiring the lack of correlations between  $E_S$  and  $E_{LO}$ , and the lack of fluctuations in  $E_{LO}$ , *on time scales comparable to that of the fluctuations of interest in  $E_S$*  (i.e., due to diffusion). Correlations between  $E_S$  and  $E_{LO}$ , and fluctuations in  $E_{LO}$ , occurring on much slower (or faster) time scales, might cause some problems (but in general not of major difficulty).

Several causes could give rise to correlated fluctuations in  $E_{LO}$  and  $E_S$ : fluctuations in laser output; fluctuations due to dust passing through either incident or scattered beams, either in the vat or in air; and fluctuations due to modulation of either incident or scattered beams on passage through time-variant thermal, hence refractive index, gradients. Slow fluctuation or long term drift in laser power will show up mainly on time scales longer than that associated with diffusion; this leads only to problems in baseline determination, as discussed later. The time scales associated with dust motion and with thermal gradients are more comparable to that of diffusion. The apparatus was designed to minimize these effects, as both can give rise to a spurious contribution to the correlation function associated with the dynamics of either dust or thermal gradients.

A more subtle possibility exists that the scattering from the porous glass matrix changes as polymer diffuses, due to change in the local refractive index of glass and solution. This could give rise to correlated changes in  $E_{LO}$  and  $E_S$  on the same time scale. (Whether field *cross-correlation* functions, between  $E_{LO}$  and  $E_S$ , would be expected to have the *same* relaxation

rate as the *autocorrelation* function of  $E_S$ , has not been considered.) To the extent that it is possible to consider the scattering from the glass as in the Rayleigh-Debye-Gans scattering (as opposed to Mie scattering) limit, these considerations will be relatively unimportant. It is noted that  $m = n_1/n_2 \approx 1.000 \pm 0.002$ , and  $qR_p|m - 1| \ll 1$ , which are the conditions for RDG scattering *if* the pores can be considered as independent scatterers. Despite the porous glass structure being rigid and bicontinuous, considering scattering from the matrix as in the RDG limit should be reasonable, given the above conditions, the randomness of the structure, and the relatively low intensity of light that is actually scattered from the nearly index matched matrix.

Fluctuations in  $E_S$  due to relative motion of the porous glass with respect to the beam, on time scales comparable to that of diffusion, leads to dire consequences for these experiments. The intensity autocorrelation function  $G^{(2)}(t)$  will then include a homodyne term for this glass motion,  $\langle E_{LO}(t)E_{LO}^*(t)E_{LO}(0)E_{LO}^*(0) \rangle$ ; normally, this term is part of the baseline. In addition, the usual heterodyne terms become "cross-heterodyne"; that is,  $\langle E_{LO}(0)E_{LO}^*(t)E_S^*(0)E_S(t) \rangle$  reduces not to  $I_{LO} \langle E_S^*(0)E_S(t) \rangle$  (under assumptions that  $E_{LO}$  and  $E_S$  are statistically independent and that  $|E_{LO}(t)| \approx |E_{LO}(0)|$ ) but to  $\langle E_{LO}(0)E_{LO}^*(t) \rangle \langle E_S^*(0)E_S(t) \rangle$  (under the assumption of statistical independence only). Since generally  $I_{LO} \gg I_S$ , these contributions of glass motion to  $G^{(2)}(t)$  can swamp the scattered field contributions of interest. The apparatus was designed to eliminate relative motion of the beam with respect to glass fragments (e.g., vibration dampening, electric heating, massive construction).

It is concluded that in the absence of glass motion, equations (3.36) and (3.37) for the heterodyne autocorrelation function are valid for the local oscillator scheme employed in this work, since most fluctuations and correlations of the local oscillator field relative to the scattered field can be largely eliminated experimentally, and in any regard, are generally on a far slower time scale than polymer diffusion. However, it is particularly important to control thermal gradients and porous glass motion, as these may occur on comparable time scales and give rise to undesired contributions to the overall correlation function.

Given the assumptions that have just been discussed, equation (3.34) for the heterodyne intensity ACF reduces to the simpler equation (3.36), which has both heterodyne and homodyne terms, with respective amplitudes of  $2 \langle I_S \rangle \langle I_{LO} \rangle / \langle I \rangle^2$  and  $\langle I_S \rangle^2 / \langle I \rangle^2$ . The fractional contribution of this homodyne term was estimated for these experiments, from experimental measurements of the coherence function, as follows.

If one assumes the coherence function  $f_C$  to be solely determined by the optical arrangement (e.g., aperture and pinhole sizes, lenses, etc.), then the amplitudes above the baseline for normalized heterodyne and homodyne intensity ACFs measured with the same optical arrangement are  $f_C^* = f_C \{ 2 \langle I_S \rangle \langle I_{LO} \rangle / \langle I \rangle^2 + \langle I_S \rangle^2 / \langle I \rangle^2 \}$  and  $f_C$  respectively. The ratio of homodyne to heterodyne *terms* in the heterodyne experiment is

$$f = \langle I_S \rangle / 2 \langle I_{LO} \rangle \quad (5.7)$$

which is given in terms of the ratio  $\xi = f_C^* / f_C$  as

$$f = (1/2) \{ (1 - \xi)^{-1/2} - 1 \} \quad (5.8)$$

and the fractional amplitude  $\alpha$  of homodyne signal is given as

$$\alpha = f/(1 + f) \quad (5.9)$$

In one experiment, the validity of this approach was tested by comparing values of  $f$  calculated from  $f_C^+$  and  $f_C$  using equation (5.8) to values of  $f$  calculated from measured  $\langle I_S \rangle$  and  $\langle I_{LO} \rangle$  using equation (5.7). The two approaches were in reasonable agreement, with the direct intensity measurements actually giving somewhat lower values for  $f$ , that is, lower estimates of the fractional homodyne contribution  $\alpha$ . For routine estimates of  $\alpha$ , equations (5.8) and (5.9) were invariably used; these equations are believed to provide a reasonable estimate of  $\alpha$  starting from the apparent coherence function  $f_C^+$  (from a heterodyne experiment), and the coherence function  $f_C$  (from a homodyne experiment), both on the same polymer sample and with the same optical arrangement. If anything, it is believed that the estimates of  $\alpha$  calculated in this fashion may err on the high side.

This entire discussion has assumed that the efficiency of mixing of the local oscillator and scattered fields is about unity. This is specifically supported by the results of the experiment above, where the coherence function predicted on the basis of intensity measurements was actually even somewhat lower than that experimentally measured. Further indirect support for a high efficiency of optical wavefront mixing comes from the relatively high values measured for  $f_C^+$  throughout the course of this work. A high efficiency of mixing is expected since the local oscillator and scattered fields arise from the same region in space, the scattering volume. This is of course a useful advantage of the porous glass as local oscillator.

Turning now to the important question of baseline determination, one source of difficulty is illustrated by a simple example.<sup>149</sup> Assume that the correlation function at very long times, that is, the baseline  $G^{(2)}(\infty)$ , is given by the square of the average intensity:

$$G^{(2)}(\infty) = N \langle n \rangle^2 \quad (5.10)$$

Say one measures the correlation function for a total duration of  $2N\Delta t$  and that the mean count rate for the first  $N$  intervals is  $\langle n \rangle$  and increases to  $\langle n \rangle(1+\beta)$  in the second  $N$  intervals. For this example:

$$G_{\text{app}}^{(2)}(\infty) = \langle n \rangle^2 \{1 + (1+\beta)^2\}/2 \quad (5.11a)$$

$$\langle n \rangle_{\text{app}} = \langle n \rangle (2+\beta)/2 \quad (5.11b)$$

with the normalized correlation function

$$g_{\text{app}}^{(2)}(\infty) = 1 + \{\beta^2/(2+\beta)^2\} \equiv 1 + \beta^2/4 \quad (5.11c)$$

showing that the increase in intensity leads to an error in the baseline. (This normalization by  $\langle n \rangle_{\text{app}}^2$  corresponds to normalization by the  $p^2/N$  baseline, equation (5.3a).) Obviously, the same result is obtained if the intensity decreases from  $\langle n \rangle(1+\beta)$  to  $\langle n \rangle$ ; hence *either* increase or decrease in intensity leads to a baseline that is too low. It is also apparent that if one normalizes not by the  $p^2/N$  baseline, but by the delayed baseline, i.e.,  $G_{\text{app}}^{(2)}(\infty)$ , such normalization error vanishes. Comparison of the delayed baseline, equation (5.11a), with the  $p^2/N$  baseline (the square of equation (5.11b)) shows that, by equation (5.11c), the delayed baseline will always be greater than or equal to the  $p^2/N$  baseline.

Before considering the effects of this misnormalization on the apparent shape of the correlation function, the sources of the difficulty in determining the baseline in these heterodyne experiments are discussed.

First and foremost, the total scattered intensity always drifts, over the course of relatively short (3-6 min) individual runs, and especially over the total run time duration (1-2 hr) for a given sample at a given angle. This drift can often be quite significant. It is this drift of the total intensity--either up or down--that makes the  $p^2/N$  baseline inherently too low as an estimate of the true baseline, with the error related to the extent of this drift. The primary cause of this intensity drift is not due to changes in the laser power output (the laser is fairly stable) but is due to changes in scattering from the sample, which is dominated by scattering from the glass. As was shown in Figure 14, the intensity shows quite sharp variation as a function of angle; and the positions of local maxima and minima change strongly with change in beam position. Even changes in position of 0.001" (25  $\mu\text{m}$ ) can change intensity by as much as a factor of 2 or 3. The maximum change in intensity that was ever observed over total run time was by a factor of about 2; typically, however, it was much less.

Any changes in the relative positions of incident beam, sample, and detector arm could thus lead to significant changes in intensity. Most likely as the cause of such shifts in relative position would be thermally induced dimensional changes, for example, of the laser cavity, optical mounts, sample cell holder, vat, etc. It is also possible that small changes in the temperature of the sample could change the relative refractive index match and hence the "location" of the scattering pattern. The exact causes of the intensity drift in

these experiments, out of the preceding suggestions and other possibilities, were not identified, in part because it was doubtful that they could be eliminated. Further, the ability to measure a delayed baseline, which does not cause any significant normalization error even when intensity drift is present, made this unnecessary.

As a consequence of the invariable unreliability of the  $p^2/N$  baseline (i.e., significantly too low), the baseline was always estimated in these experiments as the measured delayed channels baseline. As shown by equations (5.11), this delayed baseline is not expected to cause normalization error even when intensity drift is present. Nonetheless, some error can be involved in this last channels baseline if there are "moderately slow"--in comparison to diffusion--relaxations present. If such relaxations are associated with the sample (e.g., power law decay) then the delayed baseline will be too high; but if these relaxations are associated with "artifacts" (e.g., thermal gradient fluctuations, motion of dust in the beam, relative motion of the porous glass fragment and the beam), then the baseline may *in a sense* be too low. In such a case, the portion of the correlation function associated with diffusion may have totally relaxed to the baseline at the delay times given by the last channels; but if there is another more slowly relaxing "artifact" portion of the correlation function, (assumed to be of relatively low amplitude), then the measured last channels will reflect that slower decay and provide an effectively lower baseline for the (amplitude dominant) faster diffusional decay.

That such moderately slow decays were present was evident in several ways; however, the underlying causes were never identified. Even

samples of porous glass plus solvent only showed non-flat correlation functions at sufficiently long sample times ( $\Delta t$  greater than about 1 ms). Simultaneous measurements, on a single sample, of correlation functions with different  $\Delta t$  showed the fractional "amplitude" ( $<0.01$ ) of this drift to be much lower than the amplitude ( $>0.99$ ) associated with diffusion. This estimate was made by comparison of the extrapolated (to  $t=0$ ) value of the long time slope to the coherence function  $f_c^+$ . The magnitude of this drift in relative terms, that is,  $(\Delta G^{(2)}/G^{(2)})/\Delta T$ , was observed in a number of runs to be at most 0.1% per second. This drift implies absolute error in the delayed baseline (i.e., the drift at  $1280\Delta t$ ) of about 0.0001% ( $\Delta t = 1 \mu s$ ), 0.001% (10  $\mu s$ ), 0.01% (100  $\mu s$ ), and 0.1% (1 ms). However, the *relative* magnitude of this error (i.e., this error divided by  $f_c^+$ ), given the typically low  $f_c^+$ , on the order of 0.01, is thus a factor of 100 greater.

In accord with these results, the effects of this baseline drift (associated with slow decays of unknown origin) was noticeable for  $\Delta t \approx 0.5$ -1 ms, as required for the higher molecular weights at lower angles. Empirically, the relative error in the delayed baseline was at most 1% for  $\Delta t \approx 1$  ms, which is an order of magnitude less than the rough calculation above. Regardless, this drift at long times imposes a practical and quite real upper limit to the sample times that can reasonably be used,  $\Delta t_{MAX} \approx 1$  ms. Effort put into identifying and eliminating (if possible) the causes of this slow decay might enable the extension of these measurements to longer  $\Delta t$ .

Error and uncertainty in the baseline causes difficulties in analysis and establishes limits as to conclusions that can be drawn. The heterodyne intensity autocorrelation function  $G^{(2)}(t)$  can be written as:

$$G^{(2)}(t) = B_T \{ 1 + f_C^+ |g^{(1)}(t)| \} \quad (5.12)$$

where  $B_T$  is the true baseline (i.e.,  $G^{(2)}(t)$ ). Normally one considers the baseline subtracted and normalized function:

$$|g^{(1)}(t)| = \frac{G^{(2)}(t) - B_T}{f_C^+ B_T} \quad (5.13)$$

Assuming that  $f_C^+$  is known, but that the baseline  $B_0$  is used in place of  $B_T$ , where:

$$B_0 = B_T - \Delta B \quad (5.14)$$

the apparent field correlation function  $g_{app}^{(1)}(t)$  (assuming henceforth that  $g^{(1)}$  is real and even) is given by

$$g_{app}^{(1)}(t) = \frac{g^{(1)}(t) f_C^+ + (\Delta B/B_T)}{f_C^+ + (\Delta B/B_T)} \quad (5.15)$$

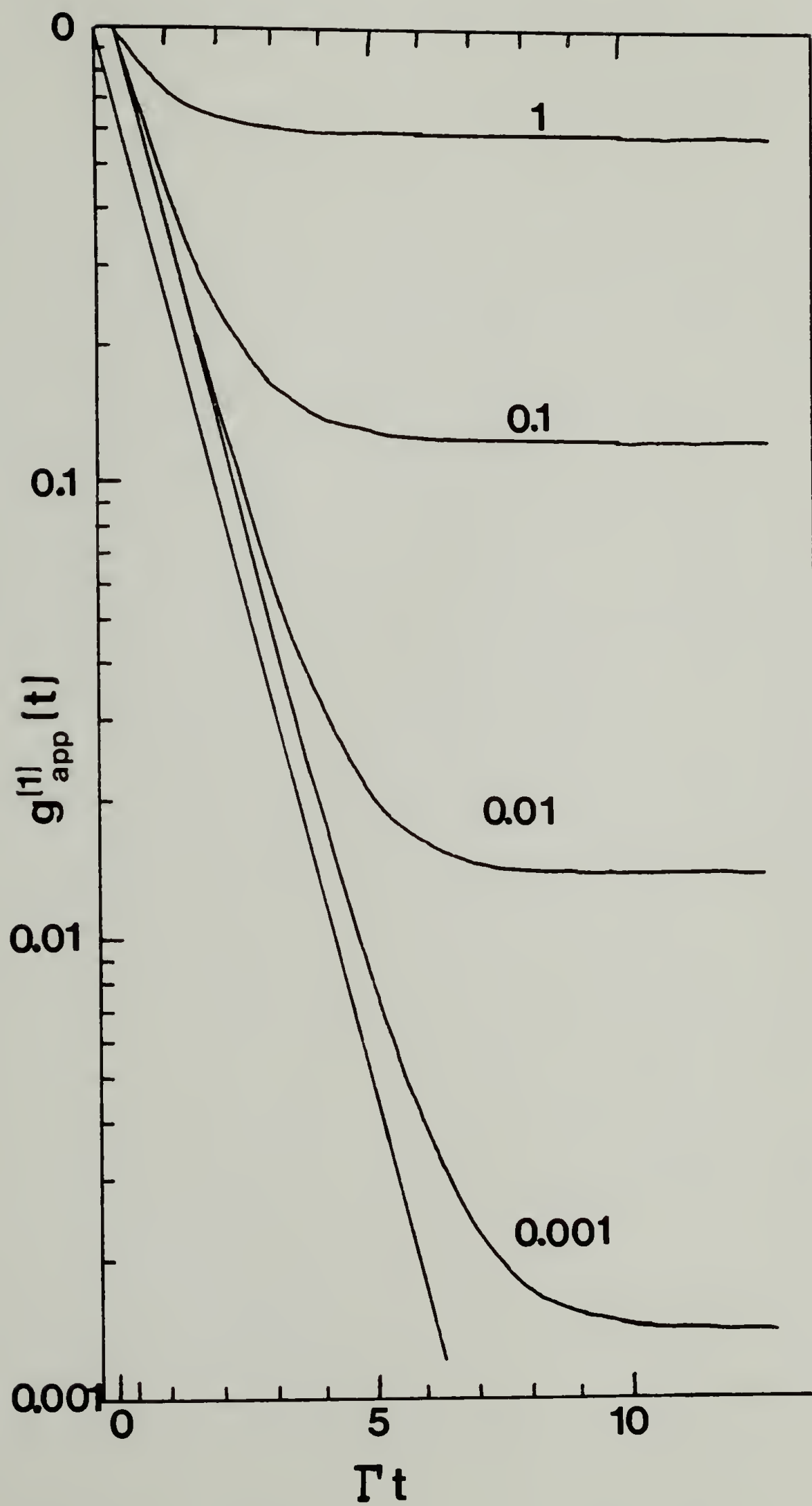
For  $\Delta B = 0$ , that is,  $B_0 = B_T$ , then  $g_{app}^{(1)}(t) = g^{(1)}(t)$ . From equation (5.15) it is seen that the extent of "misnormalization" due to baseline error depends on  $(\Delta B/B_T)/f_C^+$ , the fractional error in the baseline divided by the coherence function.

Plots of  $\log(g_{app}^{(1)}(t))$  versus  $\Gamma t$  are shown in Figure 15, for  $f_C^+ = 0.01$  and various values of  $(\Delta B/B_T)$ , shown in terms of  $(\Delta B/B_T)/f_C^+$ . For  $\Delta B > 0$  ( $B_0 < B_T$ ) there is a positive curvature in semilog plots, due to baseline misnormalization. Of course, such positive curvature is also expected for samples where there is a distribution of relaxation times (e.g., polydisperse

Figure 15.

Correlation function misnormalization due to baseline uncertainty.

These semilog plots of  $g^{(1)}_{\text{app}}(t)$  versus  $\Gamma t$  were calculated using equation (5.15) for various levels of misnormalization. Curves are identified by the value of  $(\Delta B/B_T)/f_C^+$ , which is also approximately equal to the experimental noise to signal ratio (see text). The true  $g^{(1)}(t)$  in this example is a single exponential with relaxation rate  $\Gamma$ , shown as the straight line (shifted for clarity).



polymer samples). For  $\Delta B < 0$  ( $B_0 > B_T$ ), not shown, there is a physically unrealistic negative curvature in semilog plots due to misnormalization.

It is clear from Figure 15 that even for fairly substantial misnormalization, the average relaxation rate  $\langle T \rangle$ , given by the initial slope ( $t \rightarrow 0$ ) in these semilog plots, should be determined moderately well. However, the variance of the decay rate distribution  $\mu_2/\langle T \rangle^2$  as determined by analysis of misnormalized ACFs can be significantly in error. If  $B_0 < B_T$  (positive curvature), the variance will be too high; and if  $B_0 > B_T$  (negative curvature), the variance will be too low. (Actual negative curvature might not be seen if the sample itself is intrinsically "polydisperse".)

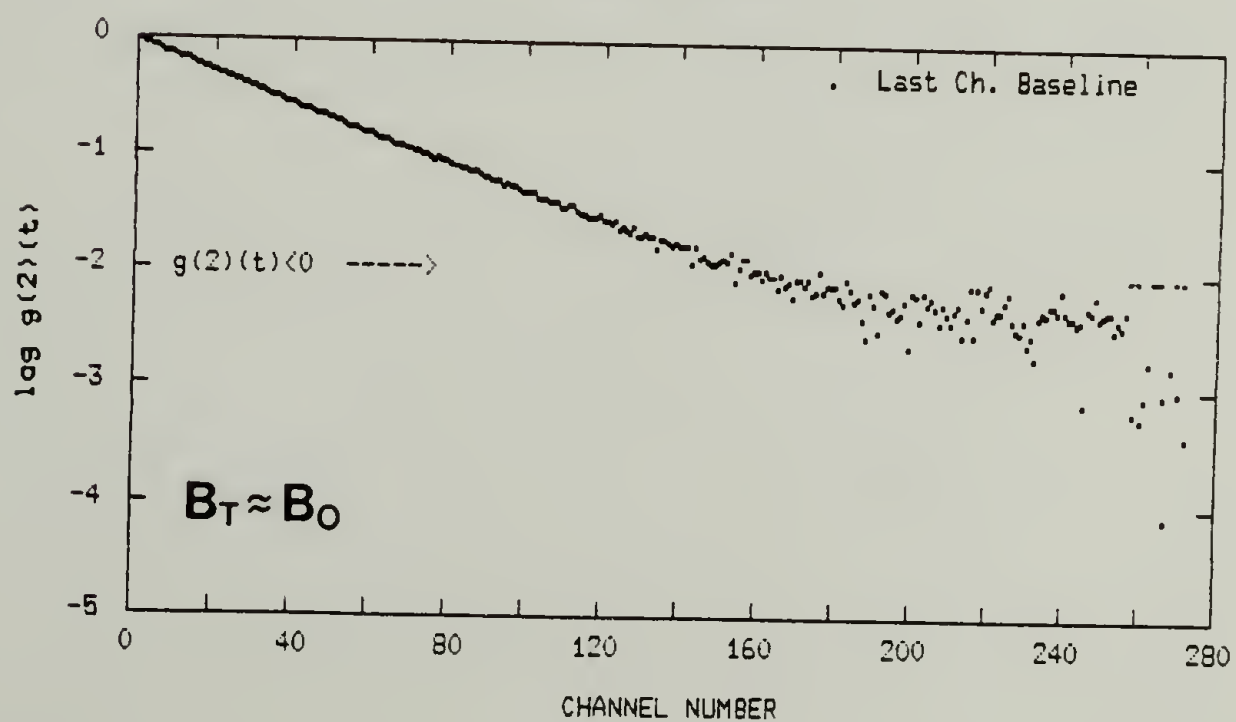
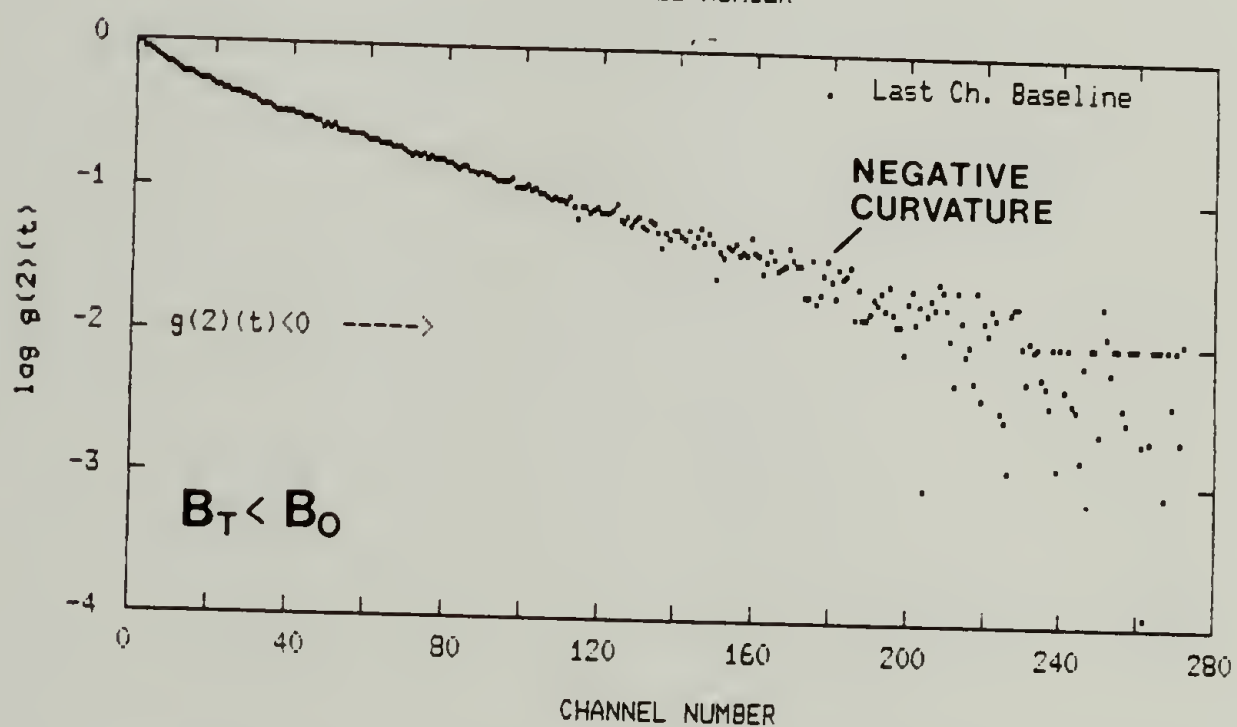
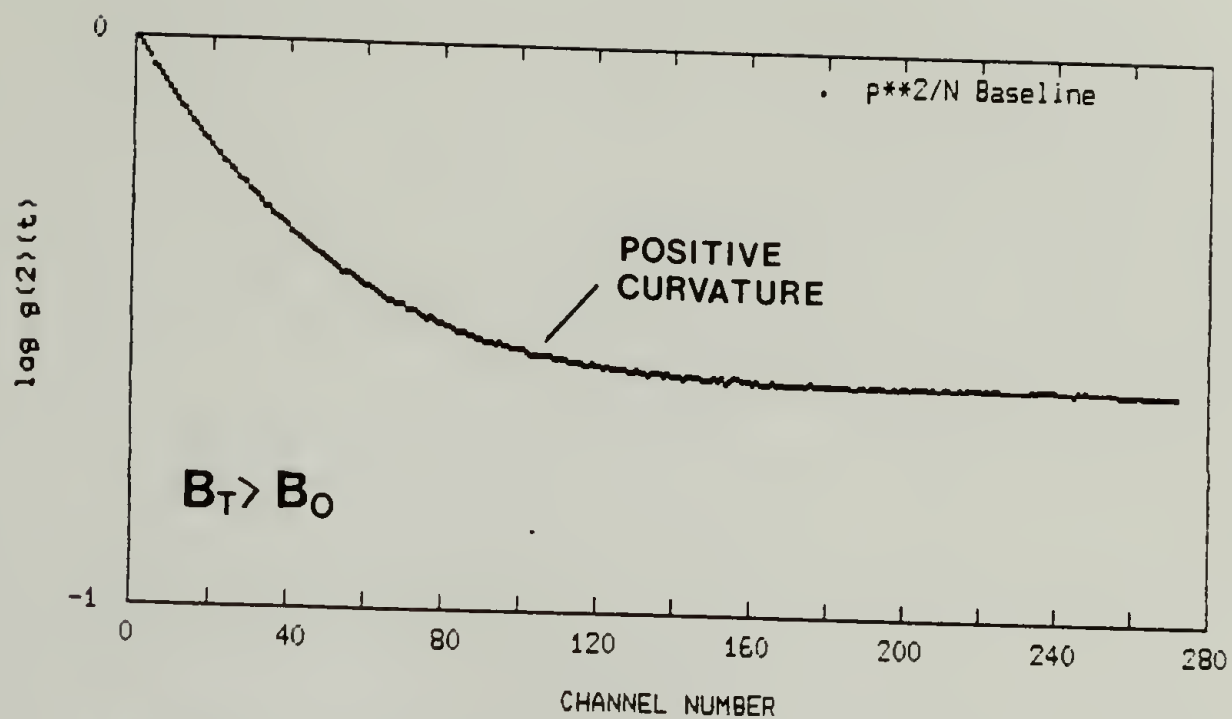
Figure 16 shows semilog plots of several experimental correlation functions, for illustration and comparison to Figure 15. The top is a typical example using the  $p^2/N$  baseline (inherently too low,  $B_0 < B_T$ , due to intensity drift) that shows quite graphically the evidence of misnormalization. The curvature when the  $p^2/N$  baseline is used is calculated fairly accurately using equation (5.15), with the experimental  $f_c^+$ , and with the "true" baseline as the last channels baseline. The middle is a result with a *non-delayed* last channels baseline; the slight negative curvature indicates  $B_0 > B_T$ .

The bottom is a typical result using the delayed last channels baseline (the same data as in the top curve), as was nearly universally used in this work. Since in real life one never knows the "true" baseline, it of course cannot be concluded whether such plots show greater or lesser curvature than if the true baseline were used. As has been discussed, the last channels baseline may be either too high (if there are slow decays associated with the sample) or effectively too low (if there are artifactual slow decays not

Figure 16.

Experimental examples of correlation function misnormalization.

The baseline used in the top figure was the  $p^2/N$  baseline. An independent estimate of  $(\Delta B/B_T)/f_C^+$  is about 0.33; comparison with Figure 15 shows that the positive curvature is about that which is expected. Obviously, the  $p^2/N$  baseline ( $B_0$ ) is less than the true baseline. The bottom figure is the same data as in the top figure, but with use of the delayed last channels baseline. The curvature may be real, or may be due to this delayed channels baseline being slightly lower than the true baseline. (For these two sets of data,  $\langle \Gamma \rangle \cdot t_{\text{MAX}} \approx 8$ .) The middle figure is for different data, where a *non-delayed* last channels baseline was used. This plot shows evidence of negative curvature, indicating  $B_0 > B_T$ .



associated with diffusion in the sample, as seen for example at long sample times). Generally, however, correlation functions in the macroscopic diffusion regime (low angles, with correspondingly long sample times) were approximately "single exponential" over two log decades, indicating  $(\Delta B/B_T)/f_C^+$  of less than about 0.5% (e.g.,  $\Delta B/B_T < 0.005\%$  for  $f_C^+ = 0.01$ ). This range of uncertainty in the baseline is about what is expected on the basis of Poisson statistics for  $G^{(2)}(t)$ . For  $B \approx 5 \times 10^8$  (typical middle of range for these experiments),  $1/\sqrt{B} \approx 4.5 \times 10^{-5}$ . It is noted also that assuming Poisson statistics,  $(\Delta B/B_T)/f_C^+$  is simply the noise to signal estimate given by equation (5.6); hence, by targeting  $N/S \approx 3 \times 10^{-3}$ , the baseline was determined sufficiently to give near "linearity" (or, more accurately, for non-single exponential correlation functions, little distortion) in semilog plots over greater than two decades in  $g_s^{(1)}(q,t)$ . (This assumes of course no significant error in the baseline as caused by artifactual decays with relaxation times comparable to that for diffusion.) This sort of precision in the baseline is sufficient for robust estimates of the average relaxation rate  $\langle T \rangle$ , and even reasonable estimates, at least for relatively "monodisperse" ACFs, of the variance  $\mu_2/\langle T \rangle^2$ .

As a last comment, it is noted that the proper analysis of the shape of normalized baseline subtracted ACFs requires an accurate estimate of  $f_C^+$ , which in turn requires knowledge not only of the baseline  $G^{(2)}(\infty)$  but also  $G^{(2)}(0)$ . This latter value cannot be measured but must be estimated by extrapolation. Improper choice of sample time, or a wide range of relaxation rates, can lead to error in extrapolation to get  $G^{(2)}(0)$ ; however, as these problems are not believed to have been significant in this work, they are not

discussed further. (One exception is the transition regime--intermediate  $qR_p$ --which is discussed in Chapter VI. Correlation functions in this regime show a wide range of apparent relaxation rates.)

### Data Analysis

The analysis of correlation functions is central to the enterprise of dynamic light scattering. The fundamental relationship between correlation functions and underlying dynamical processes--exponential decays for a random diffusive processes--and experimental uncertainties (e.g., noise to signal level, baseline determination) both serve to limit the information which can be extracted in such analysis. In this task one is generally guided by reasonable assumptions and expectations, which are in turn based on knowledge from other sources and on theoretical models for the dynamical processes in the sample. Such *a priori* knowledge increases the amount of information (e.g., fitting parameters) that can safely be extracted. Even with such knowledge, one must be content to stay within the bounds imposed by the fundamental and experimental limits to analysis, or at least realize when overstepping the bounds and speculating.

The literature on this important subject of correlation function analysis is extensive. Although the original papers<sup>150-158</sup> presenting the various analysis methods are certainly important, particularly useful are review papers and collections of papers in books where the different methods are compared.<sup>106,159-161</sup> These later sources have the benefit of hindsight--which analysis methods have withstood the test of time--and

provide critical discussion (although perhaps sometimes biased) of the relative advantages and disadvantages of the different methods.

The aim of this section is not to provide a comprehensive review of correlation function analysis, but simply to present the methods that were used, including some details of implementation; and to give the reasons why these methods were chosen, with regard to experimental and theoretical uncertainties imposed by the nature of these experiments.

The greatest efforts in correlation function analysis have been devoted to the case where the scattered electric field autocorrelation function  $g_s^{(1)}(\mathbf{q}, t)$  is given by a superposition of exponential decays:

$$g_s^{(1)}(\mathbf{q}, t) = \int_0^{\infty} G(\Gamma, \mathbf{q}) \exp(-\Gamma t) d\Gamma \quad (5.16)$$

where the function  $G(\Gamma, \mathbf{q})$  gives the normalized distribution of amplitudes of relaxation modes with relaxation rates (i.e., linewidths)  $\Gamma$ . The first moment of this distribution, the average relaxation rate  $\langle \Gamma \rangle$ , is given by

$$\langle \Gamma \rangle = \int_0^{\infty} \Gamma \cdot G(\Gamma, \mathbf{q}) d\Gamma \quad (5.17)$$

and the variance of the distribution  $\mu_2$  is given by:

$$\mu_2 = \int_0^{\infty} (\Gamma - \langle \Gamma \rangle)^2 \cdot G(\Gamma, \mathbf{q}) d\Gamma \quad (5.18)$$

Usually the variance is appropriately normalized as  $\mu_2/\langle \Gamma \rangle^2$  for more ready intercomparison.

Equation (5.16) excludes situations where there are non-exponential contributions to  $g_s^{(1)}(\mathbf{q}, t)$ , for example, in directed motion such as

electrophoresis. Other situations, of possible relevance to these experiments, were mentioned in Chapter III: fractal diffusion, and power law decays. Hence, the use of equation (5.16) for these experiments demands some justification, which, however, is deferred to later this section.

Various methods used in analyzing dynamic light scattering data can generally give the moments  $\langle \Gamma \rangle$  and  $\mu_2$  fairly accurately. Difficulty comes in performing the inverse Laplace transform (ILT) specified by equation (5.16) to obtain  $G(\Gamma)$ , because the correlation function  $g_s^{(1)}(t)$  is noisy, of finite bandwidth, and sampled at discrete points (i.e., not continuous).<sup>151,153,157</sup> For these experiments, the general difficulty in performing the ILT does not pose a severe problem. As is now argued, the distribution is expected to be unimodal and relatively narrow in the primary regimes of interest, namely, diffusion in bulk solution and macroscopic diffusion in the porous glass; hence, determination of  $\langle \Gamma \rangle$  and  $\mu_2$  should generally be sufficient.

For a polymer solution, a distribution of relaxation rates as given by equation (5.16) can arise for two primary reasons: (1) because of polydispersity in molecular weight or size or shape; and (2) because of the presence of different types of relaxation modes associated with different dynamical processes, for example, translational diffusion, rotational diffusion, internal modes (for polymers with flexibility), interactions between particles, or polymer aggregation.

For flexible polymers in porous glasses, the dynamical processes expected to be seen in dynamic light scattering experiments are translational diffusion, and, only at sufficiently high angles and for sufficiently high

molecular weights, internal modes. (If polymer adsorption is present, dynamics of adsorbed chains will also be expected to contribute to the light scattering spectrum. These adsorbed chain dynamics have in fact been observed, in experiments not discussed in this dissertation. As every effort was made in these experiments to eliminate polymer adsorption, and as it is believed to have been absent or, at the worst, quite small, e.g., see Chapter IV, dynamics of adsorbed chains will be considered absent.)

Thus, for the samples examined in this work (neglecting internal modes), a distribution of relaxation rates arises only from: (1) the molecular weight polydispersity of the samples; and (2) different translational diffusion modes. In unbounded solution, and for macroscopic diffusion in a homogeneous porous material (the primary situations examined in this work), but a single translational diffusion mode is expected, so that any distribution of relaxation rates is attributable to molecular weight polydispersity, and any other factors causing an apparent spectral broadening (e.g., divergence of the incident wavevector). However, the situation is expected to be different at higher wavevector, where the relationship of  $g_s^{(1)}(\mathbf{q}, t)$  to the underlying translational diffusion is less clear (see Chapter III, section 2). In a rough sense, a multiplicity of *apparent* relaxation modes is expected. Although equation (5.16) can be applied to such data, the physical significance of the results, that is, of the distribution  $G(\Gamma)$ , is correspondingly unclear.

As has been noted in connection with "tracer" diffusion of a polymer in an isorefractive "solvent" (i.e., solvent plus second polymer), for a given molecular weight distribution of the tracer, the decay rate distribution

will broaden relative to that in dilute solution if the translational diffusion coefficient assumes a stronger molecular weight dependence than in dilute solution (e.g.,  $D \propto M^{-2}$  for reptation, versus  $D \propto M^{-3/5}$  in dilute solution). Obviously, this effect could also be important for diffusion in a porous material, and would lead to an increase in the variance  $\mu_2$  of  $G(\Gamma)$ .

For a porous material which is inhomogeneous on a scale intermediate between  $q^{-1}$  and the size of the scattering volume, different translational diffusion modes are expected, each associated with different regions in the porous material. An example of this latter situation is for a packed bed of porous fragments, where both bulk diffusion (in interstitial regions) and intraglass diffusion (inside the fragments) contribute to the scattering spectrum. (Early experiments were performed on just such samples.) Although in principle, these contributions can be separated, this proves difficult in practice, given: (1) the problems in measuring or calculating the partitioning coefficient  $K_D$ ; and (2) the relatively minor differences between macroscopic and bulk diffusion coefficients (i.e., in this work, at most different by a factor of 4).

The method of cumulants<sup>150</sup> is based on the MacLaurin expansion of  $\ln|g_s^{(1)}(\mathbf{q}, t)|$ , which takes the form of a power series in the delay time  $t$ :

$$\ln|g_s^{(1)}(\mathbf{q}, t)| = - \langle \Gamma \rangle t + (1/2!) \mu_2 t^2 - (1/3!) \mu_3 t^3 + \dots \quad (5.19)$$

where  $\langle \Gamma \rangle$ ,  $\mu_2$ , and  $\mu_3$  are the first, second, and third cumulants. Equations (5.17) and (5.18) give the relation of  $\langle \Gamma \rangle$  and  $\mu_2$  to  $G(\Gamma, \mathbf{q})$ .

This method is computationally simple, requires no user input to run the analysis, and assumes no particular form for  $G(\Gamma)$ . It is seen from

equation (5.19) that this method can only provide moments of the distribution  $G$ . Since data is generally only of sufficient precision to permit determination of the first two moments  $\langle \Gamma \rangle$  and  $\mu_2$  (in exceptional cases also  $\mu_3$ ), essentially no detail on the shape of the distribution can be extracted (e.g., unimodal vs bimodal, skewed vs not). Also, the expansion in equation (5.19) is only reasonable for low polydispersity; hence, in practice, results are meaningful only for relatively narrow  $G(\Gamma)$ . Even then, truncation of the series (5.19) leads to bias<sup>150</sup> in the estimates of  $\langle \Gamma \rangle$  and  $\mu_2$ . The magnitude of this systematic error depends on the order of the fit, the range spanned by the experimental data (i.e.,  $\langle \Gamma \rangle t_{\text{MAX}}$ ), and the breadth of  $G(\Gamma)$ . By extrapolation to  $\langle \Gamma \rangle t_{\text{MAX}} = 0$  (i.e.,  $\Delta t \rightarrow 0$ ) this bias can be removed (e.g., see<sup>162</sup>); however, due to the necessity to rely on the delayed channel baseline, this extrapolation was not practical for these heterodyne experiments. Further, given the inevitable presence of some homodyne signal, such extrapolation is perhaps not desirable.

Actual implementation of the cumulants method involved linear least squares fits of:

$$y(j\Delta t) = a + b(j\Delta t) + c(j\Delta t)^2 \quad (5.20)$$

with

$$y(j\Delta t) = \ln \frac{\{ C(j\Delta t) - B \}}{\{ C(k\Delta t) - B \}} \quad (5.21)$$

where  $C(j\Delta t)$  is the experimental correlation function, defined by equation (5.2), and  $B$  is the baseline. The quantity  $y$  is an estimate of  $\ln |g_s^{(1)}(t)|$

(heterodyne) and  $\ln|g_s^{(1)}(t)|^2$  (homodyne); thus the parameters  $b$  and  $c$  are related by equation (5.19) to  $\langle T \rangle$  and  $\mu_2$  respectively.

Since  $C(0)$  is unmeasurable, the function must be normalized using  $\{C(k\Delta t) - B\}$ , not  $\{C(0) - B\}$ , where  $k$  is the first live channel, with  $k$  chosen so as to eliminate photomultiplier tube afterpulsing effects. The parameter  $a$  thus arises due to this necessary misnormalization, with  $a = \ln\{[C(0) - B]/[C(k\Delta t) - B]\}$ . The parameter  $a$  is used to extrapolate to  $t = 0$ , thereby allowing estimation of coherence functions  $f_c$  and  $f_c^*$ , and can be used to renormalize to give  $g_s^{(1)}(\mathbf{q}, t)$ . The accuracy of this extrapolation depends on the correlation function being "well-behaved" for  $t < (k\Delta t)$ , and on how good the cumulant fit actually is for the early channels. Due to the presence of some homodyne signal in the correlation functions, and due to the strong possibility of "anomalous" single pore diffusion contributions to the correlation functions (both more important as  $t \rightarrow 0$ ), this extrapolation can be questionable. This is especially so in the transition regime at intermediate  $qR_p$  (see Chapter VI, section 2) where the correlation functions are strongly non-exponential. The rationale for choosing sample times which give rather excessive  $\langle T \rangle t_{\text{MAX}}$  values (i.e.,  $\langle T \rangle t_{\text{MAX}} \approx 10$ , with  $t_{\text{MAX}}$  corresponding to the last contiguous, not delayed, channel) for diffusion experiments in porous glasses at low  $qR_p$  was to try to minimize the effects of homodyne and "single pore" diffusion contributions on the fits.

The effects of this "extrapolation error" were not considered in any detail. Although it is believed that no significant error was introduced in analyses of relatively single exponential correlation functions (at low  $qR_p$ ), even despite rather high  $\langle T \rangle t_{\text{MAX}}$  values, there is much more question

whether non-exponential correlation functions in the transition regime (at intermediate  $qR_p$ ) were accurately extrapolated. Significant extrapolation error of course implies error in the fit parameters; hence, the cumulants method was judged unreliable for analysis in the transition regime, as is consistent with the well-known caveat that cumulants is only good for relatively narrow decay rate distributions.

In addition to the cumulants method, data was also analyzed by performing the inverse Laplace transform (ILT) specified by equation (5.16). The method chosen was that of Provencher,<sup>151,152,159,160</sup> (program CONTIN), where a regularized solution  $G(\Gamma)$  is sought, with the additional constraint that  $G(\Gamma)$  be non-negative. Before discussing the implementation of this method, reasons for choosing it over various alternatives for ILT are given. (A computationally simpler non-negative least squares method,<sup>158,160</sup> where regularization consists of averaging solutions for shorter runs, was not evaluated.)

First, the CONTIN program is relatively automatic and operator independent, with little judgmental input required. In contrast, the histogram method<sup>155,156,159-161</sup> requires choice of number, location, and width of various bins. The "numerically filtered" ILT method<sup>153,154,159-161</sup> requires choice of the grid width, spacing, and, especially, the cutoff frequency.

The proper analysis of the ILT problem for dynamic light scattering data<sup>153,154,159,160</sup> shows that features in  $G(\Gamma)$  of higher frequency than some cutoff frequency, which is determined by the signal to noise level and the bandwidth of the data, cannot be obtained upon inversion. The Laplace transform of the function  $G(\Gamma)$  into the measurable correlation function

$g_s^{(1)}(\mathbf{q}, t)$  acts as a low-pass filter, attenuating the high frequency details in  $G(\Gamma)$ . A decrease in the support of the data  $\gamma$ , where  $\gamma$  is the ratio of maximum to minimum decay rates in the solution,  $\gamma = \Gamma_{\text{MAX}}/\Gamma_{\text{MIN}}$ , increases this cutoff frequency and allows an increase in resolution of the solution. This analysis<sup>153,157,159,160</sup> provides the limit of resolution (i.e., grid spacing of the solution) that is possible for a given noise realization and support  $\gamma$ .

Despite this, the constrained regularization ILT<sup>151,152</sup> can give a solution with *apparently* finer resolution than this limit. As follows from the nature of the regularization in this method, the solution will be the "smoothest" or most parsimonious solution consistent with the data. It nonetheless must be realized that even such smooth solutions can have a finer resolution than is warranted by noise to signal levels and the support  $\gamma$  of the inversion, and that there thus will be many other solutions consistent with the data within the noise. However, I would tentatively conclude that *if* the function  $G(\Gamma)$  is narrow, then the solution from constrained regularization ILT, although quite possibly of finer resolution than actually warranted by the data, may be closer to the true solution than would be obtained from the numerically filtered ILT method,<sup>153,154</sup> which more directly incorporates the fundamental limits to resolution into the solution. This in fact was one reason for choosing the Provencher method over that of Pike and Ostrowsky: in bulk solution, and in the macroscopic diffusion regime (see Chapter VI, section 2),  $G(\Gamma)$  is narrow, and the former method appeared more capable of giving the true distribution than the latter method (e.g., the variance from CONTIN is closer to that from cumulants than is that from the Pike-Ostrowsky method).

In these experiments, the noise to signal ratio (N/S) levels were only moderately low (e.g., targeted at  $N/S \approx 3 \times 10^{-3}$  as defined by equation (5.6)), which, taken together with lack of *a priori* knowledge of the support (i.e.,  $\Gamma$  range) of the distribution  $G(\Gamma)$ , imposes a quite limited resolution, giving a relatively large  $\ln(\Gamma)$  spacing, when using the numerically filtered ILT method. This resolution can be estimated by consulting various references.<sup>157,159,160</sup> Although the "primary" support of  $G(\Gamma)$  (e.g., for  $\approx 95\%$  of the amplitude as given by the main peak) was generally narrow enough such that, given the N/S levels, resolution comparable to that achievable with constrained regularization ILT should have been possible, in practice this was actually not possible, for the following reason. The uncertainty in determining the baseline, and "artifact" slow decays (both discussed in the second section of this chapter) in practice both necessitated the extension of the support, with concomitant loss of resolution in the numerically filtered ILT, but seemingly without much loss of resolution in the constrained regularization ILT solutions.

The implementation of the constrained regularization ILT used Provencher's CONTIN program. The approach started with the following expression for the intensity ACF,

$$G^{(2)}(t) = B_T \{ 1 + f_C^+ |g^{(1)}(t)| \}; \quad B_T = B_p + \Delta B \quad (5.22)$$

where  $B_T$  is the true baseline, and  $B_p$  the  $p^2/N$  baseline. Two options were employed. The first used a fixed baseline, usually assuming  $B_T \equiv B_L$ , with  $B_L$  the last channels baseline, solving the following equation for the scaled (by  $f_C^+$ ) distribution  $G_s(\Gamma)$ :

$$\frac{G^{(2)}(j\Delta t)}{B_L} - 1 = f_C^+ |g^{(1)}(j\Delta t)| \cong \int G_S(\Gamma) \exp(-\Gamma \cdot j\Delta t) d\Gamma \quad (5.23)$$

The second option used a floating baseline, solving the following equation (since  $\Delta B$  is constrained in the program to be non-negative, usually the  $p^2/N$  baseline, which is definitely less than  $B_T$ , was used to ensure that this be so):

$$\frac{G^{(2)}(j\Delta t)}{B_P} - 1 = \frac{\Delta B}{B_P} + f_C^+ |g^{(1)}(j\Delta t)| \cong \frac{\Delta B}{B_P} + \int G_S(\Gamma) \exp(-\Gamma \cdot j\Delta t) d\Gamma \quad (5.24)$$

In these Laplace inversions, the range of  $\Gamma$  in equations (5.23) and (5.24), given as  $\gamma = \Gamma_{MAX}/\Gamma_{MIN}$ , was chosen in the range  $100 \leq \gamma \leq 1000$ , typically  $\gamma = 200$  or  $\gamma = 500$ . Generally,  $\Gamma_{MAX}$  was chosen as  $\Gamma_{MAX} \approx 10 \langle \Gamma \rangle$ . Since the sample time  $\Delta t$  was chosen to give  $250\Delta t \langle \Gamma \rangle \approx 10$ , then  $\Gamma_{MAX} \approx (2/5\Delta t)$ , and  $(1/250\Delta t) \geq \Gamma_{MIN} \geq (1/2500\Delta t)$  (for  $100 < \gamma < 1000$ ). This range of  $\Gamma$  is basically the range for which it should be possible to extract reliable information about  $G(\Gamma)$  from the correlation function, given the sample time  $\Delta t$ . The function  $G(\Gamma)$  was calculated at  $g$  logarithmically spaced points in this range (including the end points) with spacing  $\delta = \Delta(\ln(\Gamma)) = (\ln \gamma)/(g-1)$ . Logarithmic spacing of the grid is best from the point of view of the fundamental analysis of the ILT problem. The number of points in this grid was chosen  $g \approx 15-20$ , as a compromise between fineness of (apparent) resolution required to accurately determine the moments of peaks of  $G(\Gamma)$ , and the minimization of computing expense. Use of more grid points showed no significant change in  $\langle \Gamma \rangle$  or  $\mu_2/\langle \Gamma \rangle^2$  for various peaks, whereas computational time and expense increase roughly proportional to  $g^2$ . Use of fewer grid points was somewhat unsatisfactory for narrow  $G(\Gamma)$  (e.g., as in bulk or

macroscopic diffusion) but was possible without significant inaccuracy in solutions for broad  $G(\Gamma)$  (e.g., as in the transition regime).

Attention now turns to some discussion of the justification of the use of equation (5.16) to analyze data for diffusion in porous glasses. This justification anticipates some results from later chapters.

The power law decay predicted by mode coupling theories (Chapter II, section 4) might well be present in correlation functions at low angle (low  $qR_p$ ). However, simple calculations indicate that this power law decay will only dominate the exponential (which is due to macroscopic diffusion) at long times. These times are in fact sufficiently long such that noise in the correlation function and baseline uncertainty preclude the possibility of unambiguously extracting this decay. Furthermore, calculation of the amplitude of this term requires knowledge of the extent of structural disorder (static spatial fluctuations) in the porous material, so that *a priori* knowledge of this amplitude is lacking. (Some attempt was made to look for this power law decay, but these efforts were abandoned for the reasons given here.) It is believed that if correlation functions (with sample time set to optimize the determination of the macroscopic diffusional relaxation rate) containing this power law decay were to be analyzed assuming equation (5.16), that the power law might be approximately manifested in the fits as a very slowly decaying exponential. For example, constrained regularization ILT solutions often show a "peak" at low  $\Gamma$ ; this peak might be an attempted fit of a power law decay (if present), or related to more mundane sources of baseline drift. The presence of a power law decay also has obvious implications with regard to the ability to determine the baseline accurately.

## CHAPTER VI

### RESULTS

#### Experimental Overview

An overview of the experiments is provided by considering the ranges of certain key parameters. The magnitude of the scattering wave-vector  $q$  is fixed by the apparatus; for scattering angle  $\theta$  between  $15^\circ$  and  $155^\circ$ , wavelength *in vacuo*  $\lambda_0 = 632.8$  nm, and refractive index  $n \approx 1.47$ , one has:

$$3.8 \times 10^4 < q < 2.8 \times 10^5 \text{ cm}^{-1} \quad (6.1a)$$

$$1.5 \times 10^9 < q^2 < 8.1 \times 10^{10} \text{ cm}^{-2} \quad (6.1b)$$

$$2600 > q^{-1} > 350 \text{ \AA} \quad (6.1c)$$

$$0.017 < \sin^2(\theta/2) < 0.953 \quad (6.1d)$$

In these dynamic light scattering experiments, one expects to observe different manifestations of microscopic Brownian motion as the dimensionless parameters  $qR_p$ ,  $qR_G$ , and  $R_G/R_p$  are varied. Given that  $q^{-1}$  (dimensions of length) is in essence the wavelength of the concentration fluctuations whose decay is being examined in an experiment at scattering angle  $\theta$ , these parameters are seen, respectively, as the ratio of pore size to fluctuation wavelength, the ratio of polymer coil size to fluctuation wavelength, and the ratio of polymer size to pore size. Despite the lack of

expectation of strictly universal behavior for different polymers and porous materials in terms of these dimensionless parameters, it is nonetheless obvious that these are more natural variables to use when discussing diffusion in porous materials than the individual dimensioned variables (i.e.,  $q$ ,  $R_G$ , and  $R_p$ ). The range of each of these dimensionless variables for these experiments is considered below in turn.

The ranges of  $qR_p$  for the available large glass fragments are calculated using the range of  $q$  given by equation (6.1a) together with the nominal pore radius values (Table 2, Chapter IV):

$$0.27 < qR_p < 1.97 \quad (\text{glass B13, } R_p = 703 \text{ \AA}) \quad (6.2a)$$

$$0.34 < qR_p < 2.50 \quad (\text{glass B7, } R_p = 893 \text{ \AA}) \quad (6.2b)$$

$$0.71 < qR_p < 5.23 \quad (\text{glass B5, } R_p = 1866 \text{ \AA}) \quad (6.2c)$$

The range of coil dimensions for the linear polystyrenes (Table 1, Chapter IV) in 2-fluorotoluene is calculated using the  $R_H$ - $M_D$  relationship given by equation (4.3) together with the following approximate relationship which has been observed<sup>77</sup> for linear polystyrene in toluene:

$$R_H \approx 0.69 R_G \quad (6.3)$$

This gives

$$31 < R_H < 420 \text{ \AA} \quad (6.4a)$$

$$44 < R_G < 600 \text{ \AA} \quad (6.4b)$$

Of primary concern for these light scattering experiments is that

$$qR_G < 1 \quad (6.5a)$$

which is the precondition that the concentration fluctuations are relaxing mainly by translational diffusion, or in other words, that internal modes do not make a significant contribution to the correlation function. In a porous material, where chains may be significantly deformed, equation (6.5a) is more precisely put as:

$$(\mathbf{q} \cdot \mathbf{R}_{G, \parallel}) < 1 \quad (6.5b)$$

where  $(\mathbf{q} \cdot \mathbf{R}_{G, \parallel})$  is the projection of the longest dimension of the chain onto the scattering wavevector. Considering now only polymer in unbounded solution, that is, using equation (6.5a), it is seen that for the highest molecular weight polymer used ( $M_D = 2.1 \times 10^6$ ),  $qR_G = 1$  for  $\theta = 69^\circ$ ; and for the highest value of  $q$ ,  $qR_G = 1$  corresponds to  $R_G \approx 350 \text{ \AA}$  or  $M_D \approx 8.2 \times 10^5$ . These results show that there should be no problem determining translational diffusion coefficients in bulk solution for even the highest molecular weight sample used here, since the condition given by equation (6.5a) is readily satisfied given the accessible  $q$  range; experimental verification of this is mentioned later. Given that the *maximum* value of  $(\mathbf{q} \cdot \mathbf{R}_{G, \parallel})$  (i.e., where  $\mathbf{q}$  and  $\mathbf{R}_{G, \parallel}$  are parallel) is greater than or equal to  $qR_G$  in bulk solution, these results also indicate that the condition given by equation (6.5b) might *not* be satisfied for the highest molecular weight samples, *even* at the lowest accessible  $q$  values, if the polymer chains are deformed strongly enough. Consideration of this point is given later, in relation to both experimental results and theoretical predictions.

The ranges of the relative size parameter (i.e., of polymer to pore size) are calculated using the limiting  $R_H$  values from equation (6.4a) together with nominal pore radii (Table 2, Chapter IV):

$$0.044 < R_H/R_p < 0.60 \quad (\text{glass B13, } R_p = 703 \text{ \AA}) \quad (6.6a)$$

$$0.034 < R_H/R_p < 0.47 \quad (\text{glass B7, } R_p = 893 \text{ \AA}) \quad (6.6b)$$

$$0.016 < R_H/R_p < 0.23 \quad (\text{glass B5, } R_p = 1866 \text{ \AA}) \quad (6.6c)$$

These can be converted into ranges for radius of gyration  $R_G$ , using the approximate equation (6.3); or for the root mean square end to end distance  $R_F$ , using also:

$$R_F = (6)^{1/2} R_G \quad (6.7)$$

To reintroduce notation from Chapter II, these relative size parameters will henceforth be referred to as  $\lambda_H (= R_H/R_p)$ ,  $\lambda_G (= R_G/R_p)$  and  $\lambda_F (= R_F/R_p)$ .

These ranges for the different glasses are not entirely coincident; unfortunately, the limitation imposed by equations (6.5) indicates that, even if samples were to be obtained with molecular weights high enough to give identical upper limits on  $\lambda_H$  (i.e.,  $\lambda_H = 0.60$ ), the results of light scattering experiments with those samples could not be interpreted easily in terms of translational diffusion coefficients, the object of this study. Also, although the lower limit of these ranges could have been extended by using readily available lower molecular weight samples, this was not done, for practical reasons: both the relatively low scattered intensity and the relatively high

diffusion coefficients for such samples lead to difficulties in measurements using a digital correlator.

To summarize the experiments in terms of these dimensionless parameters, it can be seen that diffusion is being examined for situations where the polymer chains are hardly confined ( $\lambda_H \approx 0$ ) to where the polymer chains are moderately confined ( $\lambda_H \approx 0.5$ ,  $\lambda_G \approx 0.7$ , and  $\lambda_F \approx 1.8$ ). The upper limit (i.e., only moderate confinement) on the relative size parameter is imposed by the requirements for measuring translational diffusion, given the pore sizes of the available glasses. (These requirements could still be satisfied at higher values of  $\lambda_H$  for smaller pore size glasses.) These ranges of the relative size parameter for the different glasses, although not identical, overlap significantly. Lastly, for the different glasses, the ranges of  $qR_p$  also differ, but again, with significant overlap; this variation in  $qR_p$  corresponds to diffusion over varying relative distances in the porous glasses.

### **Diffusion Regimes: Wavevector Dependence**

Correlation functions for diffusion within porous glasses (Figure 17) show the following features.

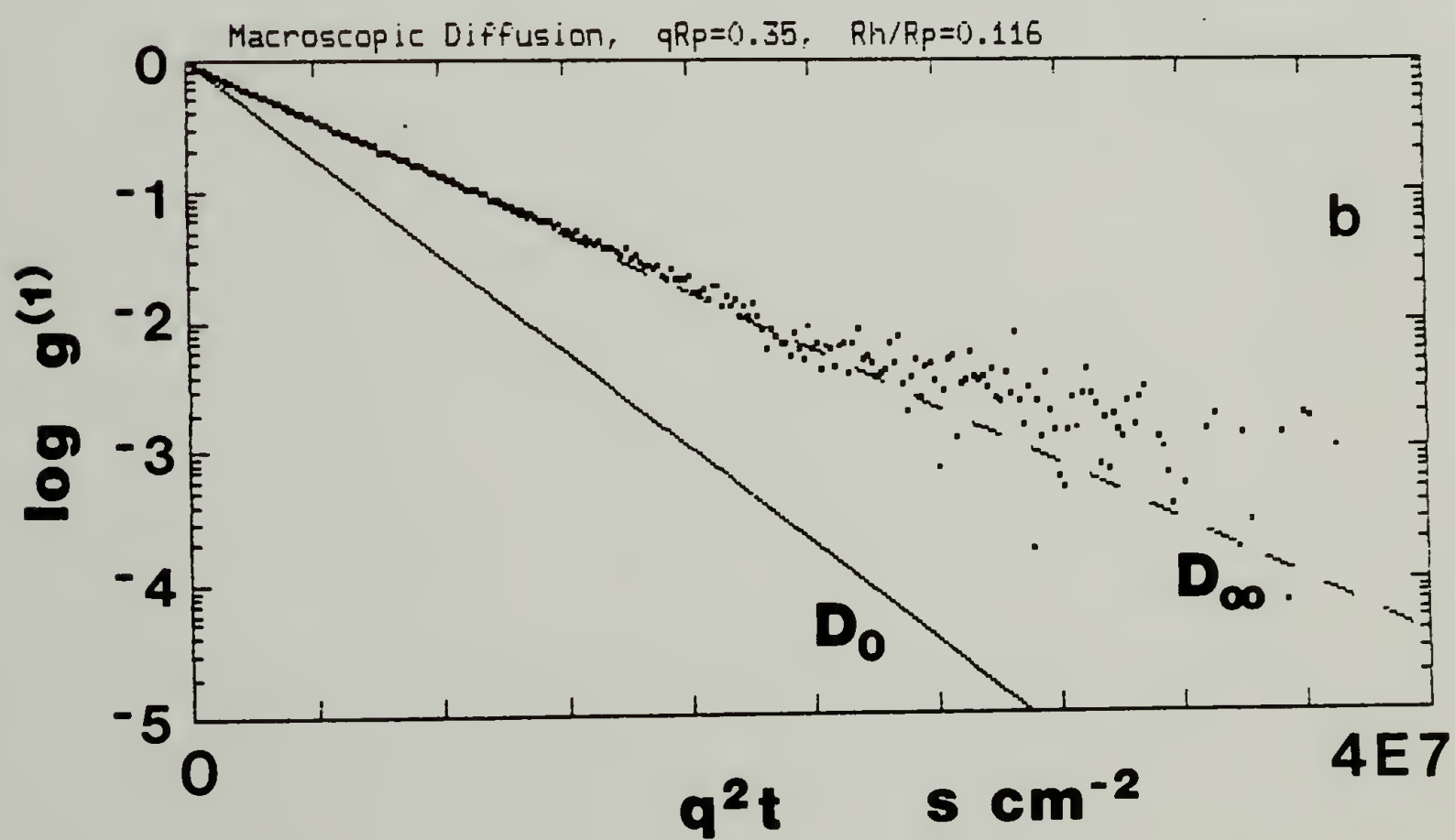
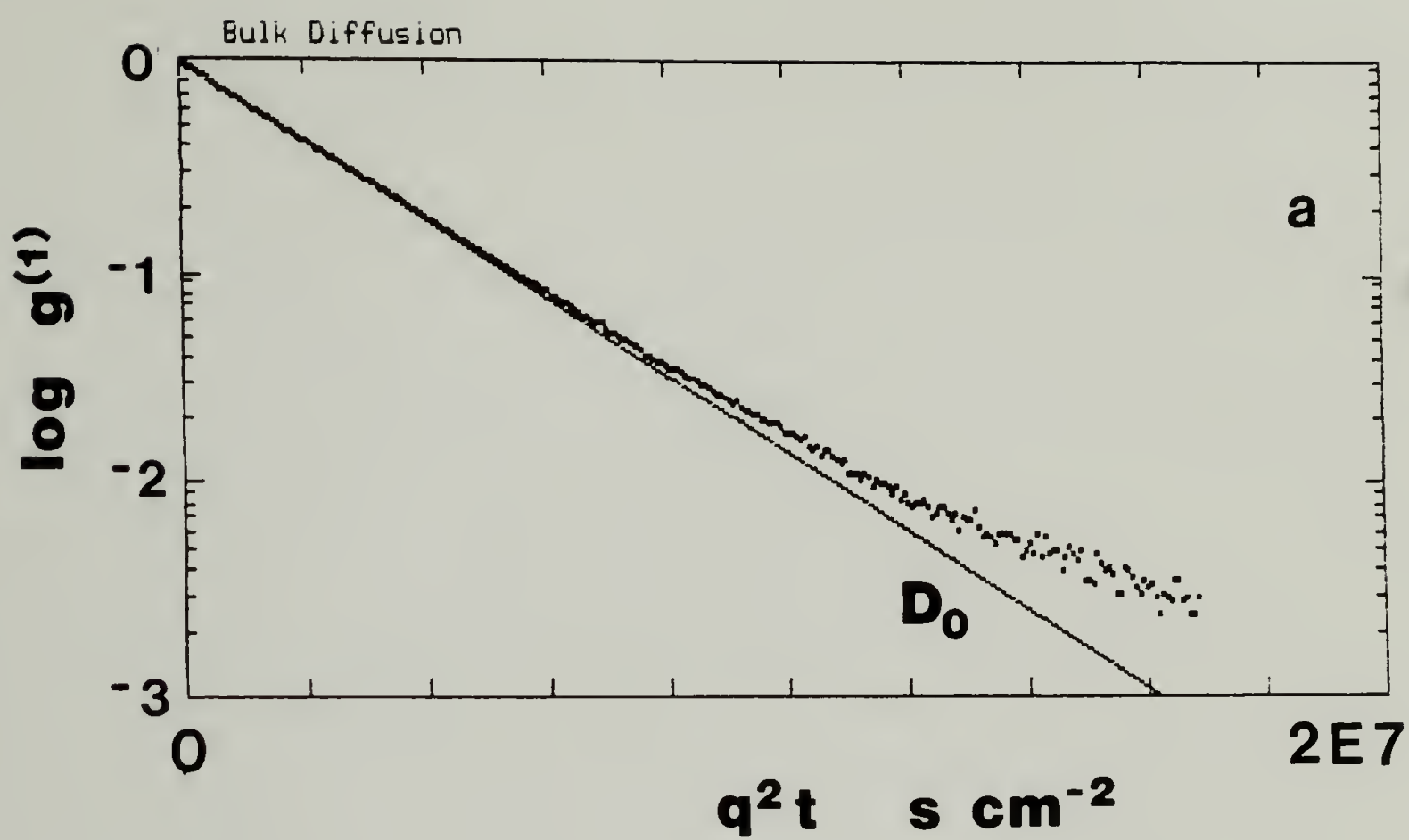
First, correlation functions decay more slowly than in bulk solution, regardless of the scattering wavevector  $q$ . This is of course expected: hydrodynamic polymer-wall interactions lead to a reduced diffusivity in the pores; and structural effects, as manifested in the intrinsic conductivity, lead to a further reduction when diffusion over macroscopic distances is considered. This deviation is seen even at the shortest time scales accessible in the light

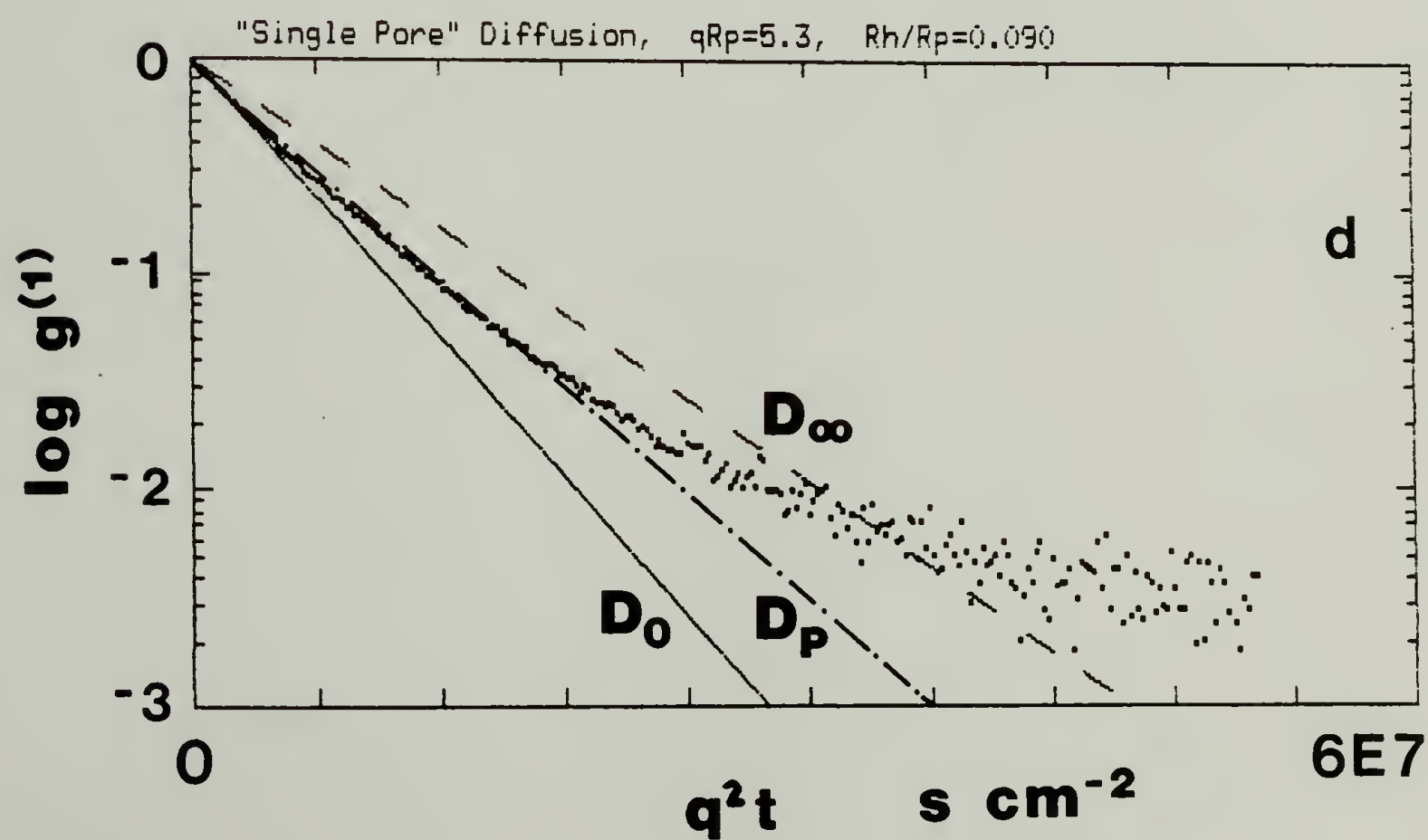
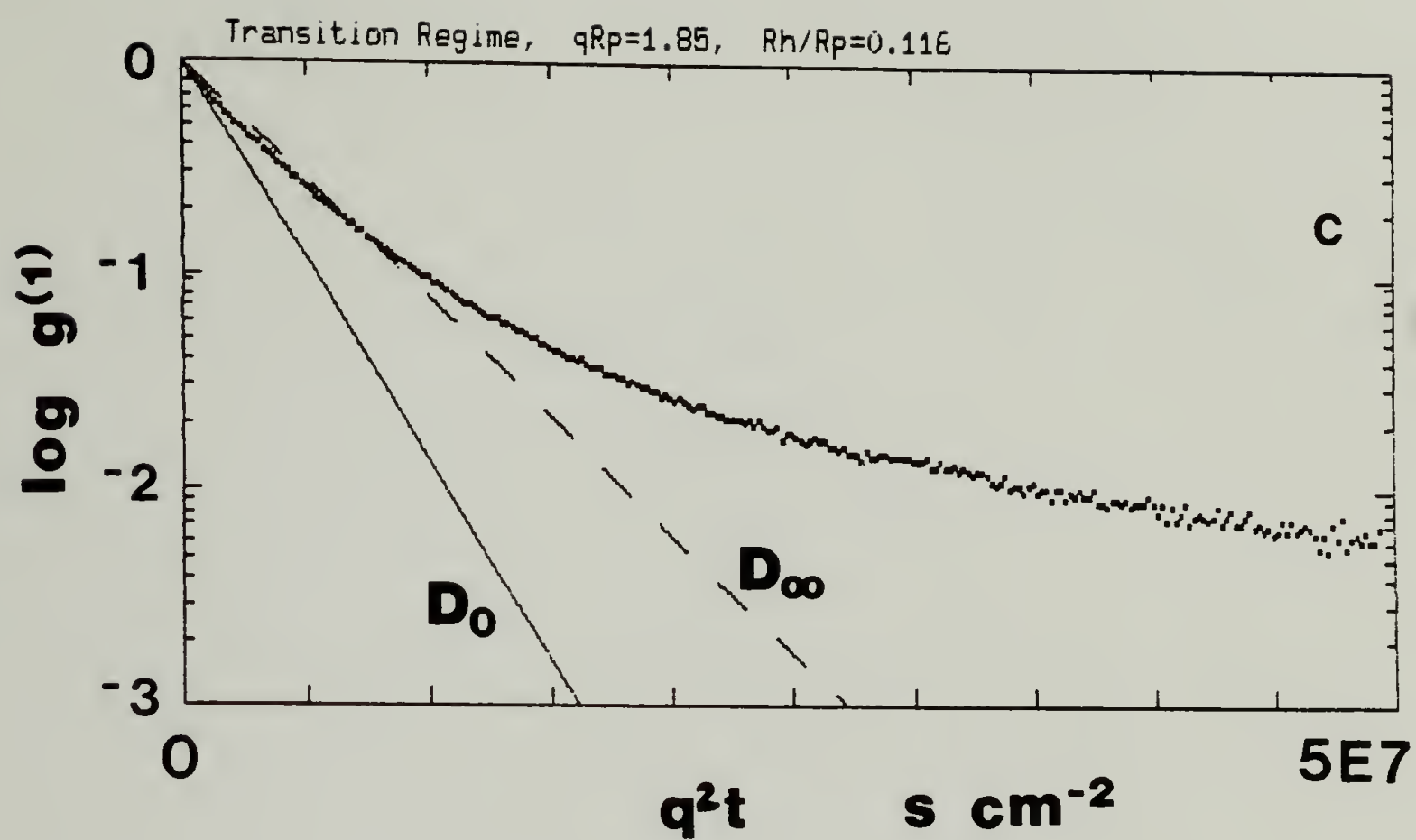
Figure 17.

Diffusion regimes: differences in the scattered electric field correlation function as  $qR_p$  is varied.

- (a) Diffusion in bulk solution
- (b) Macroscopic diffusion regime, low  $qR_p$  ( $qR_p = 0.35$ )
- (c) Transition regime, intermediate  $qR_p$  ( $qR_p = 1.85$ )
- (d) "Single pore" diffusion regime, high  $qR_p$  ( $qR_p = 5.3$ )

Figures (a) through (c) are for polymer P7 ( $M = 1.8 \times 10^5$ ,  $R_H = 104 \text{ \AA}$ ) in glass B7 ( $R_p = 893 \text{ \AA}$ ,  $\lambda_H = 0.116$ ); for this sample,  $D_0 = 4.27 \times 10^{-7} \text{ cm}^2/\text{s}$  and  $D_\infty = 2.54 \times 10^{-7} \text{ cm}^2/\text{s}$ . Figure (d) is for polymer P2 ( $M = 4.1 \times 10^5$ ,  $R_H = 168 \text{ \AA}$ ) in glass B5 ( $R_p = 1866 \text{ \AA}$ ,  $\lambda_H = 0.090$ ); for this sample,  $D_0 = 2.47 \times 10^{-7} \text{ cm}^2/\text{s}$ ,  $D_\infty = 1.51 \times 10^{-7} \text{ cm}^2/\text{s}$ , and  $D_p = 1.93 \times 10^{-7} \text{ cm}^2/\text{s}$ . This sample has  $\lambda_H$  similar to that for figures (a)-(c). Unfortunately, the entire range of behavior versus  $qR_p$  cannot be seen for a single sample, due to the limited  $q$  range of the apparatus.





scattering experiments (on the order of  $1\ \mu\text{s}$ ), since this is much longer than the time scale associated with hydrodynamic interactions (on the order of  $1\ \text{ns}$ ), which are governed by the propagation of density disturbances at the speed of sound.

Second, the behavior of the correlation functions depends significantly on  $q$ . Two limiting regimes can be distinguished, with an intermediate regime of more complex behavior. These regimes, which will be discussed with reference to Figure 17, are best considered in terms of the dimensionless variable  $qR_p$ , as opposed to simply  $q$ .

At low  $qR_p$ , correlation functions are nearly single exponential and superpose when plotted versus  $q^2t$ . At intermediate  $qR_p$ , correlation functions are definitely not single exponential and do not superpose when plotted versus  $q^2t$ . At still higher  $qR_p$ , correlation functions become more nearly single exponential and more nearly superpose when plotted versus  $q^2t$ .

Before continuing further, it is necessary to define what is meant by "single exponential". The polystyrene samples have small but non-negligible polydispersity; hence, even in bulk solution, correlation functions do not have strictly single exponential decays. Therefore, the term "single exponential" is used here to denote correlation functions with appreciably the same deviation from single exponential behavior as is seen for the same polymer in bulk solution. In figures (e.g., Figure 17) the bulk solution correlation function will usually be included to allow direct visual comparison of this curvature. Lines drawn in figures (e.g., bulk solution or pore or macroscopic diffusion lines, denoted by  $D_0$  or  $D_p$  or  $D_\infty$ ) correspond only to the

*initial* decay of these correlaton functions, that is, to the average decay rate and average diffusion coefficient; therefore these lines should *not* be interpreted as being continuous representations of the corresponding correlation functions.

Difficulties in making a precise quantitative analysis of the shape of correlation functions in the porous glass (e.g., how single exponential?) were made apparent in Chapter V, and the reasons are repeated here: uncertainty in the baseline of heterodyne correlation functions, and difficulty in accurate extrapolation of correlation fucntions to  $t=0$ , both of which lead to uncertainty in obtaining the baseline subtracted and normalized  $g_s^{(1)}(\mathbf{q},t)$ ; admixture of homodyne signal; and divergence in the wavevector. This discussion is about aspects of correlation function behavior that are clear despite these uncertainties.

The low  $qR_p$  regime (Figure 17b) shows behavior which is analogous to diffusion in bulk solution (Figure 17a). In both cases the average (essentially single) relaxation rate  $\langle\Gamma\rangle$  of the correlation functions scales with  $q^2$ ; that is,  $\langle\Gamma\rangle = Dq^2$ . This leads to superposition if  $g_s^{(1)}(\mathbf{q},t)$  is plotted versus  $q^2t$ . In bulk solution,  $D$  is the self-diffusion coefficient  $D_0$ . In the porous glass (low  $qR_p$  limit),  $D$  is identified as the effective macroscopic self-diffusion coefficient  $D_\infty$  (see Chapters II and III). As previously noted, these are actually mutual diffusion coefficients, but in order to simplify the discussion, it will be assumed that the solutions used in these experiments were sufficiently dilute to ignore this distinction. (This assumption will, however, be examined subsequently.) This low  $qR_p$  behavior is consistent with the expectation that the decay of sufficiently long wavelength fluctuations,

where structural variations should be effectively averaged, is governed by a single macroscopic relaxation rate.

Behavior at higher  $qR_p$ , where  $q^{-1}$  is comparable to the pore dimensions, is complex. As  $qR_p$  is increased, starting from the macroscopic diffusion (low  $qR_p$ ) regime, correlation functions change shape and become increasingly non-exponential. Correlation functions from this intermediate  $qR_p$  regime (e.g., Figure 17c) show extreme curvature in semilog plots, which is indicative of a high degree of non-exponentiality (for these monodisperse polystyrene samples). The initial decay rate is more rapid than in the macroscopic diffusion regime, but less rapid than in bulk solution; however, at long times the correlation functions decay even more slowly than in the macroscopic diffusion regime, at equivalent values of  $q^2t$ . It is noted that this increase in curvature as  $qR_p$  increases is a trend which runs counter to trends in curvature as caused by artifacts of baseline drift (i.e., misnormalization) and divergence of the wavevector; that is, these effects are relatively more significant at low  $q$  in causing apparent spectral broadening. This complex behavior at intermediate  $qR_p$  is a manifestation of non-Gaussian effects due to the presence of reflecting boundaries; that is to say, the probability distribution of displacements  $\Delta R$  (which are conjugate to  $q$ ) is fundamentally non-Gaussian in this intermediate  $qR_p$  regime. In this regime,  $g_s^{(1)}(\mathbf{q}, t)$  does not superpose when plotted versus  $q^2t$ , since the relative importance of these non-Gaussian effects depends on  $qR_p$ .

In fact, as  $qR_p$  is increased, the degree of non-exponentiality goes through a maximum and then decreases. The return to more nearly single exponential behavior at higher  $qR_p$  is consistent with the expectation that

the decay of fluctuations of wavelength sufficiently short compared to pore dimensions should be relatively free of non-Gaussian effects as caused by the presence of the pore walls. This is not to say that the decay rate itself is unaffected by the pore walls, since the hydrodynamic interactions (polymer-wall, and monomer-monomer) determine the diffusion coefficient governing this decay. As shown in Figure 17d, at sufficiently high  $qR_p$ , correlation functions decay at a rate intermediate between that for bulk solution and that for macroscopic diffusion in the glass, thereby showing primarily the effects of hydrodynamic interactions and only to a lesser extent structural effects as such (i.e., as are seen at lower  $qR_p$ ).

As mentioned in Chapter III, the scattered electric field autocorrelation function  $g_s^{(1)}(\mathbf{q}, t)$  can be written as:

$$g_s^{(1)}(\mathbf{q}, t) = \int_0^{\infty} G(\Gamma, \mathbf{q}) \exp(-\Gamma t) d\Gamma \quad (6.8)$$

where  $G(\Gamma, \mathbf{q})$  is the normalized distribution of the amplitudes of the generalized relaxation modes (relaxation times  $1/\Gamma$ ) at wavevector  $\mathbf{q}$ . This equation was the basis for more detailed examination of the wavevector dependence; comment as to the suitability of equation (6.8) for such analysis was given in Chapter V, section 3. The first moment of the distribution,  $\langle \Gamma \rangle$ , is given by:

$$\langle \Gamma \rangle = \int_0^{\infty} \Gamma \cdot G(\Gamma, \mathbf{q}) d\Gamma \quad (6.9)$$

and corresponds to some average *effective* relaxation rate for concentration fluctuations of wavevector  $\mathbf{q}$ . The second moment of the distribution,  $\mu_2$ ,

$$\mu_2 = \int_0^{\infty} (\Gamma - \langle \Gamma \rangle)^2 \cdot G(\Gamma, q) d\Gamma \quad (6.10)$$

gives the breadth of the distribution of *apparent* relaxation rates. Usually, this variance is appropriately normalized as  $V = \mu_2 / \langle \Gamma \rangle^2$ .

Corresponding to the average *effective* relaxation rate  $\langle \Gamma \rangle$  is a  $q$ -dependent effective diffusion coefficient  $D_{\text{EFF}}$ , which is defined by analogy to bulk solution as  $D_{\text{EFF}} = \langle \Gamma \rangle / q^2$ . The ratio of this *effective* diffusion coefficient in the porous material to the diffusion coefficient in bulk solution,  $D_{\text{EFF}} / D_0 = \langle \Gamma \rangle / \langle \Gamma \rangle_0$ , shows more clearly than  $\langle \Gamma \rangle$  or  $D_{\text{EFF}}$  changes relative to bulk solution, as a function of  $q$ , from sample to sample, and from glass to glass.

In this work, the quantities  $\langle \Gamma \rangle$  and  $\text{Var } \Gamma$  were obtained by the data analysis methods given in Chapter V, namely cumulants analysis, and Laplace inversion of equation (6.8) using Provencher's CONTIN program (i.e., constrained regularization).

Plots of  $D_{\text{EFF}} / D_0$  and  $V$  versus  $q^2$  and  $qR_p$  illustrate the wavevector dependence for typical samples in the three different glasses: B7 and B13 (Figure 18), and B5 (Figure 19).

For the smaller pore size glasses (B7 and B13) both  $D_{\text{EFF}} / D_0$  and  $V$  are constant at low  $qR_p$ , and increase significantly at higher  $qR_p$ . This transition is at  $qR_p \approx 0.7$ - $0.8$  for the effective diffusion coefficient, but at a somewhat lower value  $qR_p \approx 0.5$ - $0.6$  for the variance. For the larger pore size glass (B5),  $D_{\text{EFF}} / D_0$  is relatively constant at low  $qR_p$ , but increases significantly at higher  $qR_p$ , above  $qR_p \approx 1.3$ . The variance  $V$  has a maximum at  $qR_p \approx 1.5$ - $2.0$ , and decreases for both lower and higher  $qR_p$ . As with the smaller

Figure 18.

Wavevector dependence of the reduced average effective diffusion coefficient  $D_{\text{EFF}}/D_0$ , and of the normalized variance  $V = \mu_2/\langle\Gamma\rangle^2$  of the decay rate distribution, for glasses B7 ( $R_p = 893 \text{ \AA}$ ) and B13 ( $R_p = 703 \text{ \AA}$ ).

Two sets of results are shown for glass B7: polymer sample P4 ( $\lambda_H = 0.044$ , filled diamonds, Laplace inversion data analysis); and polymer sample P6 ( $\lambda_H = 0.084$ , empty diamonds, second order cumulants analysis). The set of results for glass B13 is for polymer sample P3 ( $\lambda_H = 0.045$ , filled circles, second order cumulants analysis).

In the graph of  $D_{\text{EFF}}/D_0$ , the lines at low  $qR_p$  were obtained from linear fits of  $\langle\Gamma\rangle = D_{\text{EFF}} q^2$  versus  $q^2$ , for data with  $q^2 < 8 \times 10^9 \text{ cm}^{-2}$ . All other lines are given to show the trends of the data.

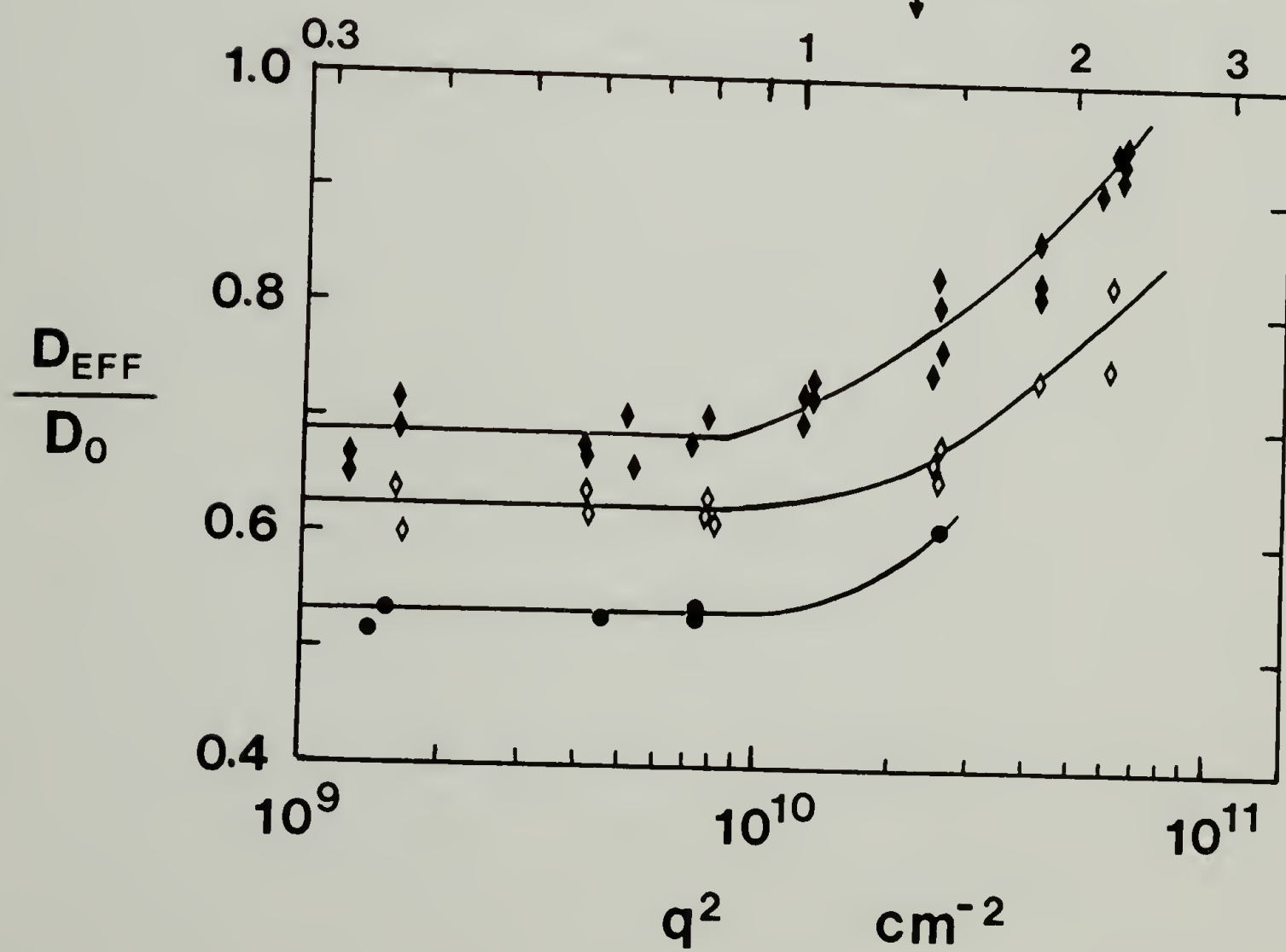
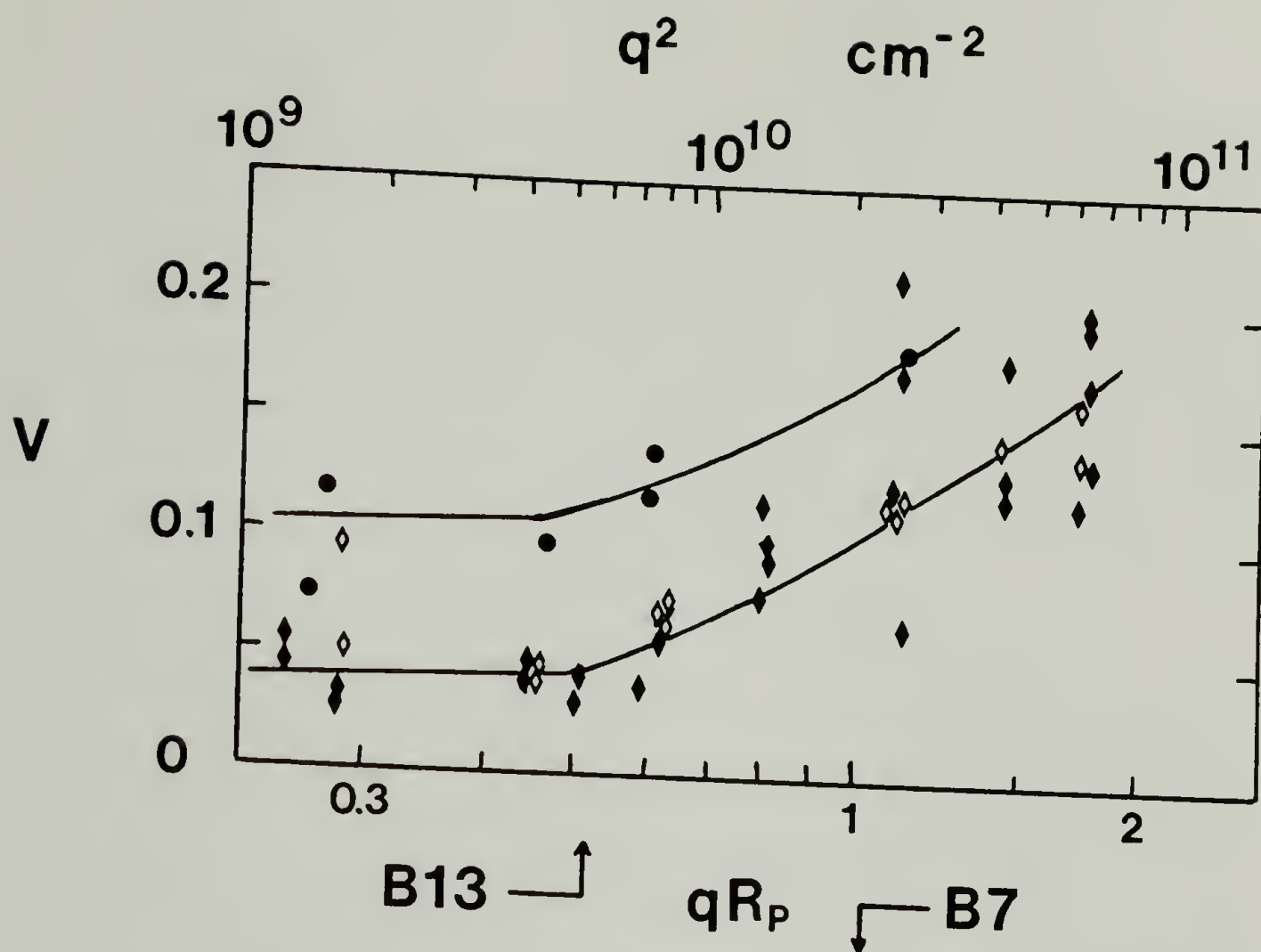
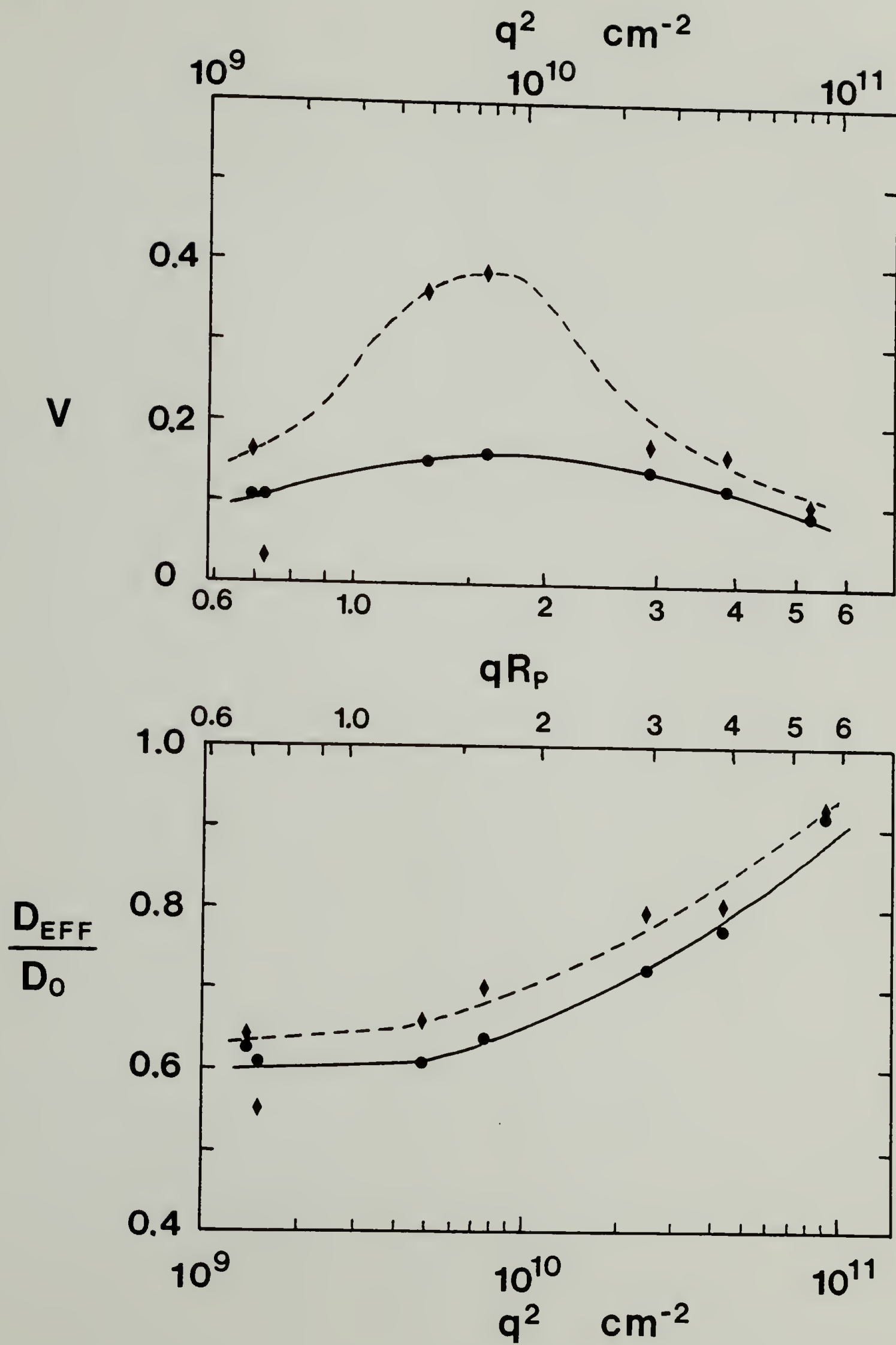


Figure 19.

Wavevector dependence of the reduced average effective diffusion coefficient  $D_{\text{EFF}}/D_0$ , and of the normalized variance  $V = \mu_2/\langle T \rangle^2$  of the decay rate distribution, for glass B5 ( $R_p = 1866 \text{ \AA}$ ).

Results are for polymer sample P2 ( $\lambda_H = 0.090$ ), using two different data analysis methods: Laplace inversion (diamonds), and second order cumulants (circles).

Lines show the trends of the data.



pore size glasses, the value of  $qR_p$  below which  $D_{\text{EFF}}/D_0$  is approximately constant is greater than the value of  $qR_p$  below which  $V$  is constant.

The range of  $qR_p$  over which correlation functions are significantly non-exponential spans about one order of magnitude,  $0.5 < qR_p < 5$ , and is centered at  $qR_p \approx 1.5$ . This relatively narrow range observed for these porous glasses is further evidence that the structure of the pore space (i.e., the pore "size distribution") is reasonably uniform. For a porous material with a broader pore size distribution, whether fractal or not, non-exponential behavior of  $g_s^{(1)}(\mathbf{q}, t)$  would be expected over a wider range of  $qR_p$ . To reiterate, this non-exponential behavior is a manifestation of the non-Gaussian nature of the probability distribution function  $P(\mathbf{R}, t|0, 0)$  for displacements  $\mathbf{R}$  in the porous material. Given that  $\mathbf{q}$  is conjugate to  $\mathbf{R}$ , the deviation from a Gaussian  $P$  and single exponential  $g_s^{(1)}(\mathbf{q}, t)$  is expected to be a maximum for  $q^{-1} \approx R_p$ , as is indeed observed.

Limited data at the highest  $qR_p$  values ( $\approx 5$ ) accessible with the available glasses and apparatus support the reasonable expectation that, for  $qR_p \gg 1$  (and also of course,  $qR_p < 1$ ), the decay rate  $\langle \Gamma \rangle$  of the correlation function is approximately  $\langle \Gamma \rangle \approx D_p q^2$ , with  $D_p$  the intrapore diffusivity, that is,  $D_0$  as modified by polymer-wall hydrodynamic interactions, and also by any changes in monomer-monomer hydrodynamic interactions due to the polymer being confined. As an example of such results, refer back to Figure 17d.

The constant  $D_{\text{EFF}}$  at low  $qR_p$  ( $qR_p \ll 1$ ) is identified as the macroscopic diffusion coefficient  $D_\infty$ , a phenomenological coefficient for diffusion over large distances or long times in the porous material as a whole. Exam-

ining the dependence of  $D_\infty$  on polymer molecular weight and on porous glass structure was the primary emphasis of this work. A few observations about the values of  $D_\infty$  for the data shown in Figures 18 and 19 are made now, although detailed discussion of the extraction of  $D_\infty$  values from such data (Chapter VI, next section) and about the molecular weight and structural dependence (Chapter VII) is deferred.

In the same porous glass (B7), polymers P4 and P6, whose relative size parameters differ by a factor of about two, have limiting values for  $D_{\text{EFF}}/D_0$  of 0.69 and 0.62. From this one concludes that a large part of the decrease of  $D_\infty$  relative to  $D_0$  is size independent, but that there is nonetheless an additional and significant size dependent decrease. Comparing between porous glasses, but for polymers with the same relative size parameters, one sees limiting values for  $D_{\text{EFF}}/D_0$  of 0.69 versus 0.53 (B7 vs B13,  $\lambda_H \approx 0.045$ ), and 0.62 versus 0.61 (B7 vs B5,  $\lambda_H \approx 0.09$ ). From this one concludes that, for the same relative size parameter, different glasses may or may not show the same overall reduction in  $D_\infty/D_0$ ; as expected, the structure of the porous glass (e.g., tortuosity) plays an important role in determining the macroscopic diffusion coefficient.

The plots of the variance  $V$  in Figures 18 and 19 indicate different limiting values for the different data sets. These limiting values are in reasonable accord with values for  $V$  in bulk solution, given that some increase in the variance is expected: P4 in B7 (0.02→0.04); P6 in B7 (0.03→0.04); P3 in B13 (0.08→0.11); and P2 in B5 (0.05→0.10). (It is noted that typical *statistical* uncertainty in  $V$  is by itself about 0.01-0.04.) The assertion that correlation functions at low  $qR_p$  are "single exponential" is thus

based not so much on the exact value of  $V$  but on the observation that  $V$  levels off at low  $qR_p$  at a similar value to that in bulk solution. This is illustrated graphically in Figure 20, where the results of Laplace inversion have been plotted as a function of  $qR_p$ ; quite clearly, the width of the shifted distribution at low  $qR_p$  is about the same as in bulk solution. It is also noted here that whereas Laplace inversion and cumulants analysis give similar results for the average decay rate  $\langle \Gamma \rangle$  over the entire  $qR_p$  range, and for the variance  $V$  for both  $qR_p \gg 1$  and  $qR_p \ll 1$ , the cumulants analysis underestimates  $V$  for  $qR_p \approx 1$  (e.g., see Figure 19).

In this dissertation research, the wavevector dependence was not examined in much detail. The light scattering spectrometer which was used only had  $q_{\text{MAX}} \approx 7.5 q_{\text{MIN}}$ . This made it impossible to examine the full range of  $qR_p$  using only a single porous glass. Further, given the  $R_p$  values of the glasses which were available for this work, and the consequently fixed ranges of  $qR_p$  (see equation (6.2)), it was also not possible to penetrate too deeply into either limiting regime, that is, towards either very low or very high  $qR_p$ . A more thorough look at the  $qR_p$  dependence could be achieved by using other porous glasses with higher and lower  $R_p$ , and by using other techniques (e.g., forced Rayleigh scattering). Dynamic light scattering appears especially well suited for studying the transition regime of  $qR_p \approx 1$ .

In concluding, it is necessary to note that this discussion of the wavevector dependence of correlation function behavior has been without a doubt oversimplified, both in order to emphasize the most important features, and because the theory on which a more detailed understanding could be based is lacking. This is particularly true in the intermediate and

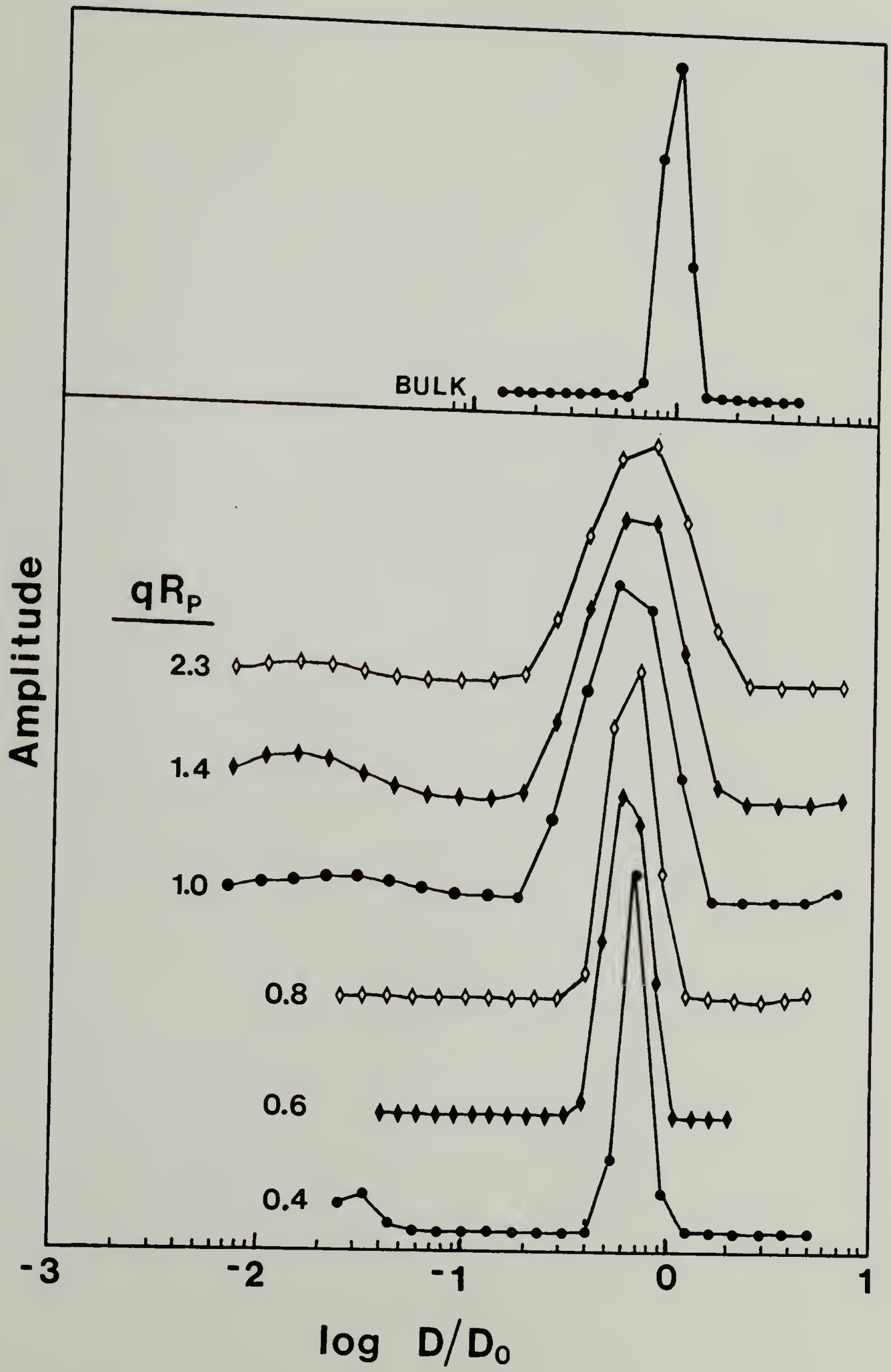
Figure 20.

Relaxation rate spectra as a function of  $qR_p$ .

Plotted are amplitude distributions (arbitrary units) of *apparent* relaxation rates normalized by the relaxation rate in bulk solution,  $\Gamma/\langle\Gamma\rangle_0 = D/D_0$ . These distributions were obtained from correlation functions by Laplace inversion using Provencher's CONTIN program.

All data are for polymer P4 ( $R_H = 40 \text{ \AA}$ ) plus glass B7 ( $R_p = 893 \text{ \AA}$ ). The top curve shows the finite dispersity of the same polymer in bulk solution. The remaining curves show the narrowing of the distribution of relaxation rates as the wavevector  $q$  decreases. For  $qR_p \leq 0.8$ , the width remains constant and is only slightly greater than in bulk solution.

Values of  $q^2$  corresponding to the denoted  $qR_p$  values are (units of  $10^9 \text{ cm}^{-2}$ ): 63.4, 25.4, 12.9, 7.81, 4.12, and 1.60, from top to bottom.



high  $qR_p$  regimes. Even at low  $qR_p$ , it is expected that the decay is not purely exponential but includes a power law term, which, however, would only be dominant at long times. From an experimental point of view, this simplified discussion is justified and perhaps preferable, due to the repeatedly mentioned experimental difficulties which preclude an exact knowledge of the shape of correlation functions.

### **Practical Data Analysis**

This section deals with important details of the extraction of diffusion coefficients from raw data: the initial analysis to obtain average relaxation rates  $\langle \Gamma \rangle$ ; the determination of the bulk solution diffusion coefficient  $D_0$  and the corresponding hydrodynamic radius  $R_H$ ; the determination of the macroscopic diffusion coefficient in the porous glass  $D_\infty$ ; estimates of random uncertainty; and discussion of sources of systematic error, in particular due to lack of extrapolations to  $c=0$  and  $t=0$ .

#### **Initial Data Fitting**

Two data analysis methods, cumulants and Laplace inversion (interchangeably referred to as CONTIN), were used. Comparison of these methods showed that the two gave nearly equivalent results in the regimes of primary interest, namely macroscopic diffusion (low  $qR_p$ ) in the porous glass, and for bulk solution measurements; hence the simpler (and less costly) cumulants method was used predominantly.

Shown in Table 5 are typical comparative results that led to this conclusion; a similar but less detailed comparison is shown graphically in

TABLE 5  
Comparison of Cumulants and Laplace Inversion Data Analysis Methods  
for Data in the Macroscopic Diffusion Regime (Polymer P4, Glass B7)

$10^{-9} \cdot q^2$ ( $\text{cm}^{-2}$ )	$\langle \Gamma \rangle$ ( $\text{s}^{-1}$ )			$\mu_2 / \langle \Gamma \rangle^2$			$f_c^+$
	L	C	C/L	L	C	C-L	
1.237	900	899	0.999	0.050	0.056	0.006	0.008
1.601	1270	1292	1.017	0.029	0.066	0.037	0.008
1.601	1228	1276	1.038	0.028	0.120	0.092	0.011
4.121	3091	3103	1.004	0.048	0.051	0.003	0.011
4.121	3043	3092	1.016	0.042	0.052	0.010	0.025
5.086	3964	4051	1.021	0.030	0.055	0.025	0.008
5.252	3825	4004	1.047	0.041	0.079	0.038	0.008
7.094	5346	5591	1.046	0.037	0.096	0.059	0.087
7.806	6100	6242	1.024	0.057	0.065	0.008	0.021

L denotes results by Laplace inversion using Provencher's CONTIN program

C denotes results by second order cumulants method

Figure 19. Generally a systematic difference in results between the two methods is seen; however, the *direction* of this difference is not always the same. For example, the results in Table 5 show  $\langle\Gamma\rangle$  and  $\mu_2/\langle\Gamma\rangle^2$  from Laplace inversion consistently lower than  $\langle\Gamma\rangle$  and  $\mu_2/\langle\Gamma\rangle^2$  from cumulants, whereas in Figure 19, the opposite is seen. This difference between the methods is due primarily to problems in baseline determination and to the presence of some homodyne signal.

If the baseline is known precisely, the presence of homodyne signal of fractional amplitude  $\alpha$  implies that:

$$\langle\Gamma\rangle_{\text{app}} = (1 + \alpha) \langle\Gamma\rangle \quad (6.11)$$

where  $\langle\Gamma\rangle_{\text{app}}$  and  $\langle\Gamma\rangle$  are the apparent and true average relaxation rates; and also that:

$$\Delta(\mu_2/\langle\Gamma\rangle^2) = \alpha(1 - \alpha)/(1 + \alpha)^2 \approx \alpha \quad (6.12)$$

where  $\Delta(\mu_2/\langle\Gamma\rangle^2)$  is the increase in the normalized variance, with the approximation for  $\alpha \ll 1$ .

Such an explanation can account for the magnitude of the observed difference in Table 5. Since the data are for a low molecular weight sample, with correspondingly short sample times (delayed baseline at  $\approx 40$  ms at the lowest  $q$ ), then problems with baseline drift are relatively negligible. Values for  $\alpha$  can be estimated from  $f_c^+$  using equation (5.9) plus  $f_c \approx 0.35$  for an aperture/pinhole of 1 mm/50  $\mu\text{m}$ ; for this data,  $\alpha \approx 0.007$ -0.07, which is of a similar magnitude to the difference in variance  $\Delta(\mu_2/\langle\Gamma\rangle^2)$  between

cumulants and CONTIN, and also to the ratio of  $\langle \Gamma \rangle$  from cumulants to  $\langle \Gamma \rangle$  from CONTIN minus one.

This explanation assumes that  $\langle \Gamma \rangle$  and  $\mu_2/\langle \Gamma \rangle^2$  from CONTIN are the "true" values; it is claimed this is approximately so *if* baseline drift is negligible. In such cases, CONTIN fits generally give a separated peak at high  $\Gamma$  with an amplitude at least roughly corresponding to  $\alpha$ , as independently estimated from  $f_c$  and  $f_c^+$ . The values given in Table 5 for CONTIN results are for the *main peak only*, thereby excluding this contribution at high  $\Gamma$ ; this main peak has  $\langle \Gamma \rangle$  and  $\mu_2/\langle \Gamma \rangle^2$  somewhat smaller than for the *entire* distribution (e.g., as determined by cumulants, or also by CONTIN).

Since some homodyne signal was always present in these experiments, the reliance on the cumulants method may have introduced some systematic error into  $\langle \Gamma \rangle$ , hence also diffusion coefficients. However, since the local oscillator was controlled to give fractional amplitude of homodyne signal  $\alpha \approx 0.005-0.025$ , the contribution of this source of error is fairly small (i.e.,  $\approx 0.5\%-2.5\%$ ).

The error introduced by uncertainty in the baseline is harder to assess. The last channels baseline ( $B_L$ ) typically exceeded the  $p^2/N$  baseline ( $B_p$ ) by about 0.5% for summed runs or about 0.05% for individual runs; however, given the low amplitudes  $\{G^{(2)}(0)/B\}-1$  of these heterodyne correlation functions at  $t=0$  (i.e., the coherence function  $f_c^+$ ), the results of fitting using  $B_L$  and  $B_p$  differ widely. (This can be seen from Figures 15 and 16 in Chapter V.) The last channels baseline  $B_L$  is a better estimate of the true baseline than  $B_p$  and was always used for cumulants analysis. Results using  $B_L$  were far more consistent than using  $B_p$ . Typically the relative

standard deviations of  $\langle \Gamma \rangle$  and  $\mu_2/\langle \Gamma \rangle^2$  from 10-20 individual runs (each run 3-6 min) were about 1-3% and 20% respectively using  $B_L$ , but much higher if  $B_p$  were used. Arguments were given in Chapter V why  $B_L$  is a better estimate of the true baseline in these heterodyne experiments. Intensity drift is particularly to blame for the unsuitability of  $B_p$ , as evidenced by the widely variable results which are obtained using  $B_p$  when significant intensity drift occurs, whereas results using  $B_L$  are essentially constant.

An idea of the sensitivity of the principal fitting parameters,  $\langle \Gamma \rangle$  and  $\mu_2/\langle \Gamma \rangle^2$ , to the choice of baseline can be gotten from Table 6, which also gives further comparison of the cumulants and Laplace inversion analysis methods. These results were for polymer P3 ( $M = 2.1 \times 10^4$ ,  $R_H = 30 \text{ \AA}$ ) in glass B7 ( $R_p = 893 \text{ \AA}$ ,  $\lambda_H = 0.034$ ) in the macroscopic diffusion regime; the coherence function  $f_C^+$  is relatively high ( $\alpha \approx 0.04$ ). Cumulant fits, and all the CONTIN fits using a multiple of  $B_L$ , employed a fixed baseline. The remaining CONTIN fit (i.e., using  $B_p$ ) allowed the baseline to float as an additional parameter (the fitted baseline was 0.9996 times  $B_L$ ).

These results illustrate a number of points. (1) The cumulant fit using  $B_p$  is obviously extremely poor ( $\chi^2 = 3300!$ ). (2) Fits with  $B > B_L$  are also poor. *For this sample*, the true baseline  $B_T$  is in the range  $B_p < B_T < B_L$ . (However, for other samples the opposite may be seen, with the true baseline  $B_T > B_L$ . Depending as to whether  $B_T > B_L$  or  $B_T < B_L$ ,  $\langle \Gamma \rangle$  and  $\mu_2/\langle \Gamma \rangle^2$  from cumulants will be either systematically lower or higher than  $\langle \Gamma \rangle$  and  $\mu_2/\langle \Gamma \rangle^2$  from Laplace inversion.) (3) As the fixed base used in fitting is decreased from  $B_L$ , several systematic effects on the fits are seen: the amplitude of the peak at low  $\Gamma$  in CONTIN fits and the overall correlation

TABLE 6  
Effect of Baseline Choice and Analysis Method on the Average  
Decay Rate  $\langle\Gamma\rangle$  and Normalized Variance  $\mu_2/\langle\Gamma\rangle^2$  for  
Polymer P3 in Glass B7, at  $q^2 = 1.5 \times 10^9 \text{ cm}^{-2}$

Baseline	Cumulants				Laplace Inversion <sup>†</sup>			
	$\langle\Gamma\rangle$	$\mu_2/\langle\Gamma\rangle^2$	$10^2 \cdot f_c^+$	$\chi^2$	$\langle\Gamma\rangle$	$\mu_2/\langle\Gamma\rangle^2$	$10^2 \cdot f_c^+$	$A_S$
1.0010 · B <sub>L</sub>	1530	-0.072	4.716	30	1685	0.015	4.864	0.0
1.0000 · B <sub>L</sub>	1597	0.045	4.894	7	1580	0.012	4.876	1.4
0.9998 · B <sub>L</sub>	1646	0.080	4.966	37	1574	0.012	4.898	1.4
0.9995 · B <sub>L</sub>	1675	0.107	5.033	58	1574	0.012	4.929	1.9
0.9990 · B <sub>L</sub>	1667	0.129	5.089	55	1587	0.012	4.979	3.2
1.0000 · B <sub>P</sub>	1277	0.050	4.554	3300	1572	0.011	4.924	1.7

<sup>†</sup> $A_S$  is the amplitude (%) of the peak at low  $\Gamma$  in these fits

function amplitude  $f_c^+$  both increase (i.e., the CONTIN program fits the dropped baseline as a slow decay); and  $\langle \Gamma \rangle$ ,  $\mu_2/\langle \Gamma \rangle^2$ , and  $\chi^2$  all increase for the cumulants fits. (4) Excluding the two fits with  $B = (1.001)B_L$ , and the cumulant fit with  $B_p$ , the relative range (from lowest to highest) in  $\langle \Gamma \rangle$  for all other fits is 7%. (5) The  $\langle \Gamma \rangle$  and  $\mu_2/\langle \Gamma \rangle^2$  results from CONTIN fits are nearly constant regardless of the initial baseline and fitting option (i.e., fixed versus floating baseline), excluding the fixed baseline ( $B = 1.001 B_L$ ) which is obviously too high. (6) The cumulant fit with  $B = B_L$  has  $\langle \Gamma \rangle = 1597$  which exceeds by only 1% the average of the  $\langle \Gamma \rangle$  from CONTIN fits; the variance from this cumulant fit exceeds that for the main peak from CONTIN. (The slightly lower  $\langle \Gamma \rangle$  value for CONTIN may be due to the aforementioned "fitting" of homodyne contributions by CONTIN--all fits had  $\approx 0.5\%$  amplitude of a high  $\Gamma$  peak--whereas this homodyne contribution may slightly influence cumulants fits.)

This discussion of data fitting has been intended to justify the use of the cumulants method in the macroscopic diffusion regime. Although Laplace inversion using the CONTIN program appears to at least roughly fit homodyne contributions (as a peak at high  $\Gamma$ ) and baseline discrepancies (as a peak at low  $\Gamma$ ), thereby providing more reliable estimates of  $\langle \Gamma \rangle$  and  $\mu_2/\langle \Gamma \rangle^2$  than the cumulants method, the differences between the two methods in the macroscopic diffusion regime are not great. (Note however that at higher  $qR_p$ , where correlation functions are more non-exponential, significant systematic differences between the methods are indeed seen.) Furthermore, as has been shown by several examples, the direction of these differences is *random* from sample to sample, but *systematic* from angle to angle for the

same sample. Since diffusion coefficients are obtained by fitting of  $\langle T \rangle$  versus  $q^2$ , each diffusion coefficient will reflect this systematic angular error; but in a series of measurements of diffusion coefficients for different samples, this fitting error is random. Also, for reasonable choice of the baseline ( $B \approx B_L$ ), results for  $\langle T \rangle$  are not extremely sensitive to the baseline even for the cumulants method; however, the variance  $\mu_2/\langle T \rangle^2$  is much more sensitive to baseline choice. Lastly, it is likely that Laplace inversion using the CONTIN program introduces some systematic error of its own (e.g., because of the constraint of "smoothness", or the criterion for choosing any one solution as best); this error may also depend on the nature of the data. Therefore, it is not possible to claim the results of Laplace inversion fits as better with any certainty. For all these reasons, it was judged satisfactory to use the cumulants method as opposed to the Laplace inversion method.

### Extraction of Diffusion Coefficients

Diffusion coefficients in bulk solution  $D_0$  and for macroscopic diffusion in the porous glass  $D_\infty$  were obtained in the usual way, as the slope of linear fits of  $\langle T \rangle$  versus  $q^2$ . Typical data and fitted lines are shown in Figure 21. Correlation coefficients  $r^2$  of these fits were always in excess of 0.999, indicating good linearity over the ranges chosen for  $q^2$ .

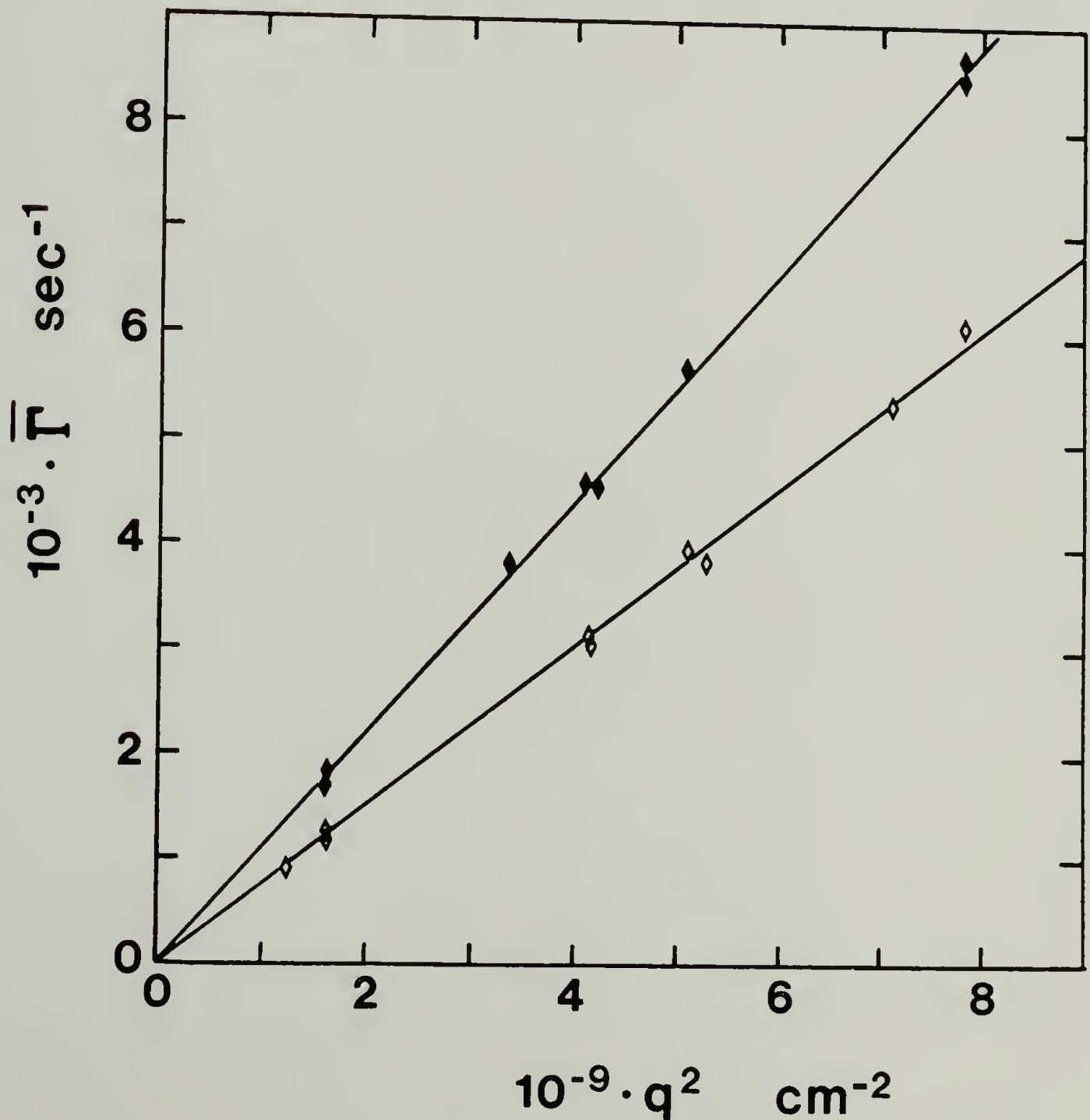
The hydrodynamic radius  $R_H$  was determined from  $D_0$  by means of the Stokes-Einstein relation, equation (3.32). As was noted there, since  $D_0$  is a mutual diffusion coefficient,  $R_H$  as thus defined is only an apparent hydrodynamic radius. The error associated with this operational definition of  $R_H$  is discussed later in connection with the concentration dependence of  $D_0$ .

Figure 21.

Average relaxation rate  $\langle \Gamma \rangle$  versus the square of the scattering wavevector  $q^2$  for diffusion in bulk solution and for macroscopic diffusion in a porous glass.

Linear fits to the data (filled diamonds, bulk solution; empty diamonds, in the porous glass), shown as solid lines, were used to obtain the diffusion coefficients  $D_0$  and  $D_\infty$  as the slopes of these lines.

Data shown are for polymer P4 in glass B7 ( $\lambda_H = 0.044$ ,  $D_0 = 1.11 \times 10^{-6} \text{ cm}^2/\text{s}$ , and  $D_\infty = 7.61 \times 10^{-7} \text{ cm}^2/\text{s}$ ).



The random error associated with the determination of  $D_0$  and  $D_\infty$  is low. Relative standard deviations of the slopes from the linear fits were 0.1-0.5% ( $D_0$ ) and 0.5-1.5% ( $D_\infty$ ). Relative standard deviations of  $D_0$  and  $D_\infty$ , as determined by the averages of  $D_0$  and  $D_\infty$  values from the individual measurements at different angles, were somewhat higher, 0.8-2% ( $D_0$ ) and 0.8-7% ( $D_\infty$ ) and perhaps better indicate the random uncertainty. Values of  $D_0$  from linear fits and from the average of individual measurements were always in agreement to within 0.5%, typically 0.1%. For  $D_\infty$ , the agreement was poorer, always within 5%, but typically less than 1%. This random error is much lower than the systematic error (to be discussed subsequently), which is primarily due to neglect of the concentration dependence of both  $D_0$  and  $D_\infty$ .

In bulk solution, the range of  $q^2$  for these fits was restricted to that where the apparent diffusion coefficient and normalized variance were constant. This corresponds to the condition  $qR_G < 1$ , and avoids the inclusion of internal modes, which lead to an increase in the apparent diffusion coefficient and the variance at higher  $qR_G$ .

The choice of the range of  $q^2$  for the determination of  $D_\infty$  (from fits of  $\langle \Gamma \rangle$  versus  $q^2$ ) is discussed now. For glasses B7 and B13 (smaller pore sizes), data with  $q^2 < 8 \times 10^9 \text{ cm}^{-2}$  were used. This limit corresponds to  $qR_p = 0.8$  for glass B7 and  $qR_p = 0.63$  for glass B13, and includes data taken through the lowest three angle windows of the light scattering vat,  $\theta = 15^\circ$ ,  $25^\circ$ , and  $35^\circ$ . The justification for this choice is clear, on reference back to Figure 18 for the wavevector dependence of  $D_{\text{EFF}} (= \langle \Gamma \rangle / q^2)$  and  $\mu_2 / \langle \Gamma \rangle^2$  for these glasses. The average effective diffusion coefficient  $D_{\text{EFF}}$  is constant,

and  $\mu_2/\langle\Gamma\rangle^2$  is nearly so, for  $q^2 < 8 \times 10^9 \text{ cm}^{-2}$ ; as discussed in section 2 of this chapter, this constancy of  $D_{\text{EFF}}$  and  $\mu_2/\langle\Gamma\rangle^2$ , and a value for  $\mu_2/\langle\Gamma\rangle^2$  near that in bulk solution, are taken as hallmarks of the macroscopic diffusion regime.

For glass B5 (larger pore size), data with  $q^2 < 5 \times 10^9 \text{ cm}^{-2}$ , corresponding to the  $15^\circ$  ( $q^2 \approx 1.5 \times 10^9 \text{ cm}^{-2}$ ,  $qR_p \approx 0.72$ ) and  $25^\circ$  ( $q^2 \approx 4.8 \times 10^9 \text{ cm}^{-2}$ ,  $qR_p \approx 1.3$ ) apparatus windows, were used to determine  $D_\infty$ . On reference back to Figure 19 for the  $q^2$  dependence of  $D_{\text{EFF}}$  and  $\mu_2/\langle\Gamma\rangle^2$ , it can be seen that  $D_{\text{EFF}}$  decreases slightly, and  $\mu_2/\langle\Gamma\rangle^2$  decreases significantly, on going from the  $25^\circ$  window to the  $15^\circ$  window. This observation clearly indicates that  $25^\circ$  window data ( $qR_p \approx 1.3$ ) are not in the macroscopic diffusion regime, as does the knowledge that the transition to macroscopic diffusion occurs at smaller values of  $qR_p$  (i.e.,  $qR_p < 0.6\text{--}0.8$ ) for the similar but smaller pore size glasses. Strictly then, only data from the  $15^\circ$  window should have been used to determine  $D_\infty$ , although even at  $15^\circ$ ,  $qR_p$  is only about 0.7, not strongly in the macroscopic diffusion regime. The inclusion of  $25^\circ$  window data was justified as providing some guard against systematic error due to alignment problems (the  $15^\circ$  and  $25^\circ$  windows are on opposite sides of the  $0^\circ\text{--}180^\circ$  axis of the vat, and are at sufficiently low  $q$  that alignment error can be a problem); and as improving the statistics of determination of  $D_\infty$  from the typically scattered data at low  $q$ . Although this leads to a bias in  $D_\infty$  (estimated at about 2%, from comparison of all data at  $15^\circ$  vs  $25^\circ$ ), this was judged preferable to total reliance on data from only the  $15^\circ$  window.

### Internal Modes of Strongly Confined Chains

A further point concerns the diffusion of high molecular weight polymer in the porous glasses. In bulk solution, the range of  $q$  was

restricted such that  $qR_G < 1$ , to ensure that correlation functions only reflected translational diffusion. The corresponding criterion in the porous glass was given by equation (6.5b), namely  $(\mathbf{q} \cdot \mathbf{R}_{G,\parallel}) < 1$ . For the higher molecular weights in the smaller pore size glasses, even the average of  $(\mathbf{q} \cdot \mathbf{R}_{G,\parallel})$  will be greater or equal to  $qR_G$  in bulk solution; that is, both  $(\mathbf{q} \cdot \mathbf{R}_{G,\parallel})_{\text{MAX}} > qR_G$  and  $\langle \mathbf{q} \cdot \mathbf{R}_{G,\parallel} \rangle > qR_G$ , where  $R_G$  is the spherically averaged radius of gyration in bulk solution. Hence, for some higher molecular weights, the conditions required to see the longitudinal internal modes of the chain (see equations (2.40)), namely,  $qR_{G,\parallel} > 1$  and  $qR_p < 1$ , might be simultaneously satisfied in some range of wavevector  $q$ .

It is noted that the internal mode structure predicted for confined chains (e.g., given by equations (2.40) for slit-like and cylindrical pore geometries) is quite different than that for chains in bulk solution, and as a consequence, contributions of internal modes might not significantly affect  $D_{\text{EFF}}$  or  $\mu_2/\langle \Gamma \rangle^2$ . (The relaxation times of these longitudinal modes of the "blob" chain should be more comparable to the translational diffusion relaxation time than are the relaxation times of the usual internal modes of an unconfined chain.) An effort was made to look for these internal modes in data at low  $qR_p$  ( $qR_p < 1$ ) for the two highest molecular weight samples in glass B7 ( $R_p = 893 \text{ \AA}$ ). This was suggested by the observations: (1) of increased difference in variance relative to bulk solution  $\Delta(\mu_2/\langle \Gamma \rangle^2)$  for these samples, as compared to  $\Delta(\mu_2/\langle \Gamma \rangle^2)$  for lower molecular weight samples; and (2) the presence of a slight "hook" in the correlation functions for these highest molecular weight samples at early times, again something not seen at all with lower molecular weight samples.

Except for the highest molecular weights (i.e., for the highest values of  $\lambda_G$ ), data for samples in glass B7 show no evidence of significant  $q$  dependence of either  $D_{\text{EFF}}$  or  $\mu_2/\langle\Gamma\rangle^2$ , for  $\theta \leq 35^\circ$  ( $q^2 < 8 \times 10^9 \text{ cm}^{-2}$ ). The maximum of  $\lambda_G$  in this work was only about 0.7 (polymer P17 in glass B7). Since, at least for most samples, the chains are relatively unconfined, then  $R_{G,\parallel}/R_G$  shouldn't be extremely large, and the measurements should mainly reflect translational diffusion. (Polymer P9, with  $R_G \approx 300 \text{ \AA}$ , giving  $\lambda_G \approx 0.4$ , was the highest molecular weight examined in the smallest pore size glass B13.) An increase in the difference in variance  $\Delta(\mu_2/\langle\Gamma\rangle^2)$  between the porous glass (at low  $qR_p$ ) and in bulk solution, as seen for the higher molecular weight samples, may indicate contributions of internal modes.

For the highest molecular weight used in this study ( $M = 2.1 \times 10^6$ ,  $R_G \approx 600 \text{ \AA}$ ),  $qR_G$  is about 0.23 ( $15^\circ$ ), 0.38 ( $25^\circ$ ), and 0.53 ( $35^\circ$ ). The isotropic average of  $\mathbf{q} \cdot \mathbf{R}_{G,\parallel}$  is  $qR_{G,\parallel} \langle \cos \theta \rangle = 2qR_{G,\parallel}/\pi$ . For the different window angles, this quantity  $2qR_{G,\parallel}/\pi$  is equal to unity for  $R_{G,\parallel}/R_G$  of about 6.9 ( $15^\circ$ ), 4.2 ( $25^\circ$ ), and 3.0 ( $35^\circ$ ); and the quantity  $qR_{G,\parallel}$  (i.e., the maximum value, corresponding to  $\mathbf{q}$  and  $\mathbf{R}_{G,\parallel}$  parallel) equals unity for  $R_{G,\parallel}/R_G$  of about 4.4 ( $15^\circ$ ), 2.6 ( $25^\circ$ ), and 1.9 ( $35^\circ$ ). These rough calculations indicate that the chains would not have to be all that strongly deformed (due to confinement) for  $qR_{G,\parallel}$  to be greater than unity.

Correlation functions for the highest molecular weight polymer (P17,  $M = 2.1 \times 10^6$ ,  $R_H = 422 \text{ \AA}$ ) in glass B7 ( $R_p = 893 \text{ \AA}$ ,  $\lambda_H = 0.472$ ) are significantly non-exponential, even at low  $qR_p$  (i.e., for data from the  $15^\circ$ ,  $25^\circ$ , and  $35^\circ$  windows). Analysis of these correlation functions (Table 7) provides strong evidence for the presence of two decay modes. The slower

TABLE 7

Internal Modes of Confined Chains: Analysis of Data for Polymer P17  
 ( $M = 2.1 \times 10^6$ ) in Glass B7 ( $R_p = 893 \text{ \AA}$ ); Relative Size  $\lambda_H = 0.47$

$10^{-9} \cdot q^2$ ( $\text{cm}^{-2}$ )	$\Delta t$ (ms)	Cumulants		Laplace Inversion <sup>1</sup>			
		$256 \langle \Gamma \rangle \Delta t$	$\langle \Gamma \rangle$ ( $\text{sec}^{-1}$ )	$\langle \Gamma \rangle_S$ ( $\text{sec}^{-1}$ )	$\langle \Gamma \rangle_F$ ( $\text{sec}^{-1}$ )	$A_S$	$A_F$
1.438	1.3	14	42	41	237	0.90	0.10
1.541	1.5	18	47	45	241	0.86	0.14
4.282	0.56	17	116	113	519	0.91	0.09
4.379	0.55	16	115	113	665	0.86	0.14
4.379	0.27	8	120	106	562	0.83	0.17
7.623	0.27	13	194	182	884	0.80	0.20

<sup>1</sup> Subscripts "S" and "F" refer to the slow and fast modes  
 Laplace inversion using Provencher's CONTIN program

mode is identified as translational diffusion. The faster mode may be due to the longitudinal internal modes of the chain (see equation (2.40d)).

As can be seen from Table 7, the average relaxation rates from cumulants fits  $\langle\Gamma\rangle_{\text{CUM}}$  are but slightly higher than that of the slow (translational diffusion) modes  $\langle\Gamma\rangle_S$  from Laplace inversion. The Laplace inversions, with both the baseline and the intercept  $f_C^+$  allowed to float (i.e., CONTIN using equation (5.24)), give two peaks with  $\langle\Gamma\rangle$  values differing by about a factor of 5. Given the rather high values of  $256 \langle\Gamma\rangle_{\text{CUM}} \Delta t$  (i.e., the time range spanned by the correlation functions) and the ratio  $\langle\Gamma\rangle_F / \langle\Gamma\rangle_S \approx 5$ , it is reasonable that the cumulants fits (which were for  $t \geq 3\Delta t$ ) do not show much evidence of the faster mode; the faster exponential, that is,  $\exp(-\langle\Gamma\rangle_F t)$ , will have decayed to about 0.4 by  $t \approx 3\Delta t$ , and to about 0.01 by  $t \approx 16\Delta t$ . With  $\langle\Gamma\rangle t_{\text{MAX}}$  so large, it should be emphasized that the fast mode cannot be expected to be determined very accurately.

The tentative identification of the faster mode as internal modes of the confined chains rests on the following. First, Laplace inversion analysis of data for lower molecular weight samples in the same glass never gives fast decay modes with such high amplitudes. Second, even admitting the possibility of significant baseline drift at such long  $\Delta t$ , the correlation functions for this sample are conclusively non-single exponential even at low angles. Third, the amplitude of the fast component increases with increase in  $q$ ; as in bulk solution, internal modes are expected to be more significant as  $qR_G$  increases. Fourth, the previous discussion indicated that for this highest molecular weight,  $qR_{G,\parallel}$  may well be greater than unity, so that internal modes could be expected to contribute to the correlation function.

Lastly, the fast relaxation rate  $\langle\Gamma\rangle_F$  appears to scale with  $q^2$ , as predicted by equation (2.40d) (which expression, it should be noted, is for *cylindrical* pores).

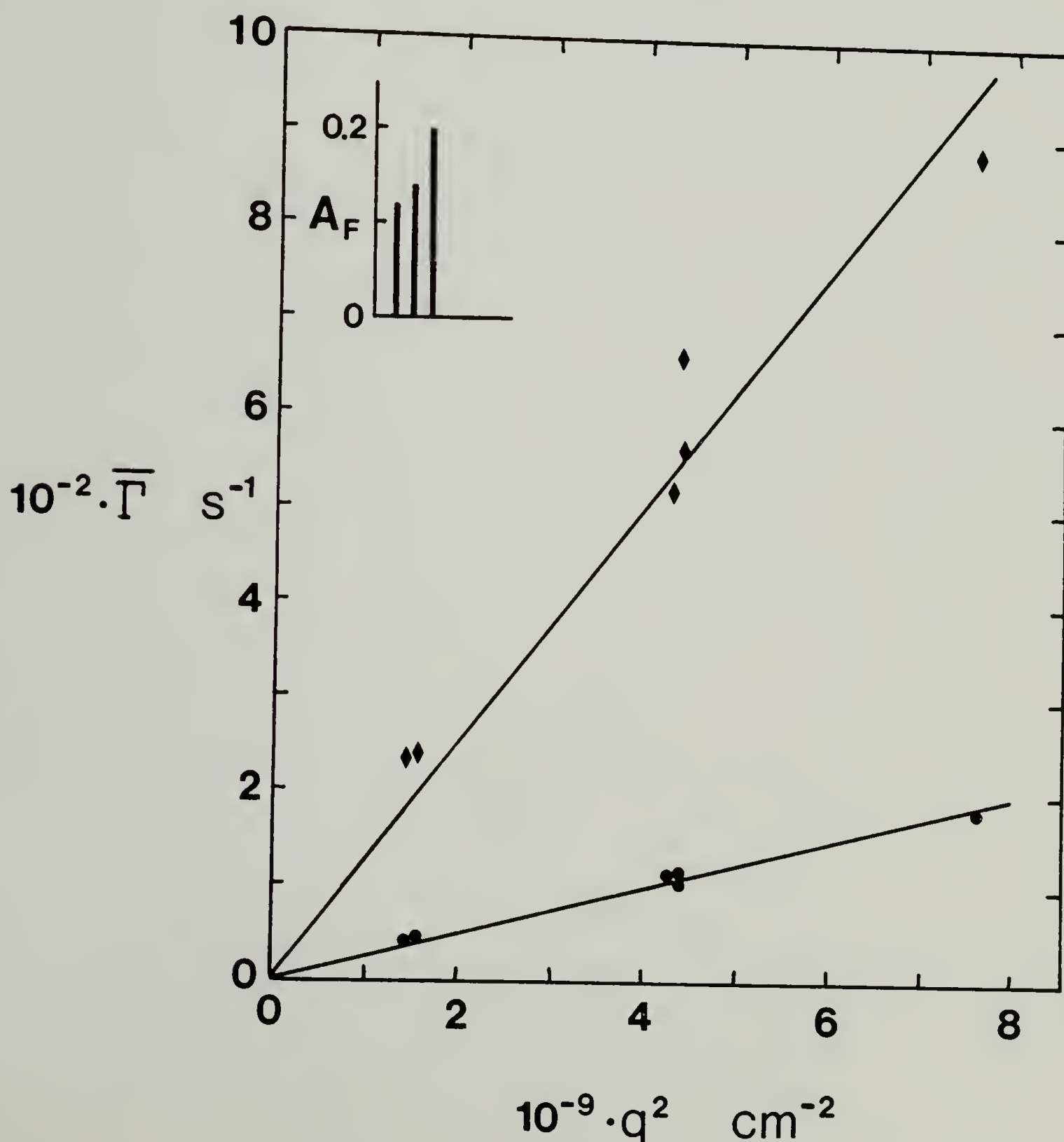
These results are plotted in Figure 22. From fits of  $\langle\Gamma\rangle_F$  and  $\langle\Gamma\rangle_S$  versus  $q^2$  (thereby assuming  $q^2$  dependence), diffusion coefficients were obtained. It is of interest to note that the diffusion coefficient obtained from a fit of  $\langle\Gamma\rangle_F$  versus  $q^2$ ,  $D_F = 1.26 \times 10^{-7} \text{ cm}^2/\text{s}$ , corresponds to an end to end distance  $R_F \approx 1.9 R_p$ ; this is of course roughly the size of a "blob" in the scaling picture (see Figure 2) of confined chains. The slow diffusion coefficient is obtained as  $D_S = 2.48 \times 10^{-8} \text{ cm}^2/\text{s}$ , as compared to the result from cumulants analysis of  $D_\infty = 2.63 \times 10^{-8} \text{ cm}^2/\text{s}$ ; as expected, the value from cumulants is higher due to inclusion of the faster mode. (N. B. The bulk solution diffusion coefficient  $D_0 = 1.09 \times 10^{-7} \text{ cm}^2/\text{s}$ , which can be compared to  $D_F$ .)

The analysis of data for the next lowest molecular weight polymer in the same glass (P16,  $M = 1.38 \times 10^6$ ,  $R_H = 330 \text{ \AA}$ ,  $\lambda_H = 0.37$ , and  $\lambda_G = 0.54$ ) yields similar results: two relaxation modes, in about the same ratio, and again with the amplitude increasing with increase in  $q$ . The ratio  $\langle\Gamma\rangle_F/\langle\Gamma\rangle_S \approx 4.3$ . Corresponding diffusion coefficients are:  $D_F = 1.48 \times 10^{-7} \text{ cm}^2/\text{s}$  (from the fast mode in Laplace inversions);  $D_S = 3.44 \times 10^{-8} \text{ cm}^2/\text{s}$  (from the slow mode in Laplace inversions);  $D_\infty = 3.97 \times 10^{-8} \text{ cm}^2/\text{s}$  (from  $\langle\Gamma\rangle$  from cumulants); and  $D_0 = 1.39 \times 10^{-8} \text{ cm}^2/\text{s}$  (from bulk solution). The end to end distance corresponding to  $D_F$  is  $R_F \approx 2.3 R_p$ , again roughly the size of a blob. (However, it is important to note that  $D_F$  is approximately the same as  $D_0$  for

Figure 22.

Average relaxation rates for slow and fast modes versus  $q^2$ , for  $M = 2.1 \times 10^6$  polystyrene in glass B7 ( $R_p = 893 \text{ \AA}$ ,  $\lambda_H = 0.47$ ).

These values are the average relaxation rates of separate peaks in the decay rate distribution obtained upon Laplace inversion. The inset shows the fractional amplitude of the fast mode. Slow mode (circles; identified as translational diffusion). Fast mode (diamonds; tentatively, identified as internal modes of confined polymer).



both P16 and P17. Although I am fairly certain that the scattering volume lay entirely within the fragments, this result perhaps suggests otherwise.)

### Concentration Dependence of Diffusion Coefficients

Attention turns now to systematic sources of error, in particular, error due to failure to extrapolate data to zero sample time and zero concentration.

Generally, correlation functions should be measured using various sample times  $\Delta t$ , and the results of analysis for  $\langle \Gamma \rangle$ ,  $\mu_2/\langle \Gamma \rangle^2$ , etc. extrapolated to  $\Delta t = 0$  (e.g., see<sup>150,162</sup>). Since the first cumulant  $\langle \Gamma \rangle$ , which corresponds to the z-average mutual diffusion coefficient, is the initial slope of  $\ln\{g_s^{(1)}(\mathbf{q}, t)\}$ , this procedure corrects both for sample polydispersity, and for the fact that the discrete photon count autocorrelation function  $C(j\Delta t)$  is only an approximation to the continuous  $g^{(2)}(t)$ . In practice, this extrapolation could not be performed. The delayed baseline  $B_L$  is the most reliable estimate of the true baseline, but as  $\Delta t \rightarrow 0$ , even  $B_L$  becomes an unreliable estimate. It is believed that the neglect of this extrapolation to  $\Delta t = 0$  introduced no significant error in these experiments. First, the correlator has 256 main channels, so even for the relatively high values of  $256 \langle \Gamma \rangle \Delta t \approx 10$ ,  $C(j\Delta t)$  should be a reasonable approximation to  $g^{(2)}(t)$ . Second, the samples used were relatively monodisperse, so even at the relatively high values of  $\{256 \langle \Gamma \rangle \Delta t\}$  employed, the apparent diffusion coefficient should not be much lower than the diffusion coefficient in the limit  $\{\langle \Gamma \rangle \Delta t\} \rightarrow 0$ . Lastly, sample times were always chosen to keep  $\{\langle \Gamma \rangle \Delta t\}$  approximately constant, both from angle to angle for the same sample, and from sample to sample; hence any

error introduced by failure to extrapolate to  $\Delta t = 0$  should presumably be approximately constant for all these measurements.

In contrast, the neglect of concentration dependence is far less justified. In this work, diffusion coefficients were measured at but a single concentration, both in bulk solution and in porous glasses. This is contrary to the usual practice of making measurements at a number of concentrations and extrapolating to  $c = 0$ , as is required to obtain the self-diffusion coefficient.

An experiment was performed with polymer P8 and glass B7 ( $M = 4.0 \times 10^5$ ,  $R_H = 165 \text{ \AA}$ ,  $R_p = 893 \text{ \AA}$ ,  $\lambda_H = 0.185$ ) in order to examine the concentration dependence of  $D$  in bulk solution and in the glass. The results are shown in Figure 23.

At relatively low concentrations, it is often assumed that the concentration dependence is linear:

$$D_{0,app} = D_0 (1 + k_{D,0} c_0) \quad (6.13)$$

$$D_{\infty,app} = D_{\infty} (1 + k_{D,G,0} c_0) \quad (6.14)$$

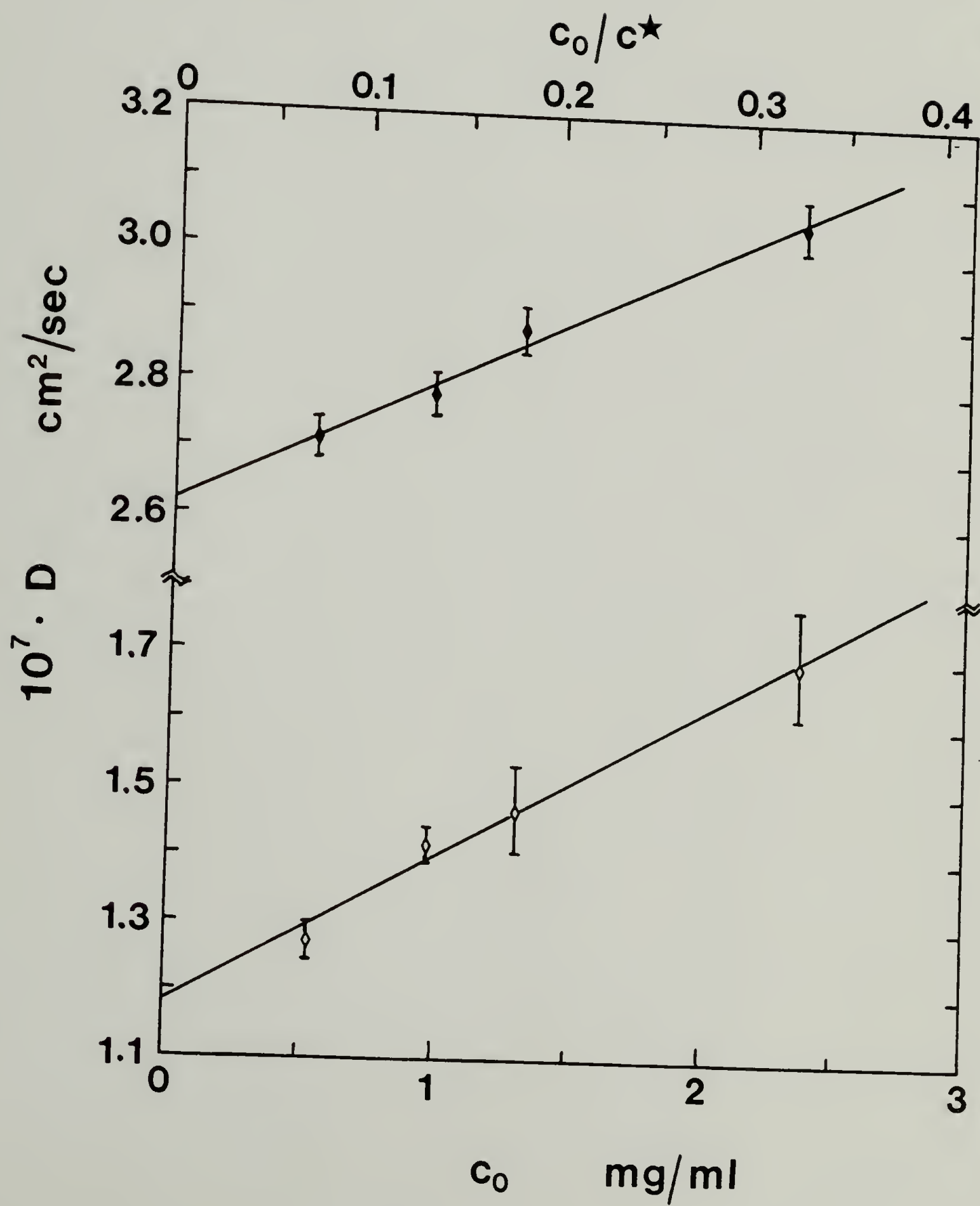
$$D_{\infty,app} = D_{\infty} (1 + k_{D,G,p} c_p) \quad (6.15)$$

Here the subscript "app" denotes concentration dependent mutual diffusion coefficients, whereas  $D_0$  and  $D_{\infty}$  without the subscript are the self-diffusion coefficients in the limit of infinite dilution. The concentration initially added is  $c_0$ , and  $c_p$  is the concentration inside the pores. Since the pore volume of a single fragment is a negligible fraction of the total sample solution volume, the relation between  $c_0$  and  $c_p$  is given by the partitioning coefficient  $K_D$ .

Figure 23.

Concentration dependence of mutual diffusion coefficients, in unbounded solution, and in solution inside a porous glass.

Data are shown for polymer P8 ( $M = 4 \times 10^5$ ) in glass B7 ( $R_p = 893 \text{ \AA}$ ). The abscissa is shown both as the concentration in bulk solution ( $c_0$ ) and as  $c_0/c^*$ , with  $c^* \approx 7.21 \text{ mg/ml}$  the overlap concentration in bulk solution, calculated using equation (4.1). The filled pips are for diffusion in unbounded solution; the porous pips are for macroscopic diffusion in the glass. The solid lines are linear fits to the data. The ratio  $D_\infty/D_0$  in the limit  $c_0 = 0$  is 0.45; this can be compared with the value  $D_{\infty,app}/D_{0,app} = 0.51$  for the second lowest concentration ( $c_0 = 0.97 \text{ mg/ml}$ ,  $c_0/c^* = 0.135$ ), which is a typical reduced concentration as used in this dissertation.



namely,  $c_p = K_D c_0$ . Note that  $k_{D,G,0}$  is the coefficient with regard to the concentration  $c_0$  in the surrounding bulk solution ( $c_0$  is easily measurable), but that  $k_{D,G,p}$  is with regard to the actual concentration  $c_p$  inside the pores ( $c_p$  is measurable with difficulty).

The results of weighted linear fits of  $D_{0,app}$  and  $D_{\infty,app}$  versus  $c_0$  are:

$$D_0 = (2.62 \pm 0.02) \times 10^{-7} \text{ cm}^2/\text{s}, \quad k_{D,0} = 70 \pm 4 \text{ cm}^3/\text{g}$$

$$D_{\infty} = (1.18 \pm 0.02) \times 10^{-7} \text{ cm}^2/\text{s}, \quad k_{D,G,0} = 186 \pm 20 \text{ cm}^3/\text{g}$$

The value of  $D_{\infty}/D_0$  in the limit  $c_0 = 0$  is 0.45. This can be compared with values at finite concentration:  $(D_{\infty}/D_0)_{app} = 0.47$  (P8,  $c_0/c^* = 0.073$ ), 0.51 (P8,  $c_0/c^* = 0.135$ ), 0.51 (P8,  $c_0/c^* = 0.180$ ), 0.55 (P8,  $c_0/c^* = 0.327$ ), and 0.49 (P2,  $c_0/c^* = 0.119$ ). (N. B. Both P8 and P2 have  $\lambda_H = 0.185$ .) These values of  $D_{\infty}/D_0$  at finite concentration show significant error relative to the  $c_0 = 0$  value: 4.5%, 13.1%, 13.3%, 23.3%, and 8.7% higher respectively.

The concentration dependence of  $D_{\infty,app}$  with respect to the actual concentration in the pores is much stronger than the concentration dependence in bulk solution. For  $\lambda_H = 0.185$ , the partitioning coefficient  $K_D$  is estimated to be in the range  $0.45 < K_D < 0.69$ , with the best estimate  $K_D \approx 0.69$ . (See Chapter IV, section 3 for details.) Using this estimate of  $K_D$  with the nominal value for  $k_{D,G,0} = 186 \text{ cm}^3/\text{g}$ , one can calculate the coefficient  $k_{D,G,p} = k_{D,G,0}/K_D = 270 \text{ cm}^3/\text{g}$ , which is nearly a factor of 4 greater than  $k_{D,0} = 70 \text{ cm}^3/\text{g}$ . (Obviously, there is much uncertainty in this estimate of  $k_{D,G,p}$ .) Intuitively, stronger concentration dependence in the pores than in bulk solution is reasonable, since the likelihood of interaction is increased

when polymer motion is confined along pore directions. (It is easier to avoid interaction with Hare Krishnas in central terminals of airports, as opposed to in connecting hallways, at constant density of people.)

Systematic error due to neglect of the concentration dependence of  $D_0$  and  $D_\infty$  is considered now. The solutions examined (with the exception of the experiment just discussed) all had  $0.10 < c_0/c^* < 0.16$ , with average  $c_0/c^* = 0.12 \pm 0.02 \approx 1/8$ . Now  $c^*$  was estimated from the intrinsic viscosity  $[\eta]$  using equation (4.1). Therefore, for the average value of  $c_0/c^*$ , equation (6.13) can be written as:

$$D_{0,app}/D_0 \approx 1 + (k_{D,0}/8[\eta]) \quad (6.16)$$

Any systematic change in  $D_{0,app}/D_0$  as a function of molecular weight is thus related to the molecular weight dependence of the quantity  $k_{D,0}/[\eta]$ . For the relatively high molecular weights used in these experiments ( $M > 2 \times 10^4$ ),  $[\eta]$  is proportional to the hydrodynamic volume  $V_H = 4\pi R_H^3/3$  divided by the molecular weight  $M$ ; hence

$$k_{D,0}/[\eta] \propto k_{D,0} (M/N_A V_H) \equiv k_D^* \quad (6.17)$$

Huber, Burchard, and Akcasu<sup>163</sup> (among others) have considered  $k_D^*$  for polystyrene in the good solvent toluene, comparing experimental results to various theories. Their results show an increase in  $k_D^*$  from about 1.0 ( $M \approx 2 \times 10^4$ ) to 1.6 ( $M \approx 2 \times 10^5$ ) to 2.2 ( $M \approx 2 \times 10^6$ ). The asymptotic value at high  $M$  is  $k_D^* \approx 2$ -2.4.

Our data for samples P8 and P2 ( $M \approx 4 \times 10^5$ ) give  $D_{0,app}/D_0 \approx 1.066$ ; and from the above,  $k_D^* \approx 1.8$  for  $M = 4 \times 10^5$ . From this one can

estimate a range of  $D_{0,app}/D_0$ : from 1.037 ( $M = 2 \times 10^4$ ) to 1.081 ( $M = 2 \times 10^6$ ) for measurements at  $c_0/c^* \approx 1/8$ , which involves a relative change in  $D_{0,app}/D_0$  of about 4% from lowest to highest molecular weight. The hydrodynamic radius, which was obtained in our experiments from  $D_{0,app}$  and not  $D_0$ , thus ranges from  $R_{H,app}/R_H \approx 0.925$  ( $M = 2 \times 10^6$ ) to  $R_{H,app}/R_H \approx 0.964$  ( $M = 2 \times 10^4$ ).

Unfortunately, theory is lacking for the corresponding dependence of  $D_{\infty,app}/D_{\infty}$  (i.e.,  $k_{D,G,P}$ ) upon molecular weight. As suggested by the observation that  $k_{D,G,P}/k_{D,0} \approx 4$  for polymer with  $M = 4 \times 10^5$  ( $\lambda_H = 0.185$ ), this dependence is probably stronger than in bulk solution. Further, it is obvious that  $k_{D,G,P}$  must be a function not only of polymer size (e.g., molecular weight, hydrodynamic radius, second virial coefficient) as it is in bulk solution, but also of the pore size; and that also, by analogy to bulk solution, this dependence will not be simply on the relative size parameter, except in the limit of very high molecular weights.

Using the value of  $k_{D,G,0} = 186 \text{ cm}^3/\text{g}$ , one can estimate  $D_{\infty,app}/D_{\infty} \approx 1.17$  at  $c_0/c^* \approx 1/8$ , which is a significant error. Supposing that there is the same relative change in  $k_{D,G,0}/[\eta]$  as in  $k_{D,0}/[\eta] = k_D^*$  over the range  $2 \times 10^4 < M < 2 \times 10^6$ , then  $D_{\infty,app}/D_{\infty}$  would range from 1.09 to 1.21 (from lowest to highest molecular weight), a 10% relative change in  $D_{\infty,app}/D_{\infty}$ . This would correspond to a range in  $D_{\infty,app}/D_{0,app}$  of 1.05 to 1.12 (6% relative change) from lowest to highest molecular weight. These ranges are probably the *best* that can be expected (i.e., smallest ranges).

From a practical standpoint with regard to the dynamic light scattering experiments, it is the concentration dependence of the quantity

$k_{D,G,0}/[\eta]$  that is important. It is perhaps reasonable that  $k_{D,G,0}/[\eta]$  is not an extremely strong function of the relative size parameter  $\lambda_H$  and molecular weight, because as  $\lambda_H$  increases, the partitioning coefficient decreases. The overall diffusion virial coefficient  $k_{D,G,0}$ , which is based on the concentration  $c_0$  in bulk solution, is the product of the diffusion virial coefficient in the pores  $k_{D,G,P}$  times the partitioning coefficient  $K_D$ . Although  $k_{D,G,P}$  will be a very strong function of  $M$  and  $\lambda_H$ , the product  $k_{D,G,0} = K_D \cdot k_{D,G,P}$  will be much less so. At large  $\lambda_H$ ,  $K_D \propto \exp(-\lambda_H^{5/3})$ , so  $k_{D,G,P}$  would have to have exponential dependence on  $\lambda_H$  for  $k_{D,G,0}$  to remain an increasing function. Exponential dependence of  $k_{D,G,P}$  might be expected on the basis of "first passage time" effects; that is, one molecule must move out of the way before another can pass.

This discussion of systematic error caused by failure to extrapolate diffusion coefficient measurements to zero concentration is now summarized, with a view towards the upcoming presentation (in Chapter VII) of data as  $D_\infty/D_0$  versus  $\lambda_H$  (where, in the notation of the current section, all these are "apparent" values). First, all measurements were made at  $c_0/c^* \approx 1/8$ , which to first order eliminates gross systematic errors from sample to sample. Second, taking the ratio  $D_{\infty,app}/D_{0,app}$  of diffusion coefficients, both measured at finite concentration, tends to reduce systematic error; nonetheless, the ratio of  $D_{\infty,app}/D_{0,app}$  to  $D_\infty/D_0$  is expected to systematically increase with increase in  $\lambda_H$  (*assuming* that  $k_{D,G,0}/[\eta]$  increases with increase in  $\lambda_H$  and  $M$ , which, however, is not assured). A rough estimate of this increase over the range of molecular weights used in this work is about 6%. Further, if  $D_{\infty,app}$  has a very strong dependence on  $\lambda_H$  or  $M$ , the slope and

even the shape of the curve could be significantly affected by this systematic error as a function of  $\lambda_H$  and  $M$ . The magnitude of this error is about  $(D_{\infty,app}/D_{0,app})/(D_{\infty}/D_0) \approx 1.10$ , as measured for a sample with a molecular weight ( $M = 4 \times 10^5$ ) and relative size parameter ( $\lambda_H = 0.185$ ) in about the middle of the investigated ranges of  $\lambda_H$  and  $M$ , at  $c_0/c^* \approx 1/8$ . This absolute error in  $D_{\infty,app}/D_{0,app}$  (versus  $D_{\infty}/D_0$ ) will significantly affect the intercept at  $\lambda_H = 0$  (i.e., the intercept will be too high). Lastly, values of  $R_{H,app}$  from  $D_{0,app}$  will be systematically low. The ratio  $R_{H,app}/R_H$  is estimated to be between 93% ( $M = 2 \times 10^6$ ) and 96% ( $M = 2 \times 10^4$ ). It is worth noting that this error ( $R_{H,app} < R_H$ ) should partially compensate the error in  $D_{\infty,app}/D_{0,app}$  (since  $D_{\infty,app}/D_{0,app} > D_{\infty}/D_0$ ) when the dependence of apparent  $D_{\infty}/D_0$  on apparent  $\lambda_H$  is considered. This error in  $R_H$  affects mainly the slope of plots of  $D_{\infty}/D_0$  versus  $\lambda_H$ , and the intercepts only to a lesser degree.

It is noted that in other studies looking at the diffusion of polymers in porous materials, this concentration dependence has heretofore always been ignored. It can be seen, both from the ratio  $(D_{\infty,app}/D_{0,app})/(D_{\infty}/D_0) \approx 1.10$  for  $c_0/c^* \approx 1/8$ , and the ratio  $k_{D,G,0}/k_{D,0} \approx 2.65$ , that this neglect of concentration dependence can lead to not insignificant systematic error, even at the low (usually considered "dilute") concentrations used in these light scattering experiments, and other experiments such as trans-membrane diffusion. In this work, the attempt has been made to remove some of the systematic concentration dependence by scaling initial solution concentrations to the overlap concentration. This certainly is better than using a single constant concentration as has often been done before.

## CHAPTER VII

### DISCUSSION AND CONCLUSIONS

#### Macroscopic Diffusion

The experimental results for macroscopic diffusion of linear polystyrenes in the three controlled pore glasses are plotted in Figure 24 as the ratio  $D_\infty/D_0$  versus the relative size parameter  $\lambda_H$ , with all of these quantities derived from light scattering data as described in Chapter VI. These results are also given in Tables 8 and 9, including the temperature, estimated  $c/c^*$ , and random measurement uncertainties.

The interpretation of these results is based on a combination of phenomenological theories for diffusion of point particles in random porous media, and microscopic theories for diffusion of rigid spheres and flexible polymers in single pores of ideal geometry. The approach to be taken is summarized in the following equation:

$$\frac{D_\infty}{D_0} = X_0 f(\lambda_H) \quad (7.1)$$

which simply states that the ratio of the effective macroscopic diffusion coefficient in the porous glass ( $D_\infty$ ) to the diffusivity in unbounded solution ( $D_0$ ), is given by the product of the intrinsic conductivity of the porous glass for point particles ( $X_0$ ), and the size-dependent ratio ( $f(\lambda_H) = D_p/D_0$ ) of the diffusivity inside a pore ( $D_p$ ) to that in bulk solution. It is to be remembered

Figure 24.

Macroscopic diffusion of linear polystyrenes in porous glasses as a function of relative size of polymer to pores.

The ratio  $D_{\infty}/D_0$  is plotted vs  $\lambda_H$ , where  $D_0$  is the macroscopic diffusion coefficient in the glass,  $D_0$  is the diffusivity in bulk solution, and  $\lambda_H$  is the ratio of polymer hydrodynamic radius  $R_H$  to pore radius  $R_p$ .

Shown are data for three glasses: B7, filled circles ( $R_p = 893 \text{ \AA}$ ,  $\Phi = 0.72$ ); B5, filled diamonds ( $R_p = 1866 \text{ \AA}$ ,  $\Phi = 0.62$ ); and B13, empty diamonds ( $R_p = 703 \text{ \AA}$ ,  $\Phi = 0.46$ ).

The solid curve through the data for glasses B7 and B5 is a fit of low  $\lambda_H$  data to the Brenner-Gajdos equation (7.3); the dashed curve through the same data is a fit of high  $\lambda_H$  data to the scaling equation (7.4). These fits are discussed in the text. The solid line through the data for glass B13 is drawn through the first two points; the dashed curve is to guide the eye to the third.

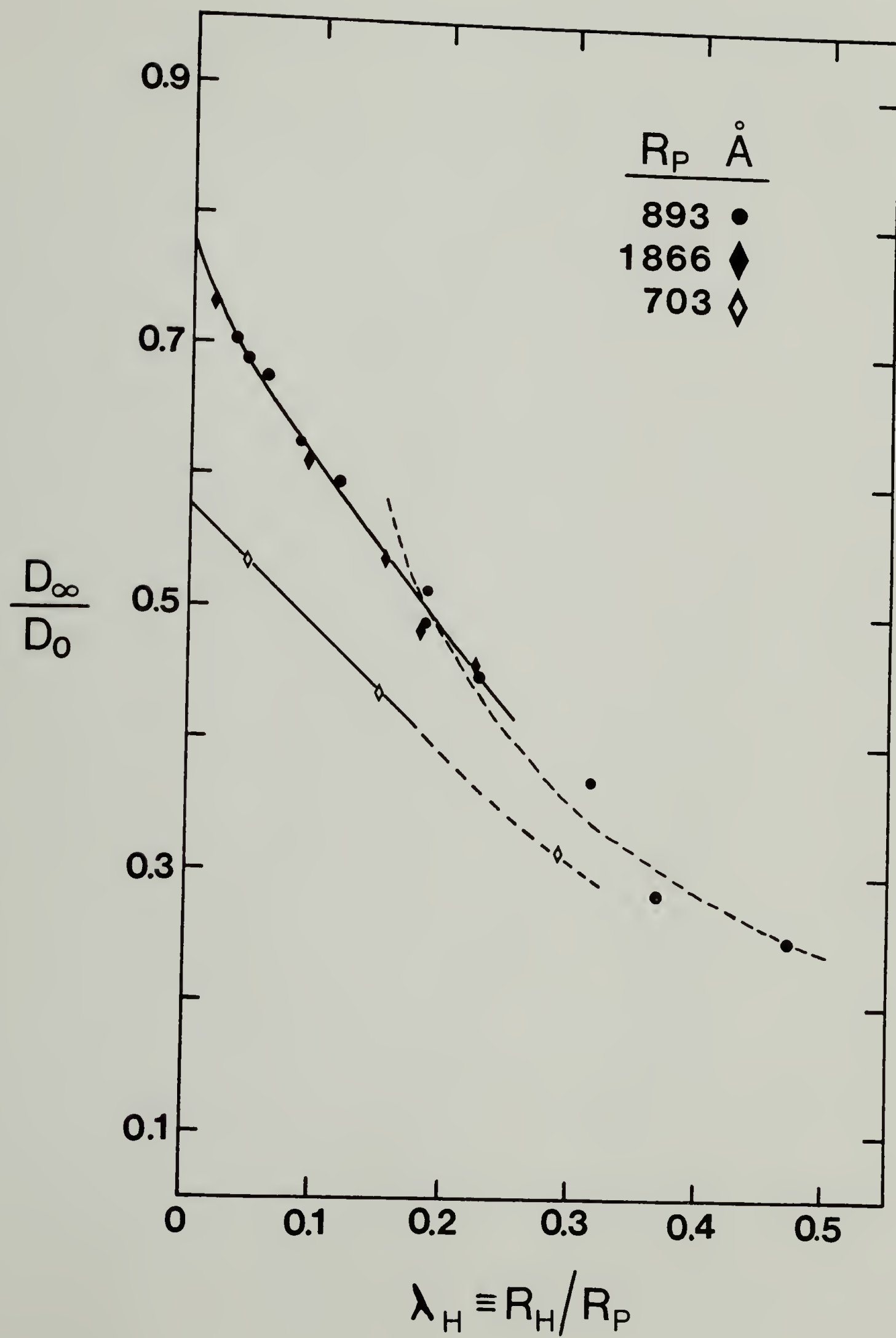


TABLE 8

Master Data Table, Part 1: Initial Concentration ( $c_0$ ), Concentration Relative to the Overlap Concentration ( $c_0/c^*$ ), Experimental Temperature (T), Hydrodynamic Radius ( $R_H$ ), and Relative Size Parameter ( $\lambda_H$ )  
 Glass B7 ( $R_p = 893 \text{ \AA}$ ), Glass B5 ( $R_p = 1866 \text{ \AA}$ ), Glass B13 ( $R_p = 703 \text{ \AA}$ )

Glass/ Polymer		$c_0$ (mg/ml)	$c_0/c^*$	T(°C)	$R_H$ (Å)	$\lambda_H$
B7	P3	8.17	0.139	44.5	$30.5 \pm 0.6$	$0.034 \pm 0.001$
	P4	7.1	0.165	42.1	$39.7 \pm 0.3$	$0.044 \pm 0.004$
	P5	3.79	0.124	42.2	$52.0 \pm 0.8$	$0.058 \pm 0.001$
	P6	2.08	0.108	42.6	$74.7 \pm 0.8$	$0.084 \pm 0.001$
	P7	1.45	0.114	42.6	$103.6 \pm 1.6$	$0.116 \pm 0.002$
	P8	0.97	0.135	45.5	$165.1 \pm 1.9$	$0.185 \pm 0.002$
	P2	0.85	0.119	45.6	$164.5 \pm 2.2$	$0.184 \pm 0.003$
	P9	0.63	0.114	42.6	$202.4 \pm 2.5$	$0.227 \pm 0.003$
	P15	0.359	0.099	45.2	$281.8 \pm 4.5$	$0.316 \pm 0.005$
	P16	0.316	0.106	45.2	$329.1 \pm 3.8$	$0.368 \pm 0.004$
	P17	0.258	0.118	45.3	$421.6 \pm 3.1$	$0.472 \pm 0.003$
B5	P3	7.29	0.124	34.6	$31.3 \pm 0.7$	$0.017 \pm 0.001$
	P2	0.78	0.109	38.0	$168.2 \pm 1.2$	$0.090 \pm 0.001$
	P15	0.359	0.099	32.8	$282.8 \pm 2.5$	$0.152 \pm 0.001$
	P16	0.316	0.106	32.5	$336.0 \pm 6.2$	$0.180 \pm 0.003$
	P17	0.258	0.118	32.8	$418.1 \pm 3.9$	$0.224 \pm 0.002$
B13	P3	7.29	0.124	38.9	$31.4 \pm 0.7$	$0.045 \pm 0.001$
	P7	1.43	0.113	34.8	$104.6 \pm 0.7$	$0.149 \pm 0.001$
	P9	0.554	0.101	35.0	$205.0 \pm 1.9$	$0.292 \pm 0.003$

TABLE 9

Master Data Table, Part 2: Diffusion Coefficient in Bulk Solution ( $D_0$ ),  
Macroscopic Diffusion Coefficient ( $D_\infty$ ), and Reduced Diffusion  
Coefficient ( $D_\infty/D_0$ ) for Glasses B7, B5, and B13

Glass/ Polymer		$10^7 \cdot D_0$ (cm <sup>2</sup> /s)		$10^7 \cdot D_\infty$ (cm <sup>2</sup> /s)		$D_\infty/D_0$	
B7	P3	14.9	± 0.3	10.4	± 0.3	0.703	± 0.024
	P4	11.1	± 0.1	7.61	± 0.07	0.688	± 0.008
	P5	8.46	± 0.14	5.71	± 0.21	0.675	± 0.027
	P6	5.92	± 0.06	3.69	± 0.07	0.624	± 0.014
	P7	4.27	± 0.07	2.54	± 0.15	0.594	± 0.027
	P8	2.78	± 0.03	1.43	± 0.03	0.513	± 0.011
	P2	2.80	± 0.04	1.37	± 0.06	0.489	± 0.022
	P9	2.18	± 0.03	0.983	± 0.019	0.450	± 0.010
	P15	1.62	± 0.03	0.599	± 0.005	0.369	± 0.007
	P16	1.39	± 0.02	0.397	± 0.022	0.285	± 0.016
	P17	1.09	± 0.01	0.270	± 0.019	0.248	± 0.018
B5	P3	12.6	± 0.3	9.21	± 0.03	0.729	± 0.017
	P2	2.47	± 0.02	1.51	± 0.03	0.610	± 0.013
	P15	1.37	± 0.01	0.734	± 0.017	0.537	± 0.013
	P16	1.14	± 0.02	0.553	± 0.016	0.484	± 0.016
	P17	0.923	± 0.009	0.423	± 0.022	0.458	± 0.024
B13	P3	13.4	± 0.3	7.15	± 0.10	0.534	± 0.014
	P7	3.80	± 0.03	1.65	± 0.05	0.435	± 0.014
	P9	1.94	± 0.02	0.615	± 0.044	0.316	± 0.023

that the justification leading to equation (7.1), where these two factors are separable, demanded that the pore space be "well-connected". The basis of equation (7.1) was given in sections 2 and 3 of Chapter II, which can be consulted for details and references.

Analysis of the experimental results in terms of equation (7.1) leads naturally in two directions: on the one hand, towards consideration of the dependence of the reduced diffusivity  $f(\lambda_H)$  on the relative size parameter  $\lambda_H$ , which, given the assumption that there are no specific polymer-wall interactions, is attributable solely to size-dependent changes in polymer-wall and also intramolecular hydrodynamic interactions; and on the other hand, towards consideration of the relation between the intrinsic conductivity  $X_0$  and the structure of the porous material.

Looking at Figure 24, it is seen that the data for glasses B7 ( $R_p = 893 \text{ \AA}$ ,  $\Phi = 0.72$ ) and B5 ( $R_p = 1866 \text{ \AA}$ ,  $\Phi = 0.62$ ) fall on the same curve, whereas the data for glass B13 ( $R_p = 703 \text{ \AA}$ ,  $\Phi = 0.46$ ) differ, showing lower  $D_\infty/D_0$  values at a given  $\lambda_H$ . For all three glasses, the values for  $D_\infty/D_0$  monotonically decrease over the investigated range of  $\lambda_H$  (up to  $\lambda_H \approx 0.47$ ). Plotted versus  $\lambda_H$ , this decrease in  $D_\infty/D_0$  is roughly linear at low  $\lambda_H$ , and becomes more gradual at higher  $\lambda_H$ .

These results provide strong evidence (which, as shown in Chapters II and III, is not really needed) that the effective diffusion coefficient  $D_\infty$  from dynamic light scattering does not include a factor of the porosity  $\Phi$ . This follows from the observations: (1) that the data for glasses B7 and B5, which have different porosities, superimpose; and (2) that if one supposed

that factors of porosity *were* included in  $D_\infty$ , it would imply intrinsic conductivities  $X_0 > 1$  (or tortuosity  $T_0 < 1$ ), a result which is unphysical.

From equation (7.1), it follows that fitting of  $D_\infty/D_0$  versus  $\lambda_H$  can be used to test theories of  $f$  and to obtain the intrinsic conductivity  $X_0$ . The value of  $X_0$  (i.e., the intercept on extrapolation to  $\lambda_H = 0$ ) is independent of any systematic error in  $\lambda_H$  as could be caused by error in the value of  $R_p$  used to calculate  $\lambda_H$ ; that is, although the slope will differ for different  $R_p$ , the intercept will be the same. The extrapolation to  $\lambda_H = 0$  does, however, depend on the model chosen for  $f(\lambda_H)$ , since different theories for  $f$  show a different functional dependence on  $\lambda_H$  (e.g., compare<sup>5,8,11</sup>). Ideally, any fitting or extrapolation should be confined to using data which lies in a range of  $\lambda_H$  where the chosen model is known to be appropriate. Any systematic error in the data will of course be reflected in fitting parameters. (The major causes of systematic error for these experiments were discussed in Chapter VI.)

The data were fit according to equation (7.1), using various theories for  $f$ . These fits are now discussed in some detail. The data for glasses B7 and B5 were combined, as they fall on the same curve, within measurement uncertainty (see Figure 24); obviously, the data for glass B13 (only 3 points) could not really be fit.

Three expressions for  $f(\lambda_H)$ , which are given below, were used; these were presented and discussed in Chapter II. The first two expressions are for the diffusion of hard spheres in cylindrical pores and are based on the results of low Reynolds number hydrodynamics. One of these two is based on the rather dubious centerline approximation (CL theory, subscript

CL), and gives the diffusivity reduction as a power series in  $\lambda_S$ , where  $\lambda_S$  is the ratio of the sphere radius to pore radius.<sup>4,5,81</sup>

$$f_{CL}(\lambda_S) = 1 - 2.10444 \lambda_S + 2.08877 \lambda_S^3 - 0.94813 \lambda_S^5 \\ - 1.372 \lambda_S^6 + 3.87 \lambda_S^8 - 4.19 \lambda_S^{10} + \dots \quad (7.2)$$

The other of these two is a more exact theory, developed by Brenner and Gajdos<sup>8,9</sup> (BG theory, subscript BG), which takes into account the radial dependence of the friction factor.

$$f_{BG}(\lambda_S) = \frac{1 + (9/8)\lambda_S \ln \lambda_S - 1.539 \lambda_S + O(\lambda_S)}{(1 - \lambda_S)^2} \quad (7.3)$$

The third expression is for the diffusion of strongly confined chains in a good solvent in regular pores of any geometry, and is based on scaling arguments<sup>10-12</sup> (subscript S).

$$f_S(\lambda_H) = \xi \lambda_H^{-2/3} \quad (7.4)$$

where  $\xi$  is an unknown numeric factor.

In this presentation, the comparison of the experimental data for  $D_\infty/D_0$  at low  $\lambda_H$  to the hard sphere diffusion theories is considered first. This is to be followed by a comparison of  $D_\infty/D_0$  at high  $\lambda_H$  to the scaling theory for flexible polymer diffusion.

The use of either equation (7.2) or (7.3) rests on the assumption that the diffusion of flexible polymers that are small compared to the pore size (i.e., small  $\lambda_H$ ) can be modeled as the diffusion of hard spheres, at least to a first approximation. This same analogy is of course the basis for the

definition of the hydrodynamic radius  $R_H$  in unbounded solution as the radius of a hard sphere that is hydrodynamically equivalent to the flexible polymer.

Fits to equations (7.2) and (7.3) were performed with two adjustable parameters: the intrinsic conductivity  $X_0$ ; and a scaling factor  $\kappa$  for the relative size parameter  $\lambda_H$ , in order to make the substitution for  $\lambda_S$  in the theoretical expressions  $f_{CL}(\lambda_S)$  and  $f_{BG}(\lambda_S)$ :

$$\lambda_S = \kappa \lambda_H \quad (7.5)$$

Results of these fits, to all glass B7 and B5 data with  $\lambda_H \leq 0.23$ , are:

$$X_0 = 0.781 \pm 0.006, \quad \kappa = 0.76 \pm 0.02 \quad (\text{Brenner-Gajdos})$$

$$X_0 = 0.748 \pm 0.006, \quad \kappa = 0.88 \pm 0.02 \quad (\text{centerline})$$

with the corresponding estimates for B13 (from the two data points with the lowest  $\lambda_H$ )

$$X_0 = 0.58, \quad \kappa = 0.78 \quad (\text{glass B13})$$

The centerline fit included terms (only) to order  $\lambda_S^6$ , since higher order terms are negligible for  $\lambda_H \leq 0.23$ . (Over this range of  $\lambda_H$ , a linear fit gives nearly identical results:  $X_0 = 0.744 \pm 0.006$ ; and  $\kappa = 0.85 \pm 0.05$ .)

Both the centerline and Brenner-Gajdos fits to the data for glasses B7 and B5 are quite good (significance level 0.0001, and correlation coefficient  $r^2 = 0.9998$ ); however, given the trend and relatively low scatter of the data, plus the functional forms of  $f_{BG}$  and  $f_{CL}$ , this quality of fit is not

surprising. The data are fit by these two theories equally well, to within the measurement uncertainty (see Figure 25), and thus are in a sense consistent with both theories. However, the Brenner-Gajdos theory must be considered as having a more realistic and rigorous theoretical basis.

The parameters  $X_0$  and  $\kappa$  from the two fits differ in the expected way. The BG theory predicts a more rapid decrease in  $f(\lambda_S)$  with increase in  $\lambda_S$  than does the CL theory; hence, in order to fit a given observed decrease in diffusivity, the scaling factor  $\kappa$  between  $\lambda_H$  and  $\lambda_S$  should be smaller for the BG fit, and the intrinsic conductivity  $X_0$  should be higher.

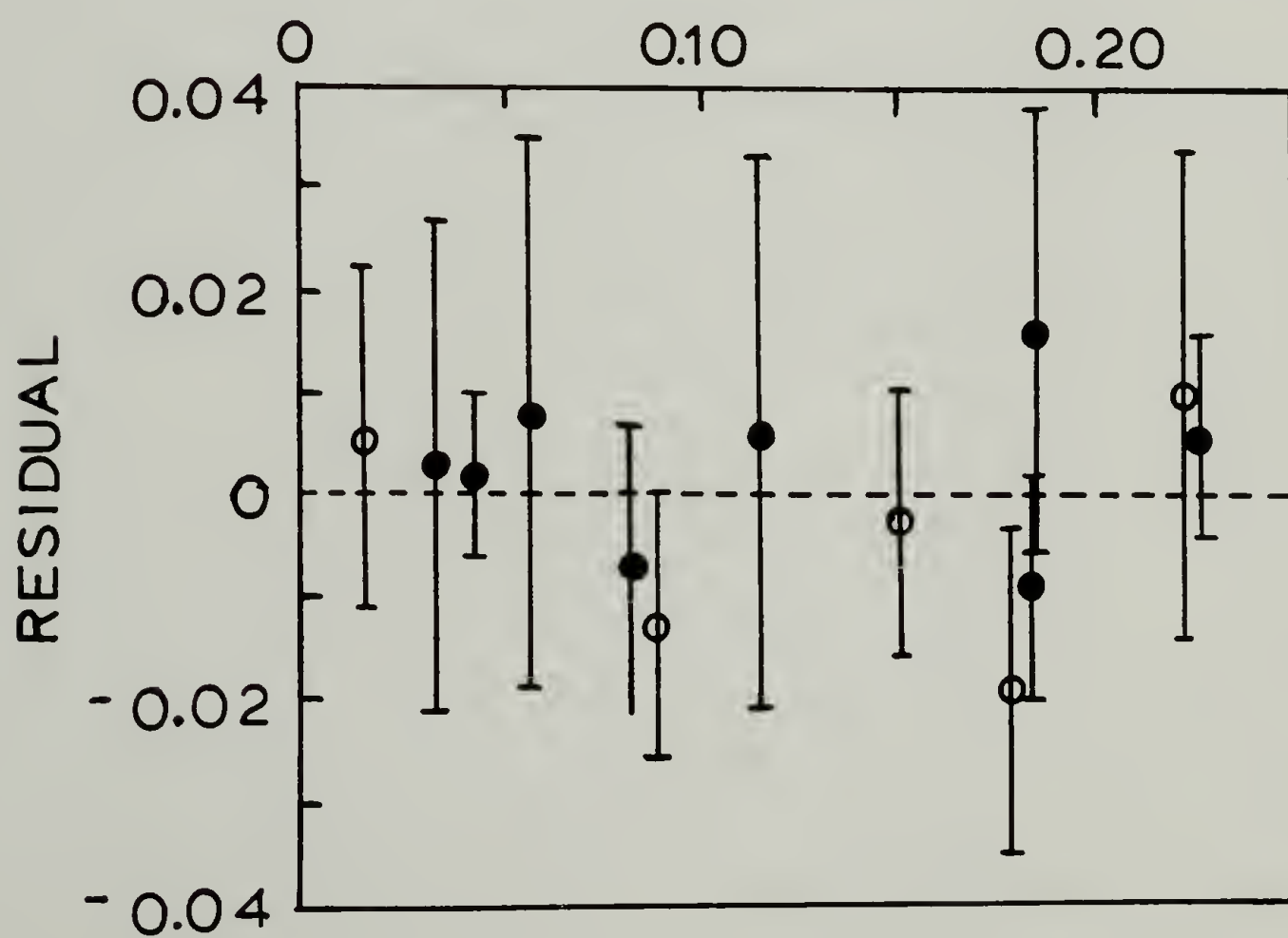
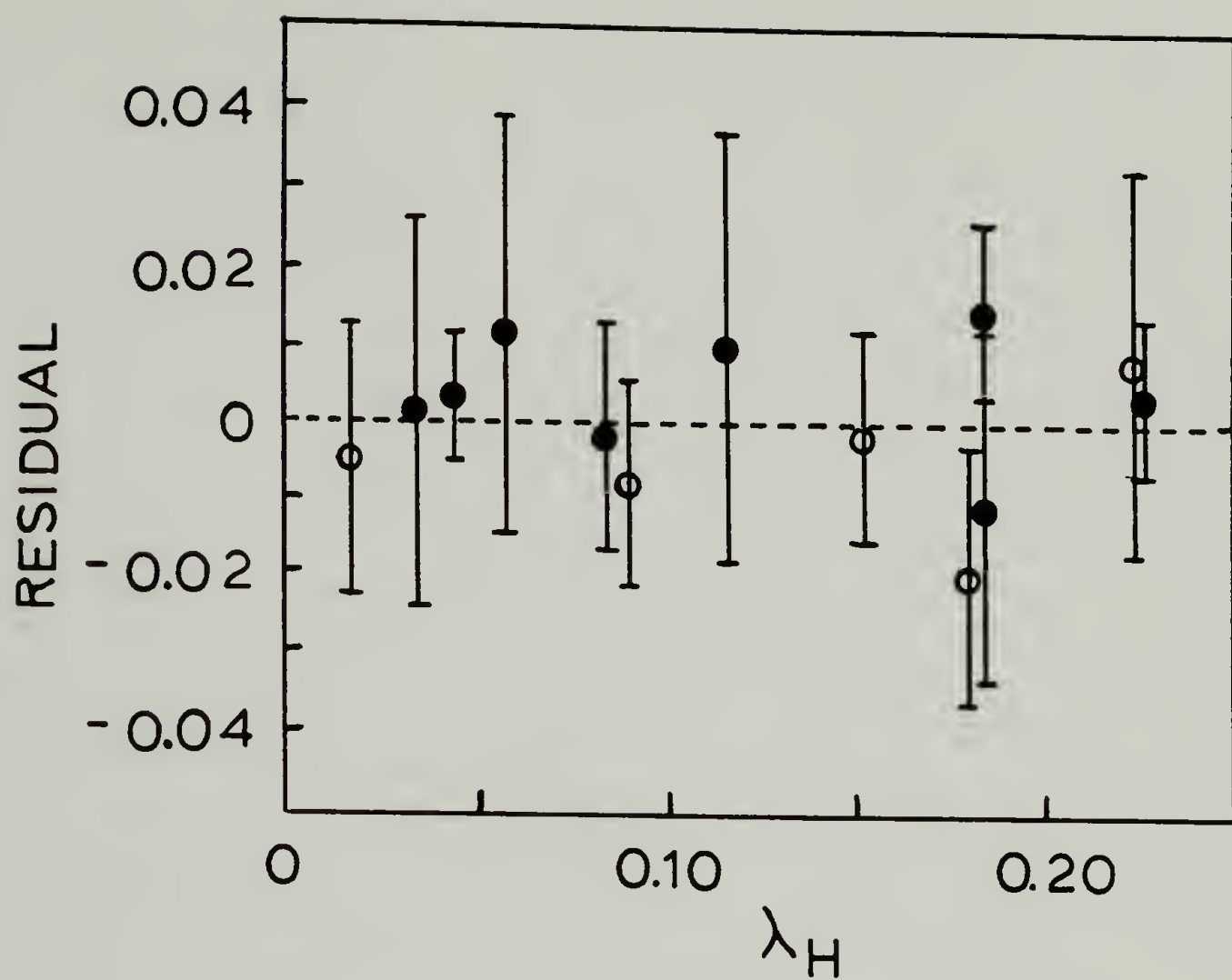
The centerline approximation, such as it is, is valid to quite high  $\lambda_S$ ; however, the Brenner-Gajdos theory is claimed applicable only for  $\lambda_S \ll 1$ , or as alternatively stated,  $\lambda_S \leq 0.1$ . (The expression is explicitly written as valid to order  $\lambda_S$ .) The upper limit of  $\lambda_H$  used in the fits ( $\lambda_H \approx 0.23$ ) translates to  $\lambda_S = \kappa \lambda_H \approx 0.17$ , which exceeds this stated range of validity. Hence using data to such high  $\lambda_H$  is perhaps not justified. Nonetheless, fits using less of the data (6 points,  $\lambda_H < 0.12$ ) give values for  $X_0$  and  $\kappa$  identical to those above, within the small limits of uncertainty of the parameters. This leads to the conclusion that use of somewhat higher  $\lambda_H$  data does not bias the fits, while helping to improve the statistical quality.

For both fits, the numerical coefficients--for cylindrical pores--were used as prescribed in the theories. Although the exact coefficients for the unknown geometry of the porous glasses would be expected to differ, this difference should not be great. The coefficient of the logarithmic term ( $=9/8$ ) in the Brenner-Gajdos theory follows directly from the result for motion of a sphere near a plane wall,<sup>85</sup> and hence, for small  $\lambda_S$ , should be

Figure 25.

Residuals of fits of low Reynolds number hydrodynamics theories to data at small relative size parameter.

These results are for fits of theories for hindered diffusion of hard spheres in cylindrical pores to data ( $\lambda_H \leq 0.23$ ) for linear polystyrenes in glasses B7 (filled circles) and B5 (empty circles). Upper plot is for the fit to the expression of Brenner and Gajdos, equation (7.3); the lower plot is for the fit to the centerline approximation expression of Bohlin, equation (7.2). The error bars indicate the measurement uncertainty (i.e., in  $D_\infty/D_0$ ) for each point.



independent of the pore space geometry. However, the coefficients of the terms linear in  $\lambda_S$  (i.e., 1.539 in the Brenner-Gajdos theory, 2.10444 in the centerline theory) and other higher order terms will depend on the geometry of the pore space. It is argued that the curved nature of the walls of the pore space implies that the actual coefficients (at least of the linear term, the most important for consideration at low  $\lambda_S$ ) would not be greatly different. For example, the result analogous to the centerline theory, for radial motion of a sphere in the center of a spherical external boundary,<sup>4</sup> gives a coefficient of 2.25. Similarly, a more exact treatment for these porous glasses (à la Brenner-Gajdos), taking into account the positional dependence of the friction factor, would not be expected to give a greatly different coefficient for the linear term. (Incidentally, a three parameter Brenner-Gajdos fit gives  $X_0 = 0.78$ ,  $\kappa = 0.72$ , and a coefficient 1.63, results which are in good agreement with the two parameter fit with the usual coefficient of 1.54.)

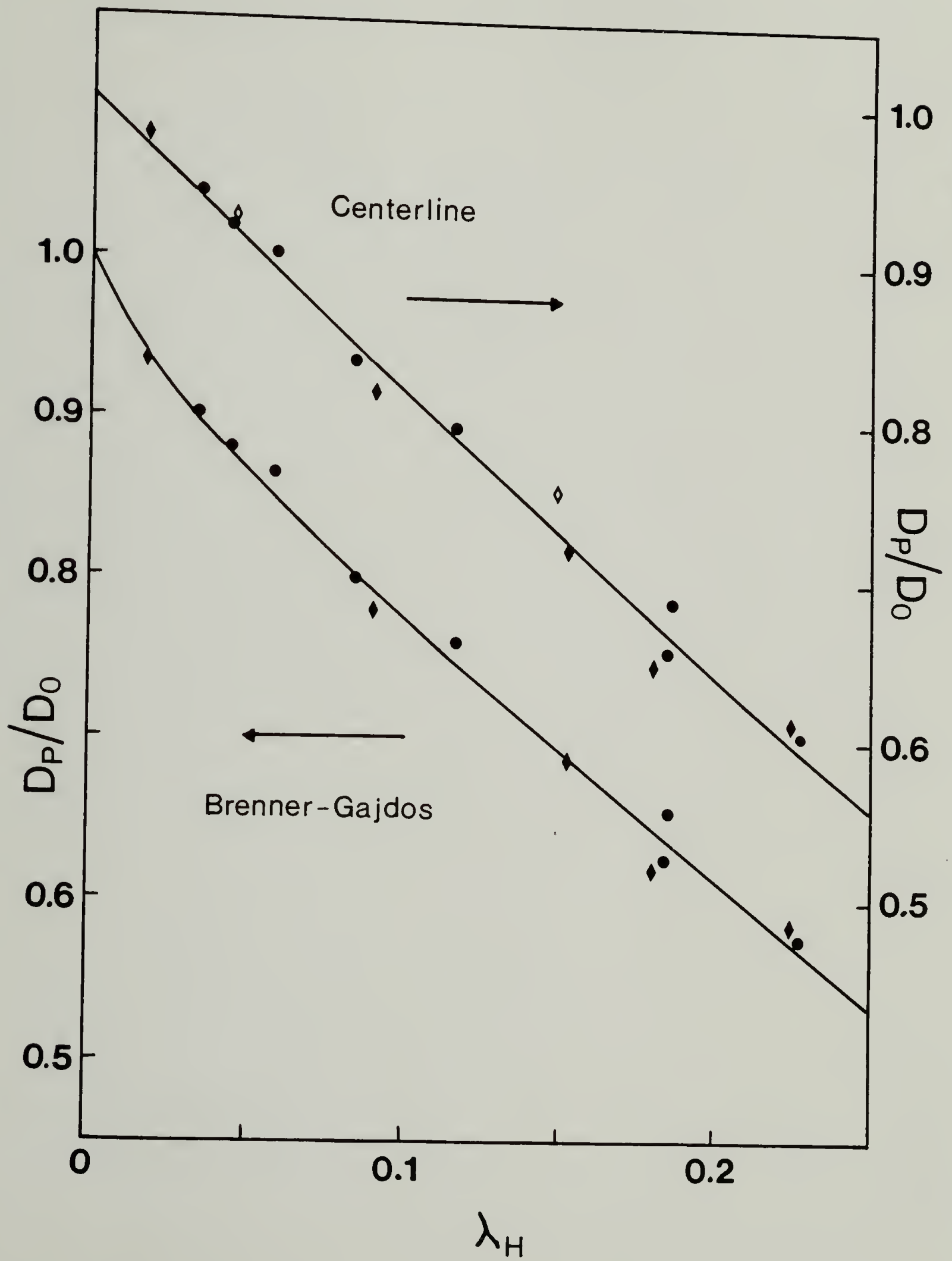
Also, the partitioning coefficient  $(1 - \lambda_S)^2 = (1 - \kappa \lambda_H)^2$  which enters the Brenner-Gajdos theory is not strictly correct for flexible polymers; nonetheless, for small  $\lambda_H$ , where the partitioning is largely a surface effect,<sup>50</sup> this expression is a good first-order approximation (e.g., see equation (2.11) for the expression for  $K_D$  in the limit  $\lambda_H \rightarrow 0$ ).

Using the values of  $X_0$  and  $\kappa$  from these fits, values of  $f(\lambda_H) = (D_\infty/D_0 X_0) = (D_p/D_0)$  can be calculated and compared to the functions  $f_{CL}(\kappa \lambda_H)$  and  $f_{BG}(\kappa \lambda_H)$  (Figure 26). Data from all three glasses fall on the same curve. This indicates that: (1) the pore sizes  $R_p$  are correct on a relative basis; and (2) the separation of intrinsic conductivity and hydrodynamic interactions as

Figure 26.

Comparison of low  $\lambda_H$  data to theories for diffusion of hard spheres in cylindrical pores.

Shown are two different fits to the data ( $\lambda_H \leq 0.23$ ) for glasses B7 (circles) and B5 (filled diamonds). Data for B13 (empty diamonds) are shown but were not used in the fits. The ordinate  $D_p/D_0$  corresponds to the function  $f$  in the text. For the experimental data,  $D_p/D_0 = D_\infty/D_0 X_0$ , where two different values of  $X_0$  (from the two different fits) have been used to normalize the data. The solid lines correspond to  $f_{CL}(\lambda_S) = f_{CL}(\kappa \lambda_H)$  and  $f_{BG}(\lambda_S) = f_{BG}(\kappa \lambda_H)$  for the centerline and Brenner-Gajdos fits respectively, where  $\kappa$  is the proportionality constant in  $\lambda_S = \kappa \lambda_H$  obtained from the fits.



represented by equation (7.1) is justified for these porous glasses. (N.B. The B13 data are shown only with the centerline- $X_0$  normalized data, since  $X_0$  for B13 was gotten by a two-point linear, hence "centerline", extrapolation.)

Examination of the extent of quantitative agreement or disagreement of the experimental  $f(\lambda_H)$  with either theory is hampered by several difficulties. First, there is uncertainty in both the absolute magnitude of the nominal pore radius  $R_p$  and in the relationship of this  $R_p$  to the actual pore space geometry (see Chapter IV, section 2). Second, there is a poorly known distribution of pore sizes (Chapter IV), which leads to the pore diffusivity  $D_p$  being some weighted average. Third, as above, the appropriate numerical coefficients for these porous glasses to use in the theories for hindered diffusion are not known. Lastly, the question of the "correct" flexible polymer radius to use in these theories is open.

Despite this negative prognosis for being able to make a quantitative comparison of these experiments with theory, the following arguments attempting just that are advanced. Certainly, the superposition of data for the different glasses shows that the  $R_p$  values are accurate in a relative sense. If the values of advancing contact angle and surface tension which were used in extracting  $R_p$  values from mercury intrusion data are reasonable, and if the pore cross sections are roughly circular, then the values obtained for  $\kappa$ , which are less than one, could be interpreted as being due to an underestimation of the average  $R_p$  for these porous glasses. This is consistent with the general recognition that the mercury intrusion method gives values for  $R_p$  which are too low. Continuing this argument, if one were to assume that  $R_H$  is indeed the correct radius for understanding the hydro-

dynamic behavior of small flexible polymers in pores, then  $\kappa$  is simply a measure of how much the pore radius is underestimated. For example, for the fits above, this would imply that the nominal pore radii used in calculating  $\lambda_H$  were about 10-25% too low, which is consistent with another independent estimate of the degree of this undervaluation of  $R_p$  (i.e., the hydraulic radii calculated in Chapter IV gave an estimate of  $R_p$  values being  $\approx 15-45\%$  too low). *If*, and this is perhaps a big if, the various assumptions in this argument are correct, then the quantitative agreement between the data for  $f(\lambda_H)$  and the theory for  $f_{BG}(\lambda_S)$  is very good, with the identification of  $\lambda_S \equiv \lambda_H$ .

In another sense, independent of any arguments of this sort, the quantitative agreement between low Reynolds number hydrodynamics theories for the diffusion of hard spheres, and experimental data for the diffusion of relatively small flexible polymers in random porous materials is excellent; it is just impossible to assign any definite and unambiguous meaning to the parameter  $\kappa$  (i.e., it could be related to a combination of pore size distribution, improper choice of contact angle, non-cylindrical geometry of the pore space, or failure of  $R_H$  as the correct equivalent hard sphere radius in the pores). These arguments show that further speculation on the degree of absolute quantitative agreement is rather pointless, since there are simply too many unknown numeric factors, with perhaps the most important being the inherent uncertainty in  $R_p$ . It is thus impossible, for example, to address directly the question of the appropriate (if any) flexible polymer dimension to use in hard sphere theories for hindered diffusivity in pores.

In these porous glasses, such an answer could perhaps come from a comparative study of linear versus star polymers versus rigid spheres.

The discussion thus far has centered on modeling the diffusion of these flexible polymers as the diffusion of hard spheres; however, it is important to ask whether this is reasonable, and if so, over what range of the relative size parameter  $\lambda_H$ . Before attempting to answer this question, it is useful to consider the comparison of our data to the scaling theory prediction for the diffusion of strongly confined flexible chains in pores.<sup>10-12</sup>

At the outset, it is noted that all the data lie outside the expected range of validity of the scaling theory. The strongly confined condition<sup>11</sup> is given as  $\lambda_F > 2$ , which translates to  $\lambda_H > 0.56$ . The scaling prediction given in equation (7.4) was derived for polymer dissolved in an ideally good solvent, that is,  $\nu = 3/5$  in the proportionality of  $R_H$  to  $M$ ,  $R_H \propto M^\nu$ . With the quite reasonable assumption that the basic scaling arguments are still valid for a less than ideally good solvent ( $1/2 < \nu < 3/5$ ), equation (7.4) can be rewritten as:

$$f_S(\lambda_H) = \xi \lambda_H^\gamma, \quad \gamma = (\nu - 1)/\nu \quad (7.6)$$

The limited data at high  $\lambda_H$  were analyzed for consistency with this scaling theory, despite doubts as to its applicability. Linear regressions were performed on  $\log(D_\infty/D_0 X_0)$  versus  $\log \lambda_H$ . The  $X_0$  value from the fit of the Brenner-Gajdos theory to the low  $\lambda_H$  data was used; obviously, however, any error in this  $X_0$  would be absorbed in the numerical factor (i.e., the intercept  $\log \xi$ ) without affecting the determination of the scaling exponent (i.e., the slope  $\gamma$ ). Two fits were performed, giving the results:

$$\gamma = -0.74 \pm 0.06, \quad \xi = 0.19 \pm 0.01 \quad (\lambda_H > 0.18, 8 \text{ points})$$

$$\gamma = -0.84 \pm 0.08, \quad \xi = 0.17 \pm 0.01 \quad (\lambda_H > 0.22, 5 \text{ points})$$

The quality of the fits (significance levels of 0.001 and 0.002, and correlation coefficients  $r^2$  of 0.96 and 0.97) is only fair considering the trend and scatter of the data.

Based on the exponent  $\nu = 0.57$ , which was obtained from the scaling of  $D_0$  versus  $M$  (Chapter IV), the expected exponent in equation (7.6) is  $\gamma = -0.75$ . Although the results are in reasonable agreement with this prediction, the significance of this agreement is open to question for the following reasons. First, the range  $0.18 \leq \lambda_H \leq 0.47$  is below the stated range of applicability of the theory. Second, this is not much of a range for concluding that power law behavior exists. Third, the agreement of the data, even at higher  $\lambda_H$ , to the scaling line is no better (actually maybe worse) than it is to the centerline fit of the *low*  $\lambda_H$  data (see Figure 27); however, there is of course no fundamental reason to believe the hard sphere centerline theory to be any more appropriate. Lastly, there is indication that at higher  $\lambda_H$  (i.e., the second vs first fits above) the dependence of  $D_\infty/D_0$  on  $\lambda_H$  is stronger than that predicted by the scaling theory (i.e.,  $|\gamma| > 0.75$ ; more on this below).

Given the limited data at higher  $\lambda_H$ , it is impossible to choose between two alternate interpretations of the stronger  $\lambda_H$  dependence of  $D_\infty/D_0$  at higher  $\lambda_H$  (e.g., in Figure 27). Is it due to increasingly strong hydrodynamic interactions of an essentially non-free draining polymer coil with the walls? Even if neither the centerline theory nor the Brenner-Gajdos

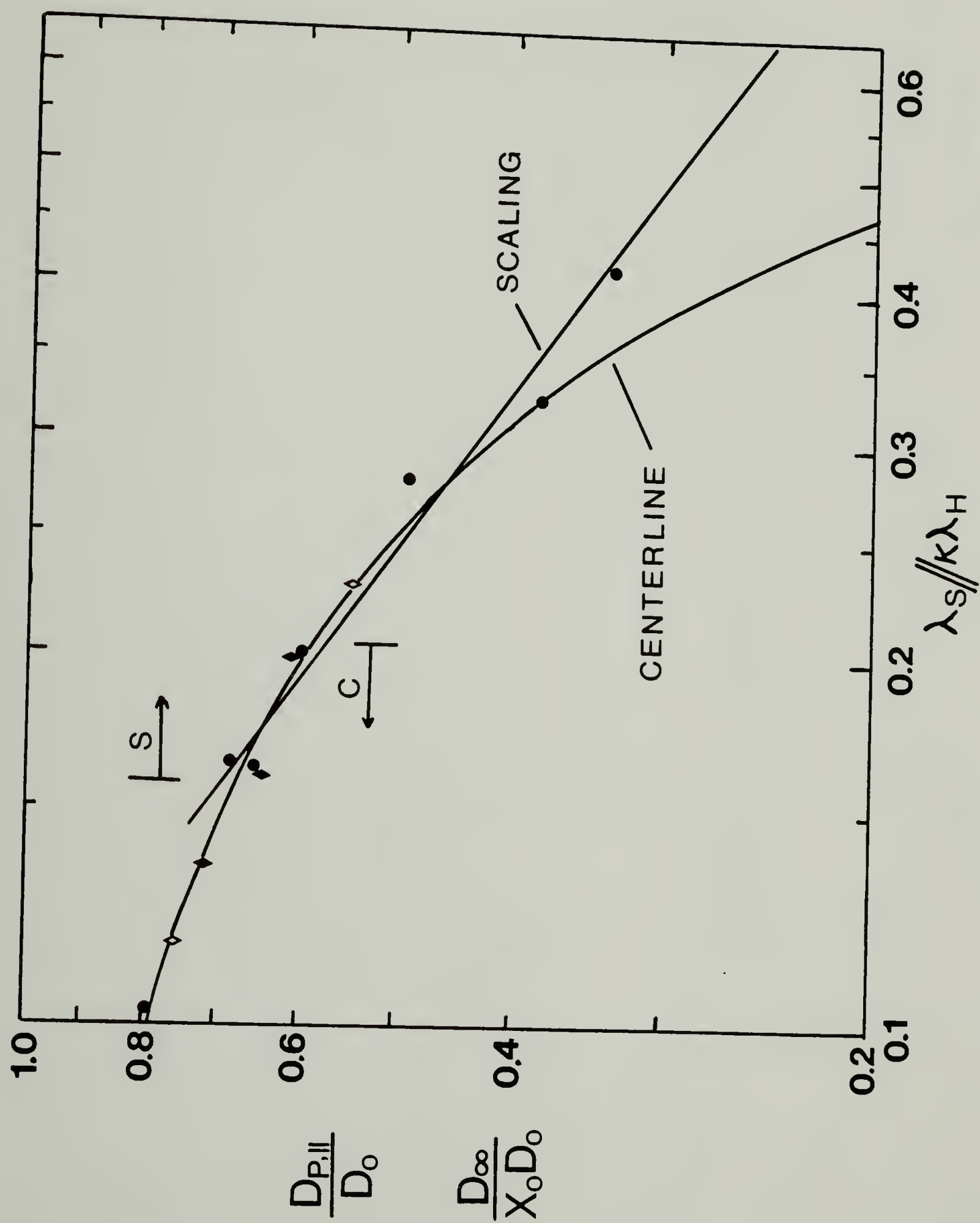
Figure 27.

Scaling theory fit to high  $\lambda_H$  data.

This double logarithmic plot shows the higher  $\lambda_H$  data in comparison to two fitted lines. The straight line is a fit to the scaling equation (7.4) for data lying to the right of the arrow labeled "S". The curved line is a fit to the centerline theory, equation (7.2), for data lying to the left of the arrow labeled "C".

The abscissa is  $\kappa \lambda_H$  for all data and curves (this also corresponds to  $\lambda_S$  for the centerline theory). The ordinate is  $f(\lambda)$  for all data and curves; this corresponds to  $D_{p,\parallel}/D_0$  for the theories, and to  $D_\infty/D_0 X_0$  for the experimental data.

Data symbols for the glasses are: B7 (circles), B5 (filled diamonds), and B13 (empty diamonds).



theory accurately describes these interactions, this is not to imply that this basic explanation is invalid. Or alternatively, is it due to increased friction because of screening of intramolecular hydrodynamic interactions? The arguments that follow indicate that this may be important even at the relatively low  $\lambda_H$  values of these experiments.

In unbounded solution, although the average conformation is spherical, the instantaneous conformation is significantly non-spherical.<sup>164,165</sup> Even for Gaussian chains, the orthogonal principal axes of  $R_G$ , relative to the average  $R_G$ , lie in the ratio 1.5/0.7/0.4. For a polymer confined to a pore space, the average conformation will become increasingly non-spherical as  $\lambda_H$  increases, even for relatively small  $\lambda_H$ . As this elongation along the perhaps ill-defined longitudinal direction of the pore becomes comparable to the transverse pore dimension (i.e.,  $2 R_p$ ), the intramolecular hydrodynamic interactions will be strongly screened for distances greater than  $2 R_p$ . These arguments indicate that the range of the scaling theory can be extended downward, as given by the condition that the average *maximum* instantaneous extension, presumed to lie in the longitudinal pore direction (i.e., not isotropically distributed as in unbounded solution), be comparable to the pore dimension. Using the simple result for Gaussian chains in unbounded solution, this lower limit becomes  $\lambda_H \approx 0.37$ ; while for non-Gaussian chains confined to pores, a still smaller lower limit would be expected.

To summarize (see Figure 28), these arguments indicate that a transition from non-free draining behavior ( $D_p \propto M^{-3/5}$ ), where the polymer can be considered as a hard sphere, to free draining behavior ( $D_p \propto M^{-1}$ ),

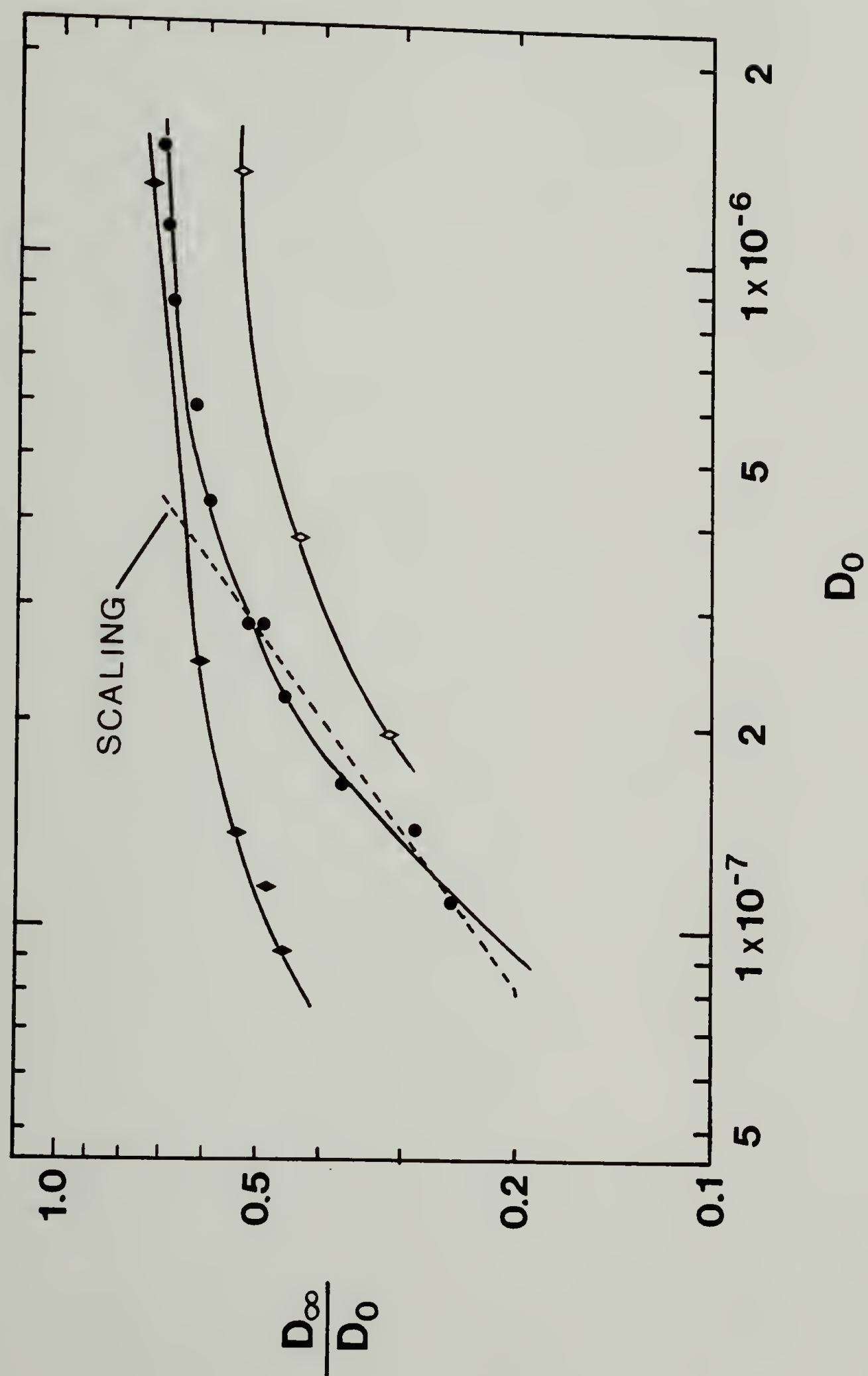
Figure 28.

Transition from non-free draining to free draining behavior.

This is a double logarithmic plot of  $D_{\infty}/D_0$  vs  $D_0$  for all three glasses: B7 (circles), B5 (filled diamonds), and B13 (empty diamonds). One interpretation of the slope of this plot is in terms of the scaling exponents of  $D_{\infty}$  and  $D_0$  on molecular weight,  $D_{\infty} \propto M^a$  and  $D_0 \propto M^b$  ( $b = -0.57$  for polystyrene in 2-fluorotoluene), giving slope =  $(a-b)/(b)$ .

The plateau at higher  $D_0$  (lower  $M$ ) can be interpreted as the behavior of non-free draining ( $a \approx b$ ) polymer coils, with the small decrease with increasing  $M$  due to hydrodynamic interactions of these "hard spheres" with the walls.

The more rapid decrease at lower  $D_0$  (higher  $M$ ) can be interpreted as the behavior of free draining ( $a = -1$ ) polymer coils, as predicted for strongly confined chains by scaling arguments. A fit to the data at lower  $D_0$  gives a slope of 0.73, very close to the value of 0.75 for  $a = -1$  and  $b = -0.57$ . (This fit is shown in Figure 27 and discussed in the text.) It is noted, however, that even hard sphere theories predict a similar decrease in  $D_{\infty}/D_0$  at low  $D_0$ ; and that the reptation theory (regular porous material) and computer simulations (random porous material) both predict a stronger molecular weight dependence of the diffusion coefficient (in a three-dimensional interconnected pore space) than is predicted for diffusion in a single pore.



where the flexible nature of the polymer must be considered, may in fact occur at fairly small values of relative size parameter. That this is reasonable is a consequence of the observation that even relatively small polymers are "strongly confined": for a flexible polymer with  $\lambda_H = 0.2$ , the equilibrium partitioning coefficient  $K_D \leq 0.44$  (this upper bound is for Gaussian coils); in other words, over half the usual (i.e., for unconfined polymer) configurational volume is excluded. (Figure 1, showing plots of  $K_D$  versus  $\lambda_H$ , can be consulted for further comparisons of this sort.) As opposed to hard spheres, where this excluded volume is simply related to center of mass position, for flexible polymers this excluded volume is also related to conformation, and hence in a sense the polymer orientation relative to the longitudinal pore direction.

A proper test of whether this transition from non-free draining to free draining behavior has occurred at such low  $\lambda_H$  obviously requires extension of these measurements to higher  $\lambda_H$  values (however, see below). For glasses B7 and B5 (the only ones available for most of this work), this would be difficult with the current light scattering apparatus, because of the requirement that  $qR_{G,\parallel} < 1$  in order to observe translational diffusion (e.g., see section 3 of Chapter VI). Using glass B13, the range could be extended to  $\lambda_H \approx 0.6$  with the same polymers. Much more desirable (again, because of the requirement  $qR_{G,\parallel} < 1$ ) would be to use a glass with smaller  $R_p$ .

However, it is unclear over what range of  $\lambda_H$  agreement with the scaling theories would be expected. The scaling theory considered thus far<sup>10-12</sup> is for a chain in an infinitely long pore (a one-dimensional cylinder; or a two-dimensional slit), whereas the pore space of the glasses is highly

interconnected in three-dimensions. Diffusion of very high molecular weight polymer ( $\lambda_H \rightarrow \text{large}$ ) in three-dimensional interconnected pore spaces will show a stronger molecular weight dependence. Reptation of a chain through a series of fixed obstacles<sup>12,166,167</sup> gives  $D_\infty \propto M^{-2}$ . Recent computer simulations<sup>168</sup> have indicated that diffusion in a random porous material shows even stronger molecular weight dependence than given by reptation.

The porous material in these computer simulations was created by random placement of solid blocks in a lattice, with probability  $(1 - \Phi)$ , where  $\Phi$  is the porosity. As  $\Phi \rightarrow 1$ , the exponent  $\nu$  in  $D \propto M^{-\nu}$  approaches the result for Rouse chains,  $\nu = 1$ . As  $\Phi$  approaches the percolation threshold from above,  $\nu$  becomes greater than 2 (which is the exponent for reptation). The natural scaling variable was shown to be  $M(1 - \Phi)^{1/2}$ .

Now our results with low molecular weight polymer indicate these glasses to be "well-connected". This well-connectedness contradicts there being a high degree of randomness in the structure (e.g., as in the computer simulations<sup>168</sup>) and instead suggests the structures to be regular, at least in some sense. Such regularity would be expected to lead to  $D_\infty \propto M^{-2}$  (reptation) in the limit  $M \rightarrow \infty$ ; this is predicted both theoretically and shown in computer simulations (e.g., see<sup>168</sup>) for regular porous materials.

That we do not see reptation is probably a consequence of insufficiently high molecular weights in our experiments. There is some indication from our data that the molecular weight dependence at the highest  $\lambda_H$  values is stronger than  $D_\infty \propto M^{-1}$ , and is becoming stronger still at higher  $\lambda_H$  (i.e., that the slope in Figure 27 would get steeper with increase in  $\lambda_H$ ; or that the slopes in Figure 28 would get steeper with decrease in  $D_0$ ). This perhaps is

indicative of a transition from Rouse-like to reptation dynamics, as has been considered by Kremer and Binder.<sup>75</sup>

Undoubtedly the stronger molecular weight dependence seen in random porous media (e.g., as in the computer simulations<sup>168</sup>) is a result of strong partitioning effects, for example, as given by the heuristic equation (2.63). The *hydrodynamics* of a polymer in either a regular or random porous material are that of a Rouse chain,  $D_p \propto M^{-1}$ . For a regular porous material, the stronger molecular weight dependence of  $D_\infty$  is simply due to the chain-like nature of the diffusant, which gives the reptation result. In a regular porous material, partitioning effects are negligible; but in a random porous material, partitioning effects are important and lead to a fundamentally different diffusion law than reptation.

The discussion now shifts, from the reduction in diffusivity due to hydrodynamic interactions, to the relation between the intrinsic conductivity  $X_0$  and the structure of the porous glasses.

One significant result is that the porous glasses B7 and B5, which have different porosities ( $\Phi = 0.72$  vs  $0.62$ ) and different pore sizes ( $R_p = 893$  vs  $1866$  Å), have the same intrinsic conductivity. Over the years, a number of theoretical and empirical expressions giving the tortuosity as a unique, single-valued (and sometimes universal) function of porosity have been proposed (e.g., see<sup>2,3,63,65</sup>), despite overwhelming evidence to the contrary. Certainly our result, that two glasses with significantly different  $\Phi$  can have the same  $X_0$ , is further evidence (as if any were needed) that no universal relation of intrinsic conductivity as a function of porosity exists.

It is of interest to compare the values for the intrinsic conductivity  $X$  of these porous glasses to both theoretical and experimental values for other porous materials. This comparison will be made primarily in terms of the tortuosity  $T$  ( $\approx 1/X$ ) and the formation factor  $F$  ( $\approx T/\Phi \approx 1/X\Phi$ ). The explicit subscript 0, denoting point particles, will be dropped.

The results for the three glasses are summarized as:

$$X = 0.78, \quad T = 1.28, \quad F = 1.78, \quad \Phi = 0.72 \quad (\text{B7})$$

$$X = 0.78, \quad T = 1.28, \quad F = 2.07, \quad \Phi = 0.62 \quad (\text{B5})$$

$$X = 0.58, \quad T = 1.73, \quad F = 3.77, \quad \Phi = 0.46 \quad (\text{B13})$$

For glasses B7 and B5, the value of  $X_0$  from the Brenner-Gajdos fit has been used. These tortuosities are relatively low, which is expected because of the high porosities and fairly uniform pore spaces possessed by these glasses. The higher tortuosity for B13, versus B7 and B5, is in accord with the general negative correlation of tortuosity with porosity.

These values are also in good accord with various experimental and theoretical values for "similar" porous materials; some such values are cited here to indicate this general agreement. (The interested reader is referred to the literature<sup>2,3,63-65</sup> for more extensive surveys; however, before doing so, he is urged to be aware that there are numerous notational variations which exist for "tortuosity".) All these literature values have been converted to the notation conventions of this dissertation (see Chapter II, section 3); and unless otherwise noted, tortuosity includes both "geometrical tortuosity" and "constrictedness".

Models of "normal" porous materials<sup>2,3,63-65</sup> give  $1 \leq T \leq 3$ ; however, models can easily be envisioned which give arbitrarily large  $T$  (e.g., fractal models<sup>94</sup>). For randomly oriented *thin* pores,  $T = \langle 1/\cos^2\theta \rangle = 3$ , which provides the upper limit above. Most real porous materials have "pores" with low aspect ratio; since flux lines can "cut across" such pores,  $T < 3$  is generally expected, with higher aspect ratio pores giving higher  $T$ .<sup>65</sup>

Packings of spheres<sup>2,3,61</sup> ( $\Phi \approx 0.4$ ) give  $T \approx 5/3$ . It is interesting to speculate whether the similarity of  $T$  for glass B13 (1.73) to this value for sphere packings might be connected with Haller's arguments that his controlled pore glasses form by nucleation and growth of eventually overlapping spherical domains. Similarly to spheres, loose packs of sand<sup>2,3</sup> have relatively low  $T \approx 3/2$ .

Various expressions relating  $T$  or  $F$  to  $\Phi$  have been proposed. Pismen<sup>65</sup> presents the formula:

$$X = 1 - (2/3)(1 + \Phi)(1 - \Phi)^{3/2} \quad (7.7)$$

This formula was derived by allowing for "shortcut" paths across pores, and has the "classic" limits, that is,  $X = 1/3$  for  $\Phi \rightarrow 0$ , and  $X = 1$  for  $\Phi \rightarrow 1$ . Values for  $X$ , calculated using equation (7.7), for our porous glasses are 0.83 (B7), 0.75 (B5), and 0.61 (B13); these are in reasonably good agreement with the experimentally measured values of  $X$ . I believe that this formula by Pismen, out of many relations proposed in the literature, is based on a model which perhaps corresponds reasonably well to the structure of the controlled pore glasses used in this work. (Of course, its universal applicability for other porous materials is not claimed.) It is also worth noting that Pismen's model

assumes no significant constrictions in the pores; hence, the agreement of our results to this theory lends support to the claim that these controlled pore glasses have fairly uniform pores without many severe constrictions.

One of the most frequently used expressions is Archie's law:<sup>2,3</sup>

$$1/F = \phi^m \quad (7.8)$$

where  $m$  is the cementation factor. For unconsolidated porous materials (e.g., loose sand),  $m \approx 1.3$ . However, for consolidated packings (e.g., sandstone),  $m$  is typically higher and quite variable.

A clearer rationale for Archie's law has recently been developed on the basis of fractal concepts, giving the cementation factor as:<sup>94</sup>

$$m = \frac{d_s + d_f (2 - d_s)}{(3 - d_f) d_s} \quad (7.9)$$

where  $d_f$  is the fractal dimension of the pore volume, and  $d_s$  is the spectral dimension;<sup>89</sup> or in terms of  $d_f$  and the fractal walk exponent<sup>90,91</sup>  $d_w$  (where  $d_s = 2d_f/d_w$ ):

$$m = \frac{1 + d_w - d_f}{(3 - d_f)} \quad (7.10)$$

For normal diffusion in three dimensions ( $d_w = 2$ ,  $d_f = 3$ ),  $m = 0$ .

This result has previously been applied towards understanding the electrical conductivity of sandstones, which on the basis of microscopy are claimed to have fractal pore spaces.<sup>94</sup> Applying equation (7.8) to the con-

trolled pore glasses, one obtains  $m=1.76$  (B7),  $m=1.52$  (B5), and  $m=1.71$  (B13).

One can then ask whether it is possible to interpret these values of  $m$  on the basis of a fractal model, as embodied in equation (7.10), which gives a relation between  $m$  and the structural and dynamical exponents  $d_f$  and  $d_w$ . Certainly these porous glasses are not fractal in the usually thought of sense, that is to say, with self-similar features spanning many orders of magnitude (e.g., as are some sandstones<sup>94</sup>); in fact, a rough guess is that they are "self-similar" over only about a three-fold range in length scales, an estimate which is based on viewing the range of pore sizes in electron micrographs and which is consistent with mercury intrusion data.

The above theory also gives a relation between the porosity and the upper  $l_2$  and lower  $l_1$  cutoff lengths of fractal structure:<sup>94</sup>

$$\Phi = A (l_1/l_2)^{3 - d_f} \quad (7.11)$$

where  $A$  is a constant of order unity. Using the above estimate  $(l_1/l_2) \approx 1/3$ , assuming  $A=1$ , and using  $\Phi = 0.72$  (glass B7), one calculates a value for  $d_f = 2.70$  from equation (7.11). Using this value with  $m=1.76$  in equation (7.10), one calculates  $d_w = 2.22$ . This value for  $d_w$  corresponds quite closely to a value obtained by choosing an exponent  $\beta = 2/d_w$  to superimpose non-exponential correlation functions measured in the high wavevector regime (see Figure 29), assuming the correlation functions in this regime scale as (see Chapter III, section 2):

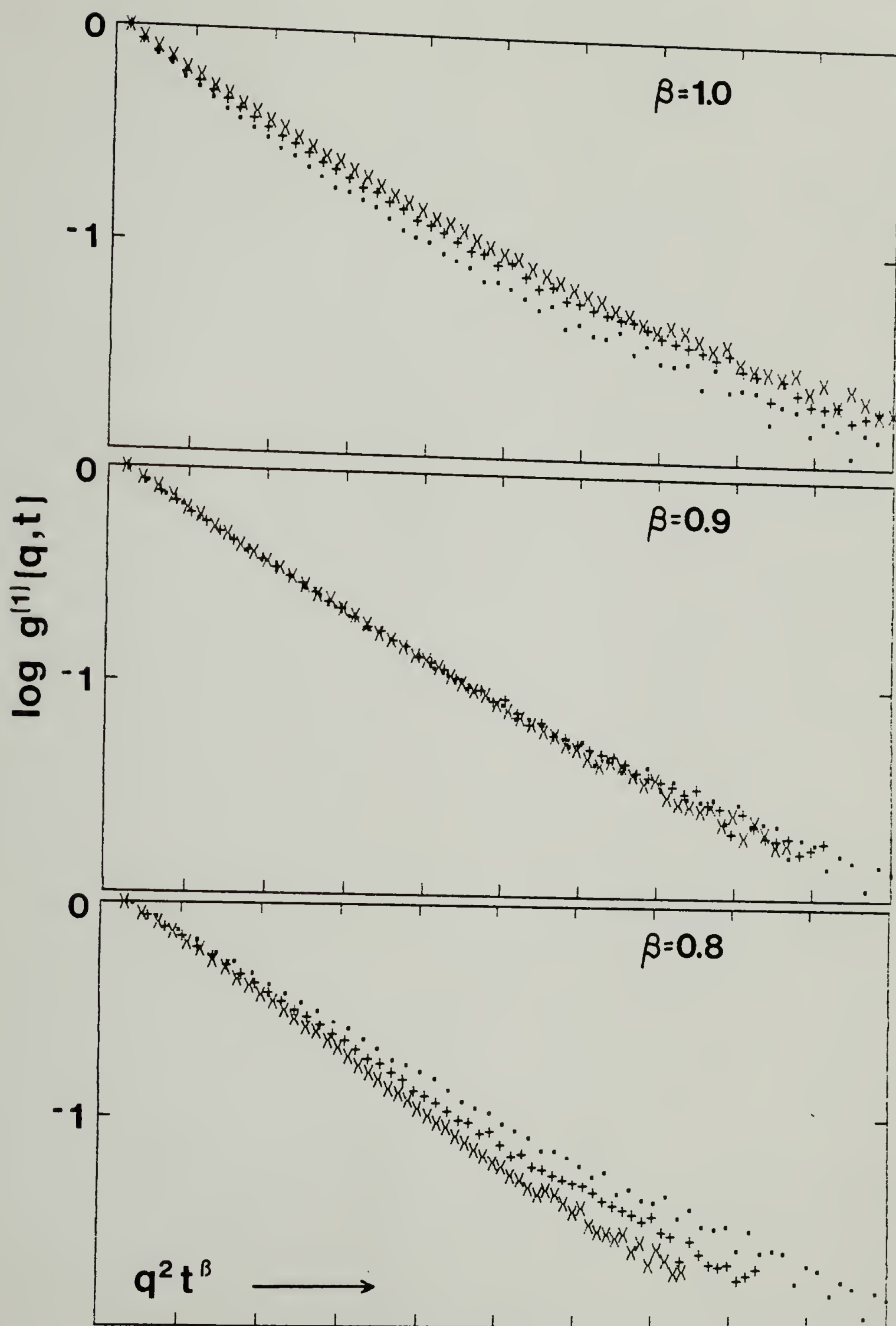
$$g_s^{(1)}(\mathbf{q}, t) = \exp(-D_{\text{EFF}} q^2 t^\beta) \quad (7.12)$$

Figure 29.

Effective fractal diffusion behavior.

Correlation functions measured at three different wavevectors are plotted as suggested by equation (7.12), to see if there is a value of  $\beta$  which will lead to superposition of the correlation functions. Empirically, a value of  $\beta \approx 0.90$  superposes the correlation functions. This exponent  $\beta$  is related to the effective fractal walk exponent as  $\beta = 2/d_w$ , giving  $d_w = 2.22$ .

These data are for polymer P4 ( $R_H = 40 \text{ \AA}$ ) in glass B7 ( $R_p = 893 \text{ \AA}$ ) at wavevectors  $q^2 = 6.34 \times 10^{10} \text{ (point)}$ ,  $2.54 \times 10^{10} \text{ (+)}$ , and  $1.29 \times 10^{10} \text{ (x) cm}^{-2}$ . Corresponding values of  $qR_p$  are 2.2, 1.4, and 1.0.



Whether this agreement has more than coincidental significance is not known. It is possible that the "non-Gaussian" effects (due to the presence of the reflecting pore walls) which are observed in this regime, intermediate between diffusion over very short and very long distances, can be considered in terms of *effectively* fractal diffusion behavior. Investigation of this idea is perhaps worthy of future study. (A loose justification of these arguments was mentioned in the fourth section of Chapter II.)

This section concludes with a general comparison of our results to those of previous investigations of diffusion of flexible polymers in porous materials. (Those studies were reviewed in Chapter II, which can be consulted for a full list of references.) Those experiments fall into three categories: transient diffusion, chromatographic peak broadening, and membrane transport.

First, the results on diffusion in porous glasses are considered. After correcting the results of Tennikov et al.<sup>17</sup> for obviously erroneous  $D_0$  values, one can conclude that their lower molecular weight data ( $\lambda_H < 0.4$ ) are at least roughly consistent with our results, both in terms of  $D_\infty/D_0$  vs  $\lambda_H$ , and in terms of the intercept at  $\lambda_H = 0$ . However, we find no support for their conclusions that  $D_\infty/D_0$  can exceed unity, and for extremal behavior (i.e., a minimum) in  $D_\infty/D_0$  vs  $\lambda_H$ . Indeed, their anomalous results at higher molecular weight cast some doubt on even their findings at lower molecular weight.

We find no support for the conclusions of Colton et al.<sup>16</sup> that flexible polystyrenes have reduced effective diffusivities  $D_\infty/D_0$  that are independent of the relative size parameter  $\lambda_H$  (i.e., independent of molecular weight)

in any given pore size glass (called erroneously by them free-draining). To the contrary, we find  $D_\infty/D_0$  to be a monotonically and significantly decreasing function of  $\lambda_H$ . Furthermore, the tortuosities estimated by Colton et al. for their porous glasses with claimed narrow pore size distributions-- $T = 2.9, 2.3, 3.1$ , and  $3.5$  for  $\Phi = 0.54, 0.70, 0.58$ , and  $0.60$ --are significantly higher and in disagreement with the values found in this work. Perhaps the most reasonable explanation for the lower and essentially constant  $D_\infty/D_0$  values observed by them would be a large boundary layer resistance<sup>7,95</sup> (it was assumed by them to be negligible) in series with the diffusive resistance of the porous glasses.

Our results are also in substantial disagreement with those of Klein and Grüneberg<sup>34</sup> (diffusion coefficients of polystyrenes in porous glasses from size exclusion chromatography peak broadening). For chromatographic partitioning coefficients  $K_C > 0.35$ , corresponding roughly to  $\lambda_H < 0.25$ , they found  $D_\infty/D_0$  independent of molecular weight; this can be contrasted to our results, where  $\approx 50\%$  reduction in  $D_\infty/D_0$  is seen at  $\lambda_H = 0.25$  relative to  $D_\infty/D_0$  at  $\lambda_H = 0$ . However, for  $K_C < 0.35$ , ( $\lambda_H > 0.25$ ) they did observe size dependent reductions in  $D_\infty/D_0$ . It is worth noting that this value of  $K_C \approx 0.35$  corresponds to  $\lambda_H \approx 0.25$ , which from our results is tentatively identified as the  $\lambda_H$  where transition to free-draining behavior is observed. It is possible that only in this free-draining regime, where the intrapore diffusivity depends more strongly on molecular weight, was their SEC peak broadening technique sensitive enough to detect changes in  $D_\infty/D_0$ . It is also noted that their (approximately constant)  $D_\infty/D_0$  values at high  $K_C$  (low  $\lambda_H$ ) are about  $0.14, 0.16$ , and  $0.23$  for glasses with porosities of  $0.48, 0.64$ , and

0.76. These values, essentially intrinsic conductivities, are far lower than those found in this work for glasses of similar porosity. As mentioned in connection with the work of Colton et al.,<sup>16</sup> it is possible that the boundary layer resistance, which is neglected in the theory of SEC peak broadening, may be larger (except for high molecular weights) than the actual intraglass diffusional resistance. (However, as noted in Chapter II, there are significant numerical questions in extracting  $D_\infty$  from these SEC experiments.)

In summary, in contrast with the results of these transient diffusion<sup>16,17</sup> and SEC peak broadening<sup>34</sup> experiments, we find that the diffusion of polystyrene in porous glasses is in no way unusual: the ratio  $D_\infty/D_0$  decreases monotonically with increase in  $\lambda_H$ . Further, we find lower tortuosities (by a factor of 2-5) than in these previous experiments. It is suggested that the significantly lower and essentially constant effective diffusivities which have been observed in these previous experiments may be due to a large boundary layer resistance. This observation, if true, implies that diffusional band broadening in gel permeation chromatography<sup>33</sup> may be due mainly to this boundary layer resistance to polymer entering and leaving packing particles, and not to diffusion within those particles.

Our dynamic light scattering results are in essential agreement with those for diffusion of flexible polymers through track-etched membranes:<sup>29-32</sup> the results of both types of experiments are consistent with both hard sphere<sup>4-9</sup> and flexible polymer<sup>10-12</sup> hindered diffusion theories, given the adjustable parameters in those theories.

It is worth noting that, in the only other work<sup>29,30</sup> where the scaling theory has been considered, the hard sphere and scaling theory fits to the data cross at values of  $\lambda_H \approx 0.15-0.30$ . This is the same as the value where the fits to our data cross. Although this may merely indicate that the scaling theory is incapable of fitting data at low  $\lambda_H$  ( $\leq 0.25$  say, where the dependence of  $D_\infty/D_0$  upon  $\lambda_H$  is nearly linear), it also lends some support to the tentative identification in our work of this value of  $\lambda_H$  as the transition from non-free draining to free draining behavior.

Dynamic light scattering experiments can potentially provide a more critical test of scaling theories and this transition in hydrodynamic behavior than can membrane transport experiments. These latter infer scaling behavior on the basis of a two parameter fit, *of a power law times an exponential*, to the experimental data for  $D_M = K_D f(\lambda_H)$ . Light scattering, in contrast, allows one to directly look for the hindered diffusivity power law, because  $K_D$  is not included in the effective diffusion coefficient which is measured.

The quantitative interpretation of the fits of our data at low  $\lambda_H$ , where hard sphere diffusion theories may be a reasonable approximation for flexible polymers, indicates that the appropriate hard sphere radius to use in these theories is the hydrodynamic radius, *that is, with a factor  $\kappa$  of very near unity*. (This is after accounting for the effect of pore polydispersity.) This is to be contrasted with previous conclusions of  $\kappa = 1.45$ ,<sup>30</sup> or  $\kappa$  significantly less than one,<sup>31,32</sup> from experiments on track-etched membranes. The higher result of Cannell and Rondelez<sup>30</sup> may be due to neglect of boundary layer resistance (estimated by them to be as high as 20%); to fit a

lower apparent  $D_M$  (i.e., including boundary layer resistance) would require a larger  $\kappa$ . Porosity, often poorly known in these membrane transport coefficients (e.g., extracted by assuming a Renkin equation fit<sup>29</sup>), can similarly affect  $\kappa$ ; as with  $K_D$ , the porosity does not enter the effective diffusion coefficient from light scattering. Nonetheless, it is difficult to reach any definitive conclusion about the exact "correct" flexible polymer radius to use in hard sphere hindered diffusion theories, because of nagging numerical details in both light scattering and membrane diffusion experiments.

### **Suggestions for Future Work**

This dissertation has demonstrated the advantages offered by a technique such as dynamic light scattering, as compared to more phenomenological techniques, in studying polymer transport in porous materials. In this work, dynamic light scattering was applied to a relatively simple problem: diffusion of linear flexible polymers in porous glasses with random but nonetheless relatively uniform pore structures, and with adsorption and convection absent. Offered here are a number of suggestions to extend the current work: to other polymers and porous materials; to the use of other complementary techniques; and to other more general problems of polymer transport in porous materials.

A relatively straightforward extension of the current work would be to examine the diffusion of different polymers in these same porous glasses. An outstanding question is the "proper" flexible polymer radius to use in considering hydrodynamic polymer-wall interactions.<sup>30,32</sup> This could be probed by examining the diffusion of star polymers of varying arm

number and size; since the ratio  $R_H/R_G$  is not constant for stars<sup>78</sup> as it is for linear polymers, comparison of  $D_\infty/D_0$  as a function of  $R_H$  and  $R_G$  for both linear and star polymers could indicate which radius (if either) is more directly related to intrapore hydrodynamics for relatively small  $\lambda_H$ . In addition, it would be of interest to see how  $D_\infty$  scales with molecular weight for strongly confined star polymers, as compared to linear polymers. (In contrast to membrane transport experiments,<sup>29-32</sup> the equilibrium partitioning factor does not cloud the interpretation.) Another point of interest would be to examine the diffusion of rigid spheres, and of "rigid rod" polymers in these same materials; a suggestion as to a candidate polymer for the latter would be poly(alkyl isocyanates), which can be obtained as relatively monodisperse fractions, which should be soluble in 2-fluorotoluene, and whose dilute solution behavior is well known.<sup>169,170</sup>

Another obvious extension of this work is to other porous materials. Certainly other porous glasses similar to those used here could be used to extend the range of the relative size parameter  $\lambda_H$  (say by using glasses with smaller  $R_p$ ), and to further examine "hindered diffusion" as a function of material parameters (pore size, porosity, intrinsic conductivity) and polymer variables. Also interesting would be to look at diffusion in better characterized porous materials. Much work on transport in porous materials, both theoretical and experimental, has been carried out on packings of non-porous spheres.<sup>3</sup> Some attempt, without success, was made to find index matchable glass spheres for such an experiment. A possibility suggested here would be to use suspension polymerized, non-porous, highly cross-linked polymer beads (e.g., of CR-39,<sup>171</sup> to be mentioned shortly). Experi-

ments in sphere packings would allow more rigorous contact with theories of tortuosity. A second example of better characterized porous materials would be track-etched membranes,<sup>172,173</sup> much utilized in membrane transport experiments.<sup>27-32</sup> As commercial membranes are unsuitable for light scattering experiments, some effort was made to find a way to make suitable track-etched materials; CR-39, a highly crosslinked and easily index matched plastic, was identified as the best starting material. (These efforts, together with my recommendations, including a rather negative prognosis for success, are summarized in Appendix B.)

Examination of diffusion in less well characterized porous materials would also be of interest. In this work, the separability of intrinsic conductivity (tortuosity) from hydrodynamic interaction effects was predicated on the relatively uniform pore sizes of the "controlled pore" glasses. However, many (if not most) porous materials have a far wider distribution of pore sizes. It is likely that at least some such porous materials have fractal pore spaces. In tune with the burgeoning interest in fractals, the study of diffusion in such materials would be timely. Results in the limit  $\lambda_H = 0$  could be compared to standard theories of fractal diffusion<sup>88-93</sup> and used to estimate fractal cutoff dimensions; and the behavior of  $D_\infty$  as a function of diffusant size could well prove quite unusual. Some suggestions of porous materials with more random structure are: other porous glasses (e.g., Vycor); macroporous crosslinked polystyrene beads, as are used in ion exchange and gel permeation chromatography; stacks of fibrous-mat membranes; and sandstones, some of which are quite possibly fractal,<sup>94</sup> and some of which, if

not too highly colored, might be sufficiently transparent and index-matchable (they are basically quartz).

Above have been suggested numerous systems--polymers and porous materials--in which diffusion could be studied. Although dynamic light scattering was the technique used in this dissertation, it is not without its limitations; hence, the additional use of other complementary techniques in future work is strongly suggested. Dynamic light scattering (DLS) measures the mutual diffusion coefficient. In contrast, forced Rayleigh scattering<sup>100</sup> (FRS) and pulsed field gradient spin-echo NMR<sup>174</sup> (PFGSE-NMR), techniques which follow the diffusion of tagged species--tagged by either a photochromic label (FRS) or nuclear spins (PFGSE-NMR)--unambiguously measure the self-diffusion coefficient. Also, both these techniques look at diffusion over longer distances (lower  $q$ ) than DLS and are thus better suited for macroscopic diffusion studies. Although FRS, like DLS, requires an optically transparent material, PFGSE-NMR is not so restricted. Thus, the primary advantages are two-fold. (1) By measuring the self-diffusion coefficient, studies can be made at higher concentration. (2) These techniques look at the relaxation of longer wavelength (low  $q$ ) fluctuations and hence are more firmly in the macroscopic diffusion regime; this could prove especially valuable for materials with large pore sizes, or for less uniform porous materials. These techniques would not be without some practical problems in adapting them to study diffusion in porous materials.

This section concludes with suggestions of other problems of polymer transport in porous media to which dynamic light scattering and

these other techniques could be applied; however, theory is less developed for these problems than for simple diffusion.

Scaling theories have had a substantial impact on polymer science in recent years.<sup>12</sup> One of the more significant results is the theory of reptation,<sup>12,166,167</sup> describing the motion of a polymer chain in the melt and concentrated solutions as being confined to a tube. The exact nature of this tube constraint and how it relaxes, when the tube itself is composed of molecules similarly in motion, is not understood. It is suggested that the study of the diffusion of flexible polymers in truly rigid "tubes" could aid in critically examining reptation. In the work of this dissertation, the regime where the chains are "strongly confined" (and hence should reptate) was scarcely reached. In accord with partitioning theories, in order to get a substantial number of long chains in very small pores, the concentration must be raised until the correlation length is less than the pore size.<sup>54-56</sup> In this regime, forced Rayleigh scattering would be the method of choice for studying whole chain diffusion, while dynamic light scattering could be used to look at the usual semi-dilute pseudogel cooperative diffusion coefficient.<sup>10,11</sup> Comparison of relatively regular (e.g., "controlled pore" glasses) to more random porous materials could be compared with computer simulations<sup>168</sup> indicating that reptation is only seen in regular porous materials. An important feature of experiments such as these, as compared to membrane transport experiments in more concentrated solutions,<sup>29</sup> is the absence of partitioning effects *per se* in the measured effective diffusion coefficients.

Other problems to which these techniques could be applied are mentioned briefly. (1) The surfaces of many porous materials can be chemically modified to introduce charged groups, perhaps allowing the study of the diffusion of charged polymers interacting with the charged walls. (2) Dynamic light scattering, in its laser Doppler velocimetry mode, could perhaps be used to directly study the flow of a polymer solution in a porous plug. (3) Dynamic light scattering is particularly well suited to the study of *less than* macroscopic diffusion (i.e., the intermediate and high  $qR_p$  regimes). The wavevector and time dependence of correlation functions in these regimes is poorly understood and is worthy of further study. In particular, the intermediate  $qR_p$  regime should show characteristic differences for structurally different pore spaces (e.g., fractal versus regular). (4) Although experimentally difficult, detailed examination of the long time behavior might be of interest (i.e., is there a long time tail as predicted by mode coupling theories?<sup>69,70</sup>) (5) The dynamics of adsorbed polymer chains is of interest and can perhaps be profitably studied using these techniques. Many porous materials, by virtue of their high specific surface area, provide a spatially concentrated surface on which adsorption, and dynamics of adsorbed chains, can be studied. Quite clearly, such dynamics have been seen by us in light scattering correlation functions, when the glass surface was untreated.

## REFERENCES

1. A. E. Scheidegger, The Physics of Flow through Porous Media, MacMillan Company, New York, 1960.
2. J. Bear, Dynamics of Fluids in Porous Media, American Elsevier Publishing, New York, 1972.
3. F. A. L. Dullien, Porous Media: Fluid Transport and Pore Structure, Academic Press, New York, 1979.
4. J. Happel and H. Brenner, Low Reynolds Number Hydrodynamics, Prentice-Hall, Englewood Cliffs, N. J., 1965.
5. C. P. Bean, "The Physics of Porous Membranes: Neutral Pores", in Membranes: A Series of Advances, V. 1, G. Eisenman, ed., Marcel Dekker, New York, 1972, p. 1.
6. J. L. Anderson and J. A. Quinn, "Restricted Transport in Small Pores: A Model for Steric Exclusion and Hindered Particle Motion", *Biophys. J.*, **14**, 130 (1974).
7. D. M. Malone, "The Convection and Diffusion of Brownian Particles within Porous Systems: A Theoretical and Experimental Approach", Ph. D. Dissertation, Cornell University, 1977.
8. H. Brenner and L. J. Gajdos, "The Constrained Brownian Movement of Spherical Particles in Cylindrical Pores of Comparable Radius: Models of the Diffusive and Convective Transport of Solute Molecules in Membranes and Porous Media", *J. Colloid Interf. Sci.*, **58**, 312 (1977).
9. L. J. Gajdos, "Boundary Effects in the Transport of Arbitrarily-Shaped Brownian Particles", Ph. D. Dissertation, Carnegie-Mellon University, 1977.
10. F. Brochard, "Dynamics of Polymer Chains Trapped in a Slit", *J. de Physique*, **38**, 1285 (1977).

11. F. Brochard and P. G. de Gennes, "Dynamics of Confined Polymer Chains", *J. Chem. Phys.*, **67**, 52 (1977).
12. P. G. de Gennes, Scaling Concepts in Polymer Physics, Cornell University Press, Ithaca, N. Y., 1979.
13. B. Chu, Laser Light Scattering, Academic Press, New York, 1974.
14. H. Z. Cummins and E. R. Pike, ed., Photon Correlation and Light Beating Spectroscopy, Plenum Press, New York, 1974.
15. B. J. Berne and R. Pecora, Dynamic Light Scattering: With Applications to Chemistry, Biology, and Physics, John Wiley and Sons, New York, 1976.
16. C. K. Colton, C. N. Satterfield, and C.-J. Lai, "Diffusion and Partitioning of Macromolecules within Finely Porous Glass", *A. I. Ch. E. Journal*, **21**, 289 (1975).
17. M. B. Tennikov, B. G. Belen'kii, V. V. Nesterov, and T. D. Anan'eva, "Measurement of Internal Diffusion Coefficients of Polystyrene Molecules in Porous Sorbents", *Colloid J. USSR*, **41**, 526 (1979); translated from *Kolloid Zh.*, **41**, 608 (1979).
18. J. D. Ferry, "Statistical Evaluation of Sieve Constants in Ultrafiltration", *J. Gen. Physiol.*, **20**, 95 (1936).
19. J. D. Ferry, "Ultrafilter Membranes and Ultrafiltration", *Chem. Rev.*, **18**, 373 (1936).
20. J. R. Papenheimer, E. M. Renkin, and L. M. Borrero, "Filtration, Diffusion, and Molecular Sieving through Peripheral Capillary Membranes: A Contribution of Pore Theory of Capillary Permeability", *Am. J. Physiol.*, **167**, 13 (1951).
21. J. R. Papenheimer, "Passage of Molecules through Capillary Walls", *Physiol. Rev.*, **33**, 387 (1953).
22. E. M. Renkin, "Filtration, Diffusion, and Molecular Sieving through Porous Cellulose Membranes", *J. Gen. Physiol.*, **38**, 225 (1954).

23. G. K. Ackers and R. L. Steere, "Restricted Diffusion of Macromolecules through Agar-gel Membranes", *Biochim. Biophys. Acta*, **59**, 137 (1962).
24. A. K. Solomon, "Characterization of Biological Membranes by Equivalent Pores", *J. Gen. Physiol.*, **51**, 335s, (1968).
25. B. M. Uzelac and E. L. Cussler, "Diffusion of Small Particles through Pores of Similar Diameter", *J. Colloid Interf. Sci.*, **32**, 487 (1970).
26. T. Conlon and B. Craven, "Hindering of Diffusion by Pores", *Austral. J. Chem.*, **25**, 695 (1972).
27. R. E. Beck and J. S. Schultz, "Hindrance of Solute Diffusion within Membranes as Measured with Microporous Membranes on Known Pore Geometry", *Biochim. Biophys. Acta*, **255**, 273 (1972).
28. D. M. Malone and J. L. Anderson, "Hindered Diffusion of Particles through Small Pores", *Chem. Eng. Sci.*, **33**, 1429 (1978).
29. G. Guillot, L. Léger, and F. Rondelez, "Diffusion of Large Flexible Polymer Chains through Model Porous Membranes", *Macromolecules*, **18**, 2531 (1985).
30. D. S. Cannell and F. Rondelez, "Diffusion of Polystyrene through Microporous Membranes", *Macromolecules*, **13**, 1599 (1980).
31. W. M. Deen, M. P. Bohrer, and N. B. Epstein, "Effects of Molecular Size and Configuration on Diffusion in Microporous Membranes", *A. I. Ch. E. Journal*, **27**, 952 (1981).
32. M. P. Bohrer, G. D. Patterson, and P. J. Carroll, "Hindered Diffusion of Dextran and Ficoll in Microporous Membranes", *Macromolecules*, **17**, 1170 (1984).
33. J. C. Giddings, L. M. Bowman, Jr., and M. N. Myers, "Isolation of Peak Broadening Factors in Exclusion (GEL) Chromatography", *Macromolecules*, **10**, 443 (1977).
34. J. Klein and M. Grüneberg, "Mass Transfer of Macromolecules in Steric Exclusion Chromatography. 1. Diffusional Transport in the Pores of SEC Materials", *Macromolecules*, **14**, 1411 (1981).

35. C. N. Satterfield, C. K. Colton, and W. H. Pitcher, "Restricted Diffusion in Liquids within Fine Pores", *A. I. Ch. E. J.*, **19**, 628 (1973).
36. B. Prasher and Y. H. Ma, "Liquid Diffusion in Microporous Alumina Pellets", *A. I. Ch. E. J.*, **23**, 303 (1977).
37. A. Chantong and F. E. Massoth, "Restrictive [sic] Diffusion in Aluminas", *A. I. Ch. E. J.*, **29**, 725 (1983).
38. E. B. Vadas, H. L. Goldsmith, and S. G. Mason, "The Microrheology of Colloidal Dispersions. I. The Microtube Technique", *J. Colloid Interf. Sci.*, **43**, 630 (1973).
39. E. B. Vadas, R. G. Cox, H. L. Goldsmith, and S. G. Mason, "The Microrheology of Colloidal Dispersions. II. Brownian Diffusion of Doublets of Spheres", *J. Colloid Interf. Sci.*, **57**, 308 (1976).
40. W. D. Dozier, J. M. Drake, and J. Klafter, "Self-Diffusion of a Molecule in Porous Vycor Glass", *Phys. Rev. Lett.*, **56**, 197 (1986).
41. J. C. Tarczoz, A. H. Thompson, W. A. Ellingson, and W. P. Halperin, "Molecular Diffusion in Porous Structures", Abstracts, Conf. on Transport and Relaxation Processes in Random Materials, 1985, p. 42.
42. S. Pickup, F. D. Blum, W. T. Ford, and M. Periyasa, "Transport of Small Molecules in Swollen Polymer Beads", *J. Am. Chem. Soc.*, **108**, 3987 (1986).
43. P. G. Cummins and E. J. Staples, "Particle Size Measurements on Turbid Latex Systems Using Heterodyne Intensity Autocorrelation Spectroscopy", *J. Phys. E: Sci. Instrum.*, **14**, 1171 (1981).
44. A. J. Hurd, R. C. Mockler, and W. J. O'Sullivan, "A Light Scattering Study of Constrained Brownian Motion", in Proceedings from the 4th International Conference on Photon Correlation Techniques in Fluid Mechanics, W. T. Mayo, Jr., and A. E. Smart, ed., Joint Institute for Aeronautics and Acoustics, Stanford Univ., Stanford, Cal., 1980, p. 22-1.

45. K. H. Lan, N. Ostrowsky, and D. Sornette, "Brownian Dynamics Close to a Wall Studied by Photon Correlation Spectroscopy from an Evanescent Wave", *Phys. Rev. Lett.*, **57**, 17 (1986).
46. R. Pecora, "Doppler Shifts in Light Scattering from Pure Liquids and Polymer Solutions", *J. Chem. Phys.*, **40**, 1604 (1964).
47. P. N. Pusey, "The Study of Brownian Motion by Intensity Fluctuation Spectroscopy", *Phil. Trans. Roy. Soc. Lond. A*, **293**, 429 (1979).
48. E. F. Casassa, "Equilibrium Distribution of Flexible Polymer Chains between a Macroscopic Solution Phase and Small Voids", *J. Polym. Sci, Polym. Lett.*, **B5**, 773 (1967).
49. E. F. Casassa and Y. Tagami, "An Equilibrium Theory for Exclusion Chromatography of Branched and Linear Polymer Chains", *Macromolecules*, **2**, 14 (1969).
50. J. C. Giddings, E. Kucera, C. P. Russell, and M. N. Myers, "Statistical Theory for the Equilibrium Distribution of Rigid Molecules in Inert Porous Networks. Exclusion Chromatography", *J. Phys. Chem.*, **72**, 4397 (1968).
51. R. J. Gaylord and D. J. Lohse, "The Configurational Statistics of a Polymeric Chain Confined by Impenetrable Barriers", *J. Chem. Phys.*, **65**, 2779 (1976).
52. D. J. Lohse and R. J. Gaylord, "The Configurational Statistics of a Polymeric Chain Confined by Impenetrable Barriers. II. The Floating Chain", *J. Chem. Phys.*, **66**, 3843 (1977).
53. M. Doi, "Equilibrium Partition Coefficient of Macromolecules between Random Porous Material and Bulk Liquid", *J. Chem. Soc., Faraday Trans. II*, **71**, 1720 (1975).
54. M. Daoud and P. G. de Gennes, "Statistics of Macromolecular Chains Trapped in Small Pores", *J. de Physique*, **38**, 85 (1977).
55. S. Daoudi and F. Brochard, "Flows of Flexible Polymer Solutions in Pores", *Macromolecules*, **11**, 751 (1978).
56. F. Brochard and P. G. de Gennes, "Conformations de Polymères Fondus dans des Pores Très Petits", *J. de Physique Lett.*, **40**, 400 (1979).

57. L. Turban, "Conformation of Confined Macromolecular Chains: Cross-over between Slit and Capillary", *J. de Physique*, **45**, 347 (1984).
58. Y. Chen and M. Muthukumar, "Free Energy of a Macromolecule in a Confined Domain", *Phys. Rev. B*, **33**, 6187 (1986).
59. Y. Chen and R. A. Guyer, "A Polymer in a Fractal Pore Space", to be published.
60. G. D. J. Phillies, "Universal Scaling Equation for Self-Diffusion by Macromolecules in Solution", *Macromolecules*, **19**, 2367 (1986).
61. J. H. Knox and L. McLaren, "A New Gas Chromatographic Method for Measuring Gaseous Diffusion Coefficients and Obstructive Factors", *Anal. Chem.*, **36**, 1477 (1964).
62. J. C. Giddings, Dynamics of Chromatography, Part I: Principles and Theory, Marcel Dekker, New York, 1965.
63. J. van Brakel and P. M. Heertjes, "Analysis of Diffusion in Macroporous Media in Terms of a Porosity, a Tortuosity, and a Constrictivity Factor", *Int. J. Heat Mass Transfer*, **17**, 1093 (1974).
64. J. van Brakel, "Pore Space Models for Transport in Porous Media", *Powder Technol.*, **11**, 205 (1975).
65. L. M. Pismen, "Diffusion in Porous Media of a Random Structure", *Chem. Eng. Sci.*, **29**, 1227 (1974).
66. J. C. Slattery, Momentum, Energy, and Mass Transfer in Continua, McGraw-Hill, New York, 1972.
67. W. G. Gray, "A Derivation of the Equations for Multi-Phase Transport", *Chem. Eng. Sci.*, **30**, 229 (1975).
68. F. K. Lehner, "On the Validity of Fick's Law for Transient Diffusion through a Porous Medium", *Chem. Eng. Sci.*, **34**, 821 (1979).
69. M. H. Ernst, J. Machta, J. R. Dorfman, and H. van Beijeren, "Long Time Tails in Stationary Random Media. I. Theory", *J. Stat. Phys.*, **34**, 477 (1984).

70. J. Machta, M. H. Ernst, H. van Beijeren, and J. R. Dorfman, "Long Time Tails in Stationary Random Media. II. Applications", *J. Stat. Phys.*, **35**, 413 (1984).
71. A. G. Ogston, "The Spaces in a Uniform Random Suspension of Fibers", *Trans. Faraday Soc.*, **54**, 1754 (1958).
72. T. C. Laurent and J. Killander, "A Theory of Gel Filtration and its Experimental Verifications", *J. Chromatog.*, **14**, 317 (1964).
73. B. H. Zimm and W. H. Stockmayer, "The Dimensions of Chain Molecules Containing Branches and Rings", *J. Chem. Phys.*, **17**, 1301 (1949).
74. C. N. Satterfield, C. K. Colton, B. de Turckheim, and J. M. Copeland, "Effect of Concentration on Partitioning of Polystyrene within Finely Porous Glass", *A. I. Ch. E. Journal*, **24**, 937 (1978).
75. K. Kremer and K. Binder, "Dynamics of Polymer Chains Confined into Tubes: Scaling Theory and Monte Carlo Simulations", *J. Chem. Phys.*, **81**, 6381 (1984).
76. H. Brenner, "Coupling between the Translational and Rotational Brownian Motions of Rigid Particles of Arbitrary Shape", *J. Colloid Interf. Sci.*, **23**, 407 (1967).
77. S. Bantle, M. Schmidt, and W. Burchard, "Simultaneous Static and Dynamic Light Scattering", *Macromolecules*, **15**, 1604 (1982).
78. W. Burchard, "Static and Dynamic Light Scattering from Branched Polymers and Biopolymers", *Adv. Polym. Sci.*, **48**, 1 (1983).
79. H. Faxén, *Ark. Mat. Astron. och Fysik*, **17**, No. 27 (1922); results given in Refs. 4, 5, and 22, among others.
80. See Refs. 4 (Chpt. 7), 5, and 81 for details.
81. P. L. Paine and P. Scherr, "Drag Coefficients for the Movement of Rigid Spheres through Liquid-Filled Cylindrical Pores", *Biophys. J.*, **15**, 1087 (1975).
82. T. Bohlin, *Trans. Roy. Inst. Technol. (Stockholm)*, No. 155 (1960); results given in Ref. 4, p. 318, and Ref. 5, p. 12.

83. W. L. Haberman and R. M. Sayre, David Taylor Model Basin Report, No. 1143, U. S. Navy Dept., Washington, D. C., 1958; results given in Ref. 4, p. 320.
84. J. Famularo, D. Eng. Sci. Thesis, New York University, 1962; results given in Ref. 4, p. 309, and in Ref. 5, p. 14.
85. A. J. Goldman, R. G. Cox, and H. Brenner, "Slow Viscous Motion of a Sphere Parallel to a Plane Wall. II. Couette Flow", Chem. Eng. Sci., **22**, 653 (1967).
86. N. Wakad and Y. Nardse, "Effective Diffusivities and Deadend Pores", Chem. Eng. Sci., **29**, 1304 (1974).
87. A. Katchalsky and P. F. Curran, Nonequilibrium Thermodynamics in Biophysics, Harvard Univ. Press, Cambridge, 1965.
88. Y. Gefen, A. Aharony, B. B. Mandelbrot, and S. Kirkpatrick, "Solvable Fractal Family, and Its Possible Relation to the Backbone at Percolation", Phys. Rev. Lett., **47**, 1771 (1981).
89. S. Alexander and R. Orbach, "Density of States on Fractals: Fractons", J. de Physique, Lett., **43**, L625 (1982).
90. Y. Gefen, A. Aharony, and S. Alexander, "Anomalous Diffusion on Percolating Clusters", Phys. Rev. Lett., **50**, 77 (1983).
91. R. Rammal and G. Toulouse, "Random Walks on Fractal Structures and Percolation Clusters", J. de Physique, Lett., **44**, L13 (1983).
92. R. A. Guyer, "Diffusive Motion on a Fractal;  $G_{nm}(t)$ ", Phys. Rev. A, **32**, 2324 (1985).
93. B. O'Shaughnessy and I. Procaccia, "Analytical Solutions for Diffusion on Fractal Objects", Phys. Rev. Lett., **54**, 455 (1985).
94. A. J. Katz and A. H. Thompson, "Fractal Sandstone Pores: Implications for Conductivity and Pore Formation", Phys. Rev. Lett., **54**, 1325 (1985).
95. M. P. Bohrer, "Diffusional Boundary Layer Resistance for Membrane Transport", Ind. Eng. Chem. Fundam., **22**, 72 (1983).

96. W. Haller, "Correlation Between Chromatographic and Diffusional Behavior of Substances in Beds of Pore Controlled Glass: Contribution to the Mechanism of Steric Chromatography", *J. Chromatogr.*, **32**, 676, (1968).
97. F. Rondelez, "Diffusion of Large Flexible Polymers through Submicroscopic Pores", *Adv. Colloid Interf.*, **16**, 403 (1982).
98. J. C. Selser, K. J. Rothschild, J. D. Swalen, and F. Rondelez, "Study of Multilamellar Films of Photoreceptor Membrane by Photon Correlation Spectroscopy Combined with Integrated Optics", *Phys. Rev. Lett.*, **48**, 1690 (1982).
99. J. Kärger, J. Lenzner, H. Pfeifer, H. Schwabe, W. Heyer, F. Janowski, F. Wolf, and S. P. Zdanov, "NMR Study of Adsorbate Self-Diffusion in Porous Glasses", *J. Am. Ceram. Soc.*, **66**, 69 (1983).
100. L. Léger, H. Hervet, and F. Rondelez, "Reptation in Entangled Polymer Solutions by Forced Rayleigh Light Scattering", *Macromolecules*, **14**, 1732 (1981).
101. H. C. van de Hulst, Light Scattering by Small Particles, Dover Publications, New York, 1981.
102. M. Kerker, The Scattering of Light and Other Electromagnetic Radiation, Academic Press, New York, 1969.
103. C. Tanford, Physical Chemistry of Macromolecules, John Wiley and Sons, 1961.
104. M. Huglin, ed., Light Scattering from Polymer Solutions, Academic Press, New York, 1972.
105. D. McIntyre and F. Gornick, ed., Light Scattering from Dilute Polymer Solutions, Gordon and Breach, New York, 1964.
106. S.-H. Chen, B. Chu, and R. Nossal, ed., Scattering Techniques Applied to Supramolecular and Nonequilibrium Systems, Plenum Press, New York, 1981.
107. M. M. Kops-Werkhoven, A. Vrij, and H. N. W. Lekkerkerker, "On the Relation between Diffusion, Sedimentation, and Friction", *J. Chem. Phys.*, **78**, 2760 (1983).

108. A. R. Altenberger and M. Tirrell, "Friction Coefficients in Self-Diffusion, Velocity Sedimentation, and Mutual Diffusion", *J. Polym. Sci., Polym. Phys. Ed.*, **22**, 909 (1984).
109. N. Yoshida, "Remarks on the Mutual Diffusion Coefficient of Brownian Particles", *J. Chem. Phys.*, **83**, 1307 (1985).
110. N. C. Ford, Jr., "Biochemical Applications of Laser Rayleigh Scattering", *Chem. Scripta*, **2**, 193 (1972).
111. E. R. Pike and E. Jakeman, "Photon Statistics and Photon-Correlation Spectroscopy", *Adv. Quant. Electr.*, **2**, 1 (1974).
112. S. Chandrasekhar, "Stochastic Problems in Physics and Astronomy", *Rev. Mod. Phys.*, **15**, 1 (1943).
113. R. A. Guyer, personal communication.
114. J. Machta and R. A. Guyer, personal communication.
115. B. Nyström and J. Roots, "Scaling Concepts in the Interpretation of Diffusion and Sedimentation Phenomena in Semi-dilute Polymer Solutions", *Progr. Polym Sci.*, **8**, 333 (1982).
116. M. T. Bishop, size exclusion chromatography calibration results.
117. Polymer Handbook, 2nd Ed., J. Brandrup and E. H. Immergut, ed., Wiley-Interscience, New York, 1975.
118. B. Chu, "Static and Dynamic Properties of Polymer Solutions", in Scattering Techniques Applied to Supramolecular and Nonequilibrium Systems, S.-H. Chen, B. Chu, and R. Nossal, ed., Plenum Press, New York, 1981, p. 231.
119. Handbook of Chemistry and Physics, 51st Ed., The Chemical Rubber Co., Cleveland, 1971.
120. Aldrich Chemical Company Catalog and Handbook, 1986.
121. W. Haller, "Chromatography on Glass of Controlled Pore Size", *Nature*, **206**, 693 (1965).

122. W. Haller, "Rearrangement Kinetics of the Liquid-Liquid Immiscible Microphases in Alkali Borosilicate Melts", *J. Chem. Phys.*, **42**, 686 (1965).
123. Dr. Yen Wong, Electro-Nucleonics, private communication.
124. Dr. Wolfgang Haller, private communication.
125. M. E. Nordberg, "Properties of Some Vycor-Brand Glasses", *J. Am. Ceram. Soc.*, **27**, 299 (1944).
126. H. P. Hood and M. E. Nordberg, U. S. Patent 2,106,744 (1938).
127. P. Volf, Technical Glasses, Pitman and Sons, London, 1961.
128. W. Haller and P. B. Macedo, "The Origin of Phase Connectivity in Microheterogeneous Glasses", *Phys. Chem. Glasses*, **9**, 153 (1968).
129. P. W. McMillan and C. E. Matthews, "Microporous Glasses for Reverse Osmosis", *J. Mater. Sci.*, **11**, 1187 (1976).
130. J. W. Cahn and R. J. Charles, "The Initial Stages of Phase Separation in Glasses", *Phys. Chem. Glasses*, **6**, 181 (1965).
131. P. Debye, H. R. Anderson, Jr., and H. Brumberger, "Scattering by an Inhomogeneous Solid. II. The Correlation Function and Its Application", *J. Appl. Phys.*, **28**, 679 (1957).
132. U. Even, K. Rademann, J. Jortner, N. Manor, and R. Reisfeld, "Electronic Energy Transfer on Fractals", *Phys. Rev. Lett.*, **52**, 2164 (1984).
133. J. van Brakel, S. Modry', and M. Svata', "Mercury Porosimetry: State of the Art", *Powder Technol.*, **29**, 1 (1981).
134. L. Moscou and S. Lab, "Practical Use of Mercury Porosimetry in the Study of Porous Solids", *Powder Technol.*, **29**, 45 (1981).
135. S. Modry', M. Svata', and J. van Brakel, "Thematic Bibliography of Mercury Porosimetry", *Powder Technol.*, **29**, 13 (1981).
136. R. J. Good and R. Sh. Mikhail, "The Contact Angle in Mercury Intrusion Porosimetry", *Powder Technol.*, **29**, 53 (1981).

137. A. A. Liabastre and C. Orr, "An Evaluation of Pore Structure by Mercury Penetration", *J. Colloid Interf. Sci.*, **64**, 1 (1978).
138. J. Kloubek, "Hysteresis in Porosimetry", *Powder Technol.*, **29**, 63 (1981).
139. R. J. Good, "The Contact Angle of Mercury on the Internal Surfaces of Porous Bodies", in Surface and Colloid Science, V. 13, E. Matijevic' and R. J. Good, ed., Plenum Press, New York, 1984, p. 283.
140. A. W. Adamson, Physical Chemistry of Surfaces, 4th Ed., Wiley-Interscience, New York, 1982.
141. B. C. Allen, in Liquid Metals. Chemistry and Physics, S. Z. Beer, ed., Marcel Dekker, New York, 1972, p. 179.
142. S. O. Farwell and S. J. Gluck, "Glass Surface Deactivants for Sulfur-Containing Gases, *Anal. Chem.*, **52**, 1968 (1980).
143. A. R. Cooper and J. F. Johnson, "Gel Permeation Chromatography: Effect of Treatment with Hexamethyldisilazane on Controlled Pore Glass Packings", *J. Appl. Polym. Sci.*, **13**, 1487 (1969).
144. C. J. Oliver, "Recent Developments in Photon Correlation and Spectrum Analysis Techniques, I. and II.", in Scattering Techniques Applied to Supramolecular and Nonequilibrium Systems, S.-H. Chen, B. Chu, and R. Nossal, ed., Plenum Press, New York, 1981, p. 87, p. 121.
145. N. C. Ford, Jr., "Theory and Practice of Correlation Spectroscopy", in Measurement of Suspended Particles by Quasi-Elastic Light Scattering, B. E. Dahneke, ed., John Wiley and Sons, New York, 1983, p. 31.
146. H. R. Haller, C. Destor, and D. S. Cannell, "Photometer for Quasi-elastic and Classical Light Scattering", *Rev. Sci. Instrum.*, **54**, 973 (1983).
147. T. Maeda and S. Fujime, "Quasielastic Light Scattering under Optical Microscope", *Rev. Sci. Instrum.*, **43**, 566 (1972).
148. I. Nishio, T. Tanaka, S.-T. Sun, Y. Imanishi, and S. T. Ohnishi, "Hemoglobin Aggregation in Single Red Blood Cells of Sickle Cell Anemia", *Science*, **220**, 1173 (1983).

149. C. J. Oliver, "Correlation Techniques", in Photon Correlation and Light Beating Spectroscopy, H. Z. Cummins and E. R. Pike, ed., Plenum Press, New York, 1974, p. 151.
150. D. E. Koppel, "Analysis of Macromolecular Polydispersity in Intensity Correlation Spectroscopy: The Method of Cumulants", *J. Chem. Phys.*, **57**, 4814 (1972).
151. S. W. Provencher, "Inverse Problems in Polymer Characterization: Direct Analysis of Polydispersity with Photon Correlation Spectroscopy", *Makromol. Chem.*, **180**, 201 (1979).
152. S. W. Provencher, J. Hendrix, L. de Maeyer, and N. Paulussen, "Direct Determination of Molecular Weight Distributions of Polystyrene in Cyclohexane with Photon Correlation Spectroscopy", *J. Chem. Phys.*, **69**, 4273 (1978).
153. J. G. McWhirter and E. R. Pike, "On the Numerical Inversion of the Laplace Transform and Similar Fredholm Integral Equations of the First Kind", *J. Phys. A: Math. Gen.*, **11**, 1729 (1978).
154. N. Ostrowsky, D. Sornette, P. Parker, and E. R. Pike, "Exponential Sampling Method for Light Scattering Polydispersity Analysis", *Opt. Acta*, **28**, 1059 (1981).
155. E. Gulari, E. Gulari, Y. Tsunashima, and B. Chu, "Photon Correlation Spectroscopy of Particle Size Distributions", *J. Chem. Phys.*, **70**, 3965 (1979).
156. B. Chu, E. Gulari, and E. Gulari, "Photon Correlation Measurements of Colloidal Size Distributions. II. Details of Histogram Approach and Comparison of Methods of Data Analysis", *Phys. Scripta*, **19**, 476 (1979).
157. M. Bertero, P. Brianzi, E. R. Pike, G. de Villiers, K. H. Lan, and N. Ostrowsky, "Light Scattering Polydispersity Analysis of Molecular Diffusion by Laplace Transform Inversion in Weighted Spaces", *J. Chem. Phys.*, **82**, 1551 (1985).
158. I. D. Morrison, E. F. Grabowski, and C. A. Herb, "Improved Techniques for Particle Size Determination by Quasi-Elastic Light Scattering", *Langmuir*, **1**, 496 (1985).

159. E. O. Schulz-DuBois, ed., Photon Correlation Techniques in Fluid Mechanics, Springer-Verlag, Berlin, 1983.
160. B. E. Dahneke, ed., Measurement of Suspended Particles by Quasi-Elastic Light Scattering, John Wiley and Sons, New York, 1983.
161. R. S. Stock and W. H. Ray, "Interpretation of Photon Correlation Spectroscopy Data: A Comparison of Analysis Methods", *J. Polym. Sci., Polym. Phys.*, **23**, 1393 (1985).
162. J. C. Brown, P. N. Pusey, and R. Dietz, "Photon Correlation Study of Polydisperse Samples of Polystyrene in Cyclohexane", *J. Chem. Phys.*, **62**, 1136 (1975).
163. K. Huber, W. Burchard, and A. Z. Akcasu, "Remarks on  $A_2$ , Hydrodynamic Coil Expansion, and Concentration Dependence of the Diffusion Coefficient for Polystyrene in Toluene", *Macromolecules*, **18**, 2743 (1985).
164. K. Solc and W. Stockmayer, *J. Chem. Phys.*, **54**, 2756 (1971).
165. K. Solc, *J. Chem. Phys.*, **55**, 335 (1971).
166. P. G. de Gennes, *J. Chem. Phys.*, **55**, 572 (1971); **72**, 4756 (1980).
167. M. Doi and S. F. Edwards, *J. Chem. Soc. Faraday Trans. II*, **74**, 1789, 1802, 1818 (1978); **75**, 38 (1979).
168. A. Baumgärtner and M. Muthukumar, "A Trapped Polymer Chain in Random Porous Media", to be published.
169. A. J. Bur and L. J. Fetters, "The Chain Structure, Polymerization, and Conformation of Polyisocyanates", *Chem. Rev.*, **76**, 727 (1976).
170. D. N. Rubingh and H. Yu, "Characterization of Stiff Shain Macromolecules. Poly(n-hexyl isocyanate) in n-Hexane", *Macromolecules*, **9**, 681 (1976).
171. CR-39 Product Information, PPG Industries.
172. R. L. Fleischer, P. B. Price, and R. H. Walker, Nuclear Tracks in Solids, University of California Press, Berkeley, 1975.

173. D. D. Peterson and M. C. Porter, "Particle Track Etching", in Kirk-Othmer: Encyclopedia of Chemical Technology, 3rd Ed., V. 16, John Wiley and Sons, New York, 1981, p. 826.
174. E. O. Stejskal and J. E. Tanner, "Spin Diffusion Measurements: Spin Echoes in the Presence of a Time-Dependent Field Gradient", *J. Chem. Phys.*, **42**, 288 (1965).
175. D. L. Camin and F. D. Rossini, "Physical Properties of 14 American Petroleum Institute Research Hydrocarbons, C<sub>9</sub> to C<sub>15</sub>", *J. Phys. Chem.*, **59**, 1173 (1955).
176. W. F. Seyer and J. D. Leslie, "The Viscosity of cis and trans Decahydronaphthalene", *J. Am. Chem. Soc.*, **64**, 1912 (1942).
177. B. G. Cartwright, E. K. Shirk, and P. B. Price, "A Nuclear Track Recording Polymer of Unique Sensitivity and Resolution", *Nucl. Instr. Meth.*, **153**, 457 (1978).
178. E. V. Benton and R. P. Henke, "Heavy Particle Range-Energy Relations for Dielectric Nuclear Track Detectors", *Nucl. Instr. Meth.*, **67**, 87 (1969).
179. R. P. Henke and E. V. Benton, "Charged Particle Tracks in Polymers No. 5: A Computer Code for the Computation of Heavy-Ion Range-Energy Relationships in Any Stopping Material", USNRDL-TR-67-122, 1967.

## APPENDIX A

### MISCELLANEOUS SOLVENT PROPERTIES

Following is assorted information on solvents other than 2-fluorotoluene that might be useful for dynamic light scattering experiments in porous materials.

The following solvents, with  $n \approx 1.47$ , could be used with porous silica: 2-fluorotoluene, 3-fluorotoluene, 4-fluorotoluene, trans-decahydronaphthalene, mixed cis- and trans-decahydronaphthalene (a standard composition, available from, e.g., Aldrich Chemical), dimethyl sulfoxide, dipropyl sulfoxide, and dibutyl sulfoxide. These polar aprotic dialkyl sulfoxides might be useful solvents for more "unusual" polymers, for example, polyelectrolytes; however, they are very hygroscopic. The following solvents, with  $n \approx 1.50$ , are good solvents for polystyrene and could be used with track-etched CR-39 plastic (Appendix B): benzene, 1,2-diethyl benzene, and ortho-xylene.

Extensive tabulations of solvents,<sup>117,119</sup> arranged in order of increasing refractive index, could aid in finding solvents to index match other porous materials.

Some early experiments used t-decahydronaphthalene; this solvent has the advantage of well known properties, namely refractive index  $n$  as a function of  $\lambda_0$  and  $T$ , and viscosity  $\eta$  as a function of  $T$ . The expression for  $n$  (modified Cauchy equation), derived based on literature data,<sup>175</sup> is:

$$n = 1.45237 + (4.39 \times 10^3)/\lambda_0^2 + (T - 30)(4.23 \times 10^{-4} + 4.06/\lambda_0^2) \quad (\text{A.1})$$

where  $\lambda_0$  is in nm and T in °C. t-decahydronaphthalene is claimed to be an "abnormal" liquid; that is, the viscosity  $\eta$  does not follow an Arrhenius relation.<sup>176</sup> Nonetheless, the viscosity can be determined by careful interpolation between literature data,<sup>176</sup> or from the approximate relation:

$$\eta \text{ (poise)} = (8.01 \times 10^{-5}) \exp(1637/T) \quad (\text{A.2})$$

with error of less than 0.5% over the range 20-45°C.

## **APPENDIX B**

### **TRACK-ETCHED POROUS PLASTICS**

This appendix relates preliminary work which was aimed at producing porous track-etched plastics suitable for light scattering experiments. This information should be useful if this idea is pursued in the future.

The dynamic light scattering experiments in this dissertation were performed in relatively random porous materials. It would of course be of great interest to perform similar experiments in porous materials having pores with well defined and regular geometry. One possible way to produce ideal porous materials is by track-etching,<sup>172,173</sup> which is based on the observation that the damage tracks created upon nuclear bombardment of dielectric materials often show different solubility than the bulk material, thereby allowing selective etching of those tracks. This has found commercial use in preparing plastic membranes with pores which are very nearly perfect cylinders. Track-etched membranes have been used extensively in trans-membrane diffusion studies, including hindered diffusion of polymers and colloids (see Chapter II).

A number of requirements must be met for a material to be suitable for making track-etched porous materials for light scattering experiments.

- (1) It must have high sensitivity to ionizing radiation, that is, be easily damaged.

- (2) It must have a high preferential rate of etching along tracks compared to the etch rate of undamaged portions. (This also requires the existence of a suitable etching reagent.
- (3) It must be of macroscopic size (minimum dimension  $> 100\ \mu\text{m}$ ) to allow easy mounting and focusing in a single piece of material.
- (4) It must have a refractive index allowing index matching with common solvents, and it must be inert to those solvents.

Commercially available membranes (Nuclepore: polycarbonate = PC; polyethylene terephthalate - PET) fail to meet these requirements. They are too thin ( $6\text{--}10\ \mu\text{m}$ ); they are not crosslinked, so solvent swelling, crazing (PC), or even dissolution could be problems; and they have refractive indices higher than common solvents (PC,  $n=1.59$ ; amorph. PET,  $n=1.58$ ; cryst. PET,  $n=1.64$ ). Common inorganic glasses, which, although inert and easily index matched, are not as sensitive to radiation as most plastics and show very low preferential etch rates<sup>172</sup> (i.e., the pores would be flat cones).

After some search, a very suitable material was found. The monomer diethylene glycol bis(allyl carbonate) can be polymerized to give a highly crosslinked plastic. (This monomer is available from PPG Industries under the tradename CR-39.)<sup>171</sup> The resultant plastic meets all the requirements listed above. It is highly sensitive to radiation and shows a high preferential etch rate; in fact, it is among the best of *all* known materials.<sup>177</sup> It has a suitable refractive index<sup>171</sup> ( $1.4956 @ 656.3\ \text{nm}$ ,  $1.4980 @ 589.3\ \text{nm}$ ,  $1.5001 @ 546.1\ \text{nm}$ ,  $1.5040 @ 486.1\ \text{nm}$ ) for matching with common solvents (see Appendix A). It is inert to and swells negligibly in common solvents<sup>171</sup> (e.g., benzene).

A basic procedure for the free-radical initiated polymerization of CR-39 has been given.<sup>171</sup> Modifications were made to this procedure in order to eliminate problems with oxygen inhibition, which is especially severe in polymerization of allylic monomers. The initiator, benzoyl peroxide, is dissolved in CR-39 (3% w/w). This solution is then passed through a 0.2  $\mu\text{m}$  filter to remove dust (which could prove troublesome in light scattering). Prior to polymerization, to avoid oxygen inhibition, the monomer solution is deoxygenated by five freeze-thaw-pump cycles, sparging the solution with nitrogen between cycles. Polymerization is carried out by heating 16 hours at 70-80°C (under nitrogen atmosphere, excluding oxygen) plus a 2 hour post-cure at 115°C. CR-39 polymer does not adhere strongly to glass and can be removed by breaking a glass container; alternatively, it can be cast in Teflon tubes for easier removal.

If the deoxygenation modification to the literature procedure is omitted, overall polymerization is slower, and all surfaces exposed to air are totally uncured to a depth of about 0.2 mm, with poor cure extending even deeper. Hence, in order to cast well-cured thin films of CR-39, complete deoxygenation is imperative. Non-uniform films of about 0.5 mm (500  $\mu\text{m}$ ) thickness were cast successfully using this procedure; however, no attempt was made to cast uniform and thinner (about 100-200  $\mu\text{m}$ ) films as would be required for irradiation. (Alternatively, cast rods of CR-39 could be machined into thin disks; however, this would be laborious, and CR-39 is brittle and does not machine easily.)

In deciding how best to irradiate CR-39, it is necessary to consider how the range ( $R$ ) and rate of energy deposition ( $dE/dx$ ) depend on the

atomic number ( $Z$ ) and energy ( $E$ ) of a nuclear particle.<sup>172,177</sup> The range increases with increase in  $E$  (same  $Z$ ) and with increase in  $Z$  (same  $E$ ). The rate of primary energy deposition has a maximum at some  $E$  (for a given  $Z$ ) and increases with  $Z$  (same  $E$ ). Representative results of approximate calculations, made using a computer program largely taken from Henke and Benton,<sup>178,179</sup> are found in Tables 10 and 11. The adjusted mean ionization potential<sup>178</sup> for CR-39 plastic, with empirical formula  $C_{12}H_{18}O_7$  and density  $1.31 \text{ g/cm}^3$ , is 70.2 eV. The desired thickness of porous CR-39 chips for light scattering experiments would be about  $150 \text{ }\mu\text{m}$ ; the range values which bracket this thickness are in boldface in Table 10. In Table 11, which gives results of  $dE/dx$  calculations, certain results are emphasized: maximum  $dE/dx$  values (for a given  $Z$ ) are underlined; values corresponding to the required range (from Table 10) are in boldface; and the approximate damage threshold is denoted by a solid line. This threshold is based on the estimate of  $dE/dx > 400 \text{ MeV cm}^2/\text{g}$  for tracks to be etchable.<sup>172,177</sup>

Recommendations for irradiation are arrived at by combining results of these calculations with the observed data<sup>177</sup> on the reduced etch rate ( $v_T/v_B$ ) for irradiated CR-39, where  $v_T$  and  $v_B$  are the etch rates along tracks and for bulk material. Heavy ions (e.g.,  $^{40}\text{Ar}$ ,  $^{56}\text{Fe}$ ) would be required. Lighter particles (e.g., protons,  $\alpha$ -particles) have sufficient range, but calculations of  $dE/dx$  and experimentally measured values of  $v_T/v_B$  indicate that lighter particles produce insufficient damage (e.g., ionization,  $\delta$ -rays) to give a high enough ratio of  $v_T/v_B$  (see below for importance of  $v_T/v_B$ ). Optimum energy, based simply on maximum  $dE/dx$  would be about 1 MeV, but for

TABLE 10  
Range (in Microns) of Nuclear Particles in CR-39 Polymer

E (MeV/amu)	<sup>1</sup> H	<sup>4</sup> He	<sup>12</sup> C	<sup>28</sup> Si	<sup>40</sup> Ar	<sup>56</sup> Fe
0.5	6.7E0	8.1E0	6.1E0	6.6E0	7.2E0	7.9E0
1.0	1.9E1	2.0E1	1.2E1	1.1E1	1.2E1	1.3E1
2.0	5.9E1	6.0E1	2.8E1	2.2E1	2.2E1	2.2E1
5.0	<b>2.8E2</b>	<b>2.8E2</b>	<b>1.0E2</b>	6.4E1	5.6E1	5.2E1
10.0	1.1E3	1.1E3	<b>3.8E2</b>	<b>1.9E2</b>	<b>1.5E2</b>	<b>1.3E2</b>
20.0	4.6E3	4.6E3	1.6E3	7.1E2	<b>5.2E2</b>	<b>4.1E2</b>
50.0	3.6E4	3.6E4	1.2E4	5.3E3	3.7E3	2.7E3

TABLE 11  
dE/dx (in MeV cm<sup>2</sup>/g) for Nuclear Particles in CR-39 Polymer

E (MeV/amu)	<sup>1</sup> H	<sup>4</sup> He	<sup>12</sup> C	<sup>28</sup> Si	<sup>40</sup> Ar	<sup>56</sup> Fe
0.05	<u>8.7E2</u>	2.1E3	6.5E3	1.3E4	1.6E4	2.0E4
0.10	8.6E2	<u>2.2E3</u>	7.6E3	1.5E4	2.0E4	2.5E4
0.20	6.5E2	2.0E3	<u>8.3E3</u>	1.8E4	2.4E4	3.2E4
0.50	4.0E2	1.6E3	8.1E3	2.2E4	3.0E4	3.9E4
1.0	2.5E2	1.0E3	6.8E3	<u>2.2E4</u>	<u>3.3E4</u>	4.5E4
2.0	1.6E2	6.3E2	5.1E3	1.9E4	3.1E4	<u>4.7E4</u>
5.0	<b>7.7E1</b>	<b>3.1E2</b>	<b>2.8E3</b>	1.3E4	2.3E4	3.8E4
10.0	3.5E1	1.4E2	<b>1.2E3</b>	<b>6.5E3</b>	<b>1.3E4</b>	<b>2.3E4</b>
20.0	1.5E1	6.2E1	5.5E2	3.0E3	<b>6.0E3</b>	<b>1.1E4</b>
50.0	4.4E0	1.8E1	1.6E2	8.7E2	1.8E3	3.5E3

sufficient range, 5-20 MeV heavy ions would be required. Specific choice would depend on CR-39 thickness and on availability of ion sources.

After irradiation, CR-39 is etched by aqueous NaOH, which hydrolyzes carbonate bonds; damaged regions are solubilized more rapidly than bulk material. References<sup>172,173,177</sup> can be consulted for details and suggestions on optimizing  $v_T/v_B$  (e.g., concentration, added substances, temperature, UV irradiation).

Certain aspects of the geometry of track-etching (see<sup>172</sup> for a detailed general discussion) have been considered (Figure 30). Given that  $v_T/v_B$  is not infinite, etched tracks will be cones not cylinders. The cone half-angle  $\theta$  is given by:

$$\theta = \sin^{-1}(v_B/v_T) \quad (\text{B.1})$$

The ratio of initial half-thickness  $L_0$  to final half-thickness  $L$  is:

$$L_0/L = (v_T/v_B)/\{(v_T/v_B) - 1\} \quad (\text{B.2})$$

and the surface diameter  $D$  of the hole when two cones which start at opposite faces on the same track meet is:

$$D = 2 L \tan \theta \quad (\text{B.3})$$

One is also interested in what number density of holes ( $N$ ,  $\text{cm}^{-2}$ ) is possible without significant overlap, and how porosity  $\Phi$  depends on  $N$  and hole geometry. A *crude* estimate of a reasonable (i.e., without much overlap)  $N$  was made by taking  $1/20$  the density of a close-packed cubic lattice of holes of area  $D^2$ :

Figure 30.

Track-etching geometry. The thicknesses before and after etching are  $2L_0$  and  $2L$ . The etch rate along the track is  $v_T$  and in the undamaged bulk material is  $v_B$  (hence the distances shown are the etch rate times the etch time). The final diameter of the hole is  $D$ .

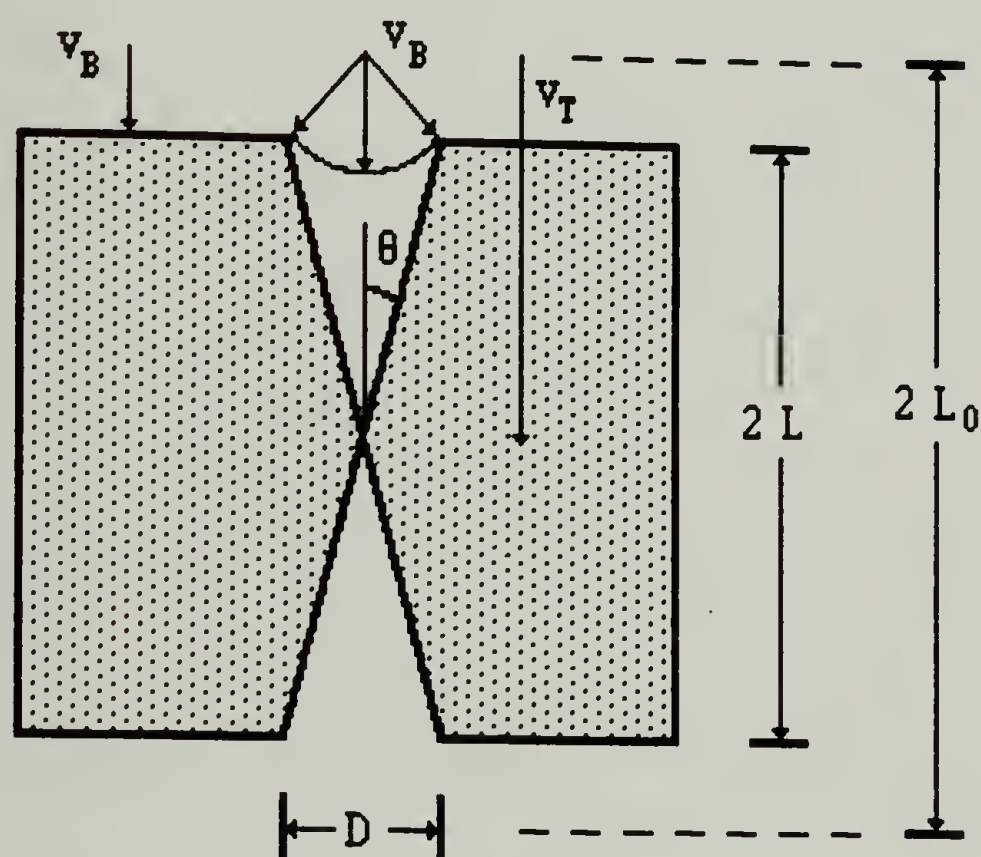


TABLE 12

Track-Etching Geometry ( $2L = 150 \mu\text{m}$ )

$v_T/v_B$	$\theta$	$D(\mu\text{m})$	$2L_0 (\mu\text{m})$	$10^{-5} \cdot N$	$\Phi$
100	$0.57^\circ$	1.5	152	22	0.013
50	$1.15^\circ$	3.0	153	5.5	0.013
20	$2.87^\circ$	7.5	158	0.9	0.013
10	$5.74^\circ$	15.1	167	0.2	0.013

$$N = 1/(20 D^2) \quad (B.4)$$

with corresponding porosity:

$$\Phi = \pi N D^2 / 12 \quad (B.5)$$

In these equations,  $D$  is in cm; obviously,  $\Phi$  is fixed by the choice of the numeric factor in equation (B.4), and is independent of cone angle. (See<sup>7</sup> for a detailed consideration of overlap, for non-conical pores only, however.)

Values of  $N$  are required to calculate radiation flux and exposure time.

The interrelations between  $v_T/v_B$ ,  $\theta$ ,  $D$ ,  $2L_0$ ,  $N$ , and  $\Phi$  are given in Table 12; these values are for a final thickness  $2L = 150 \mu\text{m}$ . From literature data,<sup>177</sup> it is apparent that for an overall thickness (i.e., range) of about  $150 \mu\text{m}$ , the maximum  $v_T/v_B$  that could be expected is about 50. This would give a surface hole diameter of  $3 \mu\text{m}$  ( $30,000 \text{ \AA}$ ), tapering to a diameter of zero in the center of the slab. Another important observation is that  $\Phi$  is quite low, even for this crude  $N$  estimate--this could lead to very low signal/noise in a light scattering experiment.

In summary, techniques for casting CR-39 have been developed, and requirements for irradiation have been determined. However, serious consideration should be given to geometrical limitations--taper, large outside hole diameter, low porosity--before attempting to pursue production of "ideal" track-etched CR-39 porous materials.

